3.4 GENERAL STANDARDS FOR CASKS

3.4.1 Chemical and Galvanic Reactions

In this subsection, it is shown that there is no credible mechanism for chemical or galvanic reactions in the HI-STAR 100 System.

The MPC, which is filled with helium, provides a nonaqueous and inert environment. Insofar as corrosion is a long-term time-dependent phenomenon, the inert gas environment in the MPC precludes the incidence of corrosion during storage on the ISFSI. Furthermore, the only dissimilar material groups in the MPC are: (1) Boral and stainless steel and (2) aluminum and stainless steel. Boral and stainless steel have been used in close proximity in wet storage for over 30 years. Many spent fuel pools at nuclear plants contain fuel racks, which are fabricated from Boral and stainless steel materials, with geometries similar to the HI-STAR 100 MPC. Not one case of chemical or galvanic degradation has been found in fuel racks built by Holtec. This experience provides a sound basis to conclude that corrosion will not occur in these materials. Additionally, the aluminum conduction inserts and stainless steel basket are very close on the galvanic series chart. Aluminum, like other metals of its genre (e.g., titanium and magnesium) rapidly passivates in an aqueous environment, leading to a thin ceramic (Al_2O_3) barrier which renders the material essentially inert and corrosion-free over long periods of application. The physical properties of the material, e.g., thermal expansion coefficient, diffusivity, and thermal conductivity, are essentially unaltered by the exposure of the aluminum metal stock to an aqueous environment. In order to eliminate the incidence of aluminum water reaction inside the MPC during fuel loading operation (when the MPC is flooded with pool water) all aluminum surfaces will be pre-passivated or anodized before installation of Boral or conduction inserts in the MPC.

The HI-STAR 100 overpack combines low alloy and nickel alloy steels, carbon steels, neutron and gamma shielding materials, thermal expansion foam, and bolting materials. All of these materials have a long history of nongalvanic behavior within close proximity of each other. The internal and external steel surfaces of each of the overpacks are sandblasted and coated to preclude surface oxidation. Therefore, chemical or galvanic reactions involving the overpack materials are highly unlikely and are not expected.

In accordance with NRC Bulletin 96-04 [3.4.7], a review of the potential for chemical, galvanic, or other reactions among the materials of the HI-STAR 100 System, its contents and the operating environments which may produce adverse reactions has been performed. Table 3.4.2 provides a listing of the materials of fabrication for the HI-STAR 100 System and evaluates the performance of the material in the expected operating environments during short-term loading/unloading operations and long-term storage operations. As a result of this review, no operations were identified which could produce adverse reactions beyond those conditions already analyzed in this FSAR.

3.4.2 Positive Closure

There are no quick-connect/disconnect ports in the confinement boundary of the HI-STAR 100 System. The all welded design of the MPC enclosure vessel precludes access to the stored nuclear fuel without use of special equipment for disconnecting Alloy X pressure vessel parts. The only access to the MPC is through the closure plate, which weighs over 7,000 pounds. The closure plate is fastened to the overpack with an array

of large bolts. Inadvertent opening of the overpack is not feasible; opening an overpack requires mobilization of special tools and heavy-load lifting equipment.

3.4.3 Lifting Devices

As required by Reg. Guide 3.61, in this subsection, analyses for all lifting operations applicable to the deployment of a HI-STAR 100 System are presented to demonstrate compliance with applicable codes and standards.

The HI-STAR 100 System has the following types of lifting devices: lifting trunnions located on the overpack top flange; threaded holes for eyebolts to lift the overpack closure plate; lifting lugs for the MPC enclosure vessel; and threaded holes for eyebolts for lifting a loaded MPC or the MPC top lid.

The evaluation of the adequacy of the lifting devices entails careful consideration of the applied loading and associated stress limits. The load combination D+H, where H is the "handling load", is the generic case for all lifting adequacy assessments. The term D denotes the dead load. Quite obviously, D must be taken as the bounding value of the dead load of the component being lifted. Table 3.2.4 gives bounding weights. In all lifting analyses considered in this document, the handling load H is assumed to be 0.15D. In other words, the inertia amplifier during the lifting operation is assumed to be equal to 0.15g. This value is consistent with the guidelines of the Crane Manufacturer's Association of America (CMAA), Specification No. 70, 1988, Section 3.3, which stipulates a dynamic factor equal to 0.15 for slowly executed lifts. Thus, the "apparent dead load" of the component for stress analysis purposes is $D^* = 1.15D$. Unless otherwise stated, all lifting analyses in this report use the "apparent dead load", D^*, in the lifting analysis.

Analysis methodology to evaluate the adequacy of the lifting device may be analytical or numerical. For the analysis of the trunnion, an accepted conservative technique for computing the bending stress is to assume that the lifting force is applied at the tip of the trunnion "cantilever" and that the stress state is fully developed at the base of the cantilever. This conservative technique, recommended in NUREG-1536, is applied to all trunnion analyses presented in this FSAR.

In general, the stress analysis to establish safety pursuant to NUREG-0612, Regulatory Guide 3.61, and the ASME Code requires evaluation of three discrete zones which may be referred to as (i) the trunnion, (ii) the trunnion/component interface, hereinafter referred to as Region A, and (iii) the rest of the component, specifically the stressed metal zone adjacent to Region A, herein referred to as Region B.

Stress limits germane to each of the above three areas are discussed below:

i. Trunnion: NUREG-0612 requires that under the "apparent dead load", D^*, the maximum primary stress in the trunnion be less than 10% of the trunnion material ultimate strength *and* less than 1/6th of the trunnion material yield strength. In otherwords, the maximum moment and shear force developed in the trunnion cantilever is less than 1/6 of the moment and shear force corresponding to incipient plasticity, and less than 1/10 of the flexural collapse moment or ultimate shear force for the section.

ii. Region A: Trunnion/Component Interface: Stresses in Region A must meet ASME Code Level A limits under applied load D*. Additionally, Regulatory Guide 3.61 requires that the maximum primary stress under $3D^*$ be less than the yield strength of the weaker of the two materials at the trunnion/component interface. In cases involving section bending, the developed section moment must be compared against the plastic moment at yield. Typically, the stresses in the component in the vicinity of the trunnion/component interface are higher than elsewhere. However, exceptional situations exist. For example, when lifting a loaded MPC, the MPC baseplate, which supports the entire weight of the fuel and the fuel basket, is a candidate location for high stress even though it is far removed from the lifting location (which is located in the top lid).

iii. Region B: This region constitutes the remainder of the component where the stress limits under the concurrent action of the apparent dead load D* and other mechanical loads that may be present during handling (e.g. internal pressure) are required to meet Level A Service Limits.

In summary, both Region A and Region B are required to meet the stress limits corresponding to ASME Level A under the load D*. Additionally, portions of the component that may experience high stress during the lift are subject to the stress criterion of Regulatory Guide 3.61, which requires satisfaction of yield strength as the limit when the sole applied load is 3D*. In general, all locations of high stress in the component under D* must also be checked for compliance with ASME Code Level A stress limits.

Unless explicitly stated otherwise, all analyses of lifting operations presented in this report follow the load definition and allowable stress provisions of the foregoing. Consistent with the practice adopted throughout this chapter, results are presented in dimensionless form, as safety factors, defined as

$$\text{Safety Factor, } SF = \frac{\text{Allowable Stress in the Region Considered}}{\text{Computed Maximum Stress in the Region}}$$

It should be emphasized that the safety factor, SF, defined in the foregoing, represents the *additional margin* that is over any beyond the margin built into NUREG 0612 (e.g. a factor of 10 on ultimate strength or 6 on yield strength).

In the following subsections, we briefly describe each of the lifting analyses performed to demonstrate compliance with regulations. Summary results are presented for each of the analyses.

It is recognized from the discussion in the foregoing that stresses in Region A are subject to two distinct criteria, namely Level A stress limits under D* and other loading that may be present (such as pressure) and yield strength at 3D*. We will use the "3D*" identifier whenever the Regulatory Guide 3.61 load case (the stresses must be bounded by the yield point at 3D*) is the applied loading.

All of the lifting analyses for the overpack reported in this subsection are designated as Load Case 03 in Table 3.1.5. All of the lifting analyses for the MPC reported in this subsection are designated as Load Case E2 in Table 3.1.4. In Subsection 3.4.4, a finite element analysis of the entire overpack is undertaken and results for Load Case 03 (Vertical Handling) in Table 3.1.5 obtained. The results for safety factors from the general finite element model are presented in a later subsection.

3.4.3.1 Overpack Lifting Trunnion Analysis

The lifting trunnion for the HI-STAR 100 overpack is presented in Holtec Drawing 1397 (Section 1.5 herein).

The two lifting trunnions for HI-STAR 100 are circumferentially spaced at 180 degrees. The trunnions are designed for a two-point lift and are sized to satisfy the aforementioned NUREG-0612 criteria. Figure 3.4.43 shows the overall lifting configuration. Appendix 3.D contains details of the lifting trunnion stress analysis. It is demonstrated in Appendix 3.D that the stresses in the trunnions, computed in the manner of the foregoing, comply with NUREG-0612 and Regulatory Guide 3.61 provisions.

Specifically, the following results are obtained:

Safety Factors from HI-STAR 100 Lifting Trunnion Stress Analysis†			
Item	Value (ksi) or (lb) or (lb-in)	Allowable (ksi) or (lb) or (lb.-in.)	Safety Factor
Bending stress (Comparison with Yield Stress/6)	17.3	24.5	1.41
Shear stress (Comparison with Yield Stress/6)	7.4	14.7	1.99
Bending Moment (Comparison with Ultimate Moment/10)	323,000	574,600	1.78
Shear Force (Comparison with Ultimate Force/10)	144,000	282,000	1.97

† The bounding lifted load is 250000 lb. (per Table 3.2.4).

We note from the above that all safety factors are greater than 1.0. A factor of safety of exactly 1.0 means that the maximum stress is equal to the yield stress in tension or shear divided by 6, or that the section moment or shear force is equal to the ultimate section moment capacity or section force capacity divided by 10.

3.4.3.2 HI-STAR 100 Overpack Lifting (Load Case 03 in Table 3.1.5)

3.4.3.2.1 Top Flange Under D*

During lifting of a loaded HI-STAR 100, the top flange of the overpack (in which the lift trunnions are located) is identified as a potential location for high stress levels.

Appendix 3.D contains calculations that analyze the top flange interface with the trunnion under the lifted load D*. The top flange is considered an NB component subject to the lifted load and internal pressure. The membrane stress intensity is computed at the interface and compared to the allowable local membrane stress intensity. The interface region is also conservatively considered as subject to the provisions of NUREG-0612 and the thread shear stress and bearing stress are compared to 1/6 of the top forging yield stress. The following table summarizes the results:

Top Flange – Minimum Safety Factors (Interface with Trunnion)			
Item	Value (ksi)	Allowable (ksi)	Safety Factor
Bearing Stress (NUREG-0612 Comparison)	3.808	5.975	1.57
Thread Shear Stress (NUREG-0612 Comparison)	3.376	3.585	1.06
Stress Intensity (NB Comparison)	7.857	34.6	4.4

It is noted from the above that all safety factors are greater than 1.0 and that the safety factors for bearing stress and thread shear stress represent the *additional* margin over the factor of safety of 6 on material yielding. A factor of safety of exactly 1.0 means that the maximum stress is equal to the yield stress in tension or shear divided by 6.

3.4.3.2.2 Overpack Top Flange and Baseplate under 3D*

Appendix 3.Y contains finite element analysis and results for the components of the HI-STAR 100 structure that are considered as Region A (namely, the top flange region and baseplate) and evaluated for safety under three times the apparent lifted load (3D*). Figure 3.Y.1 shows details of the finite element model for the top flange region. The overpack baseplate is analyzed using classical plate theory and conservatively assumes that the allowable strengths are determined at the component design temperature rather than at the lower normal operating conditions. The results from Appendix 3.Y for both regions are summarized in the table below.

Overpack Top Flange and Baseplate Minimum Safety Factors (Reg. Guide 3.61 Loading)			
Item	Value (ksi)	Allowable (ksi)	Safety Factor
Top Flange Membrane Stress Intensity (3D*)	27.44	32.2	1.17
Top Flange Membrane plus Bending Stress Intensity (3D*)	30.0	48.3	1.61
Baseplate Membrane plus Bending Stress Intensity (3D*)	1.452	32.2	22.2

It is noted from the above table that all safety factors of safety are greater than 1.0.

3.4.3.3 MPC Lifting Analysis (Load Case E2 in Table 3.1.4)

The MPC can be inserted or removed from an overpack by lifting bolts that are designed for installation into threaded holes in the top lid. The strength requirements of the bolts and base metal are examined in Appendix 3.K based on the requirements of NUREG 0612. Sufficiency of thread engagement length an bolt pre-load are also considered in Appendix 3.K. The MPC top closure is examined in Appendix 3.E, considering the top lid as "Region B", where satisfaction of ASME Code Level A requirements is demonstrated. The same appendix also considers highly stressed regions of the top closure as "Region A" where applied load is 3D*. Appendix 3.I includes structural analysis of the baseplate under normal handling and subject to the allowable strengths appropriate to a component considered in "Region B". Finally, Appendix 3.Y contains analysis and results for the same baseplate region where the loading is 3D* consistent with the baseplate of the MPC being considered as a "Region A". The definitions of "Region A", "Region B", and "3D*" as they apply to lifting analyses have been introduced at the beginning of this Subsection.

The following table summarizes the results from all of these analyses. As stated earlier, safety factors tabulated in this section represent margins that are over and beyond those implied by the loading magnification mandated in NUREG 0612 or Regulatory Guide 3.61, as appropriate.

Summary of MPC Lifting Analyses-Minimum Safety Factors			
Item	Value of Stress (ksi) or Load (lb.)	Allowable (ksi) or Capacity (lb.)	Safety Factor = Allowable/Value or Capacity/Load
Lifting Bolt Load – NUREG 0612 (Note 1)	103,500	111,300	1.08
Top Lid Peripheral Weld Load – (3D*) (Note 2)	310,500	1,055,000	3.40
Top Lid Peripheral Weld Load– "Region B" (Note 2)	460,023	1,055,000	2.29
Baseplate Bending Stress – (3D*) (Note 3)	13.26	20.7	1.56
Baseplate Bending Stress – "Region B" (Note 4)	25.78	28.05	1.09

Notes:

1. Detailed analysis presented in Appendix 3.K
2. Detailed analysis presented in Appendix 3.E
3. Detailed analysis presented in Appendix 3.Y
4. Detailed analysis presented in Appendix 3.I

We note that all factors of safety are greater than 1.0 as required. We also note that the baseplate bending stress calculation in Appendix 3.I is conservative in that the load from the fuel basket is applied as a uniform pressure over the entire baseplate; In reality, the load is applied as a ring load located near the periphery of the basket. Applying the load in this manner would increase the reported safety factor.

3.4.3.4 Miscellaneous Lifting Analyses

The closure plate of the HI-STAR 100 overpack is lifted using four eyebolt lugs that are threaded into tapped holes in the closure plate. The MPC top lid is lifted using the same tapped holes that are used for lifting a loaded MPC. Figure 8.1.2 identifies the typical lid lifting operation that is indicated as one of the steps in the cask deployment operation.

Appendix 3.K contains details of the strength qualification of the overpack top closure lifting holes. Qualification is based on the previously discussed NUREG-0612 requirement. Minimum safety factors are summarized in the table below where we note that a safety factor of 1.0 means that the stress is the lessor of yield stress/6 or ultimate stress/10.

Miscellaneous Lid Lifting – Minimum Safety Factors			
Item	Value (lb.)	Capacity (lb.)	Minimum Safety Factor
Overpack Top Closure Lifting Bolt Shear	9,200	12,010	1.31
Overpack Top Closure Lifting Bolt Tension	9,200	13,250	1.44

Synopses of lifting device, device/component interface, and component stresses, under all contemplated lifting operations for the HI-STAR 100 System have been presented in the foregoing. The results show that all factors of safety are greater than 1.0.

3.4.4 Heat

Subsection 3.4.4, labeled "Heat" in Regulatory Guide 3.61 is required to contain information on all structural (including thermoelastic) analyses performed in the cask to demonstrate positive safety margins, except for lifting operations that are covered in Subsection 3.4.3 in the preceding. Accordingly, this subsection contains all necessary information on the applied loadings, differential thermal expansion considerations, stress analysis models, and results for all normal and off-normal operations, and for natural phenomena/accident events. Assessment of potential malfunction under "Cold" conditions is required to be presented in Subsection 3.4.5.

As instructed by Regulatory Guide 3.61, the thermal evaluation of the HI-STAR 100 System is reported in Chapter 4.

3.4.4.1 Summary of Pressures and Temperatures

Design pressures and design temperatures for all conditions of storage are listed in Tables 2.2.1 and 2.2.3, respectively. Load Cases F1 (Table 3.1.3) and E4 (Table 3.1.4) are defined to study the effect of differential thermal expansion among the constituent components in the HI-STAR 100 System. Figures 3.4.1 and 3.4.2 provide the defining bounding temperature distributions used for the MPC and overpack finite element thermal stress calculations so as to maximize stresses that develop due to such radial gradients. The distribution T is applied conservatively to analyze its effect on the fuel basket, the enclosure vessel, and the overpack.

3.4.4.2 Differential Thermal Expansion

Consistent with the requirements of Reg. Guide 3.61, Load Cases F1 (Table 3.1.3) and E4 (Table 3.1.4) are defined to study the effect of differential thermal expansion among the constituent components in the HI-STAR 100 System. Tables 4.4.9 to 4.4.11 provide the temperatures necessary to perform the differential thermal expansion analyses for the MPC in the HI-STAR 100 System. The material presented

in the remainder of this paragraph demonstrates that a physical interference between discrete components of the HI-STAR 100 System (e.g. overpack and enclosure vessel) will not develop due to differential thermal expansion during any operating condition.

3.4.4.2.1 Normal Hot Environment

Closed form calculations are performed to demonstrate that initial gaps between the HI-STAR 100 overpack and the MPC canister, and between the MPC canister and the fuel basket, will not close due to thermal expansion of the system components under normal, off-normal, and accident cases, defined as F1 and E4 in Tables 3.1.3 and 3.1.4, respectively. To assess this in the most conservative manner, the thermal solutions computed in Chapter 4 are surveyed for the following information.

- The radial temperature distribution in each of the fuel baskets at the location of peak center metal temperature.
- The highest and lowest mean temperatures of the canister shell for the hot environment condition.
- The inner and outer surface temperature of the overpack shell (inner shell, intermediate shells, neutron shield, and outer enclosure shell) at the location of highest and lowest surface temperature (which will produce the lowest mean temperature).

Table 4.4.16 presents the resulting temperatures used in the evaluation of the MPC expansion in the HI-STAR 100 overpack.

Using the temperature information in the above-mentioned tables, simplified thermoelastic solutions of equivalent axisymmetric problems are used to obtain conservative estimates of gap closures. The following procedure, which conservatively neglects axial variations in temperature distribution, is utilized.

1. Use the surface temperature information for the fuel basket to define a parabolic distribution in the fuel basket that bounds (from above) the actual temperature distribution. Using this result, generate a conservatively high estimate of the radial and axial growth of the different fuel baskets using classical closed form solutions for thermoelastic deformation in cylindrical bodies.

2. Use the temperatures obtained for the canister to predict an estimate of the radial and axial growth of the canister to check the canister-to-basket gaps.

3. Use the temperatures obtained for the canister to predict an estimate of the radial and axial growth of the canister to check the canister-to-overpack gaps.

4. Use the overpack surface temperatures to construct a logarithmic temperature distribution (characteristic of a thick walled cylinder) at the location used for canister thermal growth

calculations; and use this distribution to predict an estimate of overpack radial and axial growth.

5. For given initial clearances, compute the operating clearances.

The calculation procedure outlined above is used in Appendices 3.U and 3.W (HI-STAR 100 overpack with MPC-24 and MPC-68, respectively). The results are summarized in the tables given below for normal storage conditions.

THERMOELASTIC DISPLACEMENTS IN THE MPC AND OVERPACK UNDER HOT TEMPERATURE ENVIRONMENT CONDITION				
CANISTER – FUEL BASKET				
	Radial Direction (in.)		Axial Direction (in.)	
Unit	Initial Clearance	Final Gap	Initial Clearance	Final Gap
MPC-24	0.1875	0.140	2.0	1.77
MPC-68	0.1875	0.144	2.0	1.79
CANISTER – OVERPACK				
	Radial Direction (in.)		Axial Direction (in.)	
Unit	Initial Clearance	Final Gap	Initial Clearance	Final Gap
MPC-24	0.09375	0.068	0.625	0.482
MPC-68	0.09375	0.069	0.625	0.482

It can be verified by referring to the Design Drawings provided in Section 1.5 of this report and the foregoing table, that the clearances between the MPC basket and canister structure, as well as that between the MPC shell and storage overpack, are sufficient to preclude a temperature induced interference from differential thermal expansions under normal operating conditions.

3.4.4.2.2 Fire Accident

Appendix 3.AD evaluates the growth of the fuel basket during and after the fire accident. It is shown that under the most conservative set of assumptions the fuel basket does not contact either the canister or the MPC lid due to free thermal growth. Therefore, restraint of free end expansion leading to fuel basket distortion will not occur. Hence, ready retrievability of the fuel will be maintained and the fuel will remain in a subcritical configuration. The table below summarizes the results from Appendix 3.AD

THERMOELASTIC DISPLACEMENTS IN THE MPC AND OVERPACK UNDER FIRE ACCIDENT TEMPERATURE ENVIRONMENT				
CANISTER – FUEL BASKET				
	Radial Direction (in.)		Axial Direction (in.)	
Unit	Initial Clearance	Final Gap	Initial Clearance	Final Gap
Bounding MPC	0.1875	0.106	2.0	1.604
CANISTER – OVERPACK				
	Radial Direction (in.)		Axial Direction (in.)	
Unit	Initial Clearance	Final Gap	Initial Clearance	Final Gap
Bounding MPC	0.09375	0.052	0.625	0.383

Chapter 11 shows that the fire accident has little effect on the MPC temperatures because of the short duration of the fire and the large thermal inertia of the storage overpack. Therefore, structural evaluation of the MPC under the postulated fire event is not required. The external surfaces of the HI-STAR 100 overpack that are directly exposed to the fire event experience maximum rise in temperature. The outer shell and top closure plate are the external surfaces that are in direct contact with heated air from fire. The table below, extracted from data provided in Chapter 11 (Table 11.2.2), provides maximum bulk temperatures attained.

Component Peak Temperatures due to Storage Fire Event	
Component	Maximum Fire Condition Section Temperature (°F)
Overpack Inner Shell	328
Overpack Top Flange	524
Overpack Outer Shell (external skin)	854
Overpack Baseplate	496
Overpack Closure Plate	384
Neutron Shield Inner Surface	314
Neutron Shield Outer Surface	551
MPC Shell	364

The following conclusions are readily reached from the above table.

- The maximum temperature of the ferritic steel material in the body of the HI-STAR 100 overpack is well below 50% of the material melting point. (The melting point of carbon and low alloy steels is approximately 2750°F, per Mark's Standard Handbook, Ninth Edition, pp 6-11.)

- The temperature of the neutron shielding material experiences a gradient across the thickness of the shielding. The shielding material adjacent to the hot outer enclosure shell experiences a local temperature of 551 degrees F. This means that a limited loss of shielding effectiveness may occur.

- Data published by the Oak Ridge National Laboratories indicates that low stresses from the self-weight of the most heated steel members of HI-STAR 100 (the external skin) ensures that no material rupture will occur. According to the Nuclear System Materials Handbook, TID-2666, ORNL, the time-to-rupture for carbon steels at 1250°F and 4821 psi tensile stress is 520 hours. According to the analyses summarized in Chapter 11, the duration of high temperature in the most heated portion of HI-STAR 100 is well under 1 hour, and the temperature never reaches 900°F.

3.4.4.3 Stress Calculations

This subsection presents calculations of the stresses in the different components of the HI-STAR 100 System from the effects of mechanical load case assembled in Section 3.1. Loading cases for the MPC fuel basket, the MPC enclosure vessel, the HI-STAR 100 storage overpack are listed in Tables 3.1.3 through 3.1.5, respectively. Detailed analyses for the load cases are presented in labeled appendices that are listed in the load case tables (Tables 3.1.3, 3.1.4, and 3.1.5). An abbreviated description of each of the analyses is presented in the body of the chapter.

In general, as required by Regulatory Guide 3.61, the comparison of the calculated stresses with their corresponding allowables is presented in Subsection 3.4.4.4. However, for clarity in the narrative in this subsection (3.4.4.3), unnumbered summary tables are presented within the text. However, the key stress comparisons are subsequently reproduced in numbered tables associated with Subsection 3.4.4.4 to provide strict compliance with Regulatory Guide 3.61.

The purpose of the analyses is to provide the necessary assurance that there will be no unacceptable risk of criticality, unacceptable release of radioactive material, unacceptable radiation levels, or impairment of ready retrievability.

For all stress evaluations, the allowable stresses and stress intensities for the various HI-STAR 100 System components are based on bounding high metal temperatures to provide additional conservatism (Table 3.1.17 for the MPC basket and shell, for example). Elastic behavior is assumed for all stress analyses. Elastic analysis is based on the assumption of a linear relationship between stress and strain.

In addition to the loading cases germane to stress evaluations mentioned above, three cases pertaining to the stability of HI-STAR 100 are also considered (Table 3.1.1).

The results of various stress calculations on components are reported in this subsection. The calculations are either performed directly as part of the text, or summarized in an appendix (see the list of all supporting appendices provided in Section 3.6.3) that provides details of strength of materials evaluations or finite element numerical analysis. The specific calculations reported in this subsection are:

1. MPC stress and stability calculations
2. HI-STAR 100 overpack stress and stability calculations

The MPC fuel basket and enclosure vessel have been evaluated for the load combinations in Tables 3.1.3 and 3.1.4. The HI-STAR 100 overpack has also been evaluated for certain limiting load conditions that are germane to the storage and operational modes specified for the system in Tables 3.1.1 and 3.1.5.

MPC stress and stability analyses are considered in Subsection 3.4.4.3.1. Within this subsection, the following analyses are performed:

a. Finite element analysis of the MPC fuel basket and enclosure shell under lateral loads
b. Finite element and analytical analysis of the enclosure vessel as an ASME Code pressure vessel.
c. Elastic stability and yielding analysis of the MPC fuel basket under lateral and axial compression.
d. Analysis of the MPC baseplate under lateral loads.
e. Analysis of the MPC closure lid under lateral load.
f. Analysis of the fuel support spacers under compression load.
g. Elastic stability and yielding of the MPC enclosure shell under axial and lateral loads

Overpack stress and stability analyses are considered in Subsection 3.4.4.3.2. Within this subsection, the following analyses are performed:

a. Three-dimensional finite element analysis of the overpack subjected to load cases listed in Table 3.1.5.
b. Consideration of fabrication stresses
c. Structural analysis of closure bolting for normal operation, top closure puncture, and a postulated accident drop condition.
d. Stress analysis of the overpack closure plate under lateral loads.
e. Elastic stability and yielding of the overpack inner shell.
f. Stress analysis of the enclosure shell and enclosure return under internal pressure.

3.4.4.3.1 MPC Stress and Stability Calculations

The structural function of the MPC in the storage mode is stated in Section 3.1. The calculations presented here demonstrate the ability of the MPC to perform its structural function. Analyses are performed for each of the two MPC designs. The purpose of the analyses is to provide the necessary assurance that there will be no unacceptable risk of criticality, unacceptable release of radioactive material, or impairment of ready

retrievability. The following subsections describe the model, individual loads, load combinations, and analysis procedures applicable to the MPC.

3.4.4.3.1.1 Analysis of Load Cases E.3.b, E.3.c (Table 3.1.4) and F2, F.3.b, F.3.c (Table 3.1.3)

The load cases considered herein pertain to lateral loading on the MPC components, namely the fuel basket and the enclosure vessel. For this purpose, a finite element model of the MPC is necessary.

- Description of Finite Element Models of the MPCs under Lateral Loading

A finite element model of each MPC is used to assess the effects of the normal, off normal, and accident loads. The models are constructed using ANSYS [3.4.1], and they are identical to the models used in Holtec's HI-STAR 100 10CFR71 submittal under Docket Number 71-9261. The following model description is common to all MPCs.

The MPC structural model is two-dimensional. It represents a one-inch long cross section of the MPC fuel basket and MPC canister.

The MPC model includes the fuel basket, the basket support structures, and the MPC shell. A basket support is defined as any structural member that is welded to the inside surface of the MPC shell. A portion of the overpack inner surface is modeled to provide the correct restraint conditions for the MPC. Figures 3.4.3 through 3.4.11 show the two MPC models. Detailed element numbers for the fuel basket and the enclosure vessel are provided in Appendices, 3.N through 3.S, inclusive.

The fuel basket support structure shown in the figures and in the design drawings in Section 1.5 is a multi-plate structure consisting of solid shims or support members having two separate compressive load supporting members. For conservatism in the finite element model some dual path compression members (i.e., "V" angles) are simulated as single columns. Therefore, the calculated stress intensities in the fuel basket angle supports, reported in Appendix 3.AA from the finite element solution, are conservatively overestimated in some locations.

The ANSYS model is not intended to resolve the detailed stress distributions in weld areas. Individual welds are not included in the finite element model. A separate analysis for basket welds and for the basket support "V" angles is contained in Appendix 3.M.

No credit is taken for any load support offered by the Boral panels, sheathing, and the aluminum heat conduction elements. Therefore, these so-called non-structural members are not represented in the model. The bounding MPC weight used, however, does include the mass contributions of these non-structural components.

The model is built using five ANSYS element types: BEAM3, PLANE82, CONTAC12, CONTAC26, and COMBIN14. The fuel basket and MPC shell are modeled entirely with two-dimensional beam elements (BEAM3). Plate-type basket supports are also modeled with BEAM3 elements. Eight-node plane elements (PLANE82) are used for the solid-type basket supports. The gaps between the fuel basket and the bask

supports are represented by two-dimensional point-to-point contact elements (CONTAC12). Contact between the MPC shell and the overpack is modeled using two-dimensional point-to-ground contact elements (CONTAC26) with an appropriate clearance gap.

For each MPC type, three variations of the finite element model were prepared. The basic model includes only the fuel basket and the enclosure shell (Figures 3.4.3 through 3.4.5) and is used only to study the free thermal expansion due to the temperature field developed in the system. The other two models include a representation of the overpack and are used for the two drop cases considered. Two orientations of the deceleration vector are considered. The 0-degree drop model includes the overpack-MPC interface in the basket orientation illustrated in Figure 3.1.2. The 45-degree drop model represents the overpack-MPC interface with the basket oriented in the manner of Figure 3.1.3. The 0-degree and the 45-degree drop models are shown in Figures 3.4.6 through 3.4.11. Table 3.4.1 lists the element types and number of elements for all models for all fuel storage MPC types.

A contact surface is provided in the models used for drop analyses to represent the overpack inner shell. As the MPC makes contact with the overpack, the MPC shell deforms to mate with the inside surface of the inner shell. The nodes that define the elements representing the fuel basket and the MPC shell are located along the centerline of the plate material. As a result, the line of nodes that forms the perimeter of the MPC shell is inset from the real boundary by a distance that is equal to half of the shell thickness. In order to maintain the specified MPC shell/overpack gap dimension, the radius of the overpack inner shell is decreased by an equal amount in the model.

Contact is simulated using two-dimensional point-to-ground elements (CONTAC26). The surface is tangent to the MPC shell at the initial point of impact and extends 135 degrees on both sides. This is sufficient to capture the full extent of contact between the MPC and the overpack.

The three discrete components of the HI-STAR 100 System, namely the fuel basket, the MPC shell, and the storage overpack are engineered with small diametral clearances which are large enough to permit unconstrained thermal expansion of the three components under the rated (maximum) heat duty condition. A small diametral gap under ambient conditions is also necessary to assemble the system without physical interference between the contiguous surfaces of the three components. The required gap to ensure unrestricted thermal expansion between the basket and the MPC shell is less than 0.1 inch. This gap, too, will decrease under maximum heat load conditions, but will introduce a physical nonlinearity in the structural events involving lateral loading (such as side drop of the system) under ambient conditions. It is evident from the system design drawings that the fuel basket, which is non-radially symmetric, is in proximate contact with the MPC shell at a discrete number of locations along the circumference. At these locations, the MPC shell, backed by the massive overpack weldment, provides a virtually rigid support line to the fuel basket during lateral drop events. Because the fuel basket, the MPC shell, and the overpack are all three-dimensional structural weldments, their inter-body clearances may be somewhat uneven at different azimuthal locations. As the lateral loading is increased, clearances close at the support locations, resulting in the activation of the support from the overpack.

The bending stresses in the basket and the MPC shell at low lateral loading levels which are too small to close the support location clearances are secondary stresses since further increase in the loading will activate the

overpack's support action, mitigating further increase in the stress. Therefore, to compute primary stresses in the basket and the MPC shell under lateral drop events, the gaps should be assumed to be closed. However, for conservatism, it is assumed that an initial gap of 0.1875" exists, in the direction of the applied deceleration, at all support locations between the basket and the shell and the radial gap between the shell and the overpack at the support locations is 3/32". All stresses produced by the applied loading on this configuration are compared with primary stress levels, even though the self-limiting stresses should be considered secondary in the strict definition of the Code.

- Description of Individual Loads and Boundary Conditions Applied to the MPCs

The method of applying each individual load to the MPC model is described in this subsection. The individual loads are listed in Table 2.2.14. A free-body diagram of the MPC corresponding to each individual load is given in Figures 3.4.12-3.4.15. In the following discussion, reference to vertical and horizontal orientations are made. Vertical refers to the direction along the cask axis, and horizontal refers to a radial direction.

Quasi-static structural analysis methods are used. The effects of any dynamic load factors (DLFs) are included in the final evaluation of safety margins. All analyses are carried out using the design basis decelerations in Table 3.1.2

The MPC models used for side drop evaluations are shown in Figures 3.4.6 through 3.4.11. In each model, the fuel basket and the enclosure vessel are constrained to move only in the direction that is parallel to the acceleration vector. The overpack inner shell, which is defined by three nodes needed to represent the contact surface, is fixed in all degrees of freedom. The fuel basket, enclosure vessel, and overpack inner shell are all connected at one location by linear springs (see Figure 3.4.6, for example).

(a) Accelerations

During a side impact event, the stored fuel is directly supported by the cell walls in the fuel basket. Depending on the orientation of the drop, 0 or 45 degrees (see Figures 3.4.14 and 3.4.15), either one or two walls support the fuel. The effect of deceleration on the fuel basket and canister metal structure is accounted for by amplifying the gravity field in the appropriate direction. In the finite element model this load is effected by applying a uniformly distributed pressure over the full span of the supporting walls. The magnitude of the pressure is determined by the weight of the fuel assembly (Table 2.1.6), the axial length of the fuel basket support structure, the width of the cell wall, and the impact acceleration. It is assumed that the load is evenly distributed along an axial length of basket equal to the fuel basket support structure. For example, the pressure applied to an impacted cell wall during a 0-degree side drop event is calculated as follows:

$$p = \frac{a_n W}{L \ell}$$

where:

p = pressure

a_n = ratio of the impact acceleration to the gravitational acceleration

W = weight of a stored fuel assembly

L = axial length of the fuel basket support structure

ℓ = width of a cell wall

For the case of a 45-degree side drop the pressure on any cell wall equals p (defined above) divided by the square root of 2. Figure 3.4.12 shows the details of the fuel assembly pressure load on the fuel basket.

(b) Internal Pressure

Design internal pressure in the MPC model is applied by specifying pressure on the inside surface of the enclosure vessel. The magnitude of the internal pressure applied to the model is taken from Table 2.2.1.

For this load condition, the center of the fuel basket is fixed in all degrees of freedom.

(c) Temperature

Temperature distributions are developed in Chapter 4 and applied as nodal temperatures to the finite element model of the MPC enclosure vessel (confinement boundary). Maximum design heat load has been used to develop the temperature distribution used to demonstrate compliance with ASME Code stress intensity levels. A plot of the applied temperature distribution as a function of radius is shown in Figure 3.4.1. Figure 3.4.13 shows the MPC-68 with the typical boundary conditions for all thermal and pressure load cases.

(d) Handling (Lateral Loading)

As discusses in Subsection 3.1.2.1.2, loads arise on the HI-STAR 100 System from normal handling of the cask (e.g., lateral loads while moving the system to the ISFSI). A 2g lateral acceleration, imposed on the fuel basket/enclosure shell finite element model, is assumed to bound lateral handling loads on the MPC under normal handling conditions (Level A Service Conditions).

- Analysis Procedure

The analysis procedure for this set of load cases is as follows:

1. The stress intensity and deformation field due to the combined loads is determined by the finite element solution. Results are postprocessed and listed in Appendix 3.AA.

2. The results for each load combination are compared to allowables. The comparison with allowable values is made in Subsection 3.4.4.4.

3.4.4.3.1.2 Analysis of Load Cases E1.a and E1.c (Table 3.1.4)

Load Cases E1.a and E1.c pertain to the performance of the enclosure vessel as a pressure vessel.

Since the MPC shell is a pressure vessel, the classical Lame's calculations should be performed to demonstrate the shell's performance as a pressure vessel. We note that dead load has an insignificant effect on this stress state. We first perform calculations for the shell under internal pressure. Subsequently, we perform a finite element analysis on the entire confinement boundary as a pressure vessel subject to both internal pressure and temperature gradients. Finally, we perform confirmatory hand calculations to gain confidence in the finite element predictions,

- Lame's Solution for the MPC Shell

The stress from internal pressure is found for normal and accident pressures conditions using classical formulas:

We define the following quantities:

P = pressure, r = MPC radius, and t = shell thickness.

Using classical thin shell theory, the circumferential stress, $\sigma_1 = Pr/t$, the axial stress $\sigma_2 = Pr/2t$, and the radial stress $\sigma_3 = -P$ are computed for both normal and accident internal pressures. The results are given in the following table:

Classical Shell Theory Results for Normal and Accident Internal Pressures				
Item	σ_1 (psi)	σ_2 (psi)	σ_3 (psi)	$\sigma_1 - \sigma_3$ (psi)
P= 100 psi	6,838	3,419	-100	6,938
P= 125 psi	8,548	4,274	-123	8,673

Table 3.1.17 provides the allowable membrane strength for Load Case E1 for Alloy X. We see that a safety factor greater than 1.0 exists for the case of normal and accident pressures.

- Finite Element Analysis (Load Case E1.a and E1.c of Table 3.1.4)

Having performed the classical "thin shell under pressure" evaluation, we now proceed to perform a finite element analysis where the interaction between the end closures and the MPC shell is rigorously modeled.

The MPC shell, the top lid, and the baseplate together form the confinement boundary (enclosure vessel) for storage of spent nuclear fuel. In this section, we evaluate the operating condition consisting of dead weight, internal pressure, and thermal effects for the normal heat condition of storage. The top and bottom plates of the MPC enclosure vessel (EV) are modeled using plane axisymmetric elements, while the shell is modeled using the axisymmetric thin shell element. The thickness of the top lid varies in the two MPC types; for conservative results, the minimum thickness top lid is modeled. The temperature distributions for all MPC constructions are nearly identical in magnitude and gradient. Temperature differences across the thickness of both the baseplate and the top lid exist during HI-STAR 100's operations. There is also a thermal gradient from the center of the top lid and baseplate out to the shell wall. The metal temperature profile is essentially parabolic from the centerline of the MPC out to the MPC shell. There is also a parabolic temperature profile along the length of the MPC canister. Figure 3.4.44 shows a sketch of the confinement boundary structure with identifiers A-I (also called locating points) where temperature input data is used to represent a continuous temperature distribution for analysis purposes. The overall dimensions of the confinement boundary are also shown in the figure.

Table 4.4.22 provides the desired temperatures for confinement thermal stress analysis. From the tables, we see that the distribution for the MPC-24 provides the largest temperature gradients in the baseplate (from centerline to outer edge) and in the shell (from the joint at the baseplate to the half-height of the cask). It will be shown later than stress intensities are greatest in these components of the confinement vessel. Therefore, detailed stress analyses are performed only for the MPC-24.

Figure 3.4.45 shows details of the finite element model of the top lid, canister shell, and baseplate. The top lid is modeled with 40 axisymmetric quadrilateral elements; the weld connecting the lid to the shell is modeled by a single element solely to capture the effect of the top lid attachment to the canister offset from the middle surface of the top lid. The MPC canister is modeled by 50 axisymmetric shell elements, with 20 elements concentrated in a short length of shell appropriate to capture the so-called "bending boundary layer" at both the top and bottom ends of the canister. The remaining 10 shell elements model the MPC canister structure away from the shell ends in the region where stress gradients are lower (from the physics of the problem). The baseplate is modeled by 20 axisymmetric quadrilateral elements. Deformation compatibility at the connections is enforced at the top by the single weld element, and deformation and rotation compatibility at the bottom by additional shell elements between nodes 106-107 and 107-108.

The geometry of the model is listed below (terms are defined in Figure 3.4.45):

H_t = 9.5" (the minimum thickness lid is assumed)

R_L = 0.5 x 67.25" (Bill of Materials for Top Lid, Section 1.5)

L_{MPC} = 190.5" (Drawing 1393, Sheet 1)

t_s = 0.5"

R_S = 0.5 x 68.375"

t_{BP} = 2.5"

$\beta L = 2\sqrt{R_s t_s} \approx 12$" (the "bending boundary layer")

Stress analyses are carried out for two cases as follows:

a. internal pressure = 100 psi

b. internal pressure = 100 psi, plus applied temperatures for the MPC-24

We note that dead weight of the top lid reduces the stresses due to pressure. For example, the equivalent pressure simulating the effect of the weight of the top lid is an external pressure of 3 psi, which reduces the pressure difference across the top lid to 97 psi. Thus, for conservatism, dead weight of the top lid is neglected to provide additional conservatism in the results. The dead weight of the baseplate, however, adds approximately 0.73 psi to the effective internal pressure acting on the base. The effect of dead weight is still insignificant compared to the 100 psi design pressure, and is therefore neglected. The thermal loading in the confinement vessel is obtained by developing a parabolic temperature profile to the entire length of the MPC canister and to the top lid and baseplate. The temperature data provided at locations A-I in Figures 3.4.44 and 3.4.45 are sufficient to establish the profiles. Through-thickness temperatures are assumed linearly interpolated between top and bottom surfaces of the top lid and baseplate. All material properties and expansion coefficients are considered to be temperature-dependent in the model.

Results for stress intensity are reported for the case of internal pressure alone and for the combined loading of pressure plus temperature (Load Case E1.c in Table 3.1.4). Tables 3.4.7 and 3.4.8 report results at the inside and outside surfaces of the top lid and baseplate at the centerline and at the extreme radius. Canister results are reported in the "bending boundary layer" and at a location near mid-length of the MPC canister. In the tables, the calculated value is the value from the finite element analysis, the categories are P_m = primary membrane; $P_L + P_b$ = local membrane plus primary bending; and $P_L + P_b + Q$ = primary plus secondary stress intensity. The allowable stress intensity value is obtained from the appropriate table in Section 3.1 for Level A conditions, and the safety factor SF is defined as the allowable strength divided by the calculated value. Allowable stresses for Alloy X are taken at 300°F, which bounds the temperatures everywhere except at the mid-length position of the MPC shell (Location I in Figure 3.4.44) during the normal operation. At Location I, the allowable strength is taken at 400°F. The results given in Tables 3.4.7 and 3.4.8 demonstrate the ruggedness of the MPC as a confinement boundary.

- Confirmatory Closed Form Solution

The results in Table 3.4.7 and 3.4.8 also show that the baseplate and the shell connection to the baseplate are the most highly stressed regions under the action of internal pressure. To confirm the finite element results, we perform an alternate closed form solution using classical plate and shell theory equations that are listed in or developed from the reference Timoshenko and Woinowsky-Krieger, Theory of Plate and Shells, McGraw Hill, Third Edition.

Assuming that the thick baseplate receives little support against rotation from the thin shell, the bending stress at the centerline is evaluated by considering a simply supported plate of radius a and thickness h, subjected to lateral pressure p. The maximum bending stress is given by

$$\sigma = \frac{3(3+\nu)}{8} p \left(\frac{a}{h}\right)^2$$

where:

a = .5 x 68.375"

h = 2.5"

ν = 0.3 (Poisson's Ratio)

p = 100 psi

Calculating the stress in the plate gives σ = 23,142 psi.

Now consider the thin MPC shell (t = 0.5") and first assume that the baseplate provides a clamped support to the shell. Under this condition, the bending stress in the thin shell at the connection to the plate is given as

$$\sigma_{Bp} = 3p \frac{a}{t} \frac{(1-\nu/2)}{\sqrt{3}(1-\nu^2)^{1/2}} = 10{,}553 \text{ psi}$$

In addition to this stress, there is a component of stress in the shell due to the baseplate rotation that causes the shell to rotate. The joint rotation is essentially driven by the behavior of the baseplate as a simply supported plate; the shell offers little resistance because of the disparity in thickness and will essentially follow the rotation of the thick plate.

Using formulas from thin shell theory, the additional axial bending stress in the shell due to this rotation θ can be written in the form

$$\sigma_{B\theta} = 12 \beta D_s \frac{\theta}{t^2}$$

where

$$\theta = pa^3/8D(1+\nu) * \left(1/1+\alpha\right)$$

and

$$D = \frac{Eh^3}{12(1-\nu^2)} \quad E = \text{plate Young's Modulus}$$

$$\alpha = \frac{2\beta at^3}{h^3(1+\nu)}$$

$$D_s = \frac{Et^3}{12(1-\nu^2)}$$

$$\beta^2 = \sqrt{3(1-\nu^2)}/at$$

Substituting the numerical values gives

$$\sigma_{B\theta} = 40{,}563 \text{ psi}$$

We note that the approximate solution is independent of the value chosen for Young's Modulus as long as the material properties for the plate and shell are the same.

Combining the two contributions to the shell bending stress gives the total extreme fiber stress in the longitudinal direction as 51,116 psi.

The baseplate stress value, 23,142 psi, compares well with the finite element result 20,528 psi (Table 3.4.7). The shell joint stress, 51,116 psi, is greater than the finite element result (43,986 psi in Table 3.4.7). This is due to the local effects of the shell-to-baseplate connection offset. That is, the connection between shell and baseplate in the finite element model is at the surface of the baseplate, not at the middle surface of the

baseplate. This offset will cause an additional bending moment that will reduce the rotation of the plate and hence, reduce the stress in the shell due to the rotation of the baseplate.

In summary, the approximate closed form solution confirms the accuracy of the finite element analysis in the baseplate region.

3.4.4.3.1.3 Elastic Stability and Yielding of the MPC Basket under Compression Loads (Load Case F3 in Table 3.1.3)

This load case corresponds to the scenario wherein the loaded MPC is postulated to drop causing a compression state in the fuel basket panels.

a. Elastic Stability

Following the provisions of Appendix F of the ASME Code [3.4.3] for stability analysis of Subsection NG structures, (F1331.5(a)(1)), a comprehensive buckling analysis is performed using ANSYS. For this analysis, ANSYS's large deformation capabilities are used. This feature allows ANSYS to account for large nodal rotations in the fuel basket, which are characteristic of column buckling. The interaction between compressive and lateral loading, caused by the deformation, is included in a rigorous manner. The finite element model used for the large deflection analysis of the basket is identical to the model described in Subsection 3.4.4.3.1.1 used for the fuel basket stress analysis. The large deflection option is "turned on" so that equilibrium equations for each load increment are computed based on the current deformed shape. Subsequent to the large deformation analysis, the individual basket panel that is most susceptible to buckling failure is identified by a review of the results. The lateral displacement of a node located at the mid-span of the panel is measured for the range of impact decelerations. The buckling or collapse load is defined as the impact deceleration for which a slight increase in its magnitude results in a disproportionate increase in the lateral displacement. The most critical element is a vertically oriented panel that is subject to a compressive load together with bending moments from adjacent connected lateral basket panels.

The stability requirement for the MPC fuel basket under lateral loading is satisfied if two-thirds of the collapse deceleration load is greater than the design basis horizontal acceleration (Table 3.1.2). Figures 3.4.27 through 3.4.32 are plots of the local lateral displacement versus impact deceleration for the most limiting basket panel. It should be noted that the displacements in Figures 3.4.27 through 3.4.31 are expressed in $1x10^{-1}$ inch and Figure 3.4.32 is expressed in 1×10^{-2} inch. The plots clearly show that the large deflection collapse load of the MPC fuel basket is greater than 1.5 times the inertia load corresponding to the design basis deceleration for all baskets in all orientations. Thus, the requirements of Appendix F are met for lateral deceleration loading under Subsection NG stress limit s for faulted conditions.

An alternative solution for the stability of the fuel basket panel is obtained using the methodology espoused in NUREG/CR-6322 [3.4.12]. In particular, we consider the fuel basket panels as wide plates in accordance with Section 5 of NUREG/CR-6322. We use eq.(19) in that section with the "K" factor set to the value appropriate to a clamped panel. Material properties are selected corresponding to a metal temperature of 500 degrees F which bounds computed metal temperatures at the periphery of the basket. The critical buckling stress is

$$\sigma_{cr} = \left(\pi/K\right)^2 \frac{E}{12\left(1-\nu^2\right)}\left(\frac{h}{a}\right)^2$$

where h is the panel thickness, a is the unsupported panel length, E is the Young's Modulus of Alloy X at 500 degrees F, ν is Poisson's Ratio, and K=0.65 (per Figure 6 of NUREG/CR-6322).

The MPC-24 has the smallest h/a ratio; the results of the finite element stress analyses under design basis deceleration load show that this basket is subject to the highest compressive load in the panel. Therefore, the critical buckling load is computed using the geometry of the MPC-24. The following table shows the results from the finite element stress analysis and from the stability calculation.

Panel Buckling Results From NUREG/CR-6322			
Item	Finite Element Stress (ksi)	Critical Buckling Stress (ksi)	Factor of Safety
Stress	13.717	49.22	3.588

For a stainless steel member under an accident condition load, the recommended safety factor is 2.12. We see that the calculated safety factor exceeds this value; therefore, we have independently confirmed the stability predictions of the large deflection analysis based on classical plate stability analysis by employing a simplifie method.

Stability of the basket panels, under longitudinal deceleration loading (Load Cases F3.a in Table 3.1.3), is demonstrated in the following manner. From Table 3.2.1 we have the weight of each fuel basket (including sheathing and Boral). The metal areas of the basket bearing on the MPC baseplate can be computed from the drawings in Section 1.5. Dividing weight by area and multiplying by the design basis deceleration from Table 3.1.2 gives the following results.

Fuel Basket Compressive Stress For End Drop (Load Case F3.a)			
Item	Weight (lb.)	Area (sq. inch)	Stress (psi)
MPC-68	15,263	244.9	3,739
MPC-24	17,045	295.7	3,458

To demonstrate that elastic instability in the basket panels is not credible, we compute the flat panel buckling stress, σ_{cr}, (critical stress level at which elastic buckling may occur) using the formula in reference [3.4.8].

For elastic stability, Reference [3.4.8] provides the formula for critical axial stress as

$$\sigma_{cr} = \frac{4\pi^2 E}{12(1-\nu^2)}\left(\frac{T}{W}\right)^2$$

where T is the panel thickness and W is the width of the panel, E is the Young's Modulus at the metal temperature and ν is the metal Poisson's Ratio. The following table summarizes the calculation for the critical buckling stress using the formula given above:

Elastic Stability Result for a Flat Panel	
Reference Temperature	725 degrees F
T (MPC-24)	5/16 inch
W	10.777 inch
E	24,600,000 psi
Critical Axial Stress	74,781 psi

It is noted the critical axial stress is an order of magnitude greater than the computed basket axial stress reported in the foregoing and demonstrates that elastic stability under longitudinal deceleration load is not a concern.

b. Yielding

The safety factor against yielding of the basket under longitudinal compressive stress from a design basis inertial loading is given by

SF = 17,100/3,739 = 4.57

Therefore, plastic deformation of the fuel basket under design basis deceleration is not credible.

3.4.4.3.1.4 MPC Baseplate Analysis (Load Cases E2, E3, E5)

These load cases from Table 3.1.4 consider normal handling, accidental drop, and storage fire.

Minimum safety factors have been reported for Load Case E2 in Subsection 3.4.3 where an evaluation has been performed for stresses under three times the "apparent" load D*. Load Case E3.a provides the limiting accident loading on the baseplate wherein the combined effect of a 60g deceleration plus accident internal pressure is considered. The analysis conservatively neglects support from the overpack during the storage drop accident. During a fire (Load Case E5), the MPC baseplate is subjected to the accident pressure plus dead load, and the fire temperature (which serves only to lower the allowable strengths). All of these analyses are detailed in Appendix 3.I; the results are summarized below:

MPC Baseplate Minimum Safety Factors – Load Cases E3, E5			
Item	Value (ksi)	Allowable (ksi)	Safety Factor
Center of Baseplate – Primary Bending (Load Case E3)	35.93	67.32	1.87
Center of Baseplate – Primary Bending (Load Case E5)	30.46	54.23	1.78

We note from the above that all safety factors are greater than 1.0.

3.4.4.3.1.5 Analysis of the MPC Closure Lid (Load Cases E3, E5)

The closure lid, the closure lid peripheral weld, and the closure ring are examined for maximum stresses developed during the accident drop event and the storage fire.

Analysis of the closure lid for Load Case E1 has been performed previously as part of the finite element analysis of the confinement boundary. Similarly, results for Load Case E2 have been discussed in Subsection 3.4.3 as part of a lifting device. Appendix 3.E contains stress analysis of the MPC top closure lid for Load Cases E3 and E5. The closure lid is modeled as a simply supported plate and is subject to deceleration from an end drop plus appropriate design pressures. Figure 3.E.1 shows the configuration considered. The results for minimum safety factor are reported in the table below:

MPC Top Closure Lid – Minimum Safety Factors – Load Cases E3, E5			
Item	Stress(ksi) or Load(lb.)	Allowable Stress (ksi) or Load Capacity (lb.)	Safety Factor
Lid Bending Stress – Load Case E3.a	4.67	61.05	13.1
Lid Peripheral Weld Load – Load Case E3.a	624,000	1,477,000	2.37
Lid Bending Stress – Load Case E5	1.991	54.225	27.24
Closure Ring Bending Stress – Load Case E1.a†	20.0	28.1	1.41
Closure Ring Weld Load – Load Case E1.a	140,956	632,800	4.49

† The closure ring is only subject to load subsequent to a postulated loss of integrity in the "NB" pressure boundary (such as a leak in the MPC lid that is joined to the shell using a volumetrically examined groove weld). Nevertheless, the stress results are compared to Level A allowables for conservatism. The pressure loading is assumed to correspond to the Design Pressure, which as stated before, bounds both normal and off-normal conditions of storage.

3.4.4.3.1.6 Structural Analysis of the Fuel Support Spacers (Load Cases F2 and F3.a)

Upper and lower fuel support spacers are utilized to position the active fuel region of the spent nuclear fuel within the poisoned region of the fuel basket. It is necessary to ensure that the spacers will continue to maintain their structural integrity after an accident event. Ensuring structural integrity implies that the space

will not buckle under the maximum compressive load, and that the maximum compressive stress will not exceed the compressive strength of the spacer material (Alloy X). Detailed calculations in Appendix 3.J demonstrate that large structural margins in the fuel spacers are available for the entire range of spacer lengths that may be used in HI-STAR 100 applications (for the various acceptable fuel types). For normal and off-normal operation (Level A Service Condition), a 10g deceleration load is applied (to cover the case of transport wherein the railroad longitudinal design basis g level is 10 (see the HI-STAR 100 SAR, Docket 71-9261)). For accident conditions, a 60g deceleration is the applied loading (Level D Service Condition). The following table summarizes the results:

Fuel Spacers – Minimum Safety Factors (Load Cases F2 and F3.a)			
Item	Load (lb.)	Capacity (lb.)	Safety Factor
Axial Load – Level A	16,800	46,446	2.76
Elastic Stability – Level D – Lower Spacer	100,800	1,300,000	12.9
Elastic Stability – Level D – Upper Spacer	100,800	577,000	5.72

3.4.4.3.1.7 Enclosure Vessel Stability (Load Case E1.b, E2, E3, and E5 Table 3.1.4)

The MPC shell is examined for elastic/plastic instability due to external pressure or compressive loads introduced as part of these load cases (design external pressure, normal handling, accident vertical drop, and storage fire). Each load component is examined separately. Design external pressure is applied to the outer surface of the EV shell in the MPC model. The magnitude of the external pressure applied to the model is taken from Table 2.2.1. Analysis of the MPC under the external pressure is provided in Appendix 3.H Analyses are performed using the methodology of ASME Code Case N-284 [3.4.6]. The following stability evaluations are performed in Appendix 3.H for the MPC shell:

a. A 1.15g compressive handling load.

b. Design basis deceleration inertia load.

c. Accident external pressure plus a 1g compressive dead load.

d. Design external pressure plus a 1g compressive dead load.

The interaction equations for the ASME Code Case N-284 are evaluated and shown to give results less than 1.0 for all of the above conditions. The following table summarizes the limiting result from all of the calculations performed.

MPC Shell - Elastic/Plastic Stability (ASME Code Case N-284) – Minimum Safety Factors			
Item	Value	Allowable†	Safety Factor
Load Case E3.a (Yield)	0.698	1.34	1.92
Load Case E5 (Stability Interaction Equation)	0.847	1.0	1.18
Load Case E1.b (Stability Interaction Curve)	0.832	1.0	1.20

† We note that for Load Case E3.a, the yield strength criteria in the Code Case N-284 method govern. In this event, we include the safety factor 1.34, built into the Code Case, in the tabular result in order to obtain the actual safety factor with respect to the yield strength of the material.

The results demonstrate that the MPC shell meets the requirements of Code Case N-284. We note that the stability results presented above are very conservative. The stability analyses in Appendix 3.H carried out for the MPC shell assumed no axial stiffening from the fuel basket supports that run the full length of the shell. An analysis that included the effect of the stiffening (and therefore, recognized the fact that instability will most likely occur between stiffeners) will give increased safety factors for Load Cases E5 and E1.b.

3.4.4.3.2 Overpack Stress Calculations

The structural functions of the overpack are stated in Section 3.1. The analyses presented here demonstrate the ability of components of the HI-STAR 100 overpack to perform their structural functions in the storage mode. Load cases applicable to the structural evaluation of the HI-STAR 100 overpack are compiled in Table 3.1.5.

The purpose of the analyses is to provide the necessary assurance that the design of the HI-STAR 100 overpack precludes unacceptable release of radioactive material, unacceptable radiation levels, or impairment of ready retrievability of the MPC during system deployment and throughout its service life.

In this subsection, stresses and stress intensities in the HI-STAR 100 overpack due to the combined effects of thermal gradients, pressure, and mechanical loads are presented. The results are obtained from a series of finite element analyses on the complete overpack and separate analyses on overpack components.

3.4.4.3.2.1 Finite Element Analysis – Load Cases 01 to 05 in Table 3.1.5

Load Cases 01 and 05 pertain to demonstration of the overpack helium retention boundary as an ASME "NB" component under Design Pressure and Level A Service Condition thermal loading. Other cases pertain to handling, handling accident, and natural phenomena events. To analyze these load cases, a suitable finite element model of the complete overpack is required.

- Description of Finite Element Model

The purpose of the HI-STAR 100 overpack model is to calculate stresses and stress intensities resulting from the loadings defined in Chapter 2 and compiled into load cases in Table 3.1.5 (including Load Cases 01 and 05).

A three-dimensional finite element model of the HI-STAR 100 overpack is used to assess the effects of normal, off normal, and accident condition loads. The overpack is a large structure subject to a variety of complex loads and boundary conditions. The finite element model developed for this analysis allows efficient determination of the stresses in this complex structure.

The finite element model of the overpack is constructed using ANSYS [3.4.1]. This model is duplicated in the HI-STAR 100 SAR (10CFR71) submittal for transport.

For structural analysis purposes, the overpack is assumed to be symmetric about a diametral mid-plane. This assumption is reasonable because the purpose of the model is to investigate global stresses in the model. The model is not intended to resolve effects due to small penetrations that produce peak stresses (which are significant only in cyclic fatigue conditions).

Element plots of the model are shown in four figures (Figures 3.4.17 through 3.4.20). The basic building blocks of the finite element model are 20-node brick (SOLID95), 8-node brick (SOLID45), and 6-node tetrahedron elements (SOLID45). These are 3-D solid elements with 3 degrees of freedom at each node (three linear displacement degrees of freedom). Element densities are increased towards the top and bottom of the model in order to provide increased resolution of the stress fields in those regions.

The top flange/closure plate interface is modeled using linear spring elements (COMBIN14). The concentric seals are not modeled explicitly. The model is not intended to resolve the stress field around the grooves for the seals. The status of joint seal is ascertained by "compression springs" which simulate the O-ring gaskets. Contact between the overpack top flange and closure plate is verified by checking the status of these spring elements. If contact between the closure plate and top flange is maintained (indicated by a compressive load in the "compression springs"), then the integrity of the seal is determined to have been maintained.

The overpack closure bolts are modeled with beam elements (BEAM4). The top of the beam elements represent the bolt head and are connected to the overpack closure plate. The bottom of the elements represents the threaded region of the bolt and is connected to nodes of elements representing the top flange.

The inner shell of the overpack is modeled with two element layers through the thickness of the shell.

Each of the lifting trunnions is modeled as three rigid beam elements (BEAM4) connected to the top flange. The beams extend from the flange and meet at a single node location. Trunnion stress analysis is carried out in Appendix 3.D; the inclusion of the trunnion herein is solely to provide the appropriate offset for handling loads.

The neutron shield material is not a load bearing or supporting component in the finite element model However, the weight of the neutron shield material must be included in the model in order to obtain the prope. inertia loads. The neutron shield material is modeled with SOLID45 elements having a weight density that is specified in Subsection 3.3.2.1. In the model herein, we include the neutron shield material as an element set to ensure that proper accounting of total weight (and accompanying deceleration loads) occurs. Therefore, the neutron shield material must be assigned a Young's Modulus in the model. A value approximately equal to 1% of the Modulus of the steel load carrying components is assigned to the neutron shield material to insure that the neutron shield material serves as a load rather than a structural member in the model.

It is recognized that the layered shells of the overpack are connected to each other and to innermost shell only at their top and bottom extremities. The finite element model must incorporate the potential for separation between the intermediate shells in certain regions under certain loading. Likewise, the intermediate shells cannot interpenetrate each other or the inner shell structure. This is accomplished by radially coupling adjacent intermediate shell nodes over two 60-degree spans. Figure 3.4.33 illustrates the nodal coupling pattern. The intermediate shell nodes that lie in the 60-degree sector between the top and bottom portions of the model remain uncoupled. The intermediate shells, in the uncoupled region, are free to separate from one another as the overpack cross section ovalizes during side impact. This modeling approach ensures that load transfer in a side drop is modeled correctly. With respect to the overpack model, "bottom portion" refers to the 60-degree segment of the model closest to the point of impact. Conversely, "top portion" refers to the 60-degree sector farthest from the point of impact. This nodal coupling arrangement conservatively represents the structural contribution of the intermediate shells. In addition, no axial or circumferential nodal coupling has been used between adjacent intermediate shells. Thus, axial bending stiffness of the composite shell structure is conservatively underestimated.

The two pocket trunnions at the base of the HI-STAR 100 overpack are used for rotating the overpack from horizontal to vertical orientation and are not subjected to a significant loading. During transport, these trunnions are used as restraints against longitudinal and lateral loads imposed by the action of the rail car. In particular, 10CFR71 requires that a 10g longitudinal load be supported by the two pocket trunnions during transport. In the storage mode (Part 72 certification), the pocket trunnions perform a minor structural function.

By the nature of the trunnion attachment, the two pocket trunnions also serve as two locations of support for all intermediate shell levels. In the finite element analysis of the overpack for storage, this local attachment load path which ties all intermediate shells to the overpack baseplate is conservatively neglected. In a worst case scenario under an end drop, the two pocket trunnions provide the only vertical support for the outermost intermediate shell, the neutron absorbing material and the overpack outer enclosure. For this worst case scenario, the total dead weight of these components can be computed using the dimensions given in the drawings and the appropriate weight density. An upper bound value for the total weight supported by the pocket trunnions is 38,000 lb.

Assuming the bounding design basis deceleration for the end drop, the amplified vertical load, "F", on the two pocket trunnions is given by multiplying the supported load by the design basis deceleration due to gravity. The supported load, 38,000 lb., can be confirmed from the Bills of Materials in Section 1.5 and the specified material densities. We have, $F = 38{,}000 \times 60 = 2{,}280{,}000$ lb.

For transport qualification (10CFR71), the two pocket trunnions are required to support ten times the package weight applied in the direction of the axis of the HI-STAR 100, or 2,820,000 lb. (the HI-STAR 100 SAR gives the bounding package weight, including impact limiters, as 282,000 lbs.). Therefore, the worst case storage scenario is not a bounding condition and the neglect of such support in the finite element model for storage load combinations is conservative.

Elements at locations of welds in the modeled components are assumed to have complete connectivity in all directions. Material in the model located at positions where welds exist is assumed to have material properties identical to the base material.

To summarize, the total number of nodes and elements in the overpack model are 11265 and 8642, respectively. The elements used are SOLID45, SOLID95, BEAM4, SHELL63, and COMBIN14.

For all structural analyses, material properties are obtained from the appropriate tables in Section 3.3. Property data for temperatures that are not listed in the material property tables are obtained by linear interpolation. Property values are not extrapolated beyond the limits of the code for any structural analysis.

- Description of Individual Loads and Boundary Conditions

The method of applying each individual load to the overpack model is described in this subsection. The individual loads are listed in Table 2.2.14. A free-body diagram of the overpack corresponding to each individual load is given in Figures 3.4.21 through 3.4.26. In the following discussion, reference to vertical and horizontal orientations are made. Vertical refers to the direction along the cask axis, and horizontal refers to a radial direction.

Quasi-static methods of structural analysis are used. The effects of any dynamic load factors (DLF) are discussed in the final evaluation of safety factors.

(a) Accelerations (Used to Form Load Cases 04.a and 04.b in Table 3.1.5)

Table 3.1.2 provides the bounding values of the accelerations used for design basis structural evaluation. The loading is imposed by amplifying the gravity vector by the design basis deceleration.

Boundary conditions for the model are as follows:

i. End drop - In an end drop, displacement fixities are applied to the model on a cross-section through the top flange that is normal to the drop direction. Figure 3.4.21 shows the free-body diagram for this load event. No reactions or internal body forces are shown.

ii. Side drop - In a side drop, the impacted region of the enclosure shell, radial channels, enclosure panels, and neutron shield located between the overpack and the impacting surface may sustain plastic deformation. Using a linear elastic overpack model, we cannot account for this behavior. For conservatism, the displacement constraints are placed directly at the outermost intermediate shell. That is, it is assumed that the outer radial plates and the outer enclosure have been rendered ineffective. The constraints are applied over an arc of 9 degrees. Figure 3.4.22 shows the free-body diagram. No reaction forces or internal body forces are shown.

(b) Loads on the Overpack from the MPC

Pressures are applied on the inner surfaces of the overpack model to represent loads from the MPC for the drop loads.

i. End drop - For a bottom end drop (Load Case 04.a in Table 3.1.5), the pressure load on the inside surface of the overpack bottom plate is assumed to be uniform and represents the load from the heaviest MPC (Figure 3.4.21). Note that this analysis conservatively assumes that the drop angle is not exactly 90° from the horizontal; attention is focussed on the overpack baseplate subject to the deceleration load from the heaviest MPC (applied as a uniform pressure) without the ameliorating effect of opposing distributed reaction from the impacted surface.

The magnitude of the pressure is the weight of the heaviest fully loaded MPC divided by the area of the faces of the elements over which the pressure is applied. The weight of the heaviest fully loaded MPC is taken from the tables in Section 3.2, and is amplified by the design basis deceleration.

ii. Side drop - The shape and extent of the pressure distribution is determined from the results of the structural analysis of the MPC presented in Subsection 3.4.4.3.1. In the MPC structural analysis, the extent of the support conditions of the MPC shell is determined with contact elements. The overpack is assumed to be a rigid circular surface. Based on the results of the MPC evaluations, the loaded region is taken as 81 degrees (measured from the vertical) and is applied as a sinusoid with maximum value at the line of symmetry.

The MPC load on the overpack model is applied uniformly along the axial length of the inner surface of the model. Figure 3.4.22 shows the overpack loading for the side drop event.

(c) Temperature (Used to Form Load Case 05 in Table 3.1.5)

Based on the results of the thermal evaluation for normal hot environment presented in Chapter 4, a temperature distribution with a bounding gradient is applied to the overpack model. The purpose is to determine the stress intensities that develop in the overpack under the applied thermal load. A plot of the applied temperature distribution as a function of radius is shown in Figure 3.4.2.
The temperature distribution is applied to the ANSYS finite element model at discrete nodes using a parabolic curve fit of the computed distribution. Figure 3.4.23 shows the displacement constraints for the thermal load case.

(d) Internal Pressure (Used to Form Load Cases 01 to 04 in Table 3.1.5)

Design internal pressure is applied to the overpack model. All interior overpack surfaces, including the inner shell, the bottom of the closure plate, and the top of the bottom plate are loaded with pressure. The magnitude of the internal pressure applied to the model is taken from Table 2.2.1. Figure 3.4.24 shows the displacement constraints for this load case.

(e) External Pressure (Used to Form Load Cases 01 to 04 in Table 3.1.5)

Design external pressure is applied to the overpack model. External pressure is applied to the model as a uniform pressure on the outer surface of the model. The magnitude of the external pressure applied to the model is taken from Table 2.2.1. Figure 3.4.25 shows the displacement constraints for this load case.

(f) Dead Weight in Vertical Orientation (Used in Load Cases 02 to 04 in Table 3.1.5)

A pressure load is applied on the top surface of the overpack bottom plate to represent the weight of the MPC. The magnitude of the pressure is the weight of the heaviest fully loaded MPC divided by the area of the faces of the elements over which the pressure is applied. The weight of the heaviest fully loaded MPC is taken from the tables in Section 3.2. The dead weight of the overpack itself is simulated by a 1g acceleration load in the appropriate direction. Figure 3.4.26 shows the displacement constraints for this load case.

(g) Handling Load (Used in Load Case 03 in Table 3.1.5)

As discussed in Section 3.1.2.1.2, a fully loaded HI-STAR 100 System using the lifting trunnions is a governing normal handling event. This load case is performed to determine the effects of normal condition handling loads on the overall overpack structure. This load case is intended to resolve the detailed stress distribution in the top flange in the region of the trunnion, to demonstrate that the ASME Code requirements (Level A Condition limits) are met.

Nodes in the region of the trunnions are fixed in all translational degrees-of- freedom. For additional conservatism, a vertical load amplifier of 2.0 is applied in this case (even though, as discussed in Subsection 3.4.3, the appropriate multiplier for a heavy load lift condition is 1.15).

A pressure load, applied on the top surface of the overpack bottom plate, represents the weight of the MPC. The magnitude of the pressure is the weight of the heaviest fully loaded MPC, amplified by 2.0, divided by

the area of the faces of the elements over which the pressure is applied. Figure 3.4.26 shows the displacement constraints for this load case.

(h) Bolt Pre-load (Used in Load Cases 01-05 in Table 3.1.5)

The overpack closure bolts are torqued to values given in Chapter 8. This torque generates a pre-load in the bolts and stresses in the closure plate and top flange in the region adjacent to the bolts. This load is applied to the overpack model by applying an initial strain to the beam elements representing the bolts.

- Finite Element Analysis Solution Procedure

The analysis procedure is as follows:

1. The stress and deformation field due to each individual load is determined.

2. The results for each individual load are combined in a postprocessor to create each load case. The load cases analyzed are listed in Table 3.1.5. Results are tabulated in Appendix 3.AB

3. The results for each load case are compared to allowables. The calculated values are compared with allowable values in Subsection 3.4.4.4.

3.4.4.3.2.2 Fabrication Stress

The fabrication stresses originate from welding operations to affix the intermediate shells in position. As the molten weld metal solidifies, it shrinks pulling the two parts of the shells together. Adjacent points at the weld location will close together after welding by an amount δ which is a complex function of the root opening, shape of the bevel, type of weld process, etc. The residual stresses generated by the welding process are largely confined to the weld metal and the "heat affected zone". The ASME Code recognizes the presence of residual stresses in the welds, but does not require their calculation. The Code also seeks to minimize fabrication stresses in the welds through controlled weld procedures. Nevertheless, fabrication stresses cannot be eliminated completely. Similarly, Regulatory Guide 3.61 does not require computation of stresses arising from the manufacturing operations

The computation of fabrication stresses, however, is carried out to comply with the provisions of Regulatory Guide 7.8, Article C-15 when the HI-STAR 100 is functioning as a transport cask. The Regulatory Guide requires that "Fabrication and installation stresses in evaluating transportation loadings should be consistent with the joining, forming, fitting, and aligning processes employed during the construction of casks...the phrase fabrication stresses includes the stresses caused by interference fits and the shrinkage of bonded lead shielding during solidification but does not include the residual stresses due to plate formation, welding, etc.".

A literal interpretation of the above-cited Regulatory Guide text exempts the HI-STAR 100 designer from computing the stresses in the containment shell due to welding. However, in the interest of conservatism, it was decided to compute and establish an upper bound on the stresses induced in the containment shell

("helium retention boundary" in the storage mode) and in the intermediate shells due to welding of the intermediate shell layers. Detailed calculations are presented in Appendix 3.L

To calculate the so-called fabrication stresses, we recall that in affixing the intermediate shells to the cask body, the design objective does not call for a definite radial surface pressure between the layers. Rather, the objective is to ensure that the shells are not loosely installed. Fortunately, extensive experience in fabricating multi-layer shells has been acquired by the industry over the past half-century. The technology that was developed and has matured for fabrication in older industries (such as oil and chemical) will be used in HI-STAR 100 fabrication of the multi-layered shells. Mock-up tests on carbon steel coupons indicate that the total shrinkage after welding can range from 0.010" to 0.0625" for the bevel and fit-up geometry in the HI-STAR 100 design drawings. Therefore, the calculations in Appendix 3.L are carried out using the upper bound gap of 0.0625". To bound the computed stresses even further, the inter-layer friction coefficient is set equal to zero. It is intuitively apparent that increasing the friction increases the localized stresses near the "point of pull" (i.e., the weld) while mitigating the stresses elsewhere. Since our object is to maximize the distributed (membrane) stress, the friction coefficient is set equal to zero in the analysis of Appendix 3.L.

The results from the analyses in Appendix 3.L are summarized in the table below:

Fabrication Stresses in Overpack Shells –Minimum Safety Factors (Level A Service Condition at Assembly Temperature)			
Item	Value (ksi)	Allowable (ksi) (Note 3)	Safety Factor
First Intermediate Shell (Note 1)	11.22	52.5	4.68
Fourth Intermediate Shell (Note 1)	7.79	52.5	6.74
Inner Shell Mid Plane (Note 2)	10.6	69.9	6.59
Inner Shell Outer Surface (Note 2)	16.27	69.9	4.30

Notes:

1. The fabrication stress is a tensile circumferential stress.
2. The fabrication stress is a compressive circumferential stress
3. Fabrication stresses are self-limiting and are therefore classified as "secondary" and are compared to 3 times the membrane stress or stress intensity.

The above table leads to the conclusion that the maximum possible values for stresses resulting from the HI-STAR 100 fabrication process are only a fraction of the relevant ASME Code limit.

3.4.4.3.2.3 Structural Analysis of Overpack Closure Bolting (Load Cases 01, 06 and 04.a - Table 3.1.5)

Stresses are developed in the closure bolts due to pre-load, pressure loads, temperature loads, and accident loads. Closure bolts are explored in detail in Reference [3.4.5] that was prepared for analysis of shipping

casks. The method presented is equally valid for storage casks and is considered as an acceptable analysis method by NUREG-1536. The analysis of the overpack closure bolts under normal and accident conditions appropriate for storage is carried out in Appendix 3.F and follows the procedures defined in Reference [3.4.5]. The allowable stresses used for the closure bolts follows that reference.

The following combined load cases are analyzed in Appendix 3.F.

Normal: pressure, temperature, and pre-load loads are included. (Load Case 01 in Table 3.1.5).

Top Closure Puncture: pressure, temperature, pre-load, and 8-in. diameter missile loads are included. (Load Case 06 in Table 3.1.5)

Drop: pressure, temperature, pre-load, and impact loads from a top end drop are included. We note that reference [3.4.5] is for shipping casks and therefore allows for a top end drop. There is no such credible event defined for a storage cask but it provides a bounding case for the HI-STAR 100 closure bolts (Load Case 04.a in Table 3.1.5).

Reference [3.4.5] reports safety factors defined as the calculated stress combination divided by the allowable stress for the load combination. This definition of safety factor is the inverse of the definition consistently used in this FSAR. In summarizing the closure bolt analyses performed in Appendix 3.F, we report results using the safety factor definition of allowable stress divided by calculated stress. The following results for closure lid bolting are obtained from Appendix 3.F.

Overpack Closure Bolt - Minimum Safety Factors	
Combined Load Case	Safety Factor on Bolt Tension
Normal (Load Case 01 in Table 3.1.5)	1.08
Top Closure Puncture (Load Case 06 in Table 3.1.5)	1.39
Drop (Load Case 04.a in Table 3.1.5)	1.30

It is seen from the above table that all safety factors are greater than 1.0.

3.4.4.3.2.4 Structural Analysis of the Overpack Closure Plate (Load Case 04.a in Table 3.5.1)

The simplified analysis given here complements the result from the finite element analysis of the overpack for calculation of stresses in the overpack closure plate.

The loading condition considered here is a bottom end drop where the overpack bottom plate impacts the supporting surface (Load Case 04.a in Table 3.1.5).

The following assumptions apply:

1. Stresses in the closure plate due to bolt pre-load will counteract the downward inertia load; the pre-load is conservatively ignored.
2. The closure plate is assumed to be a simply supported plate, i.e., the rotational fixity projected by the flanged joint is conservatively ignored.
3. The plate is assumed to be loaded with its own weight multiplied by the design basis deceleration from Table 3.1.2.
4. The pressure within the overpack counteracts the amplified self-weight load in a bottom end drop. Internal overpack pressure is conservatively neglected.

The geometry of the model is the same as shown in Figure 3.4.16 for the MPC lid except for the dimension change appropriate to the overpack closure plate. Using Table 24, Case 10 of reference [3.G.1], page 429 (reference is listed in Appendix 3.G), the maximum radial bending stress (σ) in the closure plate due to bending is

$$\sigma = \frac{3qa^2(3+\nu)}{8t^2}$$

where

q = load per unit area $= \frac{a_v W}{\pi a^2}$

W = weight of the plate = 8,000 lb.

a_v = design basis deceleration in an end drop = 60g's

a = radius of the simply supported plate = 38.6875 in.

υ = Poisson's ratio

t = thickness of the closure plate = 6 in.

Therefore,

$$\sigma = \frac{3(3+\nu)W\, a_v}{8\pi t^2}$$

The result is summarized in the table below:

Bending Stress in Overpack Closure Plate – Closed Form Solution (Load Case 04.a)			
Item	Value (ksi)	Allowable (ksi)	Safety Factor
Stress at Center of Plate	5.25	70.0	13.3

The safety factor is much greater than 1.0.

3.4.4.3.2.5 Elastic/Plastic Stability Considerations for the Overpack Inner Shell (Load Cases 02, 03 and 04.a in Table 3.1.5)

Appendix 3.H contains a complete stability analysis of the HI-STAR 100 System. The case of normal handling (Load Case 03 in Table 3.1.5), the accident end drop (Load Case 04.a in Table 3.1.5), and the accident external pressure plus dead load case (Load Case 02 in Table 3.1.5) are evaluated for elastic and plastic stability in accordance with the ASME Code Case N-284 [3.4.6]. All required interaction equation requirements set by [3.4.6] are met. It is shown in Appendix 3.H that yield strength limits rather than instability limits governs the minimum safety factor. Minimum safety factors from Appendix 3.H are summarized in the Table below:

Code Case N-284 Minimum Safety Factors – (Load Cases 02, 03 and 04.a in Table 3.1.5)			
Item	Calculated Interaction Value	Allowable Interaction Value†	Safety Factor against Yield†
Load Case 02 in Table 3.1.5	0.577	1.34	2.32
Load Case 03 in Table 3.1.5	0.613	2.0	3.26
Load Case 04 in Table 3.1.5	0.607	1.34	2.21

† We note that in computing the safety factor against yield for this table, we have included the safety factor implicit in the Code Case N-284 allowable interaction equation. We note also that the safety factors given above from the Code Case analysis are all safety factors against the circumferential or longitudinal stresses reaching the material yield stress. The actual safety factors against instability are larger than the factors reported in the table as can be seen by a perusal of Appendix 3.H. Finally, we note that fabrication stresses have been included in the stability calculations even though these stresses are self-limiting. Therefore, all results corresponding to the calculated stability interaction equations in Appendix 3.H are conservatively high.

3.4.4.3.2.6 Stress Analysis of Enclosure Shell

The overpack enclosure shell and the overpack enclosure return are examined for structural integrity under a bounding internal pressure in Appendix 3.AG. It is shown there that large safety factors exist agains overstress due to an internal pressure developing from off-gassing of the neutron absorber material.

3.4.4.4 Comparison with Allowable Stresses

Consistent with the formatting guidelines of Reg. Guide 3.61, calculated stresses and stress intensities from the finite element and classical elasticity evaluations are compared with the allowable stresses and stress intensities defined in Subsection 3.1.2.2 per the applicable service conditions and the ASME Code relevant for the component. Safety factors for those components that are identified as lifting devices have been reported in Subsection 3.4.3.

3.4.4.4.1 MPC Fuel Basket and Enclosure Vessel

It is recalled that the stress analyses for the load cases applicable to the fuel basket and the enclosure vessel (EV) (that together constitute the Multi-Purpose Canister) are stated in Tables 3.1.3 and 3.1.4, respectively. All detailed analyses, including finite element model details and the necessary explanations to collate and interpret the voluminous numerical results are contained in a series of appendices to this chapter. These appendices are identified in Subsection 3.6.3 and in Tables 3.1.3 and 3.1.4 for ease of reference. Summaries of results for the load cases pertinent to the fuel basket and the enclosure vessel (EV) are provided in Tables 3.4.7-3.4.9 wherein the source appendices containing detailed results are also identified. To further facilitate perusal of results, another level of summarization is performed in Tables 3.4.3-3.4.4 where the global minima of safety factor for each load case are presented. The following elements of information are relevant in ascertaining the safety factors under the various load cases presented in the tables.

- In the interest of simplification of presentation and conservatism, the total stress intensities under mechanical loading are considered to be of the primary genre' even though, strictly speaking, a portion can be categorized as secondary (that have much higher stress limits).
- In load cases involving accident events, the deceleration loads also produce internal dynamic effects, qualified as dynamic load factors (DLF). These DLF's, which depend on the duration of impact and the fundamental frequency of the internal component (e.g. the fuel basket panel) are computed in Appendix 3.X using input data from Appendix 3.A.The factors of safety presented in the above mentioned summary tables do not include the DLF's. Therefore, the tabulated factors of safety should be compared against the applicable DLF to insure that a positive design margin exists for a given load case.

The MPC stress distributions that correspond to the worst case for each MPC are provided in Figures 3.4.34 and 3.4.36. The stresses appear as colored bars where the height is proportional to the magnitude of the stress and the width equals the element length. The figures also include the design temperature of the component and the allowable stress intensity taken from Table 3.1.17 for the Level D condition of primary membrane plus bending stress. We note that for the MPC-68, the worst case is in the basket support structure.

A perusal of the results for Tables 3.4.3 and 3.4.4 under different load combinations for the fuel basket and the enclosure vessel reveals that all factors of safety are above 1.0 even if we use the most conservative value for dynamic amplification factor. The relatively modest factor of safety in the fuel basket under side drop events (Load Case F3.b and F3.c) in Table 3.4.3 warrants further explanation.

The wall thickness of the storage cells, which is by far the most significant variable in the fuel basket's structural strength, is significantly greater in the HI-STAR 100 MPCs than in comparable fuel baskets licensed in the past. For example, the cell wall thickness in the TN-32 basket (Docket No. 72-1021, M-56), is 0.1 inch and that in the NAC-STC basket (Docket No. 71-7235) is 0.048 inch. In contrast, the cell wall thickness in the MPC-24 is 0.3125 inch. In spite of their relatively high flexural rigidities, computed margins in the HI-STAR 100 fuel baskets are rather modest. This is because of some assumptions in the analysis which lead to an overstatement of the state of stress in the fuel basket. For example:

i. The section properties of longitudinal fillet welds that attach contiguous cell walls to each other are completely neglected in the finite element model (Figure 3.4.7). The fillet welds strengthen the cell wall section modulus at the very locations where maximum stresses develop.

ii. The radial gaps at the fuel basket-MPC shell and at the MPC shell-overpack interface are explicitly modeled. As the applied loading is incrementally increased, the MPC shell and fuel basket deform until a "rigid" backing surface of the overpack is contacted, making further unlimited deformation under lateral loading impossible. Therefore, some portion of the fuel basket and enclosure vessel (EV) stress has the characteristics of secondary stresses (which by definition, are self-limited by deformation in the structure to achieve compatibility). For conservativeness in the incremental analysis, we make no distinction between deformation controlled (secondary) stress and load controlled (primary) stress in the stress categorization. We treat all stresses, regardless of their origin, as primary stresses. Such a conservative interpretation of the Code has a direct (adverse) effect on the computed safety factors.

The above remarks can be illustrated simply by a simple closed-form bounding calculation. If all deformation necessary to close the gaps is eliminated from consideration, then the capacity of the fuel basket cell wall under loads which induce primary bending stress can be ascertained by considering a clamped beam (cell wall) subject to a lateral pressure representing the amplified weight of fuel assembly plus self-weight of the cell wall (e.g., see Figure 3.4.12).

Using the cell wall thickness and unsupported length for the MPC-24, for example, the fixed edge bending stress is computed as approximately 578 psi (using the actual fuel weights and cell wall weights, an unsupported length of 10.777", and a wall thickness of 0.3125")). This implies a safety factor of 1.60 for a Level D event (for a 60g deceleration, SF = 55400/(578 x 60) = 1.60) where the allowable bending stress intensity for Alloy X at 725°F (Table 3.1.16) has been used. The above scoping calculation demonstrates that the inherent safety margin under accident loading is considerably greater than is implied by the result in Table 3.4.9 (SF=1.17) for the MPC-24. Similar conclusions can be reached for the MPC-68 by performing scoping calculations in the manner just carried out.

iii. The SNF inertia loading on the cell panels is simulated by a uniform pressure, which is a most conservative approach for incorporating the SNF/cell wall structure interaction.

The above assumptions act to depress the computed values of factors of safety in the fuel basket finite element analysis and render conservative results.

As stated earlier, the reported values do not include the effect of dynamic load amplifiers. As noted in Appendices 3.A and 3.X, the duration of impact and the predominant natural frequency of the basket panels under lateral drop events, result in dynamic load factors (DLF) below 1.1. Therefore, since all reported factors of safety for the fuel basket panels (based on stress analysis) are greater than the DLF, the MPC fuel basket is structurally adequate for its intended functions during and after a lateral drop event.

Tables 3.4.7 and 3.4.8 report stress intensities and safety factors for the confinement boundary subject to internal pressure alone and internal pressure plus the normal operating condition temperature with the most severe thermal gradient. The final values for safety factors in the various locations of the confinement boundary provide assurance that the MPC enclosure vessel is a robust pressure vessel.

3.4.4.4.2 Overpack

3.4.4.4.2.1 Discussion

The overpack is subject to the load cases listed in Table 3.1.5. Results from the series of finite element analyses are reported in Appendix 3.AB and safety factors summarized in Table 3.4.10. In order to identify and to locate appropriate regions with limiting safety factors, we note that Appendix 3.AB reports the results for each load case at a select set of nodes identified as "stress report locations". Appendix 3.T defines these node locations in the overpack finite element model that are considered stress report locations. Appendix 3.T also includes tables to convert node numbers to stress report location and stress report locations to node numbers.

Figures 3.4.37 through 3.4.42 identify the locations of minimum safety margin for all overpack load combinations.

For any load case associated with a Level D Service Condition (accident event), the results listed in Appendix 3.AB report locations only where primary stresses predominate. However, in the interest of conservatism, the stress intensity reported at these locations does not separate out any secondary components. Every value is placed in the primary membrane or primary bending category, even though many locations clearly involve non-primary bending components. This simplification in stress intensity tabulation imputes considerable additional safety margin to the processed results, which is not explicitly recognized in the results presented herein.

The following text is a brief description of how the results are presented for evaluation:

- Appendix 3.AB reports the results of analyses in a series of tables for individual applied loads and for combined load cases. The stress intensity results are sorted by safety factor in ascending order.

- The extensive body of results in Appendix 3.AB is summarized in Table 3.10 wherein the minimum safety factor for different components of the overpack for each of the load cases is presented.

- Table 3.4.6 presents results of calculation of the safety factors to include "fabrication stresses" where appropriate. Table 3.4.6 summarizes safety factors, based on limits for primary plus secondary stresses, and reports the limiting safety factors for the overpack shells for events subject to Level A Service Conditions. Fabrication stresses are not included for any load case involving accident conditions since secondary stresses need not be considered for Level D Service Conditions. Fabrication stress, reported in Subsection 3.4.4.3.2.2, is "added" in absolute value to finite element stress intensity or stress results. This conservatively produces modified stress intensity or stress that is used to compute modified safety factors.

- Finally, Table 3.4.5 summarizes the minimum values of safety factors (global minima) for the overpack components.

The modifications summarized in Table 3.4.6 are briefly discussed below:

Case 01 (Pressure) – Table 3.AB.1 reports results in tabular form for Load Case 01 in Table 3.1.5. Safety factors are summarized in Table.3.4.10 prior to inclusion of fabrication stress. Table 3.4.6 shows modified safety factors that include fabrication stress. The pressure stresses result in tensile longitudinal and circumferential stresses in the inner shell and in the intermediate shells. The fabrication stress dominates the stress state in the inner and intermediate shells but comparison with the allowable values is considers a primary plus secondary stress state.

Case 03 (Normal Handling): Table 3.AB.4 reports results in tabular form for Load Case 03 in Table 3.1.5. Safety factors are summarized in Table.3.4.10 prior to inclusion of fabrication stress. Table 3.4.6 shows modified safety factors that conservatively include fabrication stress but compute safety factors considering primary plus secondary stress allowables.

Case 05 (Thermal Load) - Table 3.AB.7 reports results for Load Case 05 in Table 3.1.5. Safety factors are summarized in Table.3.4.10 prior to inclusion of fabrication stress. Table 3.4.6 shows modified safety factors that include the effect of fabrication stress in a conservative manner. Safety factors are based on allowable strengths for primary plus secondary stresses since thermal stress is a secondary stress.

3.4.4.4.3 Result Summary for the Heat Condition

- Stress Results from Overall Finite Element Models of the MPC and Overpack

Tables 3.4.7 to 3.4.10 summarize minimum safety factors from load cases analyzed using the finite element models of the MPC fuel basket plus canister and the overpack described in Subsections 3.4.4.3.1.1 and 3.4.4.3.2. All safety factors are greater than 1.0 and are greater than any credible dynamic amplifier for the

location. Table 3.4.6 provides a summary table that includes the effect of fabrication stress on safety factors for the intermediate and inner shells of the overpack. Table 3.4.6 reports safety factors based on primary plus secondary allowable strengths.

- Status of Lid Bolts and Seals on the Overpack

The finite element analysis for the overpack provides results at the lid-to top flange interface. Appendix 3.AB presents results for seals and lid bolts. The output results for each load combination indicate that all seal springs remain closed under load indicating that the sealworthiness of the bolted joint will not be breached.

Each load combination reported in Appendix 3.AB lists the total compressive force on the closure plate-overpack interface as well as the total tangential force (labeled as "friction force" in the tables). If the ratio "total friction force/total compressive force" is formed for each set of results, the maximum value of the ratio is 0.268. There will be no slip of the closure plate relative to the overpack if the interface coefficient of friction is greater than the value given above. Note that Mark's Handbook for Mechanical Engineers [3.4.9] in Table 3.2.1 shows μ = 0.74-0.79 for clean and dry steel on steel surfaces. It is concluded that there is no propensity for relative movement.

Based on the results of the finite element analysis, the following conclusions are made.

No bolt overstress is indicated under any loading event. Note that this confirms the results of closure bolt analyses performed in Appendix 3.F.

The closure plate seals do not unload under any load combination; therefore, the seals continue to perform their function.

- Stress and Stability Results from Miscellaneous Component Analyses in Subsection 3.4.4.3

Tables 3.4.11 to 3.4.19 repeats summary results from additional analyses described and reported on in Subsection 3.4.4.3 for components of the MPC and the overpack. The tables have been listed within the text of Subsection 3.4.4.3 and are reproduced in this subsection in accordance with the requirements of Regulatory Guide 3.61. The tables report comparisons of calculated values with allowable values for both stress and stability and represent a compilation of analyses detailed in appendices that form an integral part of this chapter.

- Summary of Minimum Safety Factors

Tables 3.4.3 through 3.4.5 present a concise summary of safety factors for the fuel basket, the enclosure vessel, and the overpack, respectively. Locations in this FSAR where detailed information on each summary value exists is also identified in these tables.

Based on the results of all analyses, with results presented or summarized in the text, in tabular form, and in appendices, we close by concluding that:

i. All safety factors reported in the text, summary tables, and in appendices are greater than 1.0.

ii. There is no restraint of free thermal expansion between component parts of the HI-STAR 100 System.

3.4.5 Cold

A discussion of the resistance to failure due to brittle fracture is provided in Subsection 3.1.2.3.

The value of the ambient temperature has two principal effects on the HI-STAR 100 storage system, namely:

i. The steady-state temperature of all material points in the cask system will go up or down by the amount of change in the ambient temperature.

ii. As the ambient temperature drops, the absolute temperature of the contained helium will drop accordingly, producing a proportional reduction in the internal pressure in accordance with the Ideal Gas Law.

In other words, the temperature gradients in the cask system under steady-state conditions, will remain the same regardless of the value of the ambient temperature. The internal pressure, on the other hand, will decline with the lowering of the ambient temperature. Since the stresses under normal storage condition arise principally from pressure and thermal gradients, it follows that the stress field in the MPC under -40°F ambient would be smaller than the "heat" condition of storage, treated in the preceding subsection. Therefore, th stress margins computed in Section 3.4.4 can be conservatively assumed to apply to the "cold" condition as well. Appendix 3.AE demonstrates that the overpack closure bolts will retain the helium seal under the cold ambient conditions.

Under the 80°F ambient temperature and the maximum fuel decay heat load (normal heat condition of storage), the thermal analysis in Chapter 4 reports the resultant component temperatures. These temperatures were than used in Appendices 3.U and 3.W to demonstrate that there was no restraint of free thermal expansion for the MPC-24 and MPC-68 in the HI-STAR overpack. The results from these appendices have been presented in Subsection 3.4.4.2.1. Under the postulated cold ambient temperature of -40°F the component temperatures will decrease by 80°F minus -40°F or 120°F. Thermal expansion is calculated from the product of the coefficient of thermal expansion, α, and the change in temperature, ΔT. Since the changes in temperature in each component would decrease by 120°F, the resultant thermal expansion would also decrease. This is coupled with the fact that the coefficient of thermal expansion for carbon steel and stainless steel decreases as the temperatures are decreased. Therefore, if the analysis performed in Appendicies 3.U and 3.W demonstrate that there is no restraint of thermal expansion, analysis performed at component temperatures 120°F less (to account for the cold ambient temperature, -40°F) would also show that there is no constraint of thermal expansion. That is, the operational clearances predicted in Appendices 3.U and 3.W are a conservative lower bound on the clearances with the ambient temperature corresponding to extreme cold conditions.

Finally, the HI-STAR 100 System is engineered to withstand "cold" temperatures (-40°F) without impairment of its storage function.

The structural material used in the MPC (Alloy X) and the Helium Retention Boundary is recognized to be completely immune from brittle fracture in the ASME Codes. As no liquids are included in the HI-STAR 100 overpack design, loads due to expansion of freezing liquids are not considered.

3.4.6 HI-STAR 100 Kinematic Stability under Flood Condition (Load Case A in Table 3.1.1)

The flood condition subjects the HI-STAR 100 System to external pressure, together with a horizontal load due to water velocity.

The design external pressure bounds any credible pressure due to complete submergence during flooding (see Subsection 3.1.2.1.1.3 and Appendix 3.H). The use of such a large external design pressure is mandated by 10CFR71 considerations.

Horizontal loads on the HI-STAR 100 System may, however, cause sliding (translation), or rotation (tipping); this is addressed below, where it is shown that the maximum permitted flood water velocity is limited by sliding of the cask.

Rotation of the HI-STAR 100 System due to motion of the flood water is analyzed by assuming that the overpack is pinned at the outer edge of the baseplate opposite the water flow. The pinned edge does not permit sliding.

The water velocity associated with flood produces a horizontal drag force, which may act to cause sliding or tip-over. In accordance with the provisions of ANSI/ANS 57.9, the acceptable upper bound flood velocity, V, must provide a minimum factor of safety of 1.1 against overturning and sliding. For HI-STAR 100, the design basis flood velocity is 13 feet/sec.

The overturning horizontal force, F, due to hydraulic drag, is given by the classical formula:

$$F = Cd\ A\ V^*$$

where:

V^* is the velocity head = $\frac{\rho V^2}{2g}$; (ρ is water weight density, g is acceleration due to gravity, and V is the crossflow water velocity).

A: projected area of the HI-STAR 100 cylinder perpendicular to the fluid velocity vector.

Cd: drag coefficient

The value of Cd for flow past a cylinder at Reynolds number above 5E+05 is given as 0.5 in the literature (viz. Hoerner, Fluid Dynamics, 1965).

The drag force tending to cause HI-STAR 100's sliding is opposed by the friction force, which is given by

$$F_f = \mu K W$$

where:

μ = limiting value of the friction coefficient at the HI-STAR 100/ISFSI pad interface (conservatively taken as 0.25, although literature citations give somewhat higher values).

K = buoyancy coefficient

W= Minimum weight of HI-STAR 100 with an empty MPC

Sliding Factor of Safety

The factor of safety against sliding, SF_l, is given by

$$SF_l = \frac{F_f}{F} = \frac{\mu KW}{Cd\ A\ V^*}$$

It is apparent from the above equation that SF_l will be minimized if the lower bound weight of HI-STAR 100 is used in the above equation.

As stated previously, $\mu = 0.25$, Cd = 0.5.

V^* corresponding to 13 ft./sec. water velocity (see Chapter 2 Design Criterion) is 163.75 lb. per sq. ft.

A = length × diameter of HI-STAR 100 = 96" x 203"/144 sq. in./sq.ft. = 135.33 sq. ft.

W = 189,000 lbs. (Table 3.2.1)

K = buoyancy factor = (1-weight of water displaced by HI-STAR 100/W) =0.719

Therefore, the drag force is

$$F_f = \mu K W = 33{,}973 \text{ lb.}$$

Substituting in the above formula for SF_l, we have

$$SF_l = 3.07 > 1.1 \text{ (required)}$$

Overturning Factor of Safety

For determining the margin of safety against overturning SF_2, the cask is assumed to pivot about a fixed point located at the outer edge of the contact circle at the interface between HI-STAR 100 and the ISFSI. The overturning moment due to a force F_T applied at height H^* is balanced by a restoring moment from the reaction to the cask buoyant force KW acting at radius D/2.

$$F_T H^* = KW \frac{D}{2}$$

or

$$F_T = \frac{K W D}{2 H^*}$$

W is the minimum weight of the storage overpack with an empty MPC.

We have,

W = 189,000 lb. (Table 3.2.1)

H^* = 102" (maximum height of mass center per Table 3.2.2)

D = 83.25" (Holtec Drawing 1397, Sheet 1)

K = 0.719 (calculated)

so that

F_T = 55,456 lb.

F_T is the horizontal drag force at incipient tip-over.

F = Cd A V^* = 11,080 lbs. (drag force at 13 feet/sec)

The safety factor against overturning, SF_2, is given by

$$SF_2 = \frac{F_T}{F} = 5.01 > 1.1 \text{ (required)}$$

3.4.7 Seismic Event on HI-STAR 100 (Load Case C in Table 3.1.1)

3.4.7.1 Stability

The HI-STAR 100 System plus its contents are subject to the design basis seismic event consisting of three orthogonal statistically independent acceleration time-histories (orthogonal components). The HI-STAR 100 System can be considered as a rigid body subject to a net horizontal inertia force and a vertical inertia force for the purpose of performing a conservative analysis to determine the maximum ZPA that will not cause incipient tipping. The vertical seismic loading is conservatively assumed to act in the most unfavorable direction (upwards) at the same instant. The vertical seismic load is assumed to be equal to or less than the net horizontal load with ϵ being the ratio of vertical component to one of the horizontal components. Define D as the contact patch diameter, and H_{CG} as the height of the centroid of an empty HI-STAR 100 System (no fuel).

D = 83.25" (Drawing 1397, Sheet 1)

Tables 3.2.1 and 3.2.2 give HI-STAR 100 weight data and center-of-gravity heights.

The weights and center-of-gravity heights are reproduced here for calculation of the composite center of gravity height of the overpack together with an empty MPC.

Weight (pounds)	H of C.G. Height (Inches)
Overpack - W_o = 153,710	99.7
MPC-24 - W_{24} = 39,667	108.9 + 6 = 114.9†
MPC-68 - W_{68} = 39,641	109.9 + 6 = 115.9†

† MPC centroids reported in Section 3.2 are measured from the base of the MPC.

The composite centroid, H_{CG}, is determined from the equation

$$H_{cg} = \frac{W_o \times 99.7 + W_{MPC} \times H}{W_o + W_{MPC}}$$

Performing the calculations for all of the MPC's gives the following results:

	H_{CG} (inches)
MPC-24 with overpack	102.8
MPC-68 with overpack	103.0

A conservative stability limit is achieved by using the largest value of H_{CG} (call it H) from above or from Table 3.2.2. Because the HI-STAR 100 System is a radially symmetric structure, the two horizontal seismic accelerations can be combined vectorially and applied as an overturning force at the C.G. of the cask. The overturning static moment in each of the two horizontal directions is "WGH_{CG}" where W is the total system weight, G is the zero period acceleration seismic amplifier so that WG is the inertia load due to horizontal seismic loading. The overturning moment is balanced by a vertical reaction force, acting at the outermost contact patch radial location r = D/2. At many sites, the vertical seismic acceleration is specified as a fraction of the horizontal acceleration. Let us assume that the vertical acceleration is ϵ times G. The resistive moment is minimized when the vertical acceleration tends to reduce the apparent weight of the cask. At that instant, the moment that resists "incipient tipping" is:

$$W(1-\epsilon G)\,r$$

where the vertical seismic amplifier is ϵG ($|\epsilon| \le 1$).

Equating the two moments to ensure equilibrium of moments yields

$$\sqrt{(WG)^2+(WG)^2}\,H = W(1-\epsilon G)\,r$$

$$\sqrt{2}\,WGH = W(1-\epsilon G)\,r$$

or, after canceling W and solving for G

$$G = \frac{1}{\sqrt{2}\,\frac{H}{r}+\epsilon}$$

The values of r and H for the HI-STAR 100 are r = 41.625", H = 103", which yields the following results for different values of ϵ

Acceptable Horizontal g-Level in Each of Two Orthogonal Directions	Vertical Acceleration Multiplier ϵ	Vectorial Sum of Acceptable Horizontal Accelerations (g)
0.222	1.0	0.314
0.235	0.75	0.332
0.240	0.667	0.339
0.250	0.50	0.354

The tabular results above define the envelope g-levels from the resultant inertia load from two horizontal seismic events to ensure against incipient tipping. The acceptable g-level is increased as the ratio of vertical

zero period accelerations to net horizontal g-level decreases. Additionally, in case of a 2-D earthquake plant. i.e., one horizontal and one vertical seismic acceleration, the acceptable g-level will correspond to the last tw columns in the above table.

3.4.7.2 Primary Stresses in the HI-STAR 100 Structure

A simplified calculation to assess the flexural bending stress in the HI-STAR 100 structure under the limiting seismic event (at which tipping is incipient) is presented in the following:

From the acceptable acceleration table presented above, the maximum horizontal acceleration is 0.354g. The corresponding lateral seismic load, F, is given by F = 0.354 W. This load will be maximized if the upper bound HI-STAR 100 weight (W = 245,000 lbs., from Table 3.2.4) is used. Accordingly, F = (0.354) (245,000) = 86,730 lbs.

The moment, M, at the base of the HI-STAR 100 due to this lateral force is given by

$$M = \frac{F H}{2}$$

where H = height of HI-STAR 100 (taken conservatively as 204 inches)

The flexural stress, σ, is conservatively given by the ratio of the moment M to the section modulus of the inner steel shell structure, z, which is computed to be 9,644 $in.^3$.

Therefore,

$$\sigma = \frac{(86,730)\,(204)}{(9,644)\,(2)} = 917 \text{ psi}$$

We note that the contribution from any of the intermediate shells has been neglected in the above calculation.

The maximum axial stress in the overpack shell will be reached in the "compressive" side where the flexural bending stress algebraically sums with the direct compression stress τ from vertical compression.

From the acceleration table the vertical seismic accelerations corresponding to the net 0.354g horizontal acceleration is 0.125g.

Therefore, using the maximum overpack weight

$$\tau = \frac{(245{,}000)\,(1.125)}{560} = 492 \text{ psi}$$

where 560 sq. inch is the metal area (cross section) of the inner shell in the HI-STAR 100 overpack.

The total axial stress, therefore, is

$$\sigma_T = 917 + 492 = 1{,}409 \text{ psi}$$

Per Table 3.1.7, the allowable membrane stress intensity for a Level D event is 48,200 psi at 400°F. Therefore, a factor of safety is calculated as

$$SF = \frac{48{,}200}{1{,}409} = 34.2$$

Sliding Analysis

An assessment of sliding of the HI-STAR 100 System on the ISFSI pad during a postulated limiting seismic event is performed using a one-dimensional "slider block on friction supported surface" model. The HI-STAR 100 is simulated as a rigid block of mass *m* placed on a surface which is subject to a sinusoidal acceleration of amplitude *a*. The apparent mass of the block is assumed to be reduced by a factor α to recognize the contribution of vertical acceleration in the most adverse manner (vertical acceleration acts to reduce the downward force on the friction interface). The equation of motion for such a "slider block" is given by

$$m\ddot{x} = R - m\,a\,\sin\omega t$$

where:

$\ddot{x}$: relative acceleration of the slider block (double dot denotes second derivative of displacement x in time)

a: amplitude of the sinusoidal acceleration input

ω: frequency of the seismic input motion (radians/sec)

t: time coordinate

R is the resistive Coulomb friction force which can reach a maximum value of μ (αmg) (μ = coefficient of friction) and which always acts in the direction of opposite to $\dot{x}(t)$.

Solution of the above equation can be obtained by standard numerical integration for specified values of m, a, ω and α. The following input values are used.

a = 0.354g

α = 0.875 = 1 - vertical acceleration - (vertical acceleration is 0.125g for net horizontal acceleration equal to 0.354 from the acceleration table provided in the foregoing)

m = 245,000 lbs/g

μ = 0.25

For establishing the appropriate value of ω, reference is made to the USAEC publication TID-7024, "Nuclear Reactor and Earthquakes", page 35, 1963, which states that the significant energy of all seismic events in the U.S. essentially lies in the range of 0.4 to 10 Hz. Taking the mid-point value

$\omega = (2\pi)\ (0.5)\ (0.4+10) = 32.7$ rad/sec.

The numerical solution of the above equation yields the maximum displacement of the slider block x_{max} as 0.047 inches, which is negligible compared to the spacing between casks.

Calculations performed at lower values of ω show an increase in x_{max} with reducing ω. At 1 Hz, for example, x_{max} = 1.236 inches. It is apparent from the above that there is a large margin of safety against inter-module collision within the HI-STAR 100 arrays at an ISFSI, where the minimum installed spacing is approximately 4 feet (Table 1.4.1).

3.4.8 Tornado Wind and Missile Impact (Load Case B in Table 3.1.1 and Load Case 06 in Table 3.1.5)

During a tornado event, the HI-STAR 100 System is conservatively assumed to be subjected to a constant wind force. It is also subject to impacts by postulated missiles. The maximum wind speed is specified in Table 2.2.4 and the three missiles, designated as large, intermediate, and small, are described in Table 2.2.5.

The post impact response of the HI-STAR 100 System is required to assess stability.

Appendix 3.C contains results for the post-impact response of the HI-STAR 100 where it is demonstrated there that the combination of tornado missile plus either steady tornado wind or instantaneous tornado pressure drop causes a rotation of the HI-STAR 100 to a maximum angle of inclination 18.23 degrees from vertical. This is less than the angle required to overturn the cask. The appropriate value for the drag coefficient used in the computation of the lateral force on the overpack from tornado wind is justified in Appendix 3.C

Appendix 3.C computes the maximum force acting on the projected area of the cask to be

F = 26,380 lbs.

This is bounded by the seismic overturning force computed in Section 3.4.7. Therefore, the overpack stress analysis performed in Section 3.4.7 remains governing.

The penetration potential of the missile strikes (Load Case 06 in Table 3.1.5) is examined in Appendix 3.G. It is shown in Appendix 3.G that there will be no penetration of the intermediate shells surrounding the inner shell of the overpack or penetration of the top closure plate. Therefore, there will be no radiological release associated with any missile strikes during a tornado. The following results summarize the work in Appendix 3.G.

a. The small missile will dent any surface it impacts, but no significant puncture force is generated.

b. The following table summarizes the denting and penetration analysis performed for the intermediate missile in Appendix 3.G. Denting is used to connote a local deformation mode encompassing material beyond the impacting missile envelope, while penetration is used to indicate a plug type penetration mechanism involving only the target material immediately under the impacting missile.

Intermediate Missile Strike – Denting and Penetration		
Location	Denting (in.)	Penetration
Outer Enclosure Shell	2.77	Yes (> 0.5 in.)
Intermediate shells	2.81	No (< 8.5 in.)
Closure plate	3.00	No (< 6 in.)

Since the intermediate missile generates a large puncture force for a short duration, the effect of this puncture force on the overpack closure bolts is examined in Appendix 3.F.

The primary stresses that arise due to an intermediate missile strike on the side of the overpack and in the center of the overpack top lid are also determined in Appendix 3.G. It is demonstrated there that Level D stress limits are not exceeded in either the side shell or the top lid. The safety factor in the overpack inner shell, considered as a cantilever beam under tip load, is computed, as is the safety factor in the top lid, considered as a centrally loaded plate. The applied load, in each case, is the missile impact load. A summary of the results is given in the table below:

HI-STAR 100 Missile Impact - Global Stress Results (Load Case 06 in Table 3.1.5)			
Item	Value (ksi)	Allowable (ksi)	Safety Factor
Inner Shell - Side Strike	12.6	48.2	3.83
Intermediate Shell – Side Strike -	14.3	39.1	2.73
Top Lid - (End Strike)	48.45	64.6.	1.33

The above summary table does not include the circumferential fabrication stress since these have been designated as self-limiting, and therefore fall into the category of a secondary stress which need not be included in a Level D stress evaluation.

3.4.9 Non-Mechanistic Tip-over, Side and Vertical Drop Events

Pursuant to the provision in NUREG-1536, a non-mechanistic tip-over of a loaded HI-STAR 100 System on to the ISFSI pad is considered. Analyses are also performed to determine the maximum deceleration sustained by a side or vertical free fall of a loaded HI-STAR 100 System onto the ISFSI pad. The object of the analyses is to demonstrate that the plastic deformation in the fuel basket is sufficiently limited to permit the stored SNF to be retrieved by normal means and that there is no significant loss of radiation shielding in the system.

Ready retrievability of the fuel is presumed to be ensured if stress levels in the MPC structure remain below Level D limits during the postulated drop events.

Subsequent to the accident events, the overpack must be shown to contain the shielding so that unacceptable radiation levels do not result from the accident.

Appendix 3.A provides a description of the dynamic finite element analyses undertaken to establish the decelerations resulting from the postulated event. A non-mechanistic tip-over is considered together with a side and end drop of a loaded HI-STAR 100 System. A dynamic finite element analysis of each event is performed using a commercial finite element code well suited for such dynamic analyses with interface impact and non-linear material behavior. This code and methodology have been fully benchmarked against Lawrence Livermore Laboratories test data and correlation [3.4.12].

It is shown in Appendix 3.A that the peak deceleration is less than 60g's for tip-over. Table 3.A.3 shows that the maximum deceleration level at the top of the cask is 52.8 g's, while the corresponding deceleration level at the top of the fuel basket is 47.8 g's. For the case of a vertical drop from a height of 21", the bounding longitudinal deceleration is 51.9 g's. Finally, for a side drop from a height of 72", the maximum deceleration is 49.2 g's.

Based on the above results, it is concluded that the design basis deceleration limit of 60g's (Table 3.1.2) provides a conservative input for Level D stress calculations to demonstrate retrievability of stored fuel.

3.4.10 Overpack Service Life

The term of the 10CFR72, Subpart L C of C, granted by the NRC is 20 years. Nonetheless, the HI-STAR 100 Overpack is designed for 40 years of service life, while satisfying the conservative design requirements defined in Chapter 2, including the regulatory requirements of 10CFR72. In addition, the overpack is designed, fabricated, and inspected under the comprehensive Quality Assurance Program discussed in Chapter 13 and in accordance with the applicable requirements of the ASME Codes. The pressure boundary (helium retention boundary) of the overpack is engineered to meet ASME Section III, Subsection NB (Class 1) stress intensity limits. Even though compliance to a less rigorous standard (such as the AISC Manual for Steel Construction) would be acceptable, all structural members of the HI-STAR 100 overpack located outside of the pressure boundary meet ASME Section III, Subsection NF stress limits. The aforementioned design and manufacturing measures assure high design margins, high quality fabrication, and verification of compliance through rigorous inspection and testing, as describe in Chapter 9. Technical Specifications defined in Chapter 12 assure that the integrity of the cask and the contained MPC are maintained throughout the components' service life.

The principal design considerations which bear on the adequacy of the overpack for the design basis service life are addressed as follows:

Exposure to Environmental Effects

All exposed surfaces of HI-STAR 100 are made from ferritic steels that are readily painted. Therefore, the potential of environmental vagaries are ruled out for HI-STAR 100. Under normal storage conditions, the bulk temperature of the HI-STAR 100 overpack will, because of its large thermal inertia, change very gradually with time. Therefore, material degradation from rapid thermal ramping conditions is not credible for the HI-STAR 100 overpack. The configuration of the overpack assures resistance to freeze-thaw degradation. In addition, the overpack is specifically designed for a full range of enveloping design basis natural phenomena which could occur over the 40-year service life of the overpack as defined in Section 2.2.3 and evaluated in Chapter 11.

Material Degradation

The relatively low neutron flux to which the overpack is subjected cannot produce measurable degradation of the cask's material properties and impair its intended safety function. Exposed carbon steel components are coated to prevent corrosion. The controlled environment of the ISFSI storage pad mitigates damage due to direct exposure to corrosive chemicals that may be present in other industrial applications.

Maintenance and Inspection Provisions

The requirements for periodic inspection and maintenance of the overpack throughout the 40-year service life are defined in Chapter 9. These requirements include provisions for routine inspection of the overpack exterior. ISFSIs located in areas subject to atmospheric conditions which may degrade the storage cask or

canister should be evaluated by the licensee on a site-specific basis to determine the frequency for such inspections to assure long-term performance. In addition, the HI-STAR 100 System is designed for easy retrieval of the MPC from the overpack should it become necessary to perform more detailed inspections and repairs on the overpack.

The above findings are consistent with those of the NRC's Waste Confidence Decision Review [3.4.11], which concluded that dry storage systems designed, fabricated, inspected, and operate in accordance with such requirements are adequate for a 100-year service life while satisfying the requirements of 10CFR72.

3.4.11 MPC Service Life

The term of the 10CFR72, Subpart L C of C, granted by the NRC is 20 years. Nonetheless, the HI-STAR 100 MPC is designed for 40 years of service, while satisfying the conservative design requirements defined in Chapter 2, including the regulatory requirements of 10CFR72. Additional assurance of the integrity of the MPC and the contained SNF assemblies throughout the 40-year service life of the MPC is provided through the following:

- Design, fabrication, and inspection in accordance with the applicable requirements of the ASME Code as described in Chapter 2 assures high design margins.

- Fabrication and inspection performed in accordance with the comprehensive Quality Assurance program discussed in Chapter 13 assures competent compliance with the fabrication requirements.

- Use of materials with known characteristics, verified through rigorous inspection and testing, as described in Chapter 9, assures component compliance with design requirements.

- Use of welding procedures in full compliance with Sections III and IX of the ASME Code ensures high-quality weld joints.

Technical Specifications, as defined in Chapter 12, have been developed and imposed on the MPC which assure that the integrity of the MPC and the contained SNF assemblies are maintained throughout the 40-year service life of the MPC.

The principal design considerations bearing on the adequacy of the MPC for the design basis service life are summarized below.

Corrosion

All MPC materials are fabricated from corrosion-resistant austenitic stainless steel and passivated aluminum. The corrosion-resistant characteristics of such materials for dry SNF storage canister applications, as well as the protection offered by these materials against other material degradation effects, are well established in the nuclear industry. The MPC is vacuum dried to remove all oxidizing liquids and gases and backfilled with dry inert helium at the time of closure to maintain an atmosphere in the MPC that provides corrosion protection for the SNF cladding throughout the dry storage period. The preservation of this non-corrosive atmosphere

is assured by the inherent sealworthiness of the MPC confinement boundary integrity (there are no gasketed joints in the MPC).

Structural Fatigue

The passive non-cyclic nature of dry storage conditions do not subject the MPC to conditions that might lead to structural fatigue failure. Ambient temperature and insolation cycling during normal dry storage conditions and the resulting fluctuations in MPC thermal gradients and internal pressure is the only mechanism for fatigue. These low stress, high-cycle conditions can not lead to a fatigue failure of the MPC which is made from stainless alloy stock (endurance limit well in excess of 20,000 psi). All other off-normal or postulated accident conditions are infrequent or one-time occurrences which can not produce fatigue failures. Finally, the MPC uses materials that are not susceptible to brittle fracture.

Maintenance of Helium Atmosphere

The inert helium atmosphere in the MPC provides a non-oxidizing environment for the SNF cladding to assure its integrity during long-term storage. The preservation of the helium atmosphere in the MPC is assured by the robust design of the MPC confinement boundary described in Section 7.1. Maintaining an inert environment in the MPC mitigates conditions that might otherwise lead to SNF cladding failures. The required mass quantity of helium backfilled into the canister at the time of closure as defined in the Technical Specification contained in Chapter 12, and the associated leak tightness requirements for the canister defined in the Technical Specification contained in Chapter 12, are specifically set down to assure that an inert helium atmosphere is maintained in the canister throughout a 40-year service life.

Allowable Fuel Cladding Temperatures

The helium atmosphere in the MPC promotes heat removal and thus reduces SNF cladding temperatures during dry storage. In addition, the SNF decay heat will substantially attenuate over a 40-year dry storage period. Maintaining the fuel cladding temperatures below allowable levels during long-term dry storage mitigates the damage mechanism that might otherwise lead to SNF cladding failures. The allowable long-term SNF cladding temperatures used for thermal acceptance of the MPC design are conservatively determined, as discussed in Section 4.3.

Neutron Absorber Boron Depletion

The effectiveness of the fixed borated neutron absorbing material used in the MPC fuel basket design requires that sufficient concentrations of boron be present to assure criticality safety during worst case design basis conditions over the 40-year service life of the MPC. Information on the characteristics of the borated neutron absorbing material used in the MPC fuel basket is provided in Section 1.2.1.3.1. The low neutron flux, which will continue to decay over time, to which this borated material is subjected, does not result in depletion of the material's available boron to prevent performing its intended safety function. In addition, the boron content of the material used in the criticality safety analysis is conservatively based on the minimum specified boron areal density (rather than the nominal), which is further reduced by 25% for analysis purposes, as described in Section 6.1. Analysis discussed in Section 6.2 demonstrates that the boron depletion in the Boral is

negligible over a 50-year duration. Thus, sufficient levels of boron are present in the fuel basket neutron absorbing material to maintain criticality safety functions over the 40-year service life of the MPC.

The above findings are consistent with those of the NRC's Waste Confidence Decision Review, which concluded that dry storage systems designed, fabricated, inspected, and operated in the manner of the requirements set down in this document are adequate for a 100-year service life, while satisfying the requirements of 10CFR72.

Table 3.4.1

FINITE ELEMENTS IN THE MPC STRUCTURAL MODELS

MPC Type	Model Type		
Element Type	Basic	0 Degree Drop	45 Degree Drop
MPC-24	942	1050	1050
BEAM3	898	898	898
PLANE82	8	8	8
CONTAC12	36	34	34
CONTAC26	0	107	108
COMBIN14	0	3	2
MPC-68	1234	1347	1344
BEAM3	1174	1174	1174
PLANE82	16	16	16
CONTAC12	44	43	40
CONTAC26	0	112	111
COMBIN14	0	2	3

Table 3.4.2

HI-STAR 100 SYSTEM MATERIAL COMPATIBILITY
WITH OPERATING ENVIRONMENTS

Material/Component	**Fuel Pool (Borated and Unborated Water†**	**ISFSI Pad (Open to Environment)**
Alloy X: - MPC Fuel Basket - MPC Baseplate - MPC Shell - MPC Lid - MPC Fuel Spacers	Stainless steels have been extensively used in spent fuel storage pools with both borated and unborated water with no adverse reactions or interactions with spent fuel.	The MPC internal and external environment will be inert (helium) atmosphere. No adverse interactions identified.
Aluminum: - Conduction Elements	Aluminum and stainless steels form a galvanic couple. However, they are very close in the galvanic series chart and aluminum rapidly passivates in an aqueous environment forming a thin ceramic (Al_2O_3) barrier. Therefore, during the short time they are exposed to fuel pool water, corrosion is not expected.	In a non-aqueous atmosphere galvanic corrosion is not expected.
Boral: - Neutron Absorber	The Boral will be used in passivated condition. Extensive in-pool experience on spent fuel racks with no adverse reactions.	The Boral will be in a helium environment. No adverse reactions identified.

† HI-STAR 100 System short-term operating environment during loading and unloading.

Table 3.4.2 (continued)

HI-STAR 100 SYSTEM MATERIAL COMPATABILITY WITH OPERATING ENVIRONMENT

Material/Component	Fuel Pool (Borated and Unborated Water) †	ISFSI Pad (Open to Environment)
Steels: - SA350-LF3 - SA203-E - SA515 Grade 70 - SA516 Grade 70 - SA750 630 17-4 PH - SA564 630 17-4 PH - SA106 - SA193-B7 Overpack Body	All exposed steel surfaces (except seal areas, pocket trunnions, and bolt locations) will be coated with paint specifically selected for performance in the operating environments. Even without coating, no adverse reactions (other than nominal corrosion) have been identified.	Internal surfaces of the overpack will be painted and maintained in an inert atmosphere. Exposed external surfaces (except those listed in fuel pool column) will be painted and will be maintained with a fully painted surface. No adverse reactions identified.

† HI-STAR 100 System short-term operating environment during loading and unloading.

Table 3.4.2 (continued)

HI-STAR 100 SYSTEM MATERIAL COMPATABILITY WITH OPERATING ENVIRONMENT

Material/Component	Fuel Pool (Borated and Unborated Water) †	ISFSI Pad (Open to Environment)
Stainless Steels: - SA240 304 - SA193 Grade B8 - 18-8 S/S Miscellaneous Components	Stainless steels have been extensively used in spent fuel storage pools with both borated and unborated water with no adverse reactions.	Stainless steel has a long proven history of corrosion resistance when exposed to the atmosphere. These materials are used for bolts and threaded inserts. No adverse reactions with steel have been identified. No impact on performance.
Nickel Alloy: - SB637-NO7718 Bolting	Bolts are not used in pool.	Exposed to weathering effects. No adverse reactions with overpack closure plate. No impact on performance.
Brass: - Rupture Disk	Small surface of rupture disk will be exposed. No significant adverse impact identified.	Exposed to external weathering. No loss of function expected. Disks inspected prior to transport.
Holtite-A: - Neutron Shield	The neutron shield is fully enclosed by the outer enclosure. No adverse reaction identified. No adverse reactions with thermal expansion foam or steel.	The neutron shield is fully enclosed in the outer enclosure. No adverse reaction identified. No adverse reactions with thermal expansion foam or steel.

† HI-STAR 100 System short-term operating environment during loading and unloading.

Table 3.4.2 (continued)

HI-STAR 100 SYSTEM MATERIAL COMPATABILITY WITH OPERATING ENVIRONMENT

Material/Component	Fuel Pool (Borated and Unborated Water) †	ISFSI Pad (Open to Environment)
Silicone Foam: - Thermal Expansion Foam	Fully enclosed in the outer enclosure. No adverse reaction identified. No adverse reactions with neutron shield or steel.	Foam is fully enclosed in outer enclosure. No adverse reaction identified. No adverse reactions with neutron shield or steel.
Paint: - Carboline 890 - Thermaline 450	Carboline 890 used for exterior surfaces. Acceptable performance for short-term exposure in mild borated pool water. Thermaline 450 selected for excellent high temperature resistance properties. Will only be exposed to demineralized water during in-pool operations as annulus is filled prior to placement in the spent fuel pool and the inflatable seal prevents fuel pool water in-leakage. No adverse interaction identified which could affect MPC/fuel assembly performance.	Good performance on exterior surfaces. Discoloration is not a concern. During storage, internal overpack surfaces will operate in an inert (helium) atmosphere. No adverse reaction identified.
Metallic Seals: - Alloy X750 - 304 S/S	Not installed or exposed during in-pool handling.	Seals enclosed by closure plate or port coverplates. Closure plate seals seat against stainless steel overlay surfaces. No degradation of seal integrity due to corrosion is expected.

† HI-STAR 100 System short-term operating environment during loading and unloading.

Table 3.4.3

FUEL BASKET RESULTS- GLOBAL MINIMUM OF SAFETY FACTORS

Load Case I.D.	**Loading†**	**Safety Factor**	**Location in FSAR where Results or Detailed Calculations are Presented††**
F1	T, T'	3.06	3.AA.39
F2	D + H	2.79	Table 3.4.9
F3			
F3.a	D + H' (end drop)	4.27	3.4.4.3.1.3
F3.b	D + H' (side drop 0°)	1.17	Table 3.4.9
F3.c	D + H' (side drop 45°)	1.28	Table 3.4.9

† The symbols used for the loading are defined in Table 2.2.13.

†† All Safety Factors for the Fuel Basket are conservatively evaluated using allowable stresses evaluated at 725 degrees F.

Table 3.4.4

ENCLOSURE VESSEL RESULTS – GLOBAL MINIMUM OF SAFETY FACTORS

Load Case I.D.	Load Combination[†]	Safety Factor	Component ID and Location in FSAR where Results or Detailed Calculations are Presented[†††]
E1			
E1.a	Design internal pressure, P_i	10.1 1.33 1.27	Lid Table 3.4.7 Baseplate 3.I.8.1 Shell 3.4.4.3.1.2
E1.b	Design external pressure, P_o	15 1.2 1.2	Lid 3.E.8.1.1 Baseplate Table 3.4.7[††††] Shell Table 3.4.15
E1.c	Design internal pressure, P_i, plus Temperature T	16.4 2.7 1.5	Lid Table 3.4.8 Baseplate Table 3.4.8 Shell Table 3.4.8
E2	$(P_i,P_o)^{††}$ + D + H	6.5 1.09 2.63 4.58	Lid 3.E.8.1.2 Baseplate 3.I.8.2 Shell Table 3.4.9 Supports Table 3.4.9

† The symbols used for the loadings are defined in Table 2.2.13.

†† The notation (P_i,P_o) means that one or the other pressure is applied to determine the governing condition.

††† Safety Factors computed in Table 3.4.9 are conservatively based on the design temperature given in Table 3.1.17.

†††† Safety Factor obtained by multiplication of result for internal pressure by external pressure/internal pressure ratio.

Table 3.4.4 (Continued)

Load Case I.D.	Load Combination†	Safety Factor	Component ID and Location in FSAR where Detailed Calculations are Presented††	
E3				
E3.a	$(P_I,P_o) + D + H'$, end drop	13.1	Lid	Table 3.4.13
		1.87	Baseplate	Table 3.4.12
		1.92	Shell	Table 3.4.15
E3.b	$(P_I,P_o) + D + H'$, side drop 0°	NA	Lid	
		NA	Baseplate	
		2.14	Shell	Table 3.4.9
		1.16	Supports	Table 3.4.9
E3.c	$(P_I,P_o) + D + H'$, side drop 45°	NA	Lid	
		NA	Baseplate	
		2.74	Shell	Table 3.4.9
		1.51	Supports	Table 3.4.9

† Symbols used in the loading are defined in Table 2.2.13

†† Safety Factors computed in Table 3.4.9 conservatively use allowable stresses at the design temperature of 450 degrees F (Table 3.1.17)

Table 3.4.4 (Continued)

Load Case I.D.	Load Combination†	Safety Factor	Component ID and Location in FSAR where Detailed Calculations are Presented
E4	T	No restraint of free thermal expansion under normal heat or fire accident	3.U; 3.W; 3.AD
E5	$(P_I^*, P_o^*) + D + T^*$	27.2 1.78 1.18	Lid Table 3.4.13 Baseplate Table 3.4.12 Shell Table 3.5.15

† The symbols used for the loading are defined in Table 2.2.13

Table 3.4.5
OVERPACK – GLOBAL MINIMUM SAFETY FACTORS

Load Case I.D.	Load Combination†	Safety Factor	Location in FSAR
01	(P_i, P_o)	2.86	Table 3.4.10
02	(P_i^*, P_o^*) + D + T*	3.56	Table 3.4.6
03	(P_i, P_o) + D + T + H	4.45	Table 3.4.10
04			
04.a	(P_i, P_o) + D + H (end drop)	1.27	Table 3.4.10
04.b	(P_i, P_o) + D + H (side drop)	1.48	Table 3.4.10
05	T	1.93	Table 3.4.6
06	M (small and medium penetrant missiles)	No effect on confinement boundary	3.G

† The symbols used for the loadings are defined in Table 2.2.13.

Table 3.4.6

OVERPACK SAFETY FACTORS TO INCORPORATE FABRICATION STRESS AND ACCIDENT TEMPERATURE†

Load Case (Table in 3.AA)	Inner Shell (Exterior Surface)			Inner Shell (Middle Surface)			Intermediate Shell		
	Value (ksi)	Allowable (ksi)	Safety Factor	Value (ksi)	Allowable (ksi)	Safety Factor	Value (ksi)	Allowable (ksi)	Safety Factor
01 (3.AB.1)	19.1	68.7	3.60	12.19	68.7	5.33	12.74	52.5	4.12
03 (3.AB.4)	19.28	68.7	3.56	12.30	68.7	5.59	14.61	52.5	3.59
05 (3.AB.7)	35.68	68.7	1.93	26.65	68.7	2.58	NA	NA	NA

† The Value is obtained by adding the fabrication stress from Subsection 3.4.4.3.2.2 (absolute value) to the stress intensity from the table in 3.AA to compute a conservative modified stress intensity and then re-computing the safety factor based on allowable values for primary plus secondary stresses.

Table 3.4.7
STRESS INTENSITY RESULTS FOR CONFINEMENT BOUNDARY - INTERNAL PRESSURE ONLY (Load Case E1.a in Table 3.1.4)

Component Locations (Per Fig. 3.4.44)	Calculated Value of Stress Intensity (psi)	Category	Table 3.1.13 Allowable Value (psi)†	Safety Factor (Allowable/Calculated)
Top Lid				
A	1641	$P_L + P_b$	30,000	18.3
Neutral Axis	20.2	P_m	20,000	990.1
B	1605	$P_L + P_b$	30,000	18.7
C	687	$P_L + P_b$	30,000	43.7
Neutral Axis	731	P_m	20,000	27.4
D	2960	$P_L + P_b$	30,000	10.1
Baseplate				
E	19,683	$P_L + P_b$	30,000	1.5
Neutral Axis	412	P_m	20,000	48.5
F	20,528	$P_L + P_b$	30,000	1.5
G	9,695	$P_L + P_b$	30,000	3.1
Neutral Axis	2,278	P_m	20,000	8.8
H	8,340	$P_L + P_b$	30,000	3.5

†Allowable stress intensity conservatively taken at 300 degrees F.

Table 3.4.7 Continued

Component Locations (Per Fig. 3.4.44)	Calculated Value of Stress Intensity (psi)	Category	Table 3.1.13 Allowable Value (psi)†	Safety Factor (Allowable/Calculated)
Canister				
I	6,860	P_m	18,700	2.72
Upper Bending Boundary Layer Region	7,189 7,044	$P_L + P_b + Q$ $P_L + P_b$	30,000 20,000	4.2 2.8
Lower Bending Boundary Layer Region	43,986 10,621	$P_L + P_b + Q$ $P_L + P_b$	60,000 30,000	1.36 2.82

†Allowable stress intensity conservatively based at 300 degrees F except for Location I where allowable stress intensity values are based on 400 degree F

Table 3.4.8

PRIMARY AND SECONDARY STRESS INTENSITY RESULTS FOR
CONFINEMENT BOUNDARY - PRESSURE PLUS THERMAL LOADING (Load Case E1.c in Table 3.1.4)

Locations (Per Fig. 3.4.44)	Calculated Value of Stress Intensity (psi)	Category	Allowable Stress Intensity (psi)†	Safety Factor (Allowable/Calculated)
Top Lid				
A	2,375	$P_L + P_b + Q$	60,000	25.2
Neutral Axis	765	P_L	30,000	39.2
B	1,070	$P_L + P_b + Q$	60,000	73.2
C	1,100	$P_L + P_b + Q$	60,000	56.1
Neutral Axis	1,825	P_L	30,000	16.4
D	3,517	$P_L + P_b + Q$	60,000	17.1
Baseplate				
E	21,921	$P_L + P_b + Q$	60,000	2.7
Neutral Axis	1,287	P_L	30,000	23.3
F	19,386	$P_L + P_b + Q$	60,000	3.1
G	6,152	$P_m + P_L$	60,000	9.8
Neutral Axis	4,564	P_L	30,000	6.6
H	11,306	$P_L + P_b + Q$	60,000	5.3

† Allowable stresses based on temperature of 300 degrees F

Table 3.4.8 Continued

Locations (Per Fig. 3.4.44)	Calculated Value of Stress Intensity (psi)	Category	Allowable Stress Intensity (psi)†	Safety Factor (Allowable/Calculated)
Canister				
I	6,900	P_L	28,100	4.07
Upper Bending Boundary	6,490	$P_L + P_b + Q$	60,000	9.2
Layer Region	4,834	P_L	30,000	6.2
Lower Bending Boundary Layer Region	39,929	$P_L + P_b + Q$	60,000	1.5
	7,480	P_L	30,000	4.0

† Allowable stresses based on temperature of 300 degree F except at Location I where the temperatures are based on 400 degrees F

Table 3.4.9 – FINITE ELEMENT ANALYSIS RESULTS
MINIMUM SAFETY FACTORS FOR MPC COMPONENTS (Load Cases from Tables 3.1.3 and 3.1.4)

Component – Stress Result	MPC-24		
	Handling Load Load Cases F2 or E2	0 Degree Side Drop Load Cases F3.b or E3.b	45 Degree Side Drop Load Cases F3.c or E3.c
Fuel Basket – Primary Membrane (P_m)	31.5 (982) [3.AA.2]	2.69 (852) [3.AA.8]	3.78 (852) [3.AA.14]
Fuel Basket – Local Membrane Plus Primary Bending ($P_L + P_b$)	2.79 (390) [3.AA.3]	1.17 (1012) [3.AA.9]	1.28 (632) [3.AA.15]
Enclosure Vessel - Primary Membrane (P_m)	2.63 (1156) [3.AA.4]	6.84 (1210) [3.AA.10]	6.91 (1232) [3.AA.16]
Enclosure Vessel – Local Membrane Plus Primary Bending ($P_L + P_b$)	3.11 (1225) [3.AA.5]	2.64 (1138) [3.AA.11]	3.20 (1225) [3.AA.17]
Basket Supports – Primary Membrane (P_m)	5.87 (1084) [3.AA.6]	4.81 (1096) [3.AA.12]	6.93 (1102) [3.AA.18]
Basket Supports – Local Membrane Plus Primary Bending ($P_L + P_b$)	8.96 (1075) [3.AA.7]	6.48 (1096) [3.AA.13]	5.04 (1088) [3.AA.19]

Notes:
1. Corresponding ANSYS element number shown in parentheses (Appendices 3.N-3.S provide element locations).
2. Corresponding appendix table number shown in brackets.

Table 3.4.9 (continued)

	MPC-68		
Component - Stress Result	Handling Load Load Cases F2 or E2	0 Degree Side Drop Load Cases F3.b or E3.b	45 Degree Side Drop Load Cases F3.c or E3.c
Fuel Basket - Primary Membrane (P_m)	40.0 (798) [3.AA.40]	3.07 (1603) [3.AA.46]	4.30 (1603) [3.AA.52]
Fuel Basket - Local Membrane Plus Primary Bending ($P_L + P_b$)	2.87 (438) [3.AA.41]	2.64 (1033) [3.AA.47]	1.56 (774) [3.AA.53]
Enclosure Vessel - Primary Membrane (P_m)	2.64 (1747) [3.AA.42]	5.65 (1770) [3.AA.48]	7.13 (1864) [3.AA.54]
Enclosure Vessel - Local Membrane Plus Primary Bending ($P_L + P_b$)	2.96 (1864) [3.AA.43]	3.07 (1770) [3.AA.49]	2.74 (1866) [3.AA.55]
Basket Supports - Primary Membrane (P_m)	5.85 (1714) [3.AA.44]	6.68 (1699) [3.AA.50]	8.68 (1644) [3.AA.56]
Basket Supports - Local Membrane Plus Primary Bending ($P_L + P_b$)	9.02 (1713) [3.AA.45]	1.16 (1704) [3.AA.51]	1.51 (1649) [3.AA.57]

Notes:

1. Corresponding ANSYS element number shown in parentheses (Appendices 3.N-3.S provide element locations).
2. Corresponding appendix table number shown in brackets.

Table 3.4.10 FINITE ELEMENT RESULTS
MINIMUM SAFETY FACTORS FOR OVERPACK COMPONENTS UNDER VARIOUS LOADS (Load Case from Table 3.1.5)

Component - Stress Result	Internal Pressure – Load Case 01	Accident Internal Pressure – Load Case 02	Accident External Pressure - Load Case 02	Handling Load – Load Case 03	End Drop Load Case 04.a	Side Drop – Load Case 04.b	Thermal Load – Load Case 05
Lid – Local Membrane Plus Primary Bending ($P_L + P_b$)	2.86 (501) [3.AB.1]	5.50 (501) [3.AB.2]	14.3 (501) [3.AB.3]	4.45 (501) [3.AB.4]	9.2 (501) [3.AB.5]	3.68 (501) [3.AB.6]	2.55 (479) [3.AB.7]
Inner Shell - Local Membrane Plus Primary Bending ($P_L + P_b$)	12.1 (11023) [3.AB.1]	24.6 (11023) [3.AB.2]	13.6 (47) [3.AB.3]	11.3 (8338) [3.AB.4]	2.20 (10790) [3.AB.5]	1.70 (47) [3.AB.6]	3.72 (10925) [3.AB.7]
Inner Shell - Primary Membrane (P_m)	13.7 (281) [3.AB.1]	27.7 (281) [3.AB.2]	17.4 (10791) [3.AB.3]	12.7 (2969) [3.AB.4]	2.37 (48) [3.AB.5]	2.65 (2969) [3.AB.6]	2.98 (11024) [3.AB.7]
Intermediate Shells – Local Membrane Plus Primary Bending ($P_L + P_b$)	17.2 (11025) [3.AB.1]	36.6 (11025) [3.AB.2]	24.3 (49) [3.AB.3]	7.76 (285) [3.AB.4]	3.47 (10792) [3.AB.5]	1.48 (51) [3.AB.6]	2.42 (10796) [3.AB.7]
Baseplate - Local Membrane Plus Primary Bending ($P_L + P_b$)	10.6 (1) [3.AB.1]	17.9 (1) [3.AB.2]	7.77 (1) [3.AB.3]	18.8 (1) [3.AB.4]	1.27 (1) [3.AB.5]	4.98 (1) [3.AB.6]	2.07 (27) [3.AB.7]
Enclosure Shell - Primary Membrane (P_m)	35.1 (288) [3.AB.1]	72.7 (288) [3.AB.2]	41.4 (55) [3.AB.3]	13.2 (288) [3.AB.4]	8.47 (55) [3.AB.5]	1.55 (288) [3.AB.6]	2.03 (5428) [3.AB.7]

Notes:

1. Corresponding ANSYS node number shown in parentheses (Appendices 3.N-3.S provide element locations).
2. Corresponding appendix table number shown in brackets.

Table 3.4.11

SAFETY FACTORS FROM MISCELLANEOUS CALCULATIONS

Item	Loading	Safety Factor	FSAR Text or Appendix Location Where Details are Provided
MPC Closure Ring	Internal Pressure	1.41	3.E
Fuel Basket Panels	Elastic Stability	15.9	3.4.4.3.1.3
MPC Top Lid Weld	Lifting	2.29	3.E
Fuel Support Spacers	Compression	2.76	3.J
MPC Cover Plates in MPC Lid	Accident Condition Internal Pressure	1.39	3.M
MPC Top Closure	10CFR71 Top End Drop (Transport) (Provided for Information Only)	2.8	3.E
MPC Cover Plate Weld	Accident Condition Internal Pressure	6.04	3.M

Table 3.4.12

MPC BASEPLATE MINIMUM SAFETY FACTORS FOR LOAD CASES E3 AND E5

MPC Baseplate Minimum Safety Factors – Load Cases E3, E5			
Item	Value (ksi)	Allowable (ksi)	Safety Factor
Center of Baseplate – Primary Bending (Load Case E3)	35.93	67.32	1.87
Center of Baseplate – Primary Bending (Load Case E5)	30.46	54.23	1.78

Details of calculation are in Subsection 3.4.4.3.1.4

Table 3.4.13

MPC TOP CLOSURE LID MINIMUM SAFETY FACTORS FOR LOAD CASES E3 AND E5

MPC Top Closure Lid – Minimum Safety Factors – Load Cases E3, E5			
Item	Stress(ksi) or Load(lb.)	Allowable Stress (ksi) or Load Capacity (lb.)	Safety Factor
Lid Bending Stress – Load Case E3.a	4.67	61.05	13.1
Lid Peripheral Weld Load – Load Case E3.a	624,000	1,477,000	2.37
Lid Bending Stress – Load Case E5	1.991	54.225	27.24
Closure Ring Bending Stress – Load Case E1.a†	20.0	28.1	1.41
Closure Ring Weld Load – Load Case E1.a	140,956	632,800	4.49

Details of calculation are in Subsection 3.4.4.3.1.5

† The closure ring is only subject to load subsequent to a postulated loss of integrity in the "NB" pressure boundary. Nevertheless, the stress results are compared to Level A allowables for conservatism. The pressure loading is assumed to correspond to the Design Pressure.

Table 3.4.14

MPC FUEL SPACERS – MINIMUM SAFETY FACTORS FOR LOAD CASES F2 AND F3.a

Fuel Spacers – Minimum Safety Factors (Load Cases F2 and F3.a)			
Item	Load (lb.)	Capacity (lb.)	Safety Factor
Axial Load – Level A	16,800	46,446	2.76
Elastic Stability – Level D – Lower Spacer	100,800	1,300,000	12.9
Elastic Stability – Level D – Upper Spacer	100,800	577,000	5.72

Details of calculation are in Subsection 3.4.4.3.1.6

Table 3.4.15

MPC SHELL STABILITY SAFETY FACTORS FROM ASME CODE CASE N-284

MPC Shell – Elastic/Plastic Stability (ASME Code Case N-284) – Minimum Safety Factors			
Item	Value	Allowable†	Safety Factor
Load Case E3.a (Yield)	0.698	1.34	1.92
Load Case E5 (Stability Interaction Equation)	0.847	1.0	1.18
Load Case E1.b (Stability Interaction Curve)	0.832	1.0	1.20

† We note that for Load Case E3.a, the yield strength criteria in the Code Case N-284 method governs. In this event, we include the safety factor 1.34, built into the Code Case, in the tabular result in order to obtain the actual safety factor with respect to the yield strength of the material.

Details of calculation are in Subsection 3.4.4.3.1.7

Table 3.4.16

OVERPACK FABRICATION STRESS – MINIMUM SAFETY FACTORS

Fabrication Stresses in Overpack Shells –Minimum Safety Factors (Level A Service Condition at Assembly Temperature)			
Item	Value (ksi)	Allowable (ksi) - (Note 3)	Safety Factor
First Intermediate Shell (Note 1)	11.22	52.5	4.68
Fourth Intermediate Shell (Note 1)	7.79	52.5	6.74
Inner Shell Mid Plane (Note 2)	10.6	69.9	6.59
Inner Shell Outer Surface (Note 2)	16.27	69.9	4.30

Notes:

1. The fabrication stress is a tensile circumferential stress.
2. The fabrication stress is a compressive circumferential stress
3. Fabrication stresses are self-limiting and are therefore classified as "secondary" and are compared to 3 times the membrane stress or stress intensity.

Details of calculation are in Subsection 3.4.4.3.2.2

Table 3.4.17

OVERPACK CLOSURE BOLT MINIMUM SAFETY FACTORS

Overpack Closure Bolt - Minimum Safety Factors	
Combined Load Case	Safety Factor on Bolt Tension
Normal (Load Case 01 in Table 3.1.5)	1.08
Top Closure Puncture (Load Case 06 in Table 3.1.5)	1.39
Drop (Load Case 04.a in Table 3.1.5)	1.30

Details of calculations are in Subsection 3.4.4.3.2.3

Table 3.4.18

OVERPACK CLOSURE PLATE – SAFETY FACTOR FOR LOAD CASE 04.a

Bending Stress in Overpack Closure Plate – Closed Form Solution (Load Case 04.a)			
Item	Value (ksi)	Allowable (ksi)	Safety Factor
Stress at Center of Plate	5.25	70.0	13.3

Details of calculations are in Subsection 3.4.4.3.2.4

Table 3.4.19

OVERPACK INNER SHELL SAFETY FACTORS FROM ASME CODE CASE N-284

Code Case N-284 Minimum Safety Factors – (Load Cases 02, 03 and 04.a in Table 3.1.5)			
Item	Calculated Interaction Value	Allowable Interaction Value†	Safety Factor against Yield†
Load Case 02 in Table 3.1.5	0.577	1.34	2.32
Load Case 03 in Table 3.1.5	0.613	2.0	3.26
Load Case 04 in Table 3.1.5	0.607	1.34	2.21

† We note that in computing the safety factor against yield for this table, we have included the safety factor implicit in the Code Case N-284 allowable interaction equation. We note also that the safety factors given above from the Code Case analysis are all safety factors against the circumferential or longitudinal stresses reaching the material yield stress. The actual safety factors against instability are larger than the factors reported in the table as can be seen by a perusal of Appendix 3.H. Finally, we note that fabrication stresses have been included in the stability calculations even though these stresses are self-limiting. Therefore, all results corresponding to the calculated stability interaction equations in Appendix 3.H are conservatively high.

Details of calculations are in Subsection 3.4.4.3.2.5

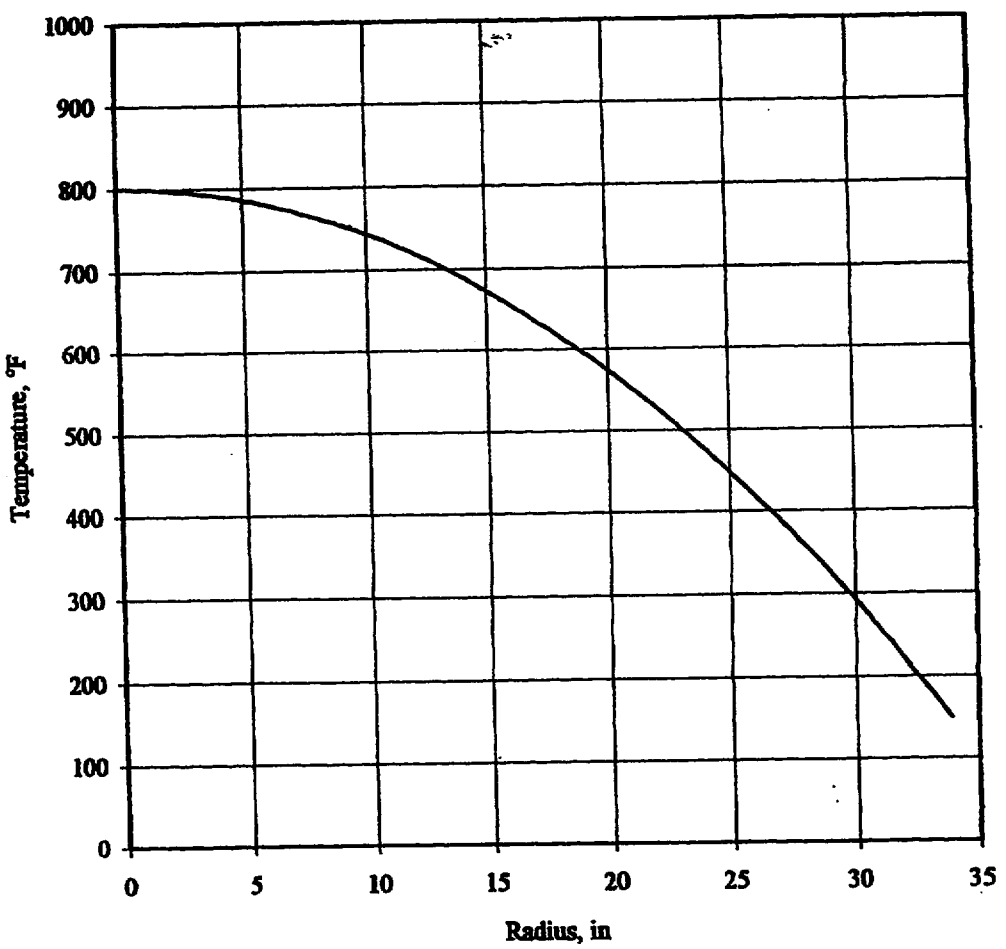

FIGURE 3.4.1; TEMPERATURE DISTRIBUTION FOR MPC THERMAL STRESS ANALYSIS

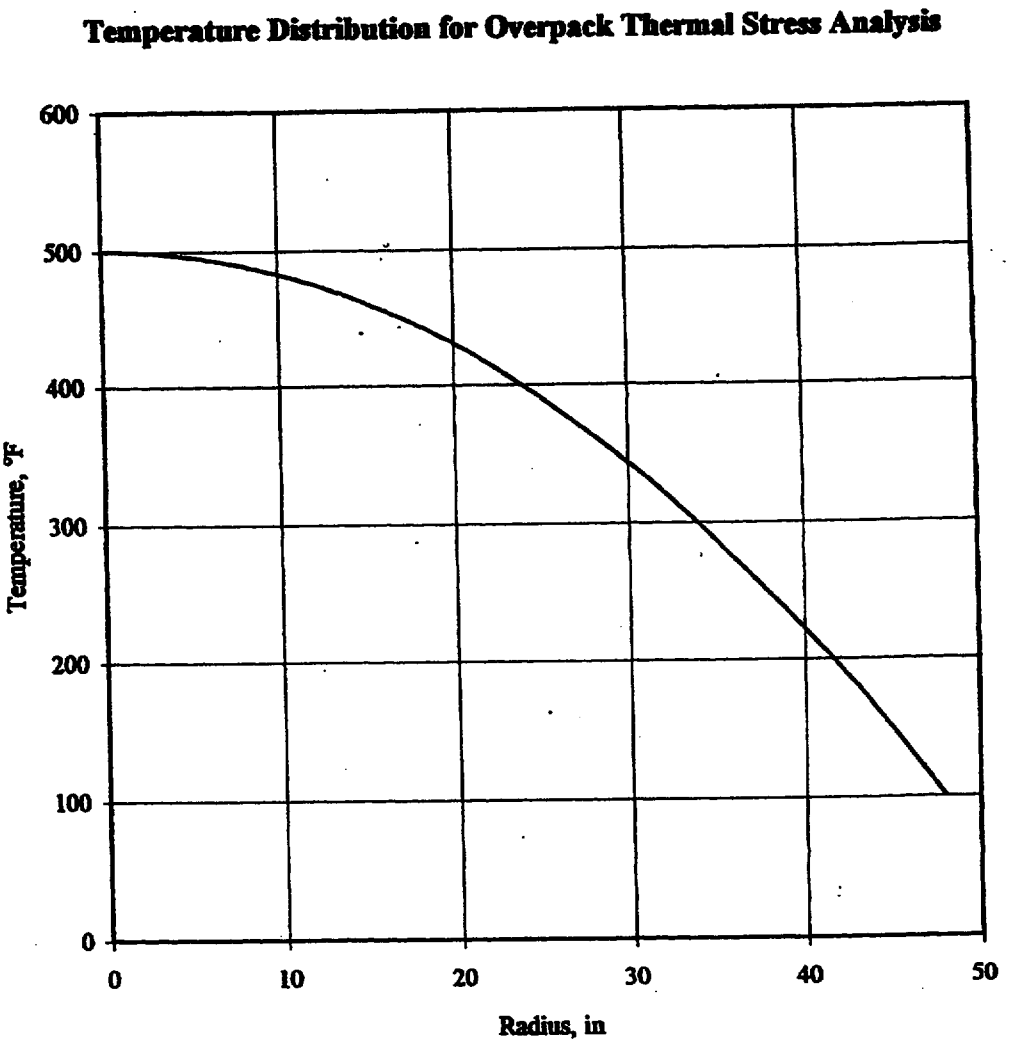

FIGURE 3.4.2; TEMPERATURE DISTRIBUTION FOR OVERPACK THERMAL STRESS ANALYSIS

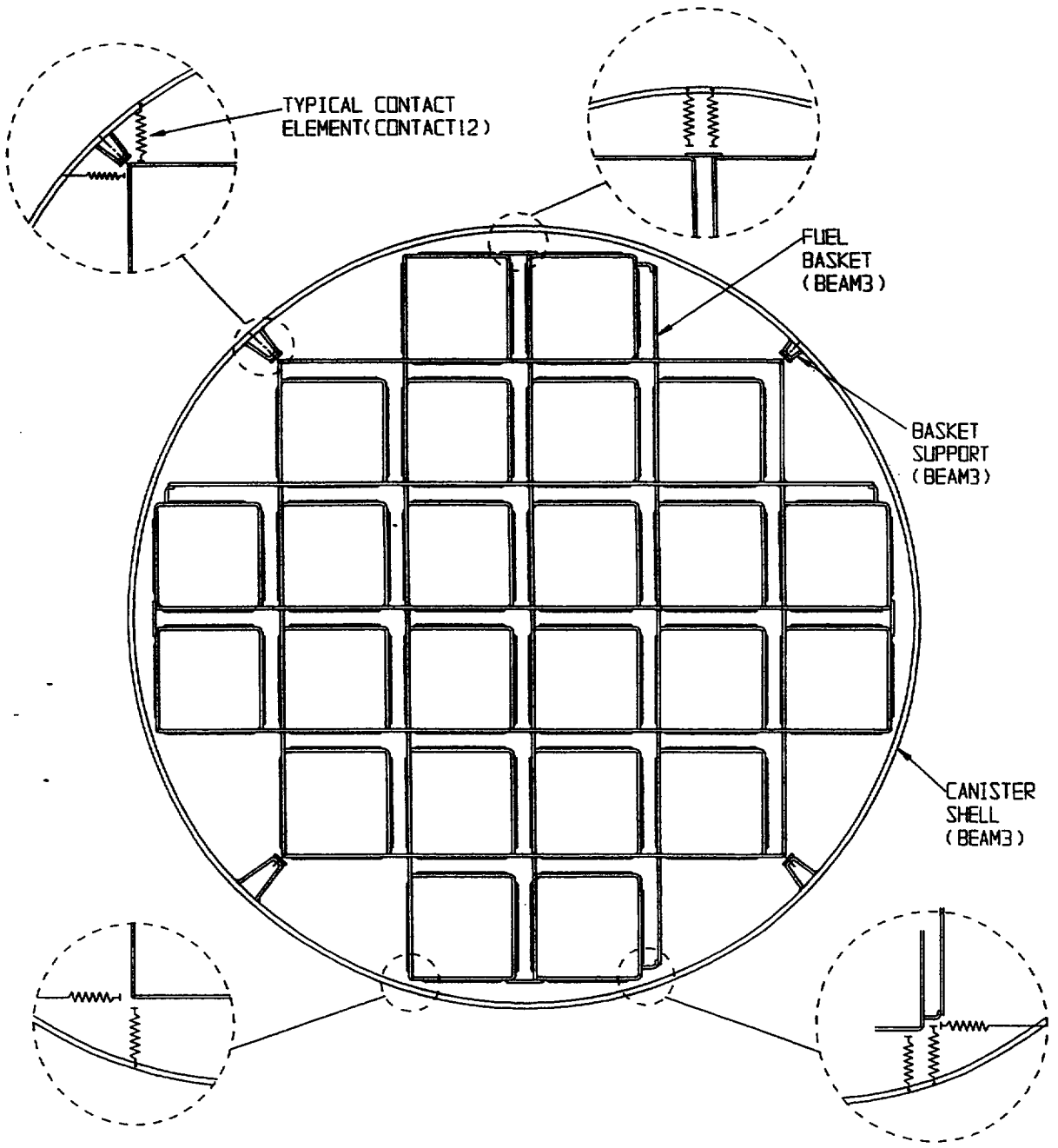

FIGURE 3.4.3: FINITE ELEMENT MODEL OF MPC-24

(BASIC MODEL)

DELETED

FIGURE 3.4.4;

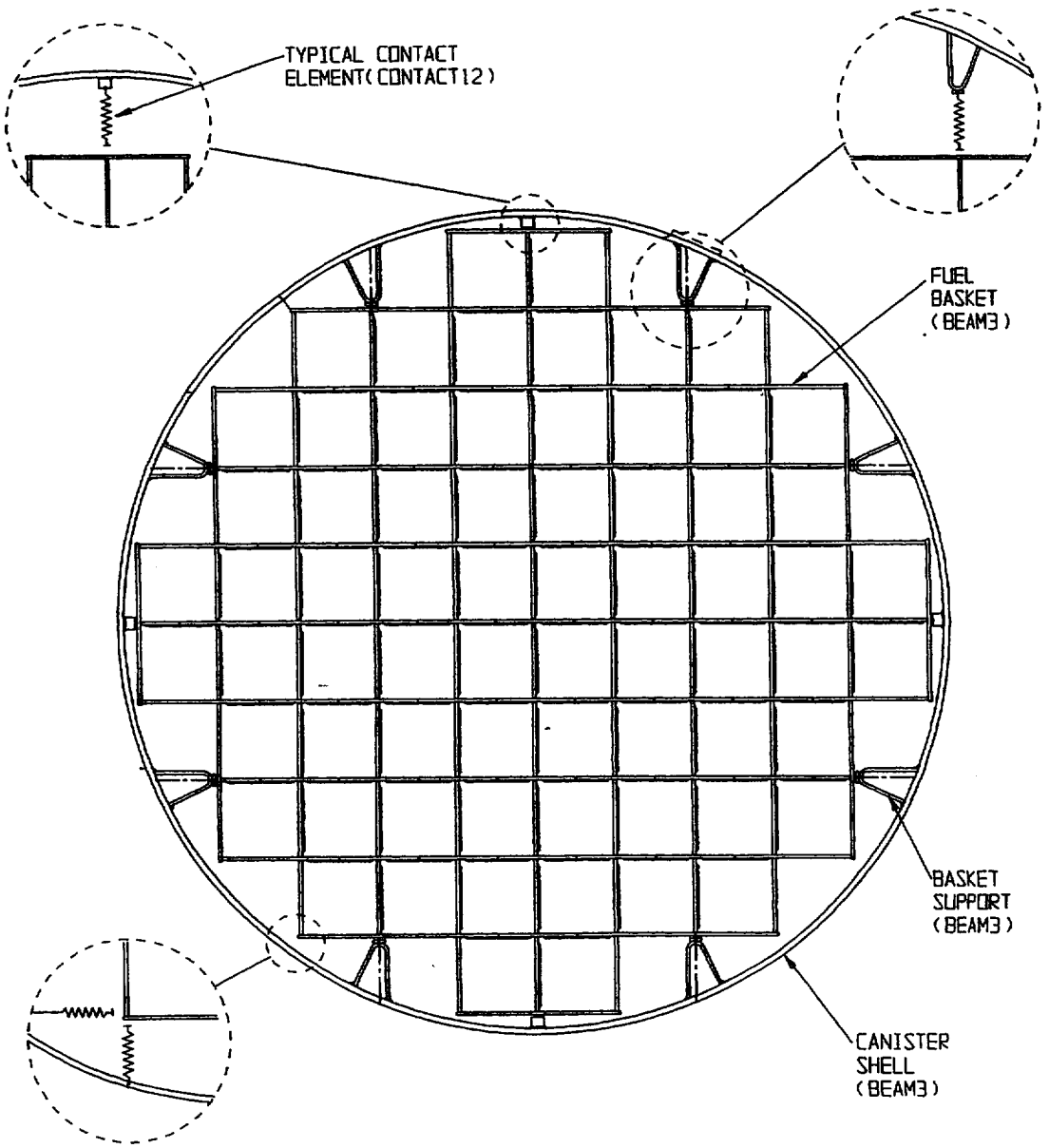

FIGURE 3.4.5: FINITE ELEMENT MODEL OF MPC-68

(BASIC MODEL)

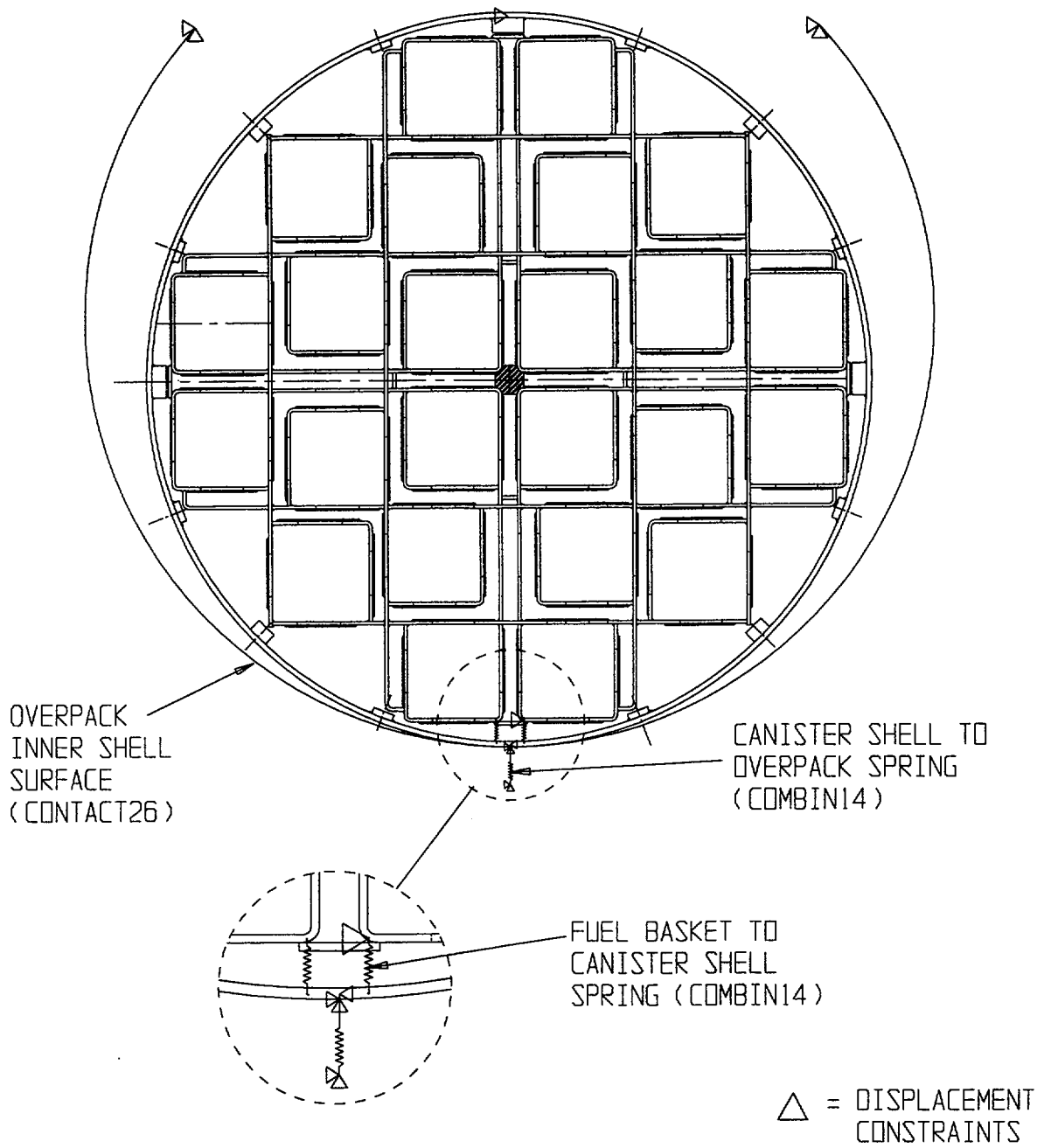

FIGURE 3.4.6: FINITE ELEMENT MODEL OF MPC-24

(0 DEGREE DROP MODEL)

DELETED

FIGURE 3.4.7;

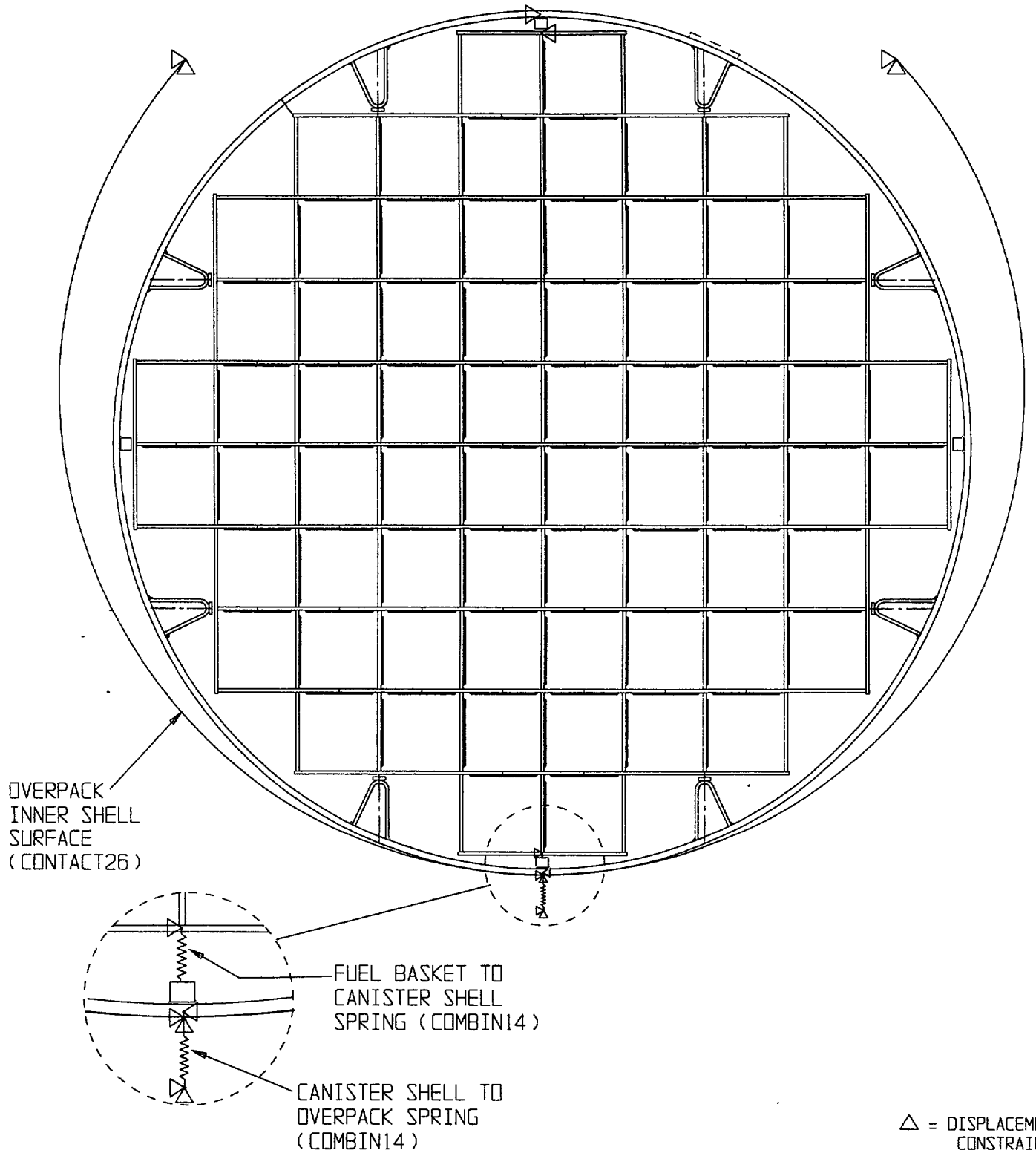

FIGURE 3.4.8; FINITE ELEMENT MODEL OF MPC-68

(0 DEGREE DROP MODEL)

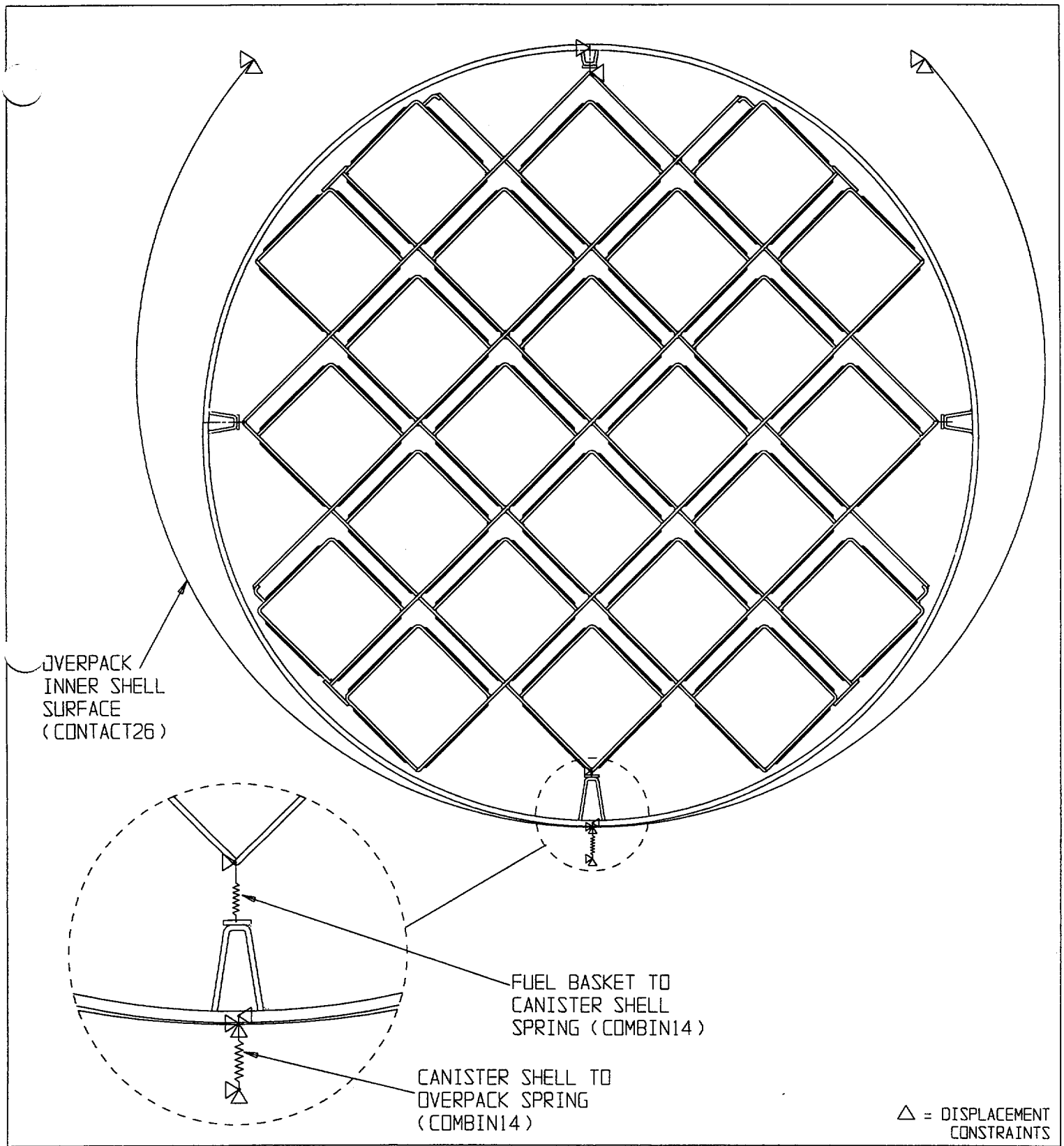

FIGURE 3.4.9; FINITE ELEMENT MODEL OF MPC-24

(45 DEGREE DROP MODEL)

DELETED

FIGURE 3.4.10; DELETED

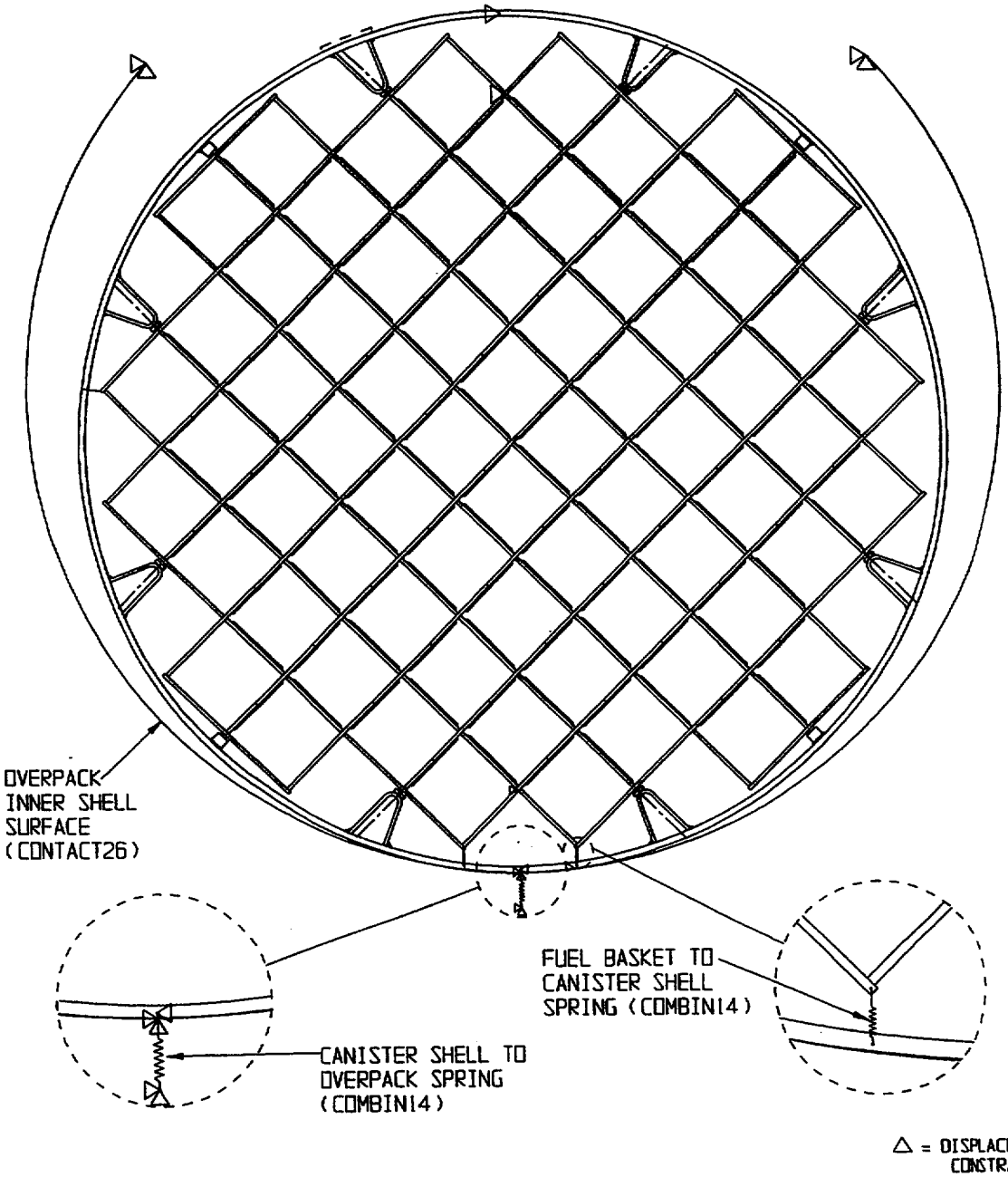

FIGURE 3.4.11: FINITE ELEMENT MODEL OF MPC-68

(45 DEGREE DROP MODEL)

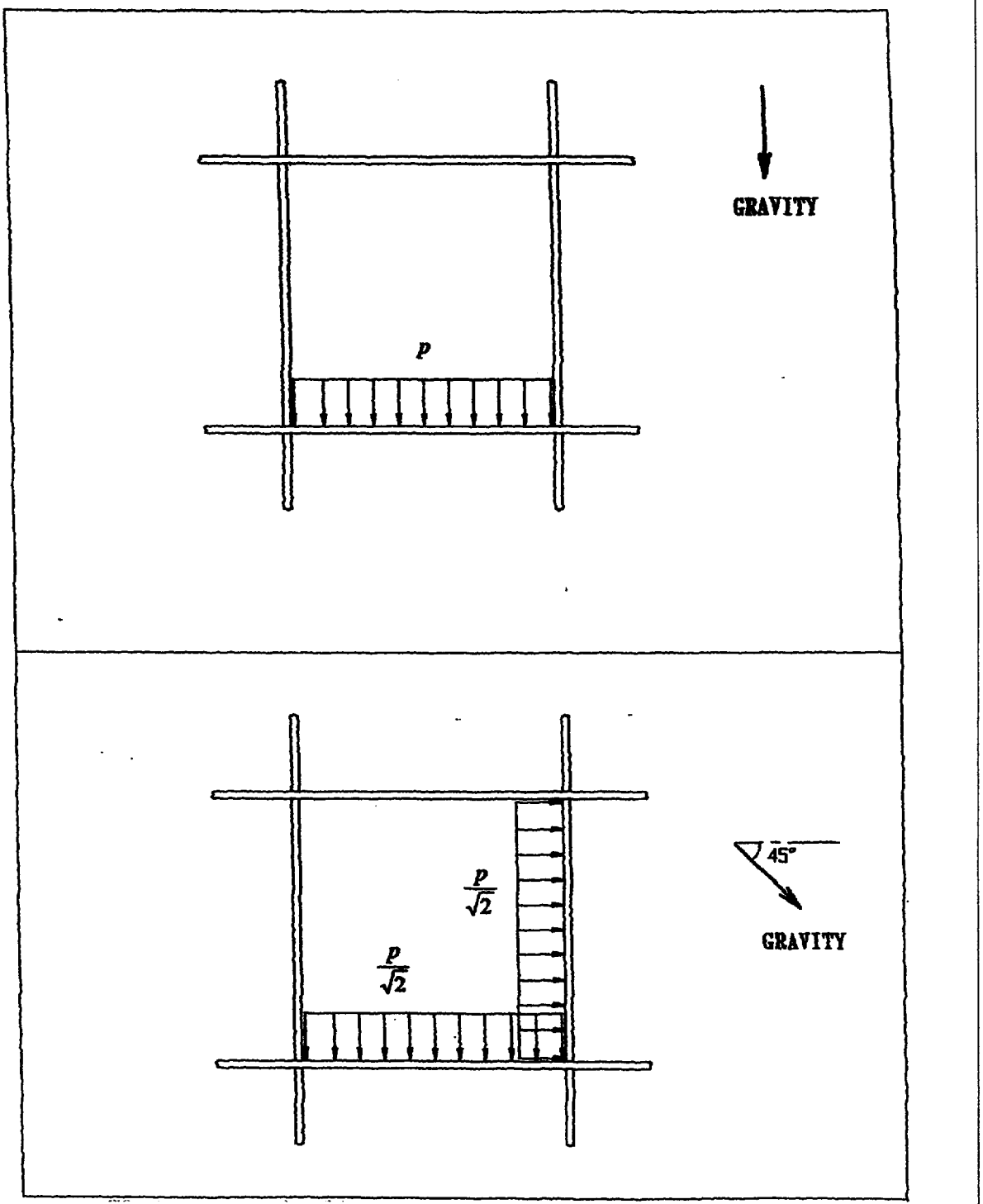

FIGURE 3.4.12: DETAIL OF FUEL ASSEMBLY PRESSURE LOAD ON MPC BASKET

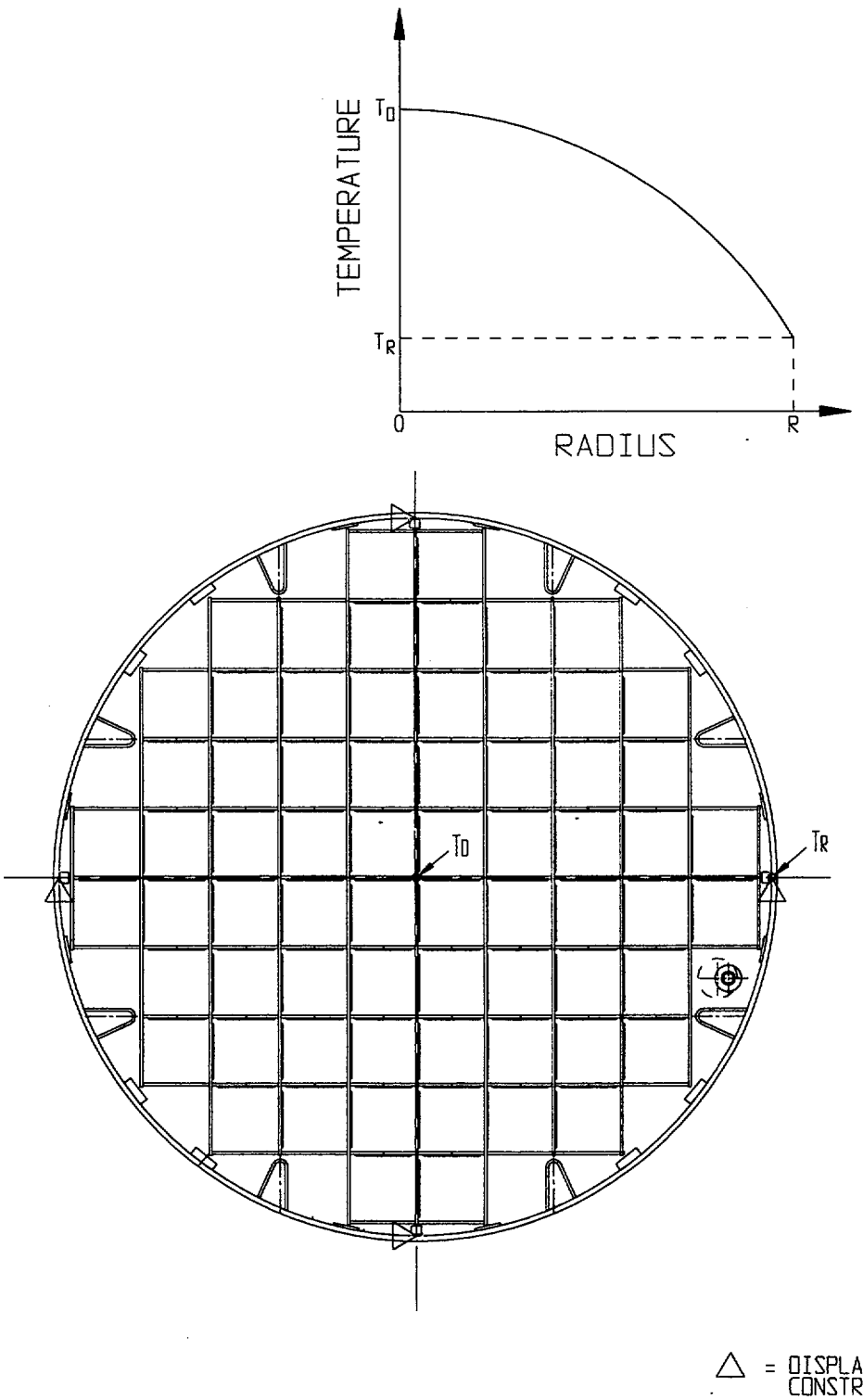

FIGURE 3.4.13; MPC THERMAL LOAD

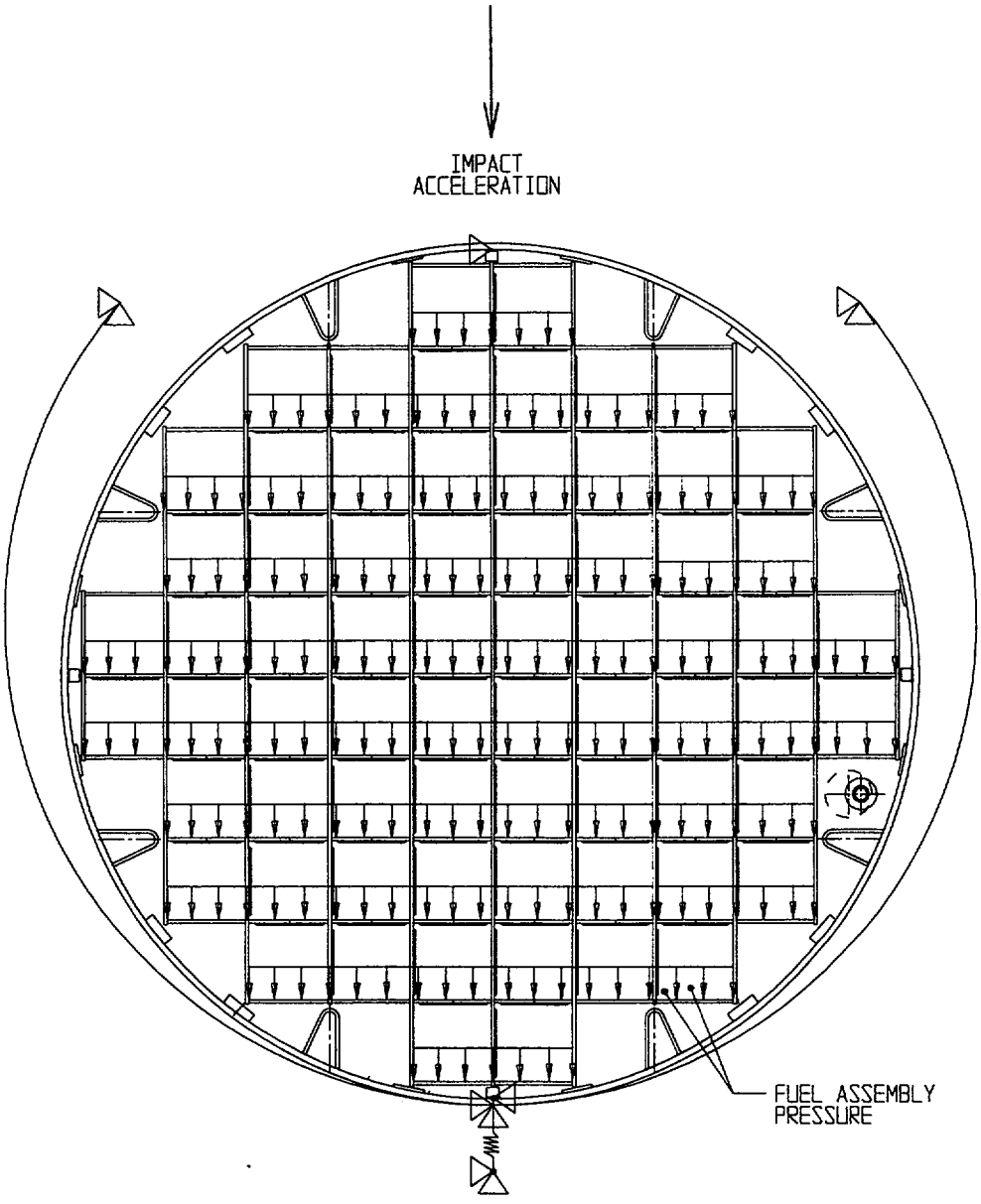

FIGURE 3.4.14; 0 DEGREE SIDE DROP OF MPC

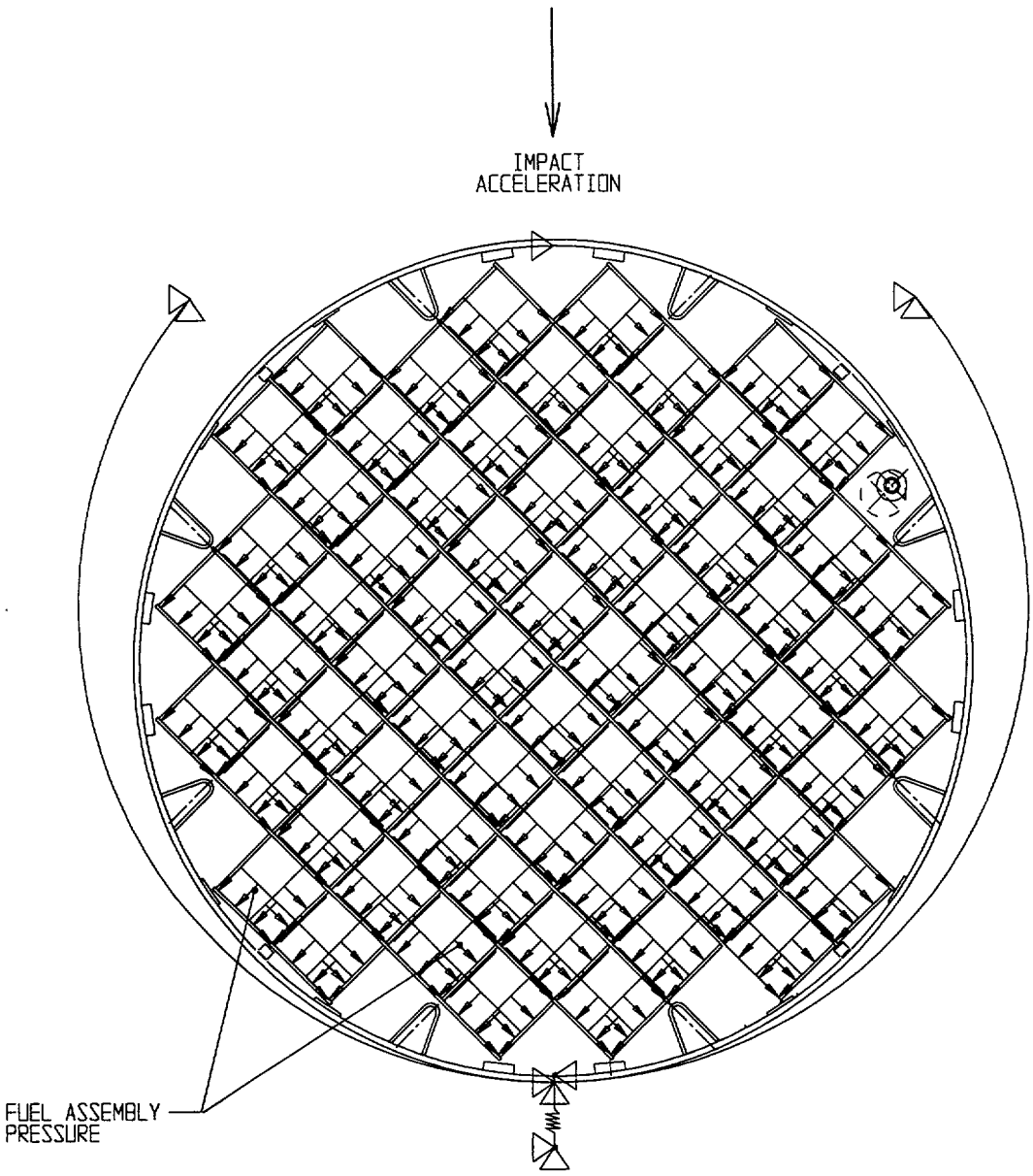

FIGURE 3.4.15; 45 DEGREE SIDE DROP OF MPC

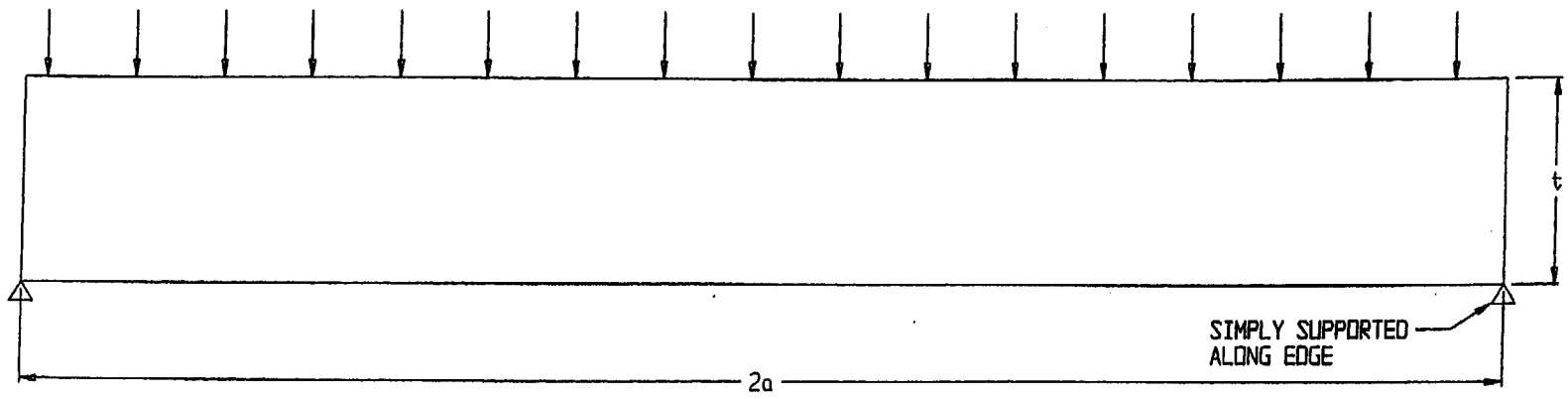

FIGURE 3.4.16; FREE BODY DIAGRAM OF THE MPC LID

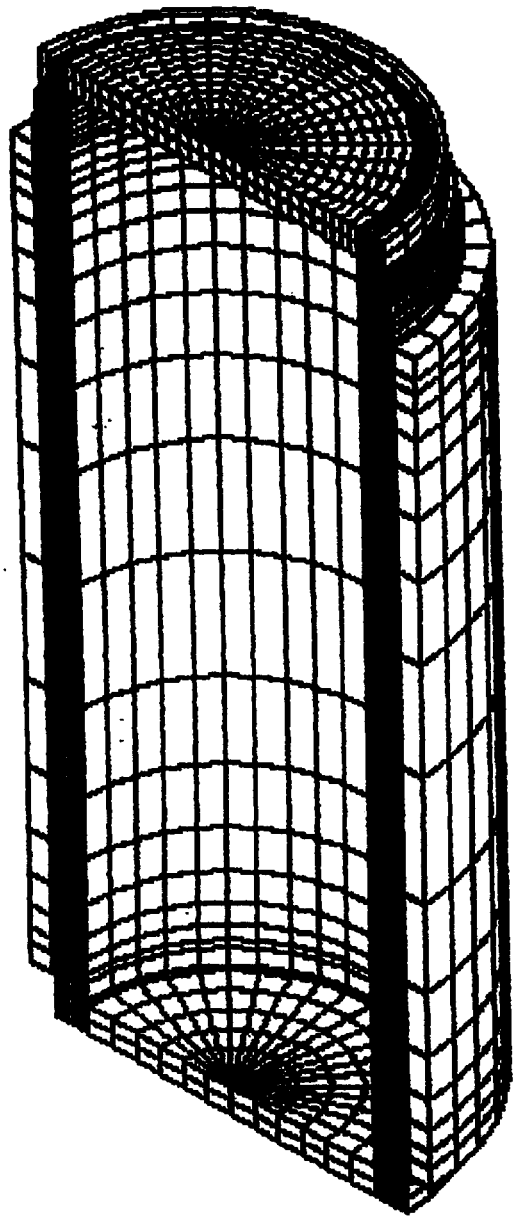

FIGURE 3.4.17; OVERPACK FINITE ELEMENT MODEL

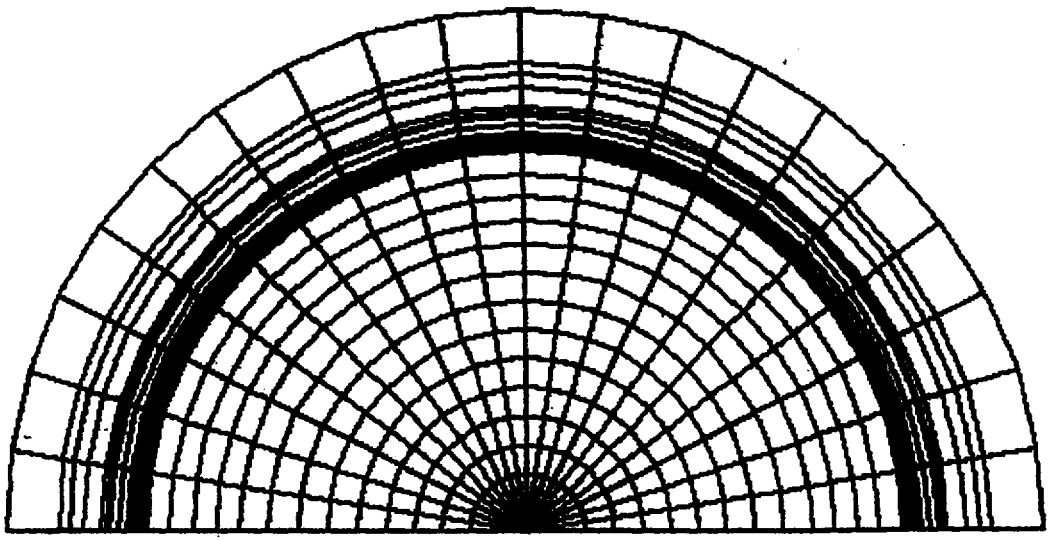

FIGURE 3.4.18; OVERPACK FINITE ELEMENT MODEL

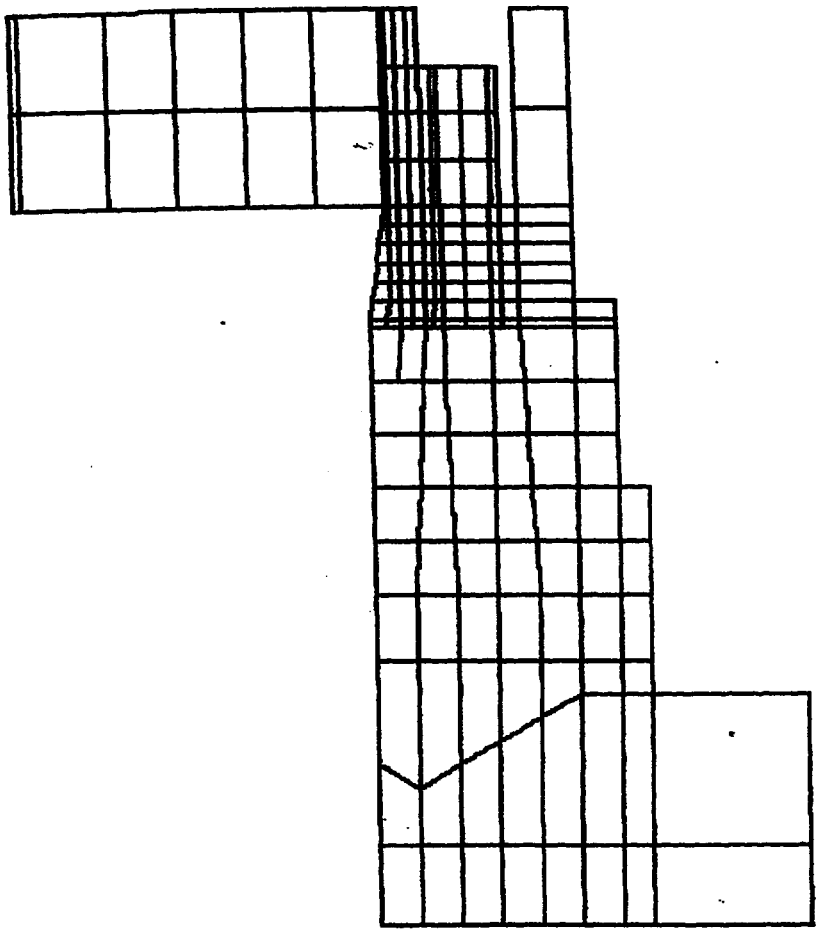

FIGURE 3.4.19; OVERPACK FINITE ELEMENT MODEL

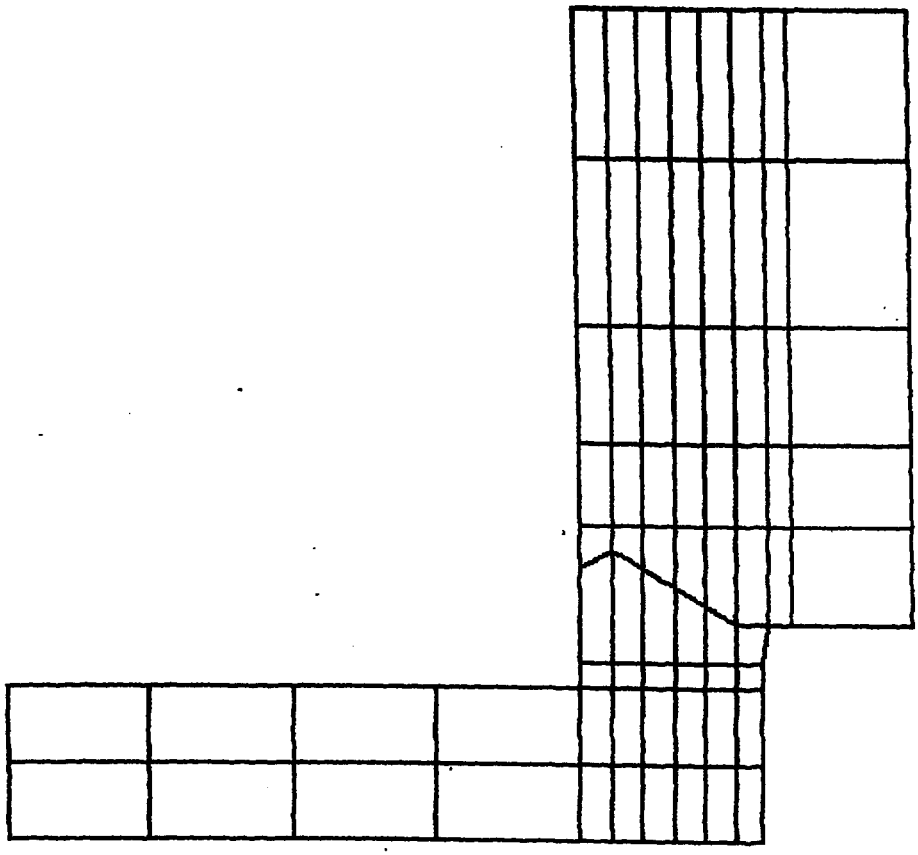

FIGURE 3.4.20; OVERPACK FINITE ELEMENT MODEL

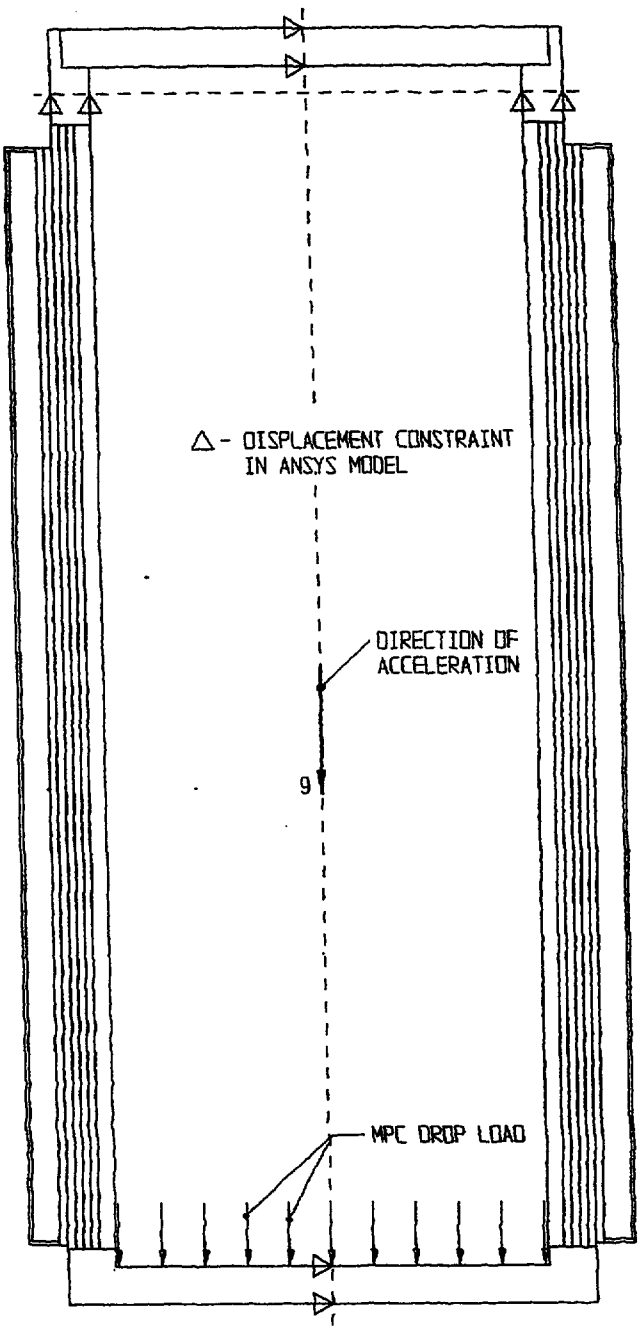

FIGURE 3.4.21; FREE BODY DIAGRAM OF OVERPACK - BOTTOM END DROP

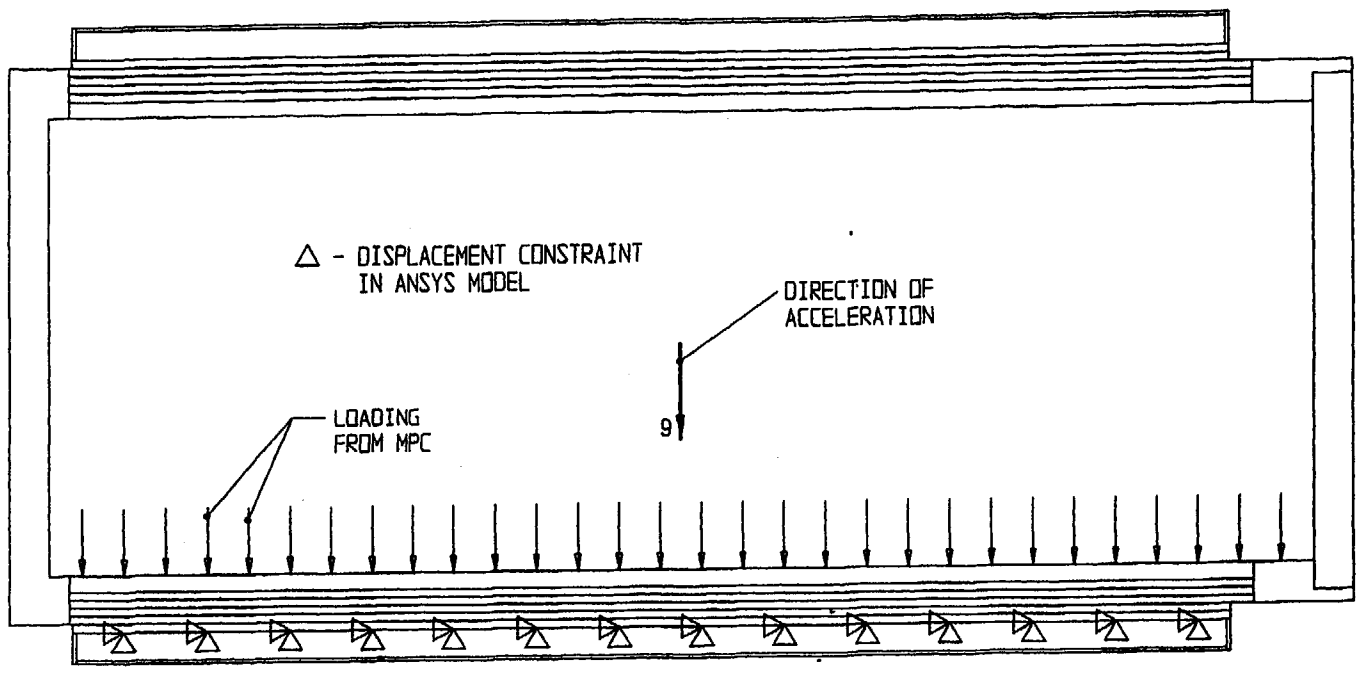

FIGURE 3.4.22; FREE BODY DIAGRAM OF OVERPACK - SIDE DROP

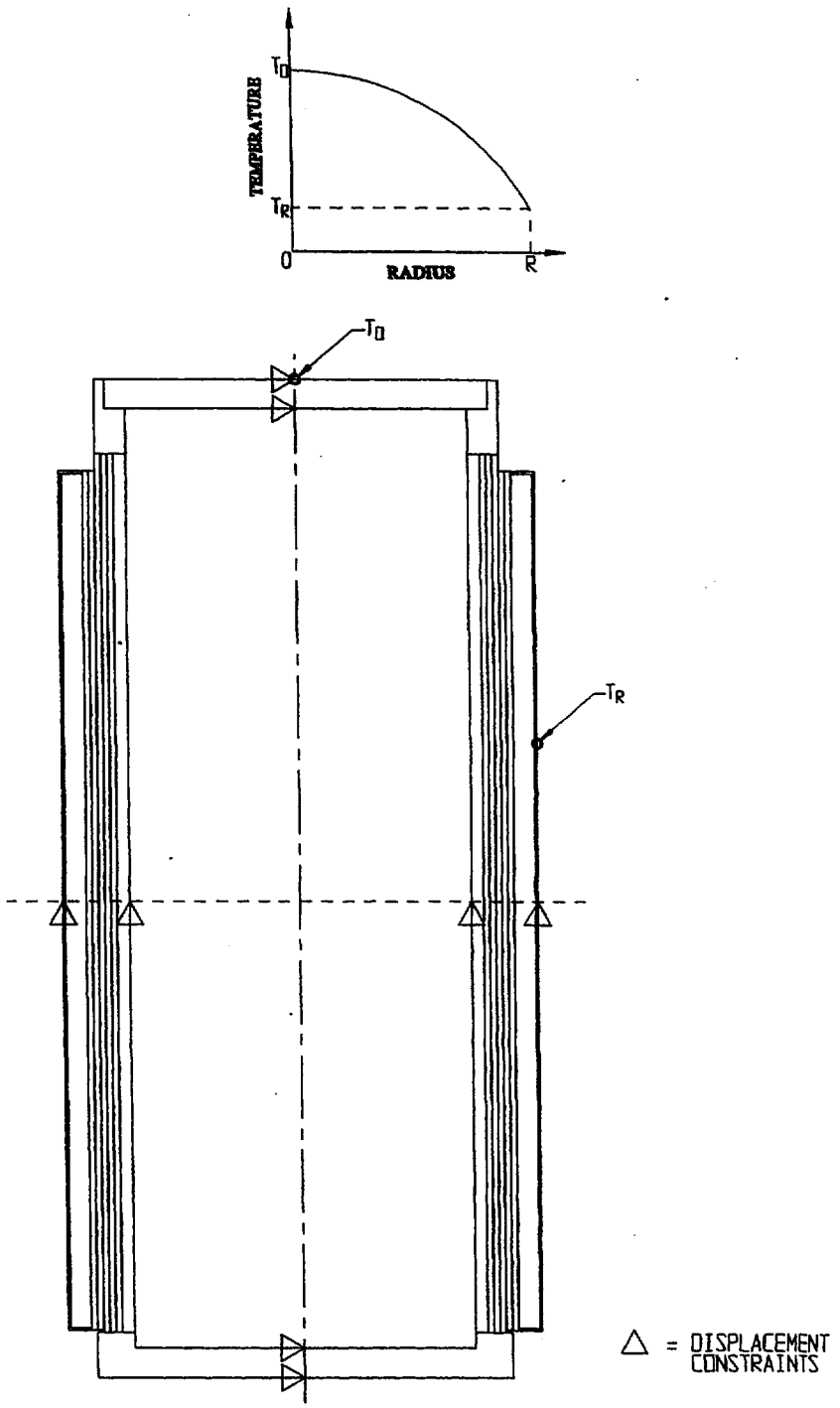

FIGURE 3.4.23; FREE BODY DIAGRAM OF OVERPACK - THERMAL LOAD

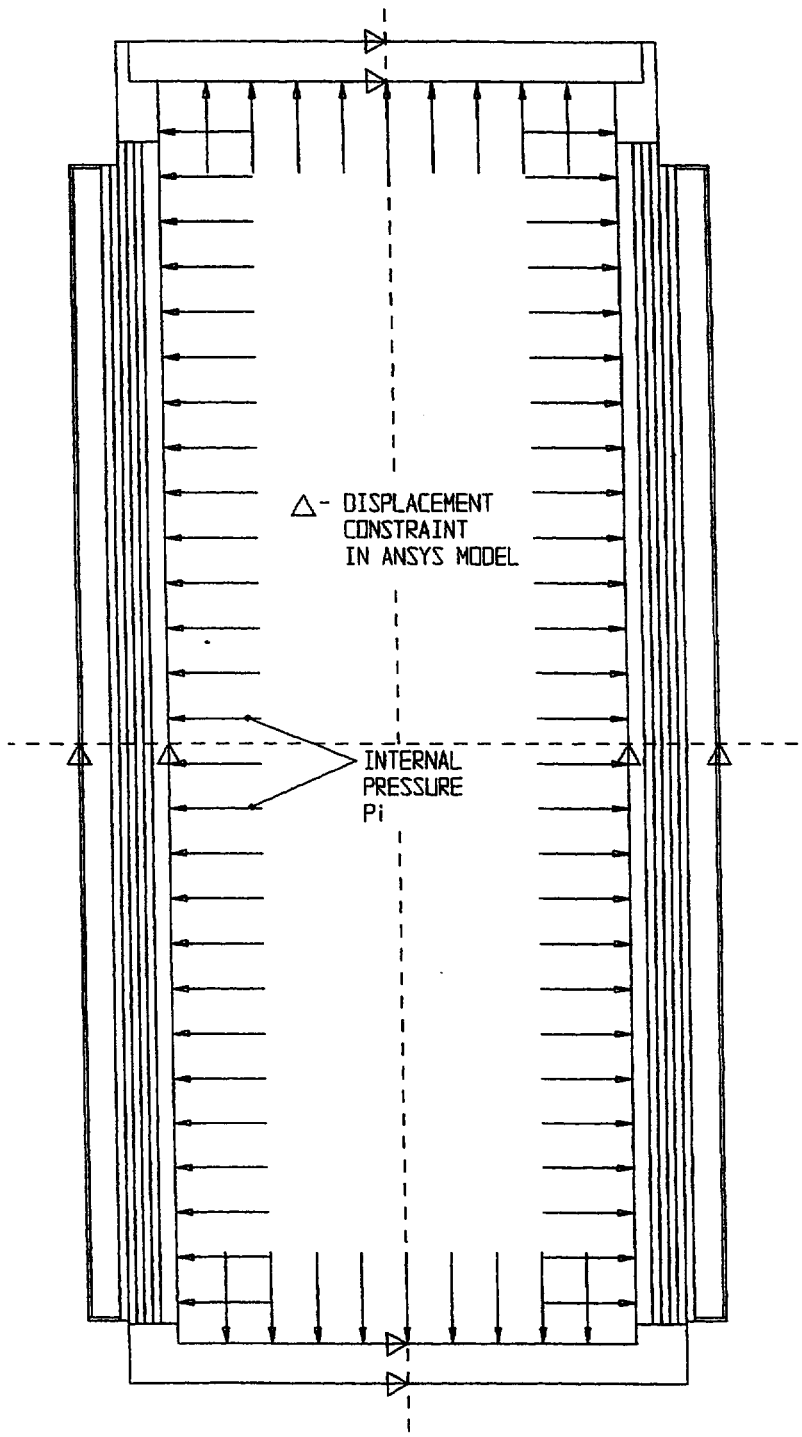

FIGURE 3.4.24; FREE BODY DIAGRAM OF OVERPACK - INTERNAL PRESSURE

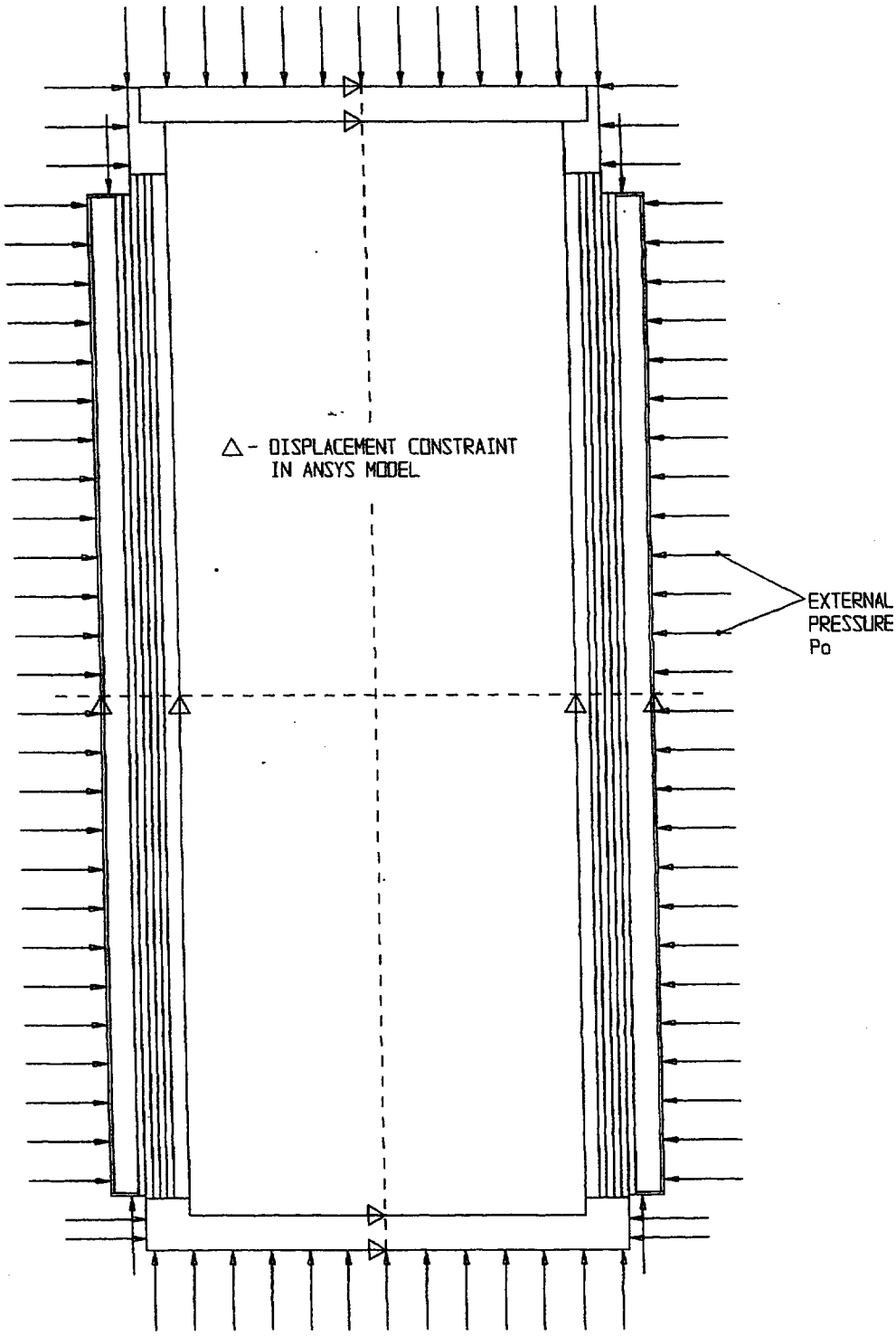

FIGURE 3.4.25; FREE BODY DIAGRAM OF OVERPACK - EXTERNAL PRESSURE

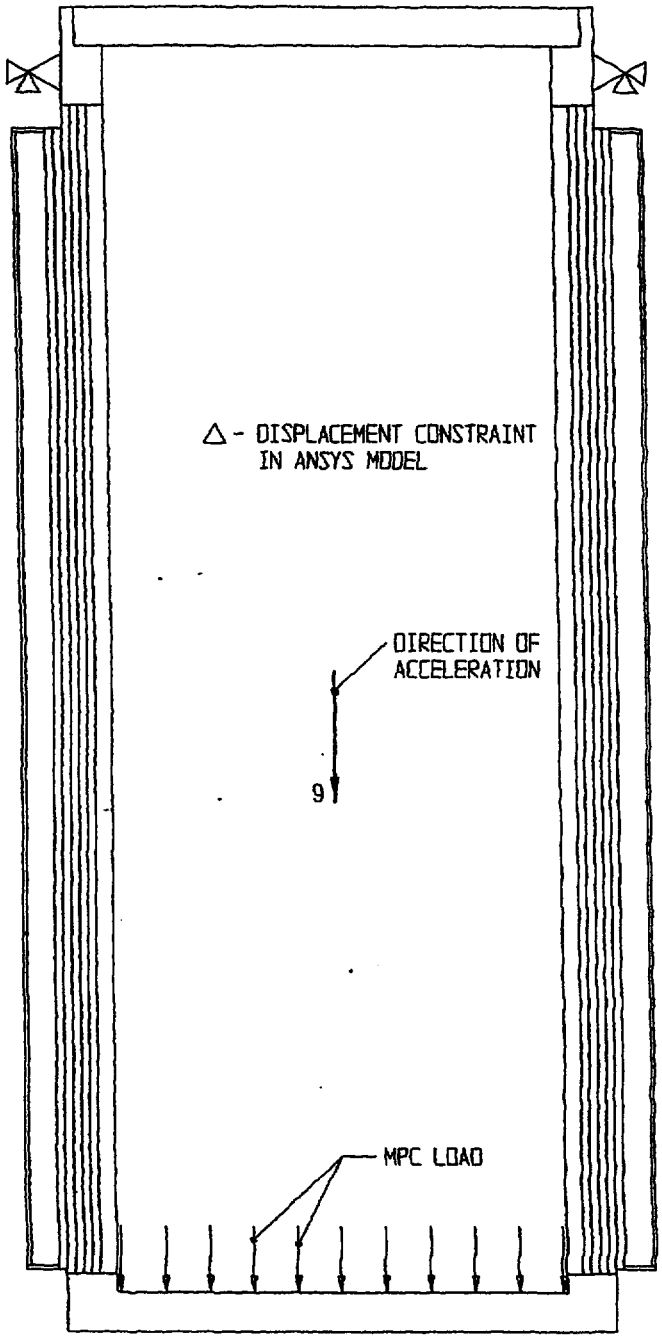

FIGURE 3.4.26; FREE BODY DIAGRAM OF OVERPACK - HANDLING LOAD

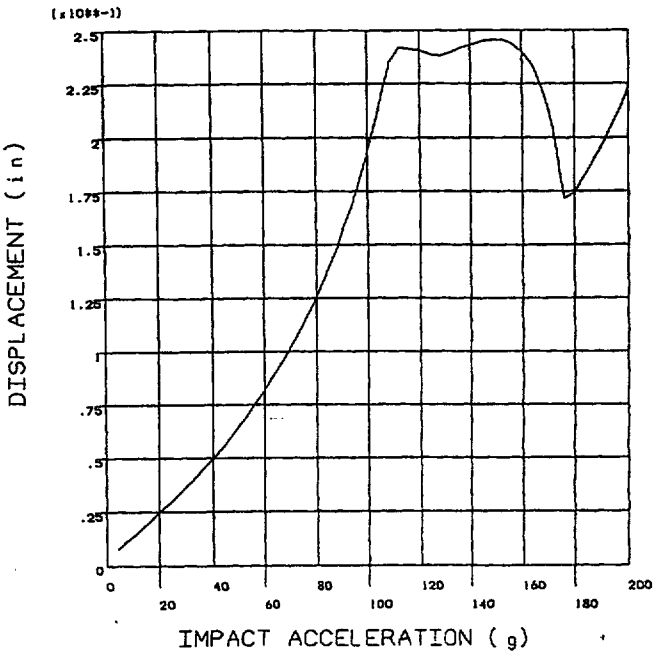

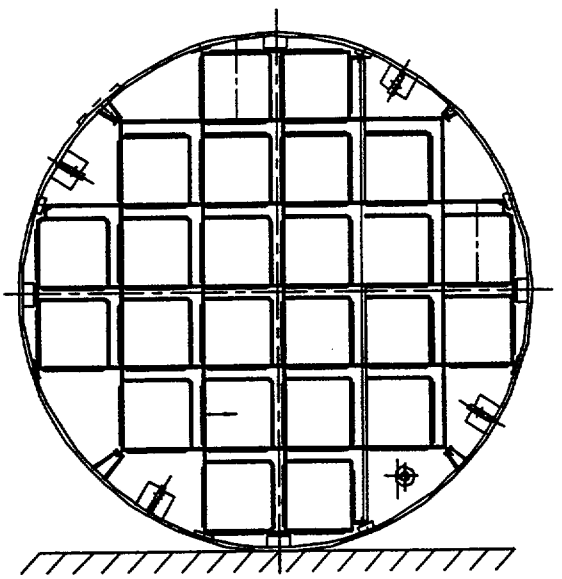

FIGURE 3.4.27; NON-LINEAR BUCKLING ANALYSIS FOR MPC-24 DISPLACEMENT Vs. IMPACT ACCELERATION (0° DROP)

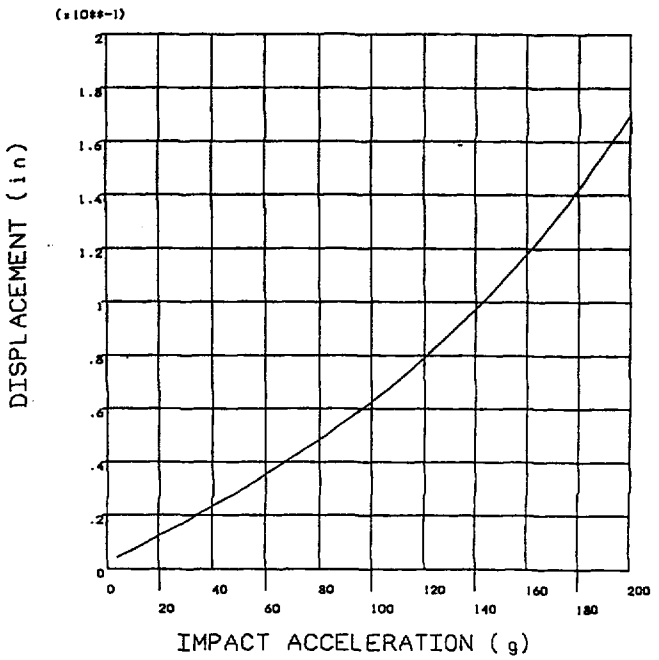

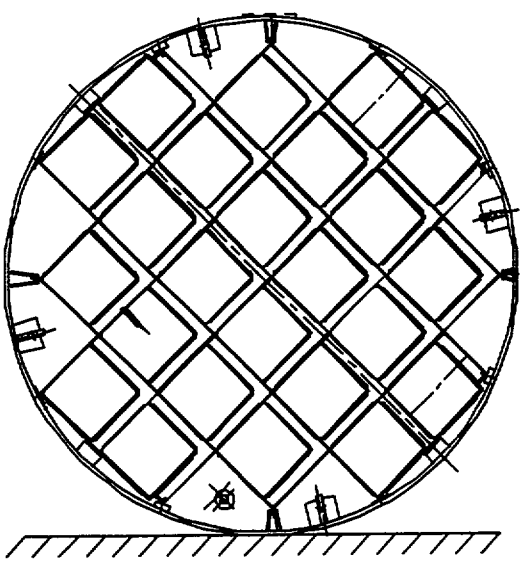

FIGURE 3.4.28; NON-LINEAR BUCKLING ANALYSIS FOR MPC-24 DISPLACEMENT Vs. IMPACT ACCELERATION (45° DROP)

DELETED

FIGURE 3.4.29;

DELETED

FIGURE 3.4.30;

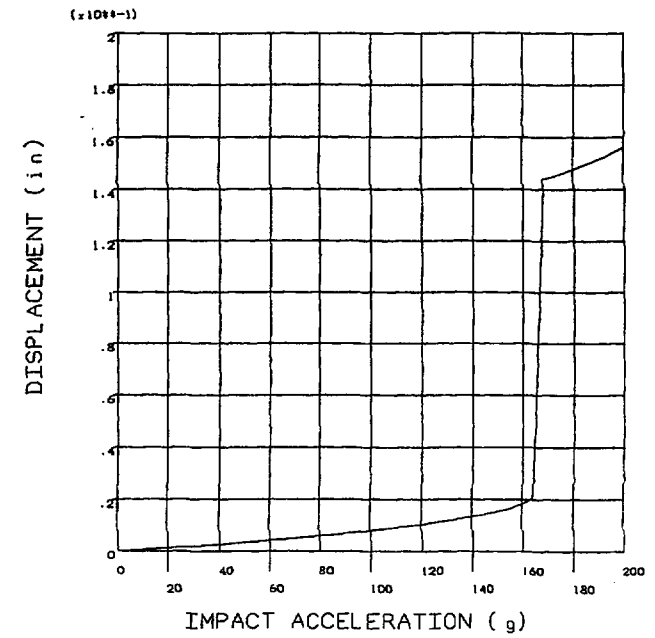

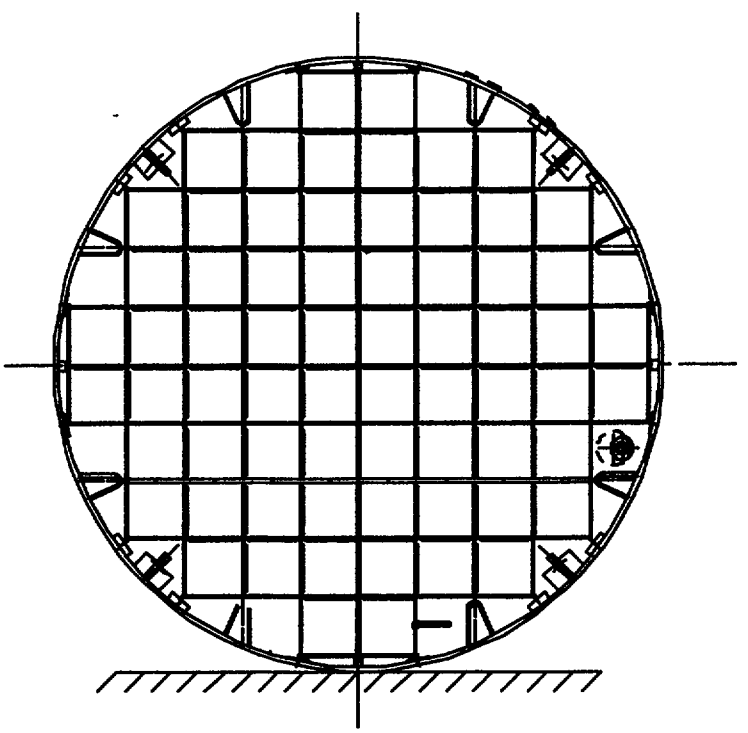

FIGURE 3.4.31; NON-LINEAR BUCKLING ANALYSIS FOR MPC-68 DISPLACEMENT Vs. IMPACT ACCELERATION (0° DROP)

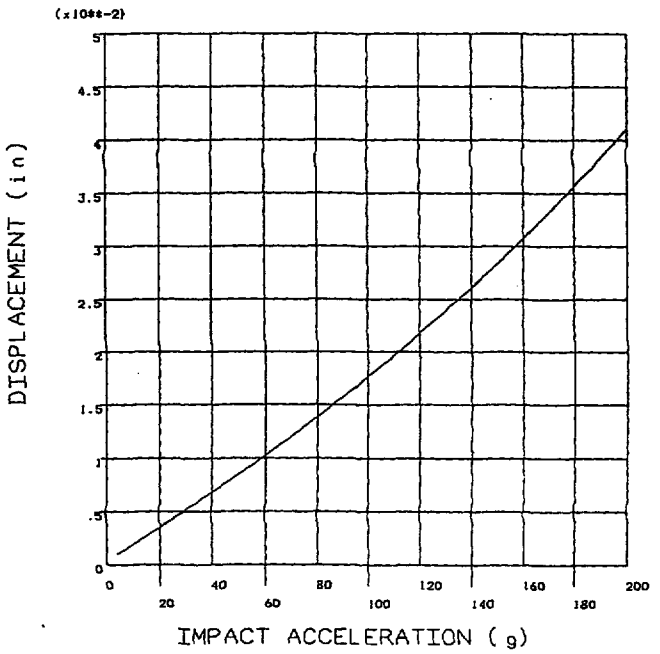

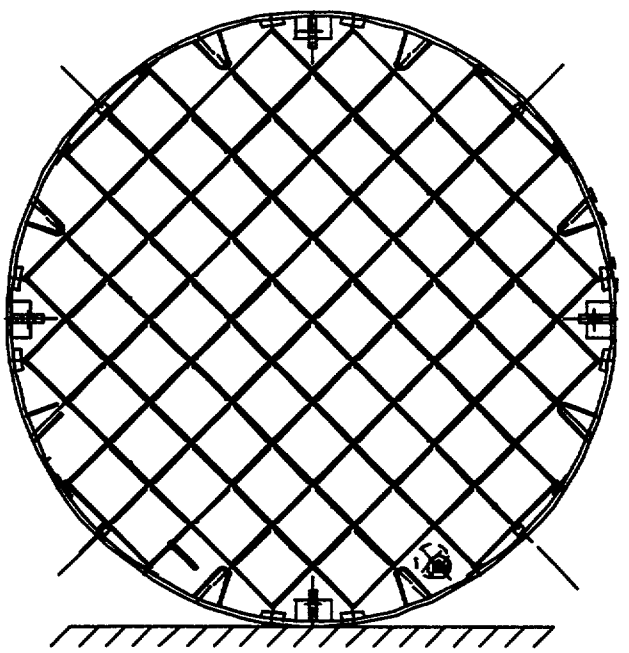

FIGURE 3.4.32; NON-LINEAR BUCKLING ANALYSIS FOR MPC-68 DISPLACEMENT Vs. IMPACT ACCELERATION (45° DROP)

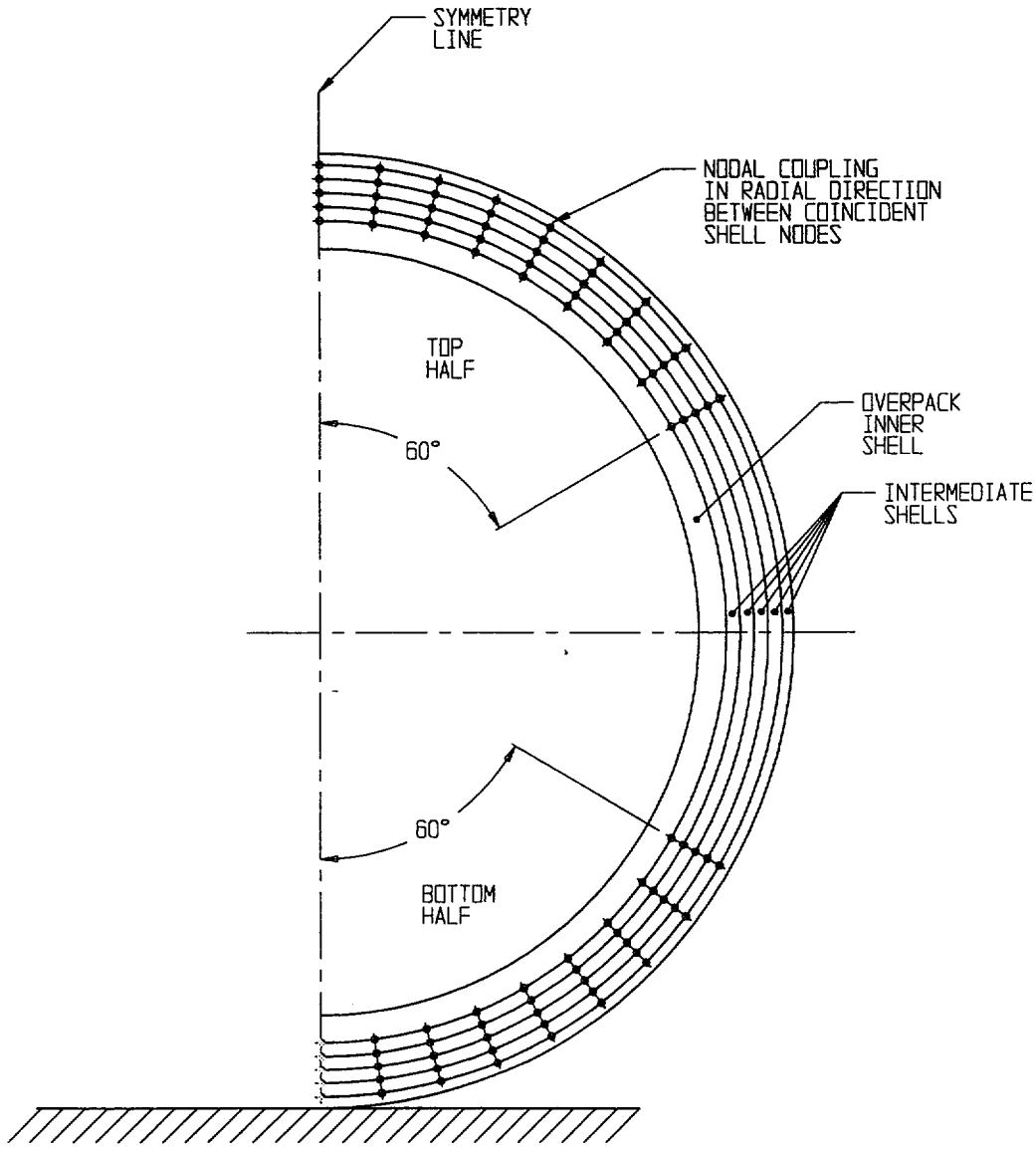

FIGURE 3.4.33; NODAL COUPLING IN OVERPACK FINITE ELEMENT MODEL

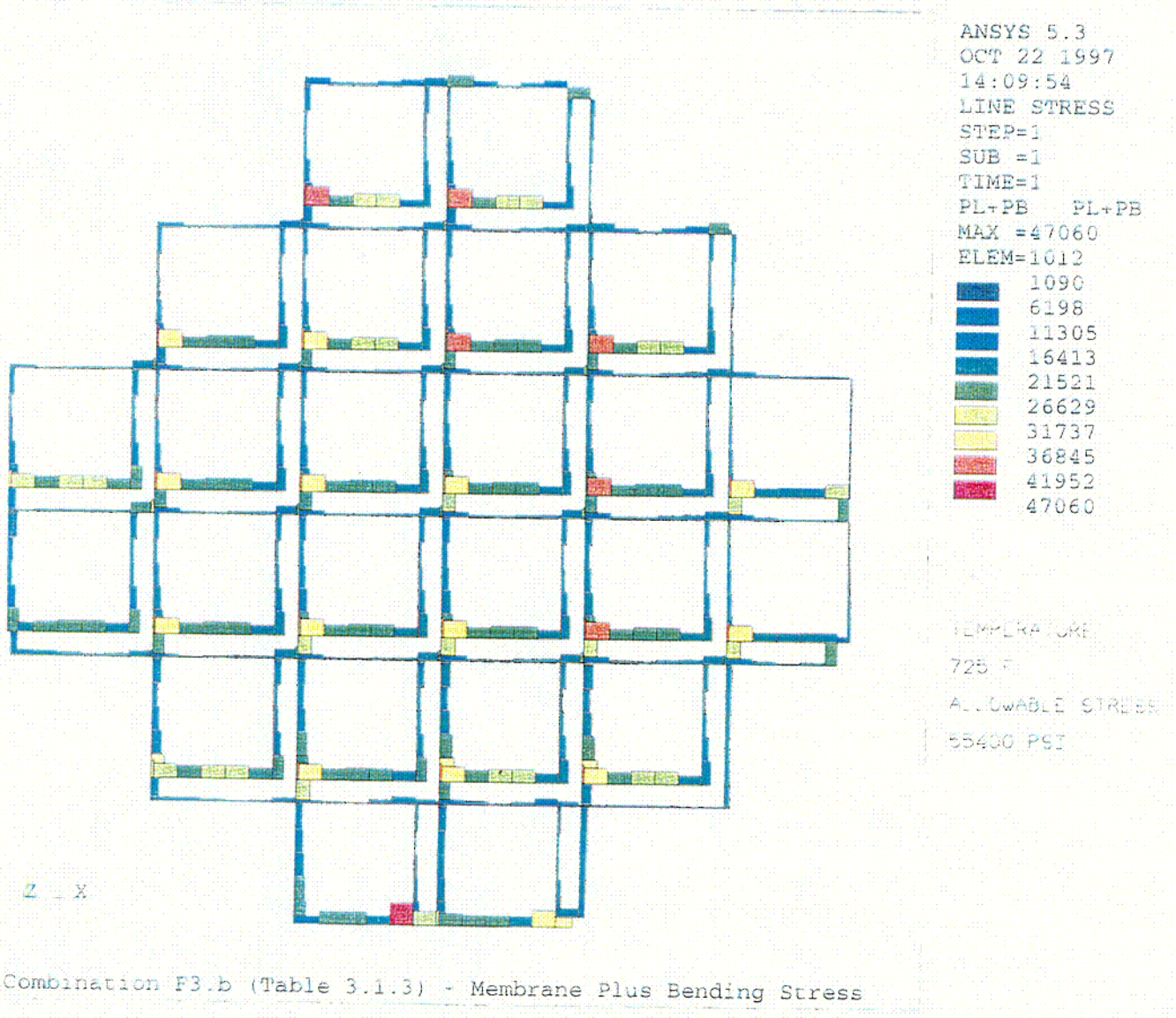

Load Combination F3.b (Table 3.1.3) - Membrane Plus Bending Stress

FIGURE 3.4.34; CRITICAL STRESS RESULTS FOR THE MPC-24

C01

DELETED

FIGURE 3.4.35;

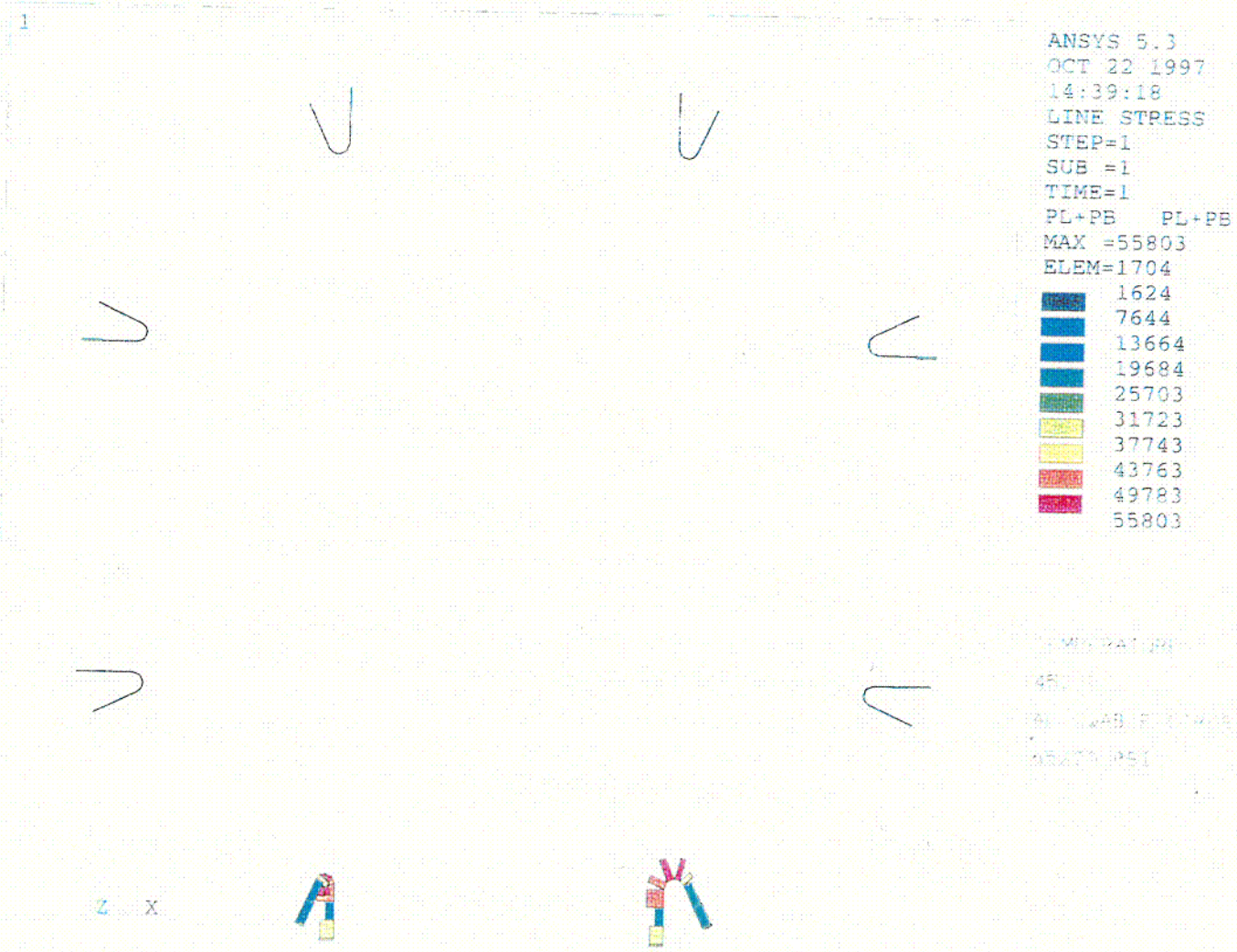

Load Combination E3.b (Table 3.1.3) - Membrane Plus Bending Stress

FIGURE 3.4.36: CRITICAL STRESS RESULTS FOR THE MPC-68

C02

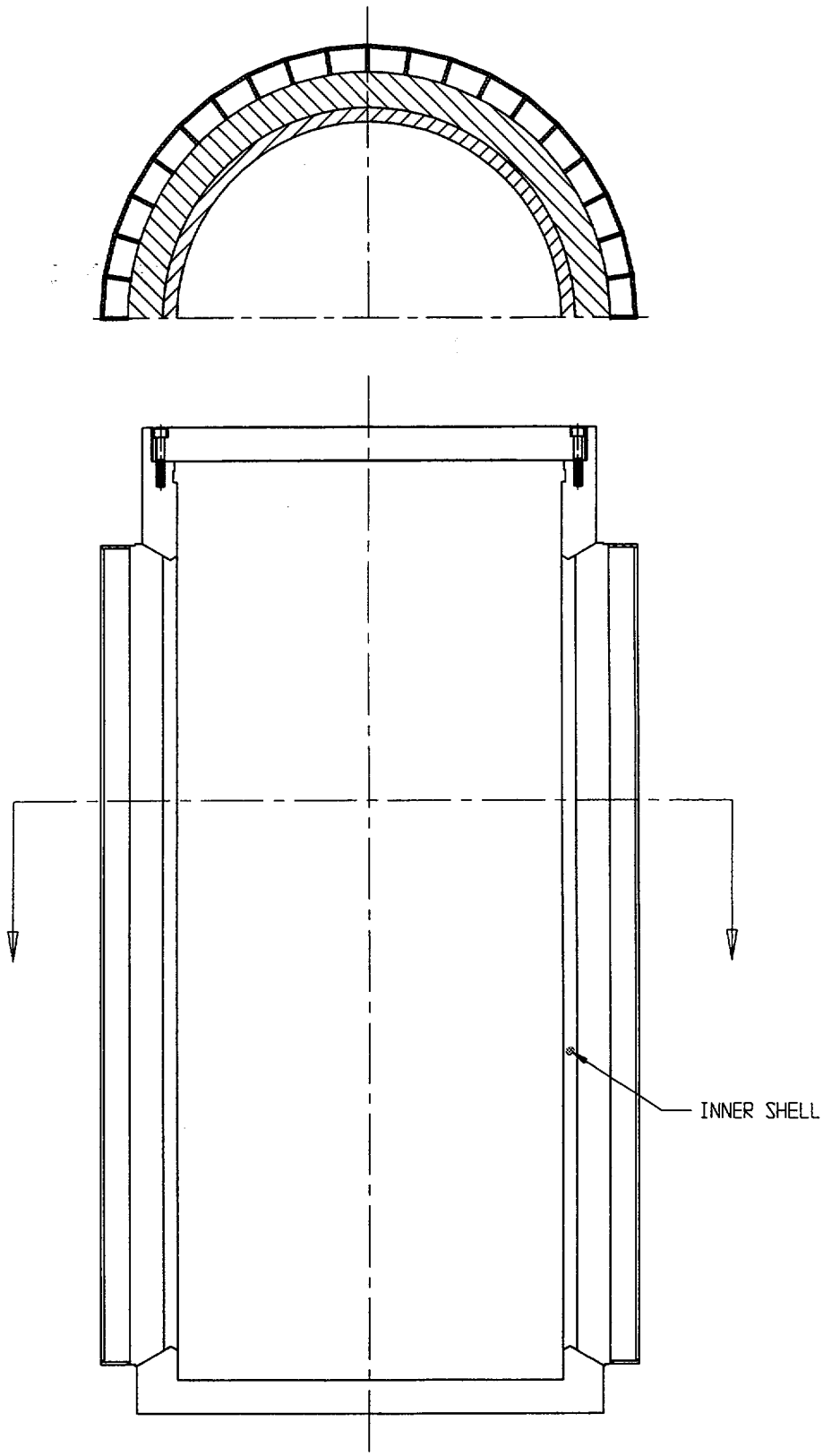

FIGURE 3.4.37; LOCATION OF MINIMUM SAFETY FACTOR FOR LOAD CASE 01

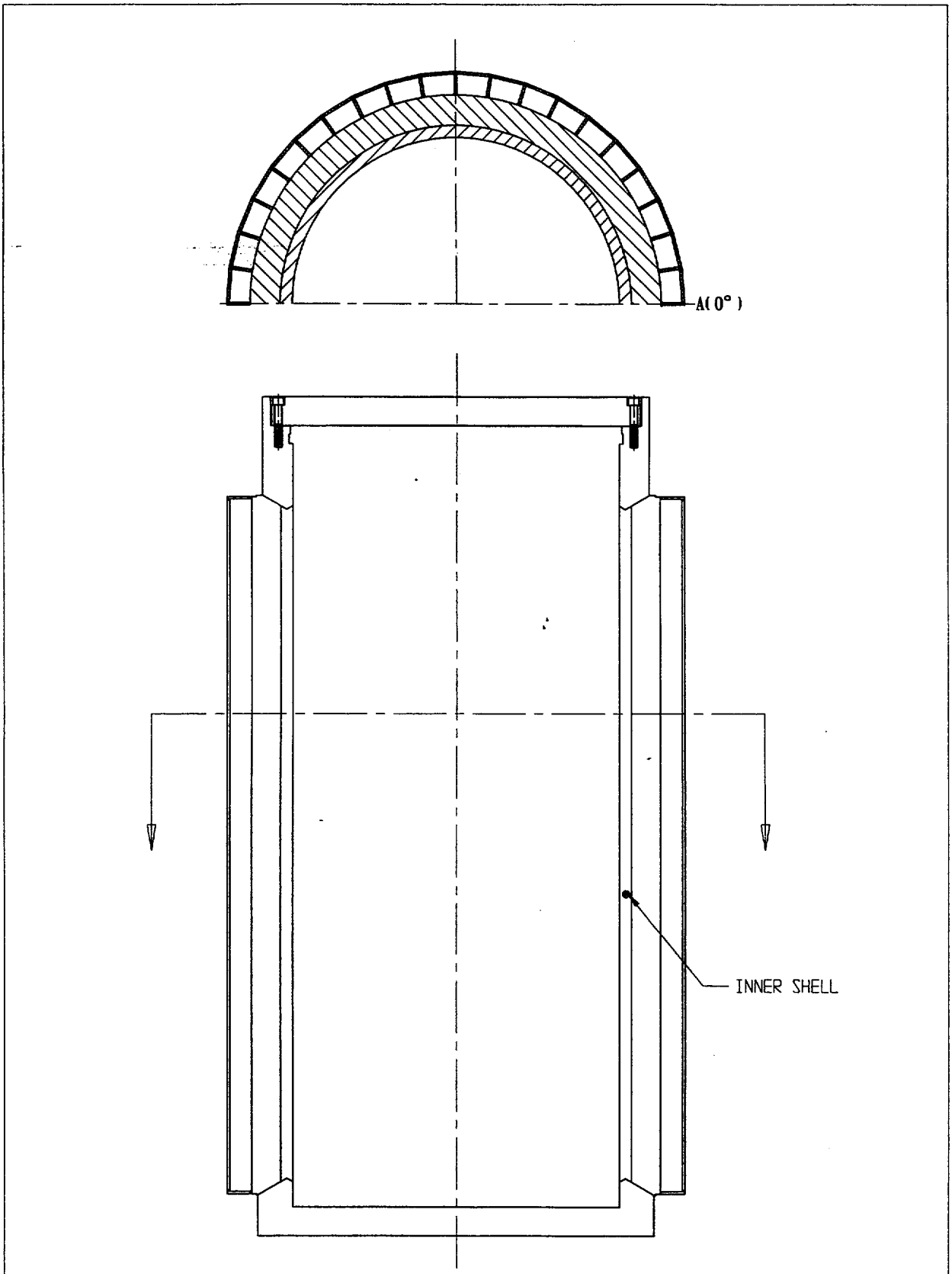

FIGURE 3.4.38; LOCATION OF MINIMUM SAFETY FACTOR FOR LOAD CASE 02

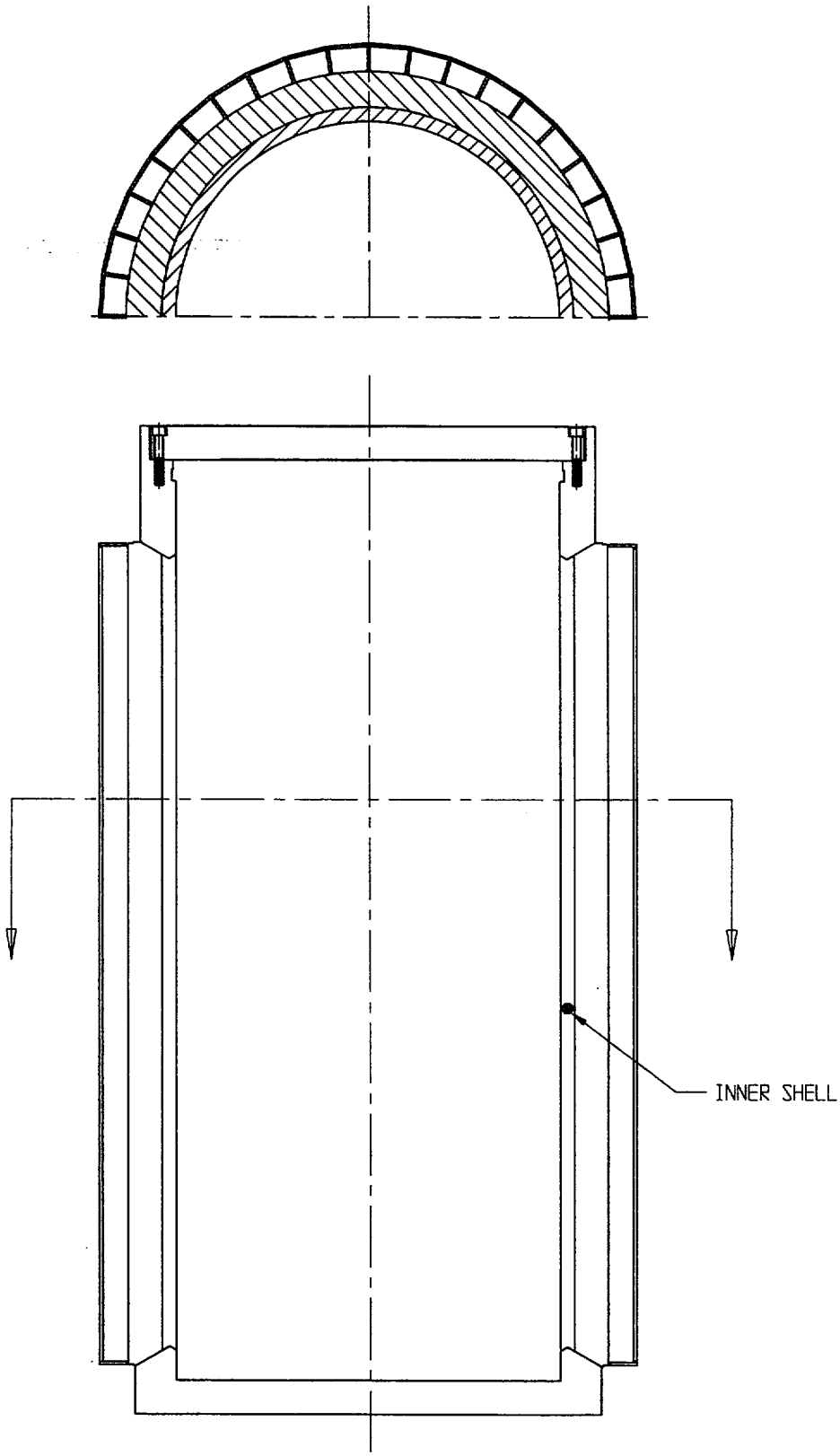

FIGURE 3.4.39; LOCATION OF MINIMUM SAFETY FACTOR FOR LOAD CASE 03

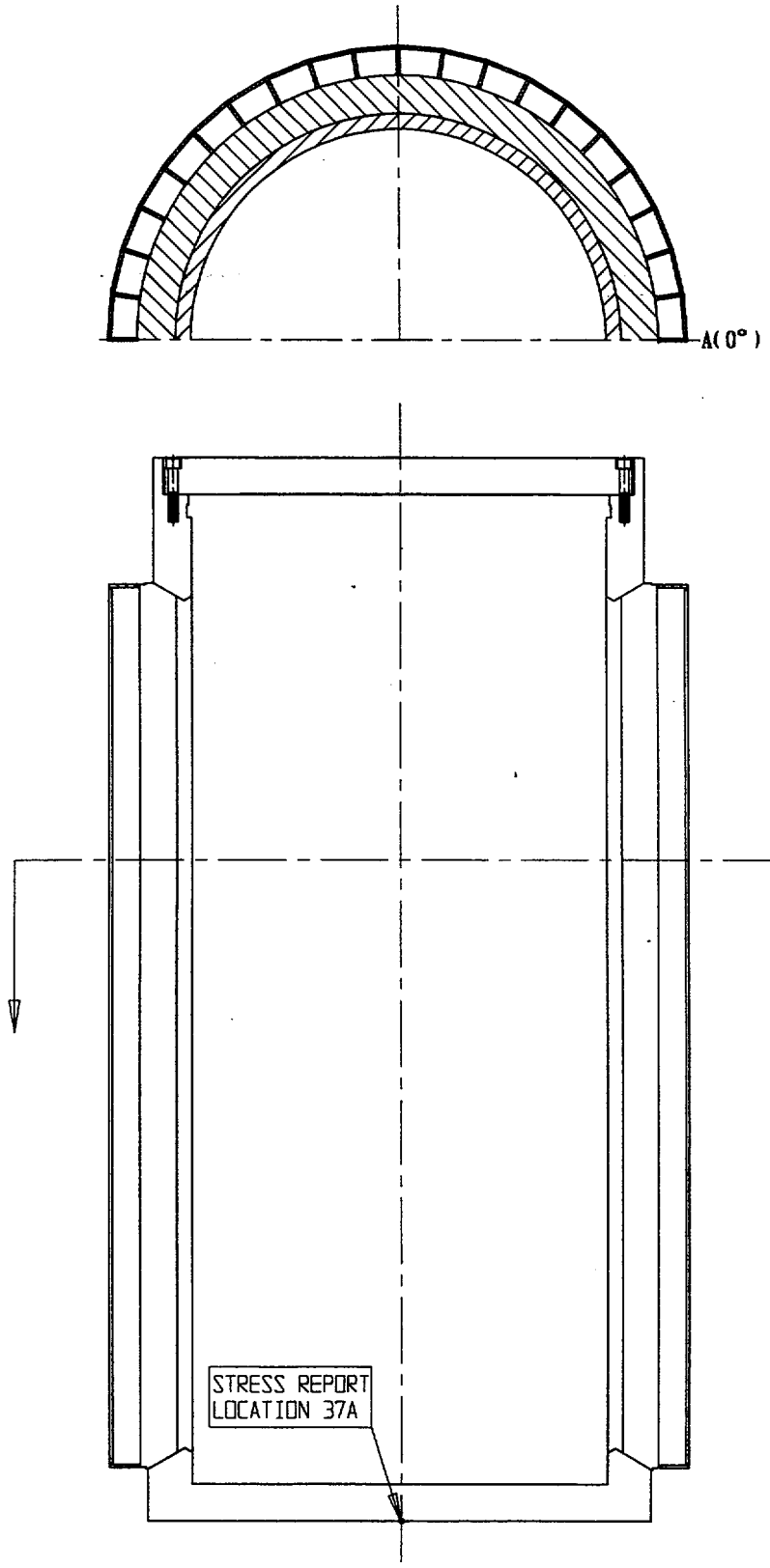

FIGURE 3.4.40; LOCATION OF MINIMUM SAFETY FACTOR FOR LOAD CASE 04.a

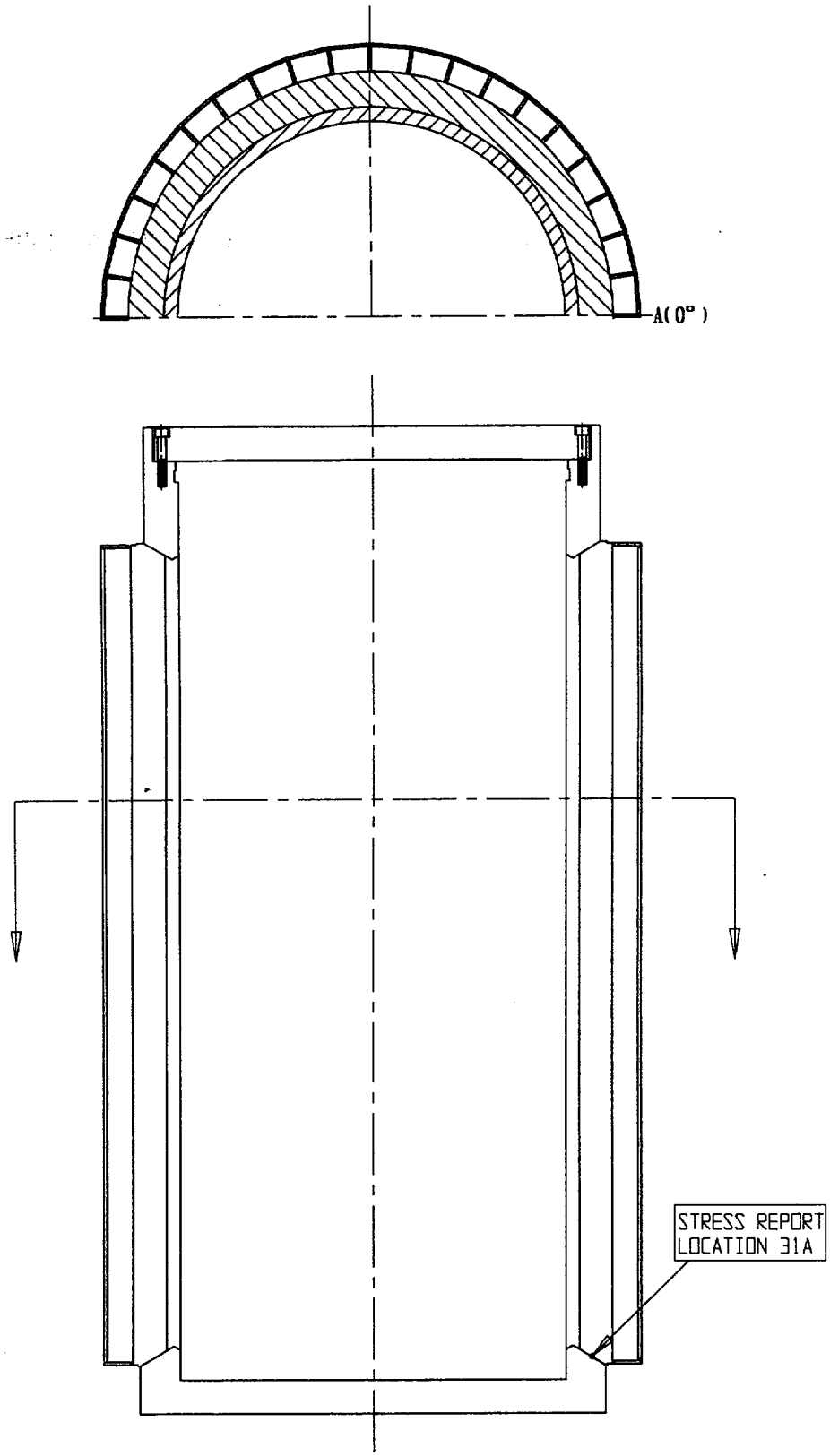

FIGURE 3.4.41; LOCATION OF MINIMUM SAFETY FACTOR FOR LOAD CASE 04.b

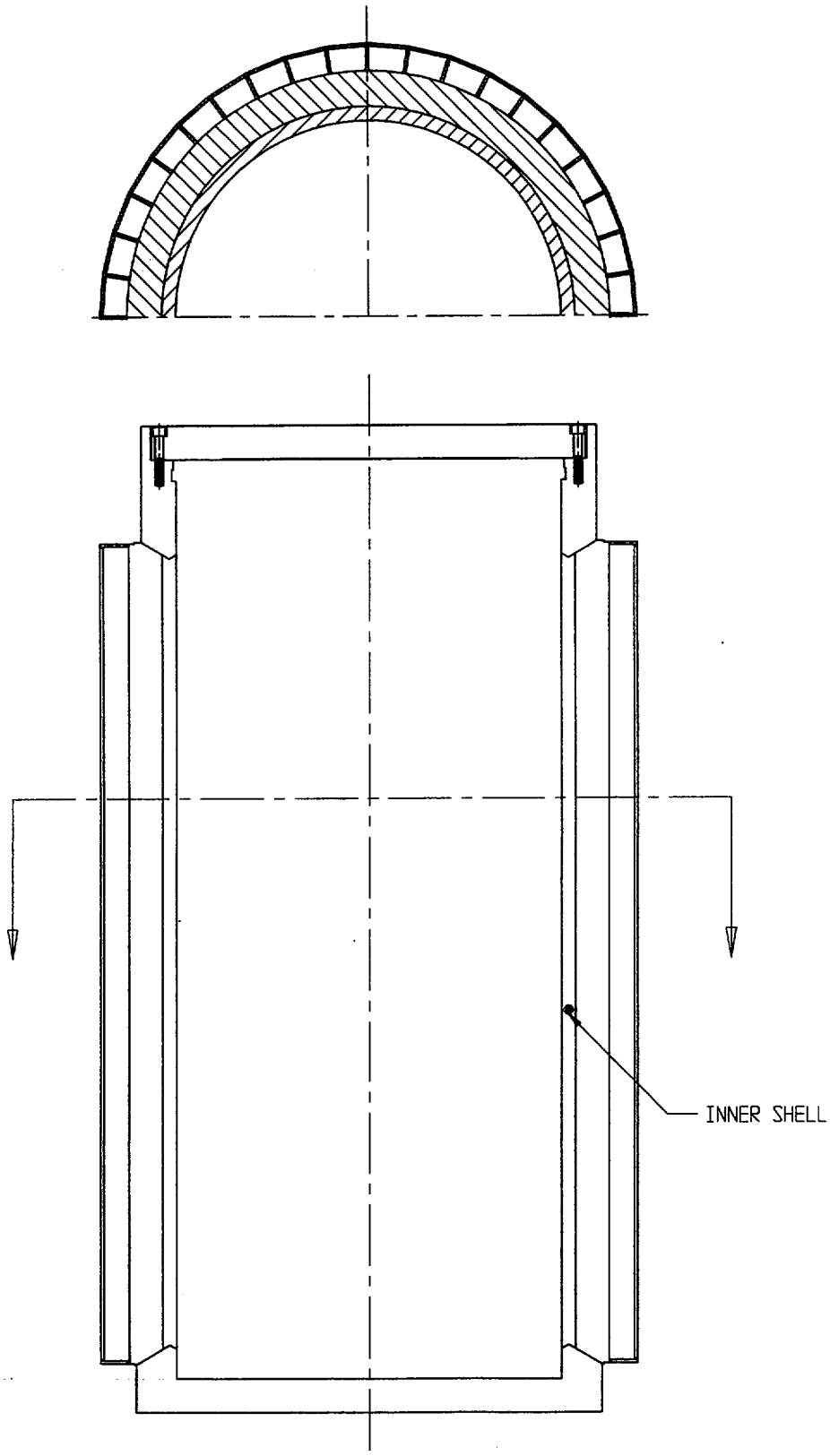

FIGURE 3.4.42; LOCATION OF MINIMUM SAFETY FACTOR FOR LOAD CASE 05

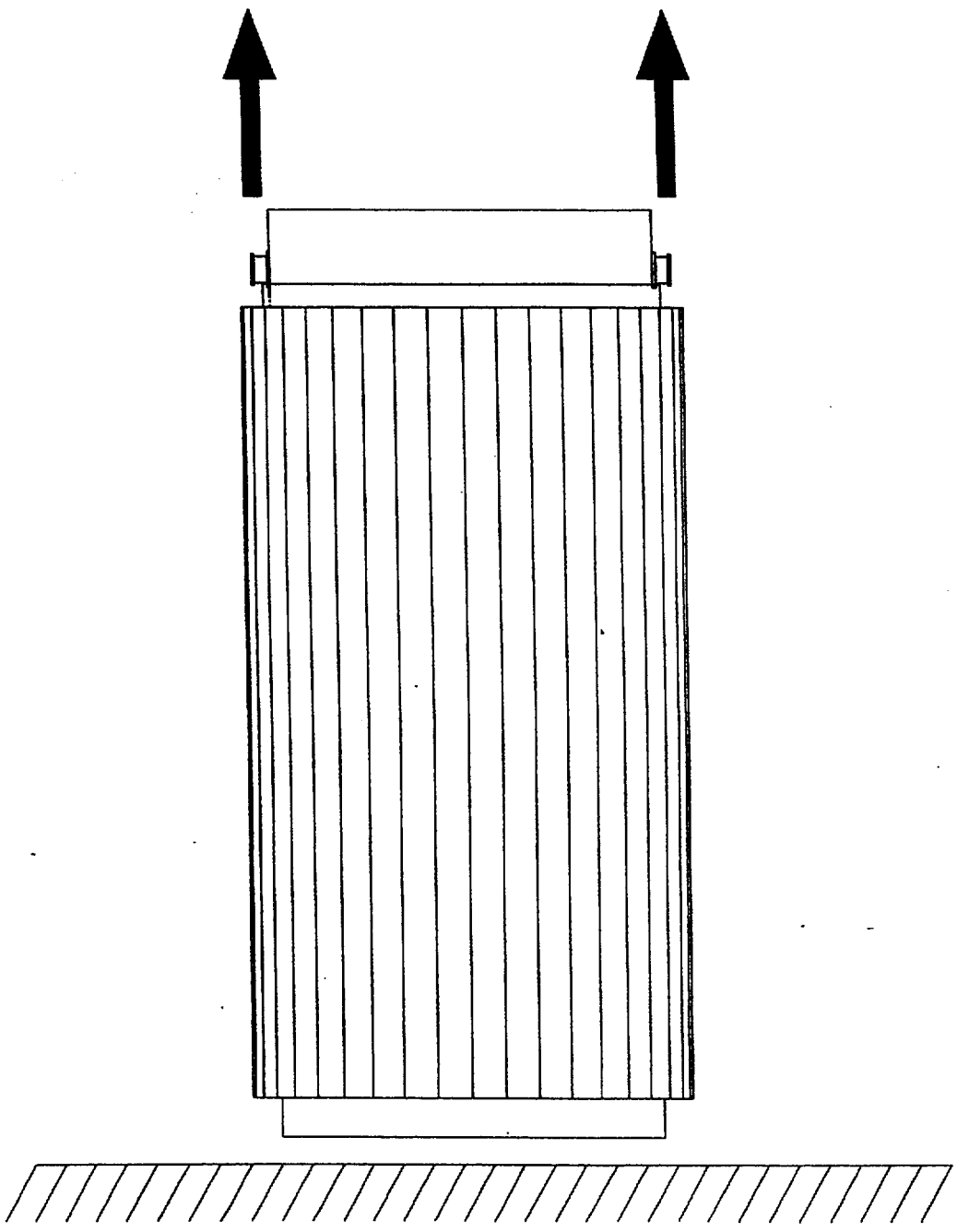

Figure 3.4.43; HI-STAR 100 Vertical Lifting

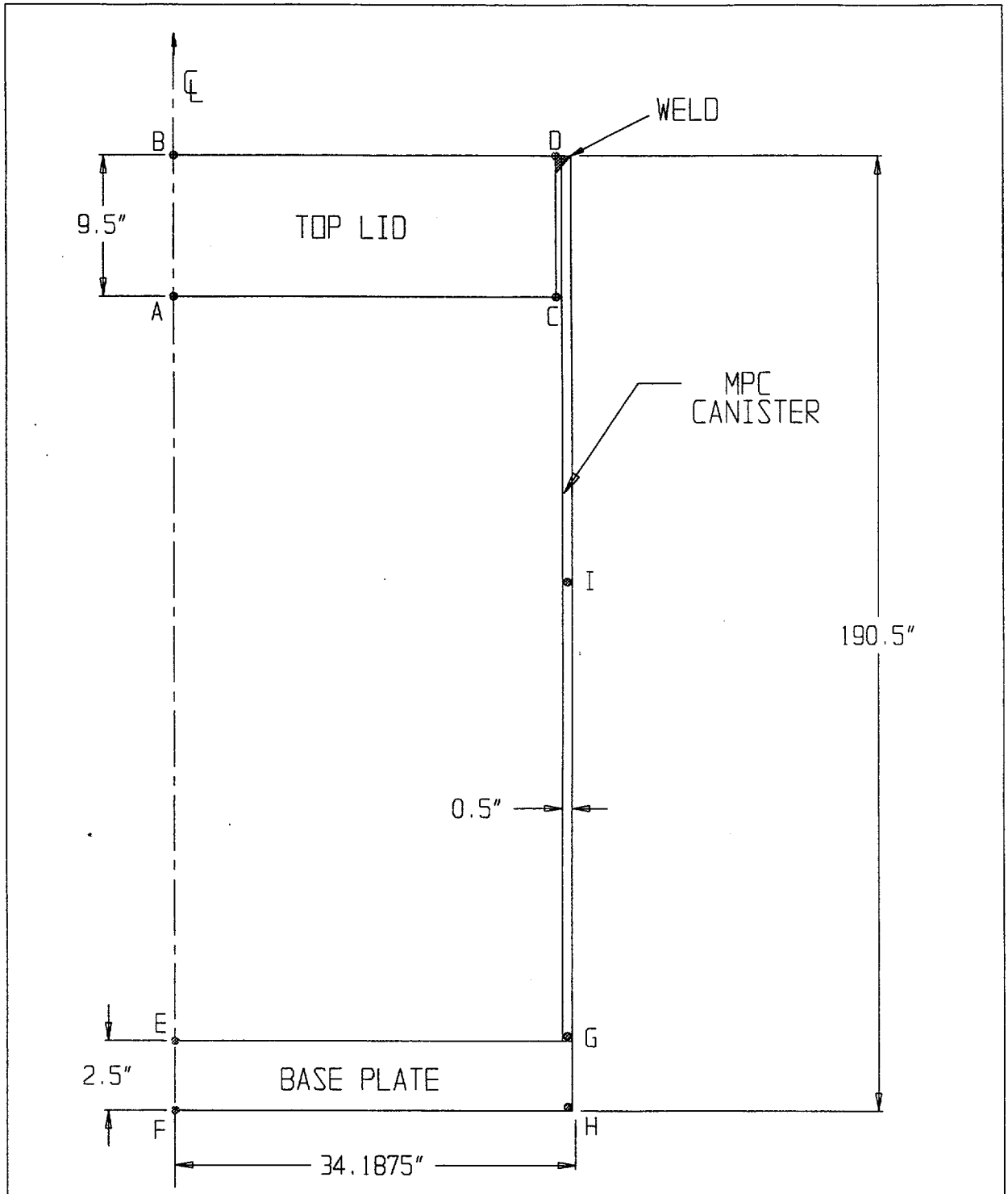

FIGURE 3.4.44 CONFINEMENT BOUNDARY MODEL SHOWING TEMPERATURE DATA POINTS

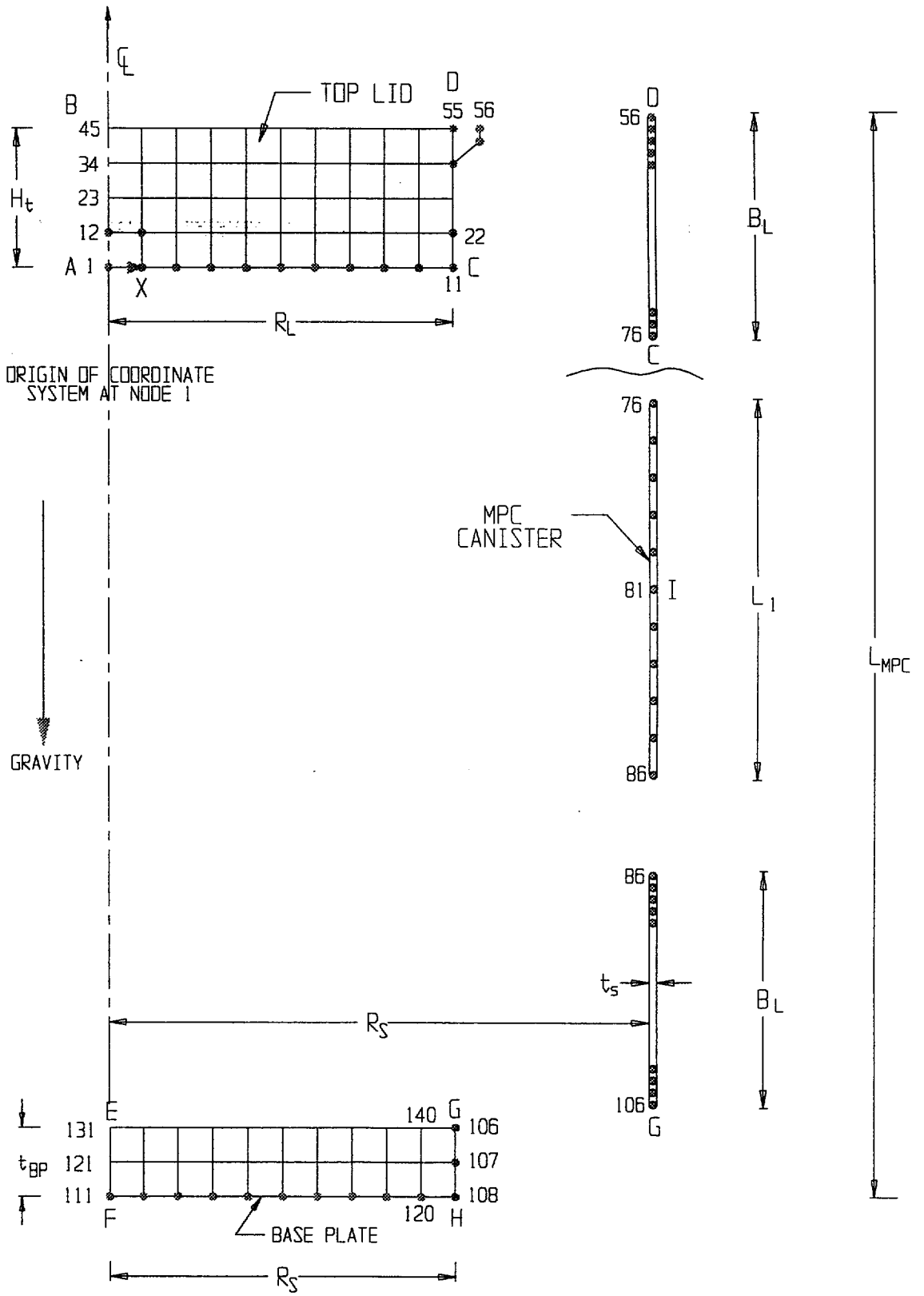

FIGURE 3.4.45 MPC - CONFINEMENT BOUNDARY FINITE ELEMENT GRID (EXPLODED VIEW)

3.5 FUEL RODS

The cladding of the fuel rods is the initial confinement boundary in the HI-STAR 100 System. Analyses have been performed in Chapter 4 to ensure that the maximum temperature of the fuel cladding is below the Pacific Northwest Laboratory's threshold values for various cooling times. These temperature limits ensure that the fuel cladding will not degrade in an inert helium environment. Additional details on the fuel rod cladding temperature analyses for the spent fuel to be loaded into the HI-STAR 100 System are provided in Chapter 4.

The dimensions of the storage cell openings in the MPC are equal to or greater than those used in spent fuel racks supplied by Holtec International. Thousands of fuel assemblies have been shuffled in and out of these cells over the years without a single instance of cladding failure. The vast body of physical evidence provides confirmation that the fuel handling and loading operations with the HI-STAR 100 MPC will not endanger or compromise the integrity of the cladding or the structural integrity of the assembly.

The HI-STAR 100 System is designed and evaluated for a maximum deceleration of 60g's. Studies of the capability of spent fuel rods to resist impact loads [3.5.1] indicate that the most vulnerable fuel can withstand 63 g's in the most adverse orientation. Therefore, designing the HI-STAR 100 System to a maximum deceleration of 60 g's will ensure that fuel rod cladding integrity is maintained during all normal, off-normal, and accident conditions.

3.6 SUPPLEMENTAL DATA

3.6.1 Additional Codes and Standards Referenced in HI-STAR 100 System Design and Fabrication

The following additional codes, standards and practices were used as aids in developing the design, manufacturing, quality control and testing methods for HI-STAR 100 System:

a. Design Codes

(1) AISC Manual of Steel Construction, 1964 Edition and later.

(2) ANSI N210-1976, "Design Requirements for Light Water Reactor Spent Fuel Storage Facilities at Nuclear Power Stations".

(3) American Concrete Institute Building Code Requirements for Reinforced Concrete, ACI-318.

(4) Code Requirements for Nuclear Safety Related Concrete Structures, ACI349-85/ACI349R-85, and ACI349.1R-80.

(5) ASME NQA-1, Quality Assurance Program Requirements for Nuclear Facilities.

(6) ASME NQA-2-1989, Quality Assurance Requirements for Nuclear Facility Applications.

(7) ANSI Y14.5M, Dimensioning and Tolerancing for Engineering Drawings and Related Documentation Practices.

(8) ACI Detailing Manual - 1980.

(9) Crane Manufacturer's Association of America, Inc., CMAA Specification #70, Specifications for Electric Overhead Traveling Cranes, Revised 1988.

b. Material Codes - Standards of ASTM

(1) E165 - Standard Methods for Liquid Penetrant Inspection.

(2) A240 - Standard Specification for Heat-Resisting Chromium and Chromium-Nickel Stainless Steel Plate, Sheet and Strip for Fusion-Welded Unfired Pressure Vessels.

(3) A262 - Detecting Susceptibility to Intergranular Attack in Austenitic Stainless Steel.

(4) A276 - Standard Specification for Stainless and Heat-Resisting Steel Bars and Shapes.

(5) A479 - Steel Bars for Boilers & Pressure Vessels.

(6) ASTM A564, Standard Specification for Hot-Rolled and Cold-Finished Age-Hardening Stainless and Heat-Resisting Steel Bars and Shapes.

(7) C750 - Standard Specification for Nuclear-Grade Boron Carbide Powder.

(8) A380 - Recommended Practice for Descaling, Cleaning and Marking Stainless Steel Parts and Equipment.

(9) C992 - Standard Specification for Boron-Based Neutron Absorbing Material Systems for Use in Nuclear Spent Fuel Storage Racks.

(10) ASTM E3, Preparation of Metallographic Specimens.

(11) ASTM E190, Guided Bend Test for Ductility of Welds.

(12) NCA3800 - Metallic Material Manufacturer's and Material Supplier's Quality System Program.

c. Welding Codes: ASME Boiler and Pressure Vessel Code, Section IX - Welding and Brazing Qualifications, 1995 Edition.

d. Quality Assurance, Cleanliness, Packaging, Shipping, Receiving, Storage, and Handling Requirements

(1) ANSI 45.2.1 - Cleaning of Fluid Systems and Associated Components during Construction Phase of Nuclear Power Plants.

(2) ANSI N45.2.2 - Packaging, Shipping, Receiving, Storage and Handling of Items for Nuclear Power Plants (During the Construction Phase).

(3) ANSI - N45.2.6 - Qualifications of Inspection, Examination, and Testing Personnel for Nuclear Power Plants (Regulatory Guide 1.58).

(4) ANSI-N45.2.8, Supplementary Quality Assurance Requirements for Installation, Inspection and Testing of Mechanical Equipment and Systems for the Construction Phase of Nuclear Power Plants.

(5) ANSI - N45.2.11, Quality Assurance Requirements for the Design of Nuclear Power Plants.

(6) ANSI-N45.2.12, Requirements for Auditing of Quality Assurance Programs for Nuclear Power Plants.

(7) ANSI N45.2.13 - Quality Assurance Requirements for Control of Procurement of Equipment Materials and Services for Nuclear Power Plants (Regulatory Guide 1.123).

(8) ANSI N45.2.15-18 - Hoisting, Rigging, and Transporting of Items for Nuclear Power Plants.

(9) ANSI N45.2.23 - Qualification of Quality Assurance Program Audit Personnel for Nuclear Power Plants (Regulatory Guide 1.146).

(10) ASME Boiler and Pressure Vessel, Section V, Nondestructive Examination, 1995 Edition.

(11) ANSI - N16.9-75 Validation of Calculation Methods for Nuclear Criticality Safety.

e. Reference NRC Design Documents

(1) NUREG-0800, Radiological Consequences of Fuel Handling Accidents.

(2) NUREG 0612, "Control of Heavy Loads at Nuclear Power Plants", USNRC, Washington, D.C., July, 1980.

(3) NUREG-1536, "Standard Review Plan for Dry Cask Storage Systems", USNRC, January 1997, Final Report.

f. Other ANSI Standards (not listed in the preceding)

(1) ANSI/ANS 8.1 (N16.1) - Nuclear Criticality Safety in Operations with Fissionable Materials Outside Reactors.

(2) ANSI/ANS 8.17, Criticality Safety Criteria for the Handling, Storage, and Transportation of LWR Fuel Outside Reactors.

(3) N45.2 - Quality Assurance Program Requirements for Nuclear Facilities - 1971.

(4) N45.2.9 - Requirements for Collection, Storage and Maintenance of Quality Assurance Records for Nuclear Power Plants - 1974.

(5) N45.2.10 - Quality Assurance Terms and Definitions - 1973.

(6) ANSI/ANS 57.2 (N210) - Design Requirements for Light Water Reactor Spent Fuel Storage Facilities at Nuclear Power Plants.

(7) N14.6 (1993) - American National Standard for Special Lifting Devices for Shipping Containers Weighing 10,000 pounds (4500 kg) or more for Nuclear Materials.

(8) ANSI/ASME N626-3, Qualification and Duties of Personnel Engaged in ASME Boiler and Pressure Vessel Code Section III, Div. 1, Certifying Activities.

g. Code of Federal Regulations

(1) 10CFR20 - Standards for Protection Against Radiation.

(2) 10CFR21 - Reporting of Defects and Non-compliance.

(3) 10CFR50 - Appendix A - General Design Criteria for Nuclear Power Plants.

(4) 10CFR50 - Appendix B - Quality Assurance Criteria for Nuclear Power Plants and Fuel Reprocessing Plants.

(5) 10CFR61 - Licensing Requirements for Land Disposal of Radioactive Material.

(6) 10CFR71 - Packaging and Transportation of Radioactive Material.

h. Regulatory Guides

(1) RG 1.13 - Spent Fuel Storage Facility Design Basis (Revision 2 Proposed).

(2) RG 1.25 - Assumptions Used for Evaluating the Potential Radiological Consequences of a Fuel Handling Accident in the Fuel Handling and Storage Facility of Boiling and Pressurized Water Reactors.

(3) RG 1.28 - (ANSI N45.2) - Quality Assurance Program Requirements.

(4) RG 1.29 - Seismic Design Classification (Rev. 3).

(5) RG 1.31 - Control of Ferrite Content in Stainless Steel Weld Material.

(6) RG 1.38 - (ANSI N45.2.2) Quality Assurance Requirements for Packaging, Shipping, Receiving, Storage and Handling of Items for Water-Cooled Nuclear Power Plants.

(7) RG 1.44 - Control of the Use of Sensitized Stainless Steel.

(8) RG 1.58 - (ANSI N45.2.6) Qualification of Nuclear Power Plant Inspection, Examination, and Testing Personnel.

(9) RG 1.61 - Damping Values for Seismic Design of Nuclear Power Plants, Rev. 0, 1973.

(10) RG 1.64 - (ANSI N45.2.11) Quality Assurance Requirements for the Design of Nuclear Power Plants.

(11) RG 1.71 - Welder Qualifications for Areas of Limited Accessibility.

(12) RG 1.74 - (ANSI N45.2.10) Quality Assurance Terms and Definitions.

(13) RG 1.85 - Materials Code Case Acceptability - ASME Section 3, Div. 1.

(14) RG 1.88 - (ANSI N45.2.9) Collection, Storage and Maintenance of Nuclear Power Plant Quality Assurance Records.

(15) RG 1.92 - Combining Modal Responses and Spatial Components in Seismic Response Analysis.

(16) RG 1.122 - Development of Floor Design Response Spectra for Seismic Design of Floor-Supported Equipment or Components.

(17) RG 1.123 - (ANSI N45.2.13) Quality Assurance Requirements for Control of Procurement of Items and Services for Nuclear Power Plants.

(18) RG 1.124 - Service Limits and Loading Combinations for Class 1 Linear-Type Component Supports, Revision 1, 1978.

(19) Reg. Guide 3.4 - Nuclear Criticality Safety in Operations with Fissionable Materials at Fuels and Materials Facilities.

(20) RG 3.41 - Validation of Calculational Methods for Nuclear Criticality Safety, Revision 1, 1977.

(21) Reg. Guide 8.8 - Information Relative to Ensuring that Occupational Radiation Exposure at Nuclear Power Plants will be as Low as Reasonably Achievable (ALARA).

(22) DG-8006, "Control of Access to High and Very High Radiation Areas in Nuclear Power Plants".

i. Branch Technical Position

(1) CPB 9.1-1 - Criticality in Fuel Storage Facilities.

(2) ASB 9-2 - Residual Decay Energy for Light-Water Reactors for Long-Term Cooling.

j. Standard Review Plan (NUREG-0800)

(1) SRP 3.2.1 - Seismic Classification.

(2) SRP 3.2.2 - System Quality Group Classification.

(3) SRP 3.7.1 - Seismic Design Parameters.

(4) SRP 3.7.2 - Seismic System Analysis.

(5) SRP 3.7.3 - Seismic Subsystem Analysis.

(6) SRP 3.8.4 - Other Seismic Category I Structures (including Appendix D), Technical Position on Spent Fuel Rack.

(7) SRP 3.8.5 - Foundations

(8) SRP 9.1.2 - Spent Fuel Storage, Revision 3, 1981.

(9) SRP 9.1.3 - Spent Fuel Pool Cooling and Cleanup System.

(10) SRP 9.1.4 - Light Load Handling System.

(11) SRP 9.1.5 - Overhead Heavy Load Handling System.

(12) SRP 15.7.4 - Radiological Consequences of Fuel Handling Accidents.

k. AWS Standards

(1) AWS D1.1 - Structural Welding Code, Steel.

(2) AWS A2.4 - Standard Symbols for Welding, Brazing and Nondestructive Examination.

(3) AWS A3.0 - Standard Welding Terms and Definitions.

(4) AWS A5.12 - Tungsten Arc-welding Electrodes.

(5) AWS QC1 - Standards and Guide for Qualification and Certification of Welding Inspectors.

l. Others

(1) ASNT-TC-1A - Recommended Practice for Nondestructive Personnel Qualification and Certification.

(2) SSPC SP-2 - Surface Preparation Specification No. 2 Hand Tool Cleaning.

(3) SSPC SP-3 - Surface Preparation Specification No. 3 Power Tool Cleaning.

(4) SSPC SP-10 - Near-White Blast Cleaning.

3.6.2 Computer Programs

Three computer programs, all with a well established history of usage in the nuclear industry, have been utilized to perform structural and mechanical analyses documented in this report. These codes are ANSYS, DYNA3D, and WORKING MODEL. ANSYS is a public domain code which utilizes the finite element method for structural analyses.

WORKING MODEL, Version V.3.0

This code is primarily used in the analysis of cask drop events for the 10CFR71 submittal. It is also used in this 10CFR72 submittal to verify the results reported in Appendix 3.A for tip-over and to compute the dynamic load resulting from intermediate missile impact on the overpack closure in Appendix 3.G.

"WORKING MODEL" (V3.0) is a Computer Aided Engineering (CAE) tool with an integrated user interface that merges modeling, simulation, viewing, and measuring. The program includes a dynamics algorithm that provides automatic collision and contact handling, including detection, response, restitution, and friction.

Numerical integration is performed using the Kutta-Merson integrator which offers options for variable or fixed time-step and error bounding.

The Working Model Code is commercially available. Holtec has performed independent QA validation of the code by comparing the solution of several classical dynamics problems with the numerical results predicted by Working Model. Agreement in all cases is excellent.

Additional theoretical material is available in the manual: "Users Manual, Working Model, Version 3", Knowledge Revolution, 66 Bovet Road, Suite 200, San Mateo, CA, 94402.

DYNA3D

"DYNA3D" is a nonlinear, explicit, three-dimensional finite element code for solid and structural mechanics. It was originally developed at Lawrence Livermore Laboratories and is ideally suited for study of short-time duration, highly nonlinear impact problems in solid mechanics. DYNA3D is commercially available for both UNIX work stations and Pentium class PCs running Windows 95 or Windows NT. The PC version has been fully validated at Holtec following Holtec's QA procedures for commercial computer codes. This code is used to analyze the drop accidents and the tip-over scenario for the HI-STAR 100. Benchmarking of DYNA3D for these storage analyses is discussed and documented in Appendix 3.A.

3.6.3 Appendices Included in Chapter 3

3.A	HI-STAR Deceleration Under Postulated Drop Events and Tipover
3.B	Damaged Fuel Container
3.C	Response of Cask to Tornado Wind Load and Large Missile Impact
3.D	Lifting Trunnion Stress Analysis
3.E	Analysis of MPC Top Closure
3.F	Stress Analysis of Overpack Closure Bolts
3.G	Missile Penetration Analysis
3.H	Code Case N-284 Stability Calculations
3.I	Structural Qualification of MPC Baseplate
3.J	Fuel Support Spacer Strength Evaluations
3.K	Lifting Bolts - MPC Lid and Overpack Top Closure
3.L	Fabrication Stresses
3.M	Miscellaneous Calculations
3.N	Detailed Finite Element Listings for MPC-24 Fuel Basket
3.O	Detailed Finite Element Listings for MPC-24 Enclosure Vessel
3.P	Deleted
3.Q	Deleted
3.R	Detailed Finite Element Listings for MPC-68 Fuel Basket
3.S	Detailed Finite Element Listings for MPC-68 Enclosure Vessel
3.T	Stress Report Locations for the Overpack
3.U	HI-STAR 100 Component Thermal Expansion - MPC-24
3.V	Deleted
3.W	HI-STAR 100 Component Thermal Expansion - MPC-68
3.X	Calculation of Dynamic Load Factors
3.Y	Cask Under Three Times Dead Load
3.Z	Top Flange Bolt Hole Analysis
3.AA	ANSYS Finite Element Results for the MPCs
3.AB	ANSYS Finite Element Results for the Overpack

3.AC MPC Enclosure Vessel Lifting
3.AD Thermal Expansion During Fire Accident
3.AE Stress Analysis of Overpack Closure Bolts Under Cold Conditions of Storage
3.AF Stress Analysis of Overpack Closure Bolts for the Storage Fire Accident
3.AG Stress Analysis of the HI-STAR 100 Enclosure Shell Under 30 psi Internal Pressure
3.AH MPC Lift Lugs
3.AI Analysis of Transnuclear Damaged Fuel Canister and Thoria Rod Canister

3.7 COMPLIANCE TO NUREG-1536

Supporting information to provide reasonable assurance with respect to the adequacy of the HI-STAR 100 System to store spent nuclear fuel in accordance with the stipulations of the Technical Specifications (Chapter 12) is provided throughout this Final Safety Analysis Report. An itemized table (Table 3.0.1 at the beginning of this chapter) has been provided to locate and collate the substantiating material to support the technical evaluation findings listed in NUREG-1536 Chapter 3, Article VI.

The following statements are germane to the finding of an affirmative safety evaluation for HI-STAR 100 spent fuel storage system:

- The design and structural analysis of the HI-STAR 100 System is in full compliance with the provisions of Chapter 3 of NUREG-1536. No exceptions are taken.

- The list of Regulatory Guides, Codes, and standards presented in Section 3.6 herein is in full compliance with the provisions of NUREG-1536.

- All HI-STAR 100 structures, systems, and components (SSC) that are important to safety (ITS) are identified in Table 2.2.6. Section 1.5 contains the design drawings which describe the HI-STAR 100 SSCs in complete detail. Explanatory narrations in Subsections 3.4.3, 3.4.4, and appendices to this chapter provide sufficient textual details to allow an independent evaluation of their structural adequacy.

- The requirements of 10CFR72.24 with regard to information pertinent to structural evaluation is provided in Chapters 2, 3, and 11.

- Technical Specifications pertaining to the structures of the HI-STAR 100 System have been provided in Section 12.3 herein pursuant to the requirements of 10CFR72.26.

- A series of analyses to demonstrate compliance with the requirements of 10CFR72.122(b) and (c), and 10CFR72.24(c)(3) have been performed which show that SSCs designated as ITS possess an adequate margin of safety with respect to all load combinations applicable to normal, off-normal, accident, and natural phenomenon events. In particular, the following information is provided:

    i. Load combinations for the fuel basket, enclosure vessel, and the HI-STAR 100 overpack for normal, off-normal, accident, and natural phenomenon events are compiled in Tables 2.2.14, 3.1.1, and 3.1.3 through 3.1.5, respectively.

    ii. Stress limits applicable to the materials are provided in Subsection 3.3.

iii. Stresses at various locations in the fuel basket, the enclosure vessel, and the HI-STAR 100 overpack have been computed by analysis. Descriptions of stress analyses are presented in Sections 3.4.3 and 3.4.4, which are further elaborated in a series of appendices listed at the end of this chapter.

iv. Factors of safety in the components of the HI-STAR 100 System are reported as below:

a.	Fuel basket	Tables 3.4.3, 3.4.9, and 3.4.11
b.	Enclosure vessel	Tables 3.4.4, 3.4.7, 3.4.8, 3.4.9, 3.4.11, 3.4.12, 3.4.13, 3.4.15
c.	HI-STAR 100 overpack	Tables 3.4.5, 3.4.6, 3.4.10, and 3.4.16-3.4.19
d.	Miscellaneous components	Tables 3.4.11 and 3.4.14
e.	Lifting devices	Subsection 3.4.3

- The structural design and fabrication details of the fuel baskets whose safety function in the HI-STAR 100 System is to maintain nuclear criticality safety, have been carried out to comply with the provisions of Subsection NG of the ASME Code (loc. cit.) Section III. The structural factors of safety, summarized in Tables 3.4.3 and 3.4.6 for all credible load combinations under normal, off-normal, accident, and natural phenomenon events demonstrate that the Code limits are satisfied in all cases. As the stress analyses have been performed using linear elastic methods and the computed stresses are well within the respective ASME Code limits, it follows that the physical geometry of the fuel basket will not be altered under any load combination to create a condition adverse to criticality safety. This conclusion satisfies the requirement of 10CFR72.124(a), with respect to structural margins of safety for SSCs important to nuclear criticality safety.

  Structural margins of safety during handling, packaging, and transfer operations, mandated by the provisions of 10CFR Part 72.236(b), require that the lifting and handling devices are engineered to comply with the stipulations of ANSI N14.6, NUREG-0612, Regulatory Guide 3.61, and NUREG-1536, and that the components being handled meet the applicable ASME Code service condition stress limits. The requirements of the governing codes for handling operations are summarized in Subsection 3.4.3 herein. A summary table of factors of safety for all ITS components under lifting and handling operations, presented in Subsection 3.4.3, shows that adequate structural margins exist in all cases.

- Consistent with the requirements of 10CFR72.236(i), the confinement boundary for the HI-

STAR 100 System has been engineered to maintain confinement of radioactive materials under normal, off-normal, and postulated accident conditions. This assertion of confinement integrity is made principally on the strength of the following information provided in this FSAR.

i. The MPC Enclosure Vessel which constitutes the confinement boundary is designed and fabricated in accordance with Section III, Subsection NB (Class 1 nuclear components) of the ASME Code to the maximum extent practicable.

ii. The MPC lid of the MPC Enclosure Vessel is welded using a strength groove weld and is subjected to volumetric examination, hydrostatic testing, liquid penetrant (root and final), and leakage testing to establish maximum confidence in weld joint integrity.

iii. The closure of the MPC Enclosure Vessel consists of *two* independent isolation barriers.

iv. The confinement boundary is constructed from stainless steel alloys with a proven history of material integrity under environmental conditions encountered in terrestrial applications.

v. The load combinations for normal, off-normal, accident, and natural phenomena events have been compiled (Table 2.2.14) and applied on the HI-STAR 100 MPC Enclosure Vessel (confinement boundary) and on the HI-STAR 100 overpack. The results, summarized in Tables 3.4.4 through 3.4.19, show that the factor of safety (with respect to the appropriate ASME Code limits) is greater than one in all cases. Design Basis natural phenomena events such as tornado-borne missiles (large, intermediate, or small) have also been analyzed to evaluate their potential for breaching the helium retention boundary and the confinement boundary. Analyses presented in Subsection 3.4.8 (summarized in unnumbered tables in Subsection 3.4.8 and in the appendices to this chapter), show that the integrity of the helium retention boundary and the confinement boundary is preserved under all design basis projectile impact scenarios.

- The information on structural design included in this FSAR complies with the requirements of 10CFR72.120 and 10CFR72.122, and can be ascertained from the information contained in Table 3.7.1.

- The provisions of features in the HI-STAR 100 structural design, listed in Table 3.7.2, demonstrate compliance with the specific requirements of 10CFR72.236(e), (f), (g), (h), (i), (j), (k), and (m).

Table 3.7.1

COMPLIANCE MATRIX FOR 10CFR72.120 AND 10CFR72.122 REQUIREMENTS

Item	Compliance		Location of Supporting Information in This Document
i. Design and fabrication to acceptable quality standards	All ITS components designed and fabricated to recognized Codes and Standards:		
	• Basket:	Subsection NG, Section III	Subsections 2.0.1 and 3.1.1 Tables 2.2.6 and 2.2.7
	• Enclosure Vessel:	Subsection NB, loc. cit.	Subsections 2.0.1 and 3.1.1 Tables 2.2.6 and 2.2.7
	• HI-STAR 100 Structure:	Subsection NF, loc. cit.	Subsections 2.0.2 and 3.1.1

Table 3.7.1 (continued)

COMPLIANCE MATRIX FOR 10CFR72.120 AND 10CFR72.122 REQUIREMENTS

Item	Compliance	Location of Supporting Information in This Document
ii. Erection to acceptable quality standards	HI-STAR 100 will be installed in a vertical orientation using proven deployment procedures which are in full compliance with established construction practices at nuclear power plants.	Section 8.1
iii. Testing to acceptable quality standards	• All non-destructive examination of ASME Code components for provisions in the Code (see exceptions in Table 2.2.15). • Hydrotest of pressure vessel per the Code (see Table 12.3.18). • Testing for radiation containment per provisions of NUREG-1536 (see Tables 12.3.8 and 12.3.9).	Section 9.1 Section 9.1 Sections 7.1 and 9.1

Table 3.7.1 (continued)

COMPLIANCE MATRIX FOR 10CFR72.120 AND 10CFR72.122 REQUIREMENTS

Item	Compliance	Location of Supporting Information in This Document
iv. Adequate structural protection against environmental conditions and natural phenomena.	Analyses presented in Chapter 3 demonstrate that the confinement boundary will preserve its integrity under all postulated off-normal and natural phenomena events listed in Chapter 2.	Section 2.2 Chapter 11

Table 3.7.1 (continued)

COMPLIANCE MATRIX FOR 10CFR72.120 AND 10CFR72.122 REQUIREMENTS

Item	Compliance	Location of Supporting Information in This Document
v. Adequate protection against fires and explosions	• The extent of combustible (exothermic) material in the vicinity of the cask system is procedurally controlled (the sole source of hydrocarbon energy is diesel in the tow vehicle).	Chapter 8
	• Analyses show that the heat energy released from the postulated fire accident condition surrounding the cask will not result in impairment of the confinement boundary and will not lead to structural failure of the overpack. The effect on shielding will be localized to the external surfaces directly exposed to the fire which will cause no significant change in the HI-STAR 100 overpack.	Subsection 11.2.4
	• Explosion effects are shown to be bounded by the Code external pressure design basis. Pressure pulse from explosion will act on the HI-STAR 100 overpack; the MPC (confinement boundary) is completely protected.	Subsection 11.2.11 and Subsection

Table 3.7.1 (continued)

COMPLIANCE MATRIX FOR 10CFR72.120 AND 10CFR72.122 REQUIREMENTS

Item	Compliance	Location of Supporting Information in This Document
vi. Appropriate inspection, maintenance, and testing	Inspection, maintenance, and testing requirements set forth in this FSAR are in full compliance with the governing regulations and established industry practice.	Sections 9.1 and 9.2 Chapter 12
vii. Adequate accessibility in emergencies.	• The HI-STAR 100 overpack lid can be removed to gain access to the multi-purpose canister.	Chapter 8

Table 3.7.1 (continued)

COMPLIANCE MATRIX FOR 10CFR72.120 AND 10CFR72.122 REQUIREMENTS

Item	Compliance	Location of Supporting Information in This Document
viii. A confinement barrier that acceptably protects the spent fuel cladding during storage.	• The peak temperature of the fuel cladding at design basis heat duty of each MPC has been demonstrated to be maintained below the limits recommended in the reports of national laboratories. • The confinement barriers consist of highly ductile stainless steel alloys. The multi-purpose canister is housed in the overpack, built from a steel structure whose materials are selected and examined to maintain protection against brittle fracture under off-normal ambient (cold) temperatures (minimum of -40°F).	Subsection 4.4.2 Subsection 3.1.1 Subsection 3.1.2.3
ix. The structures are compatible with the appropriate monitoring systems.	The HI-STAR 100 overpack	Section 1.5, Subsection 2.3.3.2

Table 3.7.1 (continued)

COMPLIANCE MATRIX FOR 10CFR72.120 AND 10CFR72.122 REQUIREMENTS

Item	Compliance	Location of Supporting Information in This Document
x. Structural designs that are compatible with ready retrievability of fuel.	• The fuel basket is designed to be an extremely stiff honeycomb structure such that the storage cavity dimensions will remain unchanged under all postulated normal and accident events. Therefore, the retrievablity of the spent nuclear fuel from the basket will not be jeopardized.	Subsection 3.1.1
	• The MPC canister lid is attached to the shell with a groove weld which is made using an automated welding device. A similar device is available to remove the weld. Thus, access to the fuel basket can be realized.	Sections 8.1 and 8.3

Table 3.7.2

COMPLIANCE OF HI-STAR 100 SYSTEM WITH 10CFR72.236(e), ET AL.

Item	Compliance	Location of Supporting Information in This Document
i. Redundant sealing of confinement systems.	Two physically independent lids, each separately welded to the MPC shell (Enclosure Vessel shell) provide a redundant confinement system.	Section 1.5 Drawing Nos. 1392, 1395, and 1401; Figure 7.1.2 Section 7.1.
ii. Adequate heat removal without active cooling systems.	Thermal analyses presented in Chapter 4 show that the HI-STAR 100 System will remove the decay heat generated from the stored spent fuel by strictly passive means and maintain the system temperature within prescribed limits.	Sections 4.4 and Sections 9.1 and 9.2
iii. Storage of spent fuel for a minimum of 20 years.	The service life of the overpack and MPC are engineered to be in excess of 20 years.	Subsections 3.4.10 and 3.4.11
iv. Compatibility with wet or dry spent fuel loading and unloading facilities.	The system is designed to eliminate any material interactions in the wet (spent fuel pool) environment.	Subsection 3.4.1

Item		Compliance	Location of Supporting Information in This Document
v.	Ease of decontamination.	The external surface of the multi-purpose canister is protected from contamination during fuel loading through a custom designed sealing device.	Figures 8.1.13 and 8.1.14
vi.	Inspection of defects that might reduce confinement effectiveness.	Post-fabrication inspection of the shielding materials will be performed to ensure that no HI-STAR 100 Systems containing unacceptable voids are deployed at the ISFSI for long-term storage.	Section 9.1 and Chapter 12
vii.	Conspicuous and durable marking.	The stainless steel lid of each MPC will have model number and serial number engraved for ready identification.	Section 1.5, Design Drawings
viii.	Compatibility with removal of the stored fuel from the site, transportation, and ultimate disposal by the U.S. Department of Energy.	The MPC is designed to be in full compliance with the DOE's draft specification for transportability and disposal published under the now dormant "MPC" program.	Section 2.4 Subsection 1.2.1.1

3.8 REFERENCES

[3.1.1] NUREG-0612, "Control of Heavy Loads at Nuclear Power Plants," United States Nuclear Regulatory Commission.

[3.1.2] ANSI N14.6-1993, "American National Standard for Special Lifting Devices for Shipping Containers Weighing 10000 Pounds (4500 kg) or More for Nuclear Materials," American National Standards Institute, Inc.

[3.1.3] Regulatory Guide 7.11, "Fracture Toughness Criteria of Base Material for Ferritic Steel Shipping Cask Containment Vessels with a Maximum Wall Thickness of 4 Inches."

[3.1.4] Regulatory Guide 7.12, "Fracture Toughness Criteria of Base Material for Ferritic Steel Shipping Cask Containment Vessels with a Wall Thickness Greater Than 4 Inches but Not Exceeding 12 Inches."

[3.1.5] NUREG/CR-1815, "Recommendations for Protecting Against Failure by Brittle Fracture in Ferritic Steel Shipping Containers Up to Four Inches Thick."

[3.1.6] Aerospace Structural Metals Handbook, Manson.

[3.1.7] Armco Product Data Bulletin S-22.

[3.3.1] ASME Boiler & Pressure Vessel Code, Section II, Part D, 1995.

[3.4.1] ANSYS 5.2, ANSYS, Inc., 1995.

[3.4.2] ASME Boiler & Pressure Vessel Code, Section III, Subsection NF, 1995.

[3.4.3] ASME Boiler & Pressure Vessel Code, Section III, Appendices, 1995.

[3.4.4] ASME Boiler & Pressure Vessel Code, Section III, Subsection NB, 1995.

[3.4.5] Mok, Fischer, Hsu, "Stress Analysis of Closure Bolts for Shipping Casks" (NUREG/CR 6007 UCRL-ID-110637), Lawrence Livermore National Laboratory/Kaiser Engineering, 1993.

[3.4.6] Code Case N-284, "Metal Containment Shell Buckling Design Methods", Section III, Division 1, Class MC, Approval Date 8/25/80.

[3.4.7] NRC Bulletin 96-04: Chemical, Galvanic or Other Reactions in Spent Fuel Storage and Transportation Casks, July 5, 1996.

[3.4.8] Theory of Elastic Stability, S.P. Timoshenko and J. Gere, McGraw Hill, 2nd Edition.

[3.4.9] Marks Standard Handbook for Mechanical Engineering, 9th ed.

[3.4.10] ASME Boiler and Pressure Vessel Code, Section III, Subsection NG, 1995.

[3.4.11] 10CFR71, Waste Confidence Decision Review, USNRC, September 11, 1990.

[3.4.12] NUREG/CR-6322, Buckling Analysis of Spent Fuel Basket, Lawrence Livermore National Laboratory, May, 1995.

[3.5.1] Chun, Witte, Schwartz, "Dynamic Impact Effects on Spent Fuel Assemblies", UCID-21246, Lawrence Livermore National Laboratory, October 20, 1987.

APPENDIX 3.A: HI-STAR DECELERATION UNDER POSTULATED DROP EVENTS AND TIPOVER

3.A.1 INTRODUCTION

Handling accidents with a HI-STAR overpack containing a loaded MPC are credible events (Section 2.2.3). The stress analyses carried out in Chapter 3 of this safety analysis report assume that the inertial loading on the load bearing members of the MPC, fuel basket, and the overpack due to a handling accident are limited by the Table 3.1.2 decelerations. The maximum deceleration experienced by a structural component is the product of the rigid body deceleration sustained by the structure and the dynamic load factor (DLF) applicable to that structural component. The dynamic load factor (DLF) is a function of the contact impulse and the structural characteristics of the component. A solution for dynamic load factors is provided in Appendix 3.X.

The rigid body deceleration is a strong function of the load-deformation characteristics of the impact interface, weight of the cask, and the drop height. For the HI-STAR 100 System, the weight of the structure and its surface compliance characteristics are known. However, the contact stiffness of the ISFSI pad (and other surfaces over which the HI-STAR 100 may be carried during its movement to the ISFSI) is site-dependent. The contact resistance of the collision interface, which is composed of the HI-STAR 100 and the impacted surface compliances, therefore, is not known a priori for a site. For conservatism, the HI-STAR 100 cask is simulated as a rigid body (infinite surface stiffness) which has the effect of maximizing the stiffness of the contact interface. Analyses for the rigid body decelerations are presented here for a reference ISFSI pad (which is the pad used in a recent Lawrence Livermore National Laboratory report). The surface compliance of the pad, therefore, is the only source of interface deformation in the dynamic simulations considered in this appendix.

3.A.2 Purpose

The purpose of this appendix is to demonstrate that the rigid body decelerations are sufficiently low so that the design basis deceleration of 60g is not exceeded. Three scenarios of accidental drop of a loaded HI-STAR 100 cask on the ISFSI pad are considered in this appendix. They are:

i. Side drop: A loaded HI-STAR 100 free-falls in a horizontal orientation (casks's axis is horizontal) from a height "h" before impacting the ISFSI pad.

ii. Tipover: A loaded HI-STAR 100 is assumed to undergo a non-mechanistic tipover event at an ISFSI pad resulting in an impact with a pre-incipient impact angular velocity of ω which is readily calculated from elementary dynamics.

iii. End drop: The loaded cask is assumed to drop with its longitudinal axis in the vertical orientation such that its bottom plate hits the pad after free-falling from a height, h.

It is shown in Appendix 3.X that dynamic load factors are a function of the dominant natural frequency of vibration of the component for a given input load pulse shape. Therefore, for the purposes of this Appendix 3.A, it is desired to demonstrate that the rigid body deceleration experienced in each of the drop scenarios is below the 60g HI-STAR 100 design basis.

3.A.3 Background and Methodology

An earlier revision of this FSAR contained an analytical treatment of the three cask drop scenarios. In the earlier submittal, the cask/ISFSI interface was simulated by a linear spring with the spring stiffeners calculated using the Bousinesq elastic half-space solution. All three scenarios reduced to the solution of a simple mass-spring system. The need for such an idealized solution was eliminated when the Lawrence Livermore National Laboratory (LLNL) published results of the so-called fourth series billet tests [3.A.1] with a companion report [3.A.2] documenting a numerical solution based methodology which simulated the drop test results with reasonable accuracy. Subsequently, USNRC personnel published a paper [3.A.3] affirming the NRC's endorsement of the LLNL methodology. The LLNL simulation used modeling and simulation algorithms contained within the commercial computer code DYNA3D [3.A.6].

The LLNL cask drop model is not completely set forth in the above-mentioned LLNL reports. Using the essential information provided by the LLNL [3.A.2] report, however, Holtec is able to develop a finite element model for implementation on DYNA3D which is fully consistent with LLNL's (including the use of the Butterworth filter for discerning rigid body deceleration from "noisy" impact data). The details of the DYNA3D dynamic model, henceforth referred to as the Holtec model, are contained in the proprietary benchmark report [3.A.4] wherein it is shown that the peak deceleration in *every* case of billet drop analyzed by LLNL is replicated within a small tolerance by the Holtec model. The case of the so-called "generic" cask for which LLNL provided predicted response under side drop and tipover events is also bounded by the Holtec model. In summary, the benchmarking effort documented in [3.A.4] is in full compliance with the guidance of the Commission [3.A.3].

Having developed and benchmarked an LLNL-consistent cask impact model, this model is applied to prognosticate the HI-STAR drop scenarios.

In the tipover scenario, the angular velocity of approach is readily calculated using planar rigid body dynamics and is used as an initial condition in the DYNA3D simulation.

For the side drop and end drop scenarios, considering the reference target (pad) elasto-plastic-damage characteristics, the object is to determine the maximum allowable drop height "h" such that the rigid body deceleration is below the design basis.

It is recognized, from the elementary analogy of the spring-mass impact, that the maximum deceleration increases monotonically as the rigidity of the cask is increased. Therefore, an upper bound on the deceleration of HI-STAR is obtained by replacing the polymeric zone in HI-STAR also by a rigid medium, making the entire cask a rigid body. Simulations for side drop and tipover conditions under the complete rigid body assumption provide an upper bound on the cask response. For the case of vertical drop, the impacting region is bottom plate forging which, without excessive conservatism, can be also modeled as a rigid body. Thus, all drop simulations presented in this appendix assume the HI-STAR 100 cask to simulate a rigid body for conservatism.

A description of the work effort and a summary of the results are presented in the following sections. In all cases, the reported decelerations are below the design basis of 60 g's.

3.A.4 Assumptions and Input Data

3.A.4.1 Assumptions

The assumptions used to create the model are completely described in Reference [3.A.4] and are shown there to be consistent with the LLNL simulation. There are two key aspects which are restated here:

The cask pad is assumed to be identical to the pad defined by LLNL [3.A.2]. It is also identical to the pad utilized in the benchmark report [3.A.4]. For a specific ISFSI site, the reinforced concrete section, as well as the underlying engineered fill, may be different; in that case, the site-specific conditions must be shown to perform in a manner to ensure compliance with the design limits of the HI-STAR system (e.g., maximum rigid body g-load less than specified limits). The essential data which define the reference pad used to qualify the HI-STAR 100 is provided in Table 3.A.1.

3.A.4.2 Input Data

Table 3.A.1 characterizes the properties of the reference target pad used in the analysis. The inputs are taken from References [3.A.2] and [3.A.4].

Table 3.A.2 details the geometry of the HI-STAR 100 used in the drop simulations. This data is taken from applicable HI-STAR 100 drawings.

3.A.5 Finite Element Model

The finite-element model of the Holtec HI-STAR 100 cask (bottom plate, shells, forging, lid, Holtite polymer and its connectors), concrete pad and a portion of the subgrade soil is constructed using the pre-processor integrated with the LS-DYNA3D software [3.A.5]. The deformation field for all postulated drop events, the end-drop, the side-drop and the tipover, exhibits symmetry with the vertical plane passing through the vertical diameter of the cask and the concrete pad length. Using

this symmetry condition of the deformation field a half finite-element model is constructed. The finite-element model is organized into five independent parts (the cask, the MPC steel plates, the basket fuel zone, the concrete pad and the soil). The final model contains 35431 nodes, 29944 solid type finite-elements, five (5) materials, one (1) property and four (4) interfaces. The finite-element model used for the side-drop and tipover-drop events is depicted in Figures 3.A.1 through 3.A.4. Figures 3.A.5 through 3.A.8 show the end-drop finite-element model.

The half portion of the cylindrical cask contains 7,320 solid finite-elements. Figure 3.A.11 depicts details of the cask finite-element mesh.

The elasto-plastic behavior characteristic of all HI-STAR components (shells, lids, Holtite, outer skin, connectors, etc.) are simulated as rigid materials using a DYNA3D built-in command.

The soil grid, shown in Figure 3.A.9, is a rectangular prism (800 inches long, 375 inches wide and 470 inches deep), is constructed from 13294 solid type finite-elements. The material defining this part is an elastic orthotropic material. The central portion of the soil (400 inches long, 150 inches wide and 170 inches deep) where the stress concentration is expected to appear is discretized with a finer mesh.

The concrete pad is 320 inches long, 100 inches wide and is 36 inches thick. This part contains 8208 solid finite-elements. A uniform sized finite-element mesh, shown in Figure 3.A.10, is used to model the concrete pad. The concrete behavior is described using a special constitutive law and yielding surface contained within DYNA3D. The geometry, the material properties, and the material behavior are identical to the LLNL reference pad.

The MPC and the contained fuel is modeled in two parts which represent the lid and baseplate, and the fuel area. An elastic material is used for both parts. The finite-element mesh pertinent to the MPC contains 1122 solid finite-elements and is shown in Figure 3.A.14. The mass density is appropriate to match a representative weight of 241,937 lb which is an approximate mean of the upper and lower weight estimates for a loaded HI-STAR 100. The total weight used in the analysis is approximately 8,000 lb heavier than the HI-STAR 100 containing the lightest weight MPC.

Analysis of a single mass impacting a spring with a given initial velocity shows that both the maximum deceleration "a_M" of the mass and the time duration of contact with the spring "t_c" are related to the dropped weight "w" and drop height "h" as follows:

$$a_M \sim \frac{\sqrt{h}}{\sqrt{w}} \; ; \; t_c \sim \sqrt{w}$$

Therefore, the most conservatism is introduced into the results by using the minimum weight. However, since the difference between the heaviest and the lightest HI-STAR 100 is only 9,500 lb, a small percentage of the total weight, the results using the minimum weight will yield a 2% increase in the maximum deceleration and a 2% decrease in the duration of the impact. This small difference is neglected in the presentation of results.

It is emphasized that the finite element model described in the foregoing is identical in its approach to the "Holtec model" described in the benchmark report [3.A.4]. Gaps between the MPC and the overpack are included in the model.

3.A.6 Impact Velocity

a. Linear Velocity: Vertical Drops

For the side drop and vertical drop events, the impact velocity, v, is readily calculated from the Newtonian formula:

$$v = \sqrt{(2gh)}$$

where

g = acceleration due to gravity
h = free-fall height

b. Angular velocity: Tipover

The tipover event is an artificial construct wherein the HI-STAR 100 overpack is assumed to be perched on its edge with its C.G. directly over the pivot point A (Figure 3.A.15). In this orientation, the overpack begins its downward rotation with zero initial velocity. At angle ψ_1 (Figure 3.A.16), the pivot point shifts to point B; but otherwise the downward rotation of the overpack continues with increasing angular velocity. Towards the end of the tipover, the overpack is horizontal with its downward velocity ranging from zero at the pivot point to a

maximum at the farthest point of impact (point E in Figure 3.A.18). The angular velocity at the instant of impact defines the downward velocity distribution along the contact line.

In the following, we derive an explicit expression for calculating the angular velocity of the cask at the instant when it impacts on the ISFSI pad.

Referring to Figure 3.A.15, let r be the length AC where C is the cask centroid. Therefore,

$$r = \left(\frac{d^2}{4} + (h+a)^2 \right)^{1/2} \qquad \textbf{(3.A.1)}$$

The mass moment of inertia of the HI-STAR 100 System, considered as a rigid body, can be written about an axis through point A, as

$$6I_A = I_c + \frac{W}{g} r^2 \qquad \textbf{(3.A.2)}$$

where I_c is the mass moment of inertia about a parallel axis through the cask centroid C, and W is the weight of the cask (W = Mg).

Let $\theta_1(t)$ be the rotation angle between a vertical line and the line AC. The equation of motion for rotation of the cask around point A, during the time interval prior to contact with point B (Figure 3.A.15), is

$$I_A \frac{d^2 \theta_1}{dt^2} = Mgr \sin \theta_1 \qquad \textbf{(3.A.3)}$$

This equation can be rewritten in the form

$$\frac{I_A}{2} \frac{d (\dot{\theta}_1)^2}{d \theta_1} = Mgr \sin \theta_1 \qquad \textbf{(3.A.4)}$$

which can be integrated over the limits $\theta_1 = 0$ to $\theta_1 = \psi_1$. (See Figure 3.A.17).

The final angular velocity $\dot{\theta}_1$ at the time instant just prior to contact at point B is given by the expression

$$\dot{\theta}_1\ (t_B) = \sqrt{\frac{2\ Mgr}{I_A}\ (1 - \cos\ \psi_1)} \qquad \textbf{(3.A.5)}$$

The angle ψ_1 between AC and the vertical, at the time just prior to contact, is given by geometry as

$$\psi_1 = \psi_A - \psi_B \qquad \textbf{(3.A.6)}$$

where $\psi_A = \tan^{-1}\ (\frac{a}{b})$

$\psi_B = \tan^{-1}\ (\frac{d}{2h})$

and a and b are shown in Figure 3.A.17. At contact with point B at time t_B (Figure 3.A.16), the angular impulse momentum equation can be used to determine a new initial angular velocity for subsequent determination of the angular motion about point B. Ignoring the small impulsive moment from the cask weight due to the instantaneous change in moment arm, the angular momentum balance gives

$$I_A\ \dot{\theta}_1\ (t_B) = I_B\ \dot{\theta}_2\ (0) \qquad \textbf{(3.A.7)}$$

where $I_B = I_C + Mr_1^2$ is the mass moment of inertia of the cask about point B. Solving for $\theta_2\ (0)$ and eliminating $\theta_1\ (t_b)$ using Eq. (3.A.5) gives

$$\dot{\theta}_2(0) = \sqrt{\frac{2\ Mg\ r_1}{I_B}\ \frac{I_A}{I_B}\ (1 - \cos\ \psi_1)\ (\frac{r}{r_1})} \qquad \textbf{(3.A.8)}$$

The angle $\theta_2(0)$, which is the starting point for the rotational motion around point B, is easily obtained from the cask geometry. With X defined in Figure 3.A.16.

$$\sin\theta_2(0) = \frac{X(0)}{r_1} \qquad \textbf{(3.A.9)}$$

where X(0) can be determined from Figure 3.A.17 as

$$X(0) = r \sin \psi_1 - (a^2 + b^2)^{1/2}$$

so that

$$\sin\theta_2(0) = \frac{r}{r_1} \sin \psi_1 - \frac{(a^2 + b^2)^{1/2}}{r_1} \qquad \textbf{(3.A.10)}$$

where

$$r_1 = \left[(\frac{D}{2})^2 + h^2 \right]^{1/2}$$

With the initial conditions determined by Eq. (3.A.9) and (3.A.10), the solution for the motion $\theta_2(t) \geq \theta_2(0)$ is easily obtained.

The angular velocity θ_{2f} at the instant of ground contact is

$$\dot{\theta}_{2f}^2 - \dot{\theta}_2^2(0) = \frac{2\,Mgr_1}{I_B} \left(\cos\,\theta_2(0) - \cos\,\theta_{2f}\right) \qquad \textbf{(3.A.11)}$$

where, from Figure 3.A.18

$$\theta_{2f} = \cos^{-1}\left(\frac{D}{2r_1}\right) \qquad \textbf{(3.A.12)}$$

Using Eq. (3.A.8) to eliminate θ_2 (0) from Eq. (3.A.11) leads to a solution for the angular velocity θ_{2f} when interface contact occurs, in the form

$$\dot{\theta}_{2f} = \sqrt{\frac{2Mgr_1}{I_B}\,\beta} = \omega \qquad \textbf{(3.A.13)}$$

$$\text{where } \beta = \frac{I_A r}{I_B r_1} (1 - \cos \psi_1) + \cos \theta_2(0) - \cos \theta_{2f} \qquad \textbf{(3.A.14)}$$

Equations (3.A.13) and (3.A.14) establish the initial conditions for the final phase of the tipover analysis; namely, the portion of the motion when the cask is decelerated by the resistive force at the ISFSI pad interface.

Using the data germane to HI-STAR 100 (Table 3.A.2), and the above equations, the angular velocity of impact is calculated as 1.79 rad/sec.

3.A.7 Results

The LS-DYNA3D time-history results are processed using the Butterworth filter (in conformance with the LLNL methodology) to establish the time-history rigid body motion of the cask. The material points on the cask where the acceleration displacement and velocity are computed for each of the three drop scenarios are shown in Figure 3.A.19.

Node 2901 (Channel A2), which is located midway on the outermost shell generator at the top in side drop events serves as the reference point.

Node 5151 (Channel A1), which is located at the center of the outer surface of the bottom forging, serves as the reference point for end-drop scenarios.

Node 6000 (Channel A3), which is located at the center of the cask top lid outer surface, serves as the reference point for the tipover scenario with the pivot point indicated as Point 0 in Figure 3.A.19.

The results reported below for maximum cask-ISFSI contact force have been multiplied by 2.0 to reflect the fact that only 50% of the dropped mass is included in the model due to the symmetry assumption.

i. Side Drop:

Figures 3.A.20-3.A.23, respectively, show the time-histories of the impact force and displacement, velocity, and deceleration at the reference node point (Channel A2). The drop height is h = 72". Using the data from Figure 3.A.20, the peak cask/pad impact force is 9.636E+06 lbs and the contact duration associated with the initial peak is 9.5 milli-seconds.

The maximum rigid body deceleration (filtered at 350 Hz cut-off frequency) as shown in Figure 3.A.23 is 49.67 g's, value which is below the design basis limit of 60 g's. The time duration of the peak deceleration pulse is 4.4 milli-seconds.

ii. Tipover:

Figures 3.A.24-3.A.27, respectively, show the time-histories of the impact force and displacement, velocity and vertical deceleration of Channel A3 (in Figure 3.A.19) for this event.

The deceleration at the tip of the fuel basket is obtained by ratioing the filtered deceleration of Node 6000. The maximum filtered deceleration at the tip of the fuel basket is found from Figure 3.A.27 to be 66.02 x 0.906 = 59.81 g's which is below the design basis limit. The 0.906 multiplier is based on the geometry of the loaded HI-STAR 100 (further explained in Table 3.A.3). The maximum contact force in this event is 6.43E+06 lbs and the contact duration associated with the initial peak is approximately 8.8 milli-seconds. It should be emphasized that the calculated deceleration for Node 6000 was filtered at 350 Hz cut-off frequency.

The duration of the initial deceleration pulse is obtained from Fig. 3.A.27 as 4.4 milli-seconds.

iii. End Drop:

As in all other impact cases analyzed in this appendix, the overpack is treated as a completely rigid body in the end drop scenario. One drop height is considered: h = 21". The results are summarized in Table 3.A.3 and Figures 3.A.28-3.A.31, respectively, show the contact force, displacement, velocity, and acceleration time-histories at Channel A1 (Figure 3.A.19) for the 21" end drop. The duration of the contact force initial pulse is approximately 2.7 milli-seconds, and the filtered cask deceleration pulse is 2.1 milli-seconds.

A carry height of 21" gives peak filtered deceleration in the event of an end drop of approximately 53 g's.

Decelerations obtained from the DYNA3D numerical solutions are filtered through a Butterworth type filter identical to the filter used by LLNL to investigate the "generic" cask [3.A.2]. The filter has the following characteristics: 350 Hz passband frequency, 10,000 Hz stopband frequency, 0.15 maximum passband ripple, and 10 minimum stopband attenuation.

The computer code utilized in this analysis is LS-DYNA3D [3.A.5] validated under Holtec's QA system.

3.A.8 Computer Codes and Archival Information

The input and output files created to perform the analyses reported in this appendix are listed for future retrievability.

The computer code utilized in this analysis is LS-DYNA3D [3.A.5] validated under Holtec's QA system.

LS-DYNA3D computer code has an extensive finite-element and material description library and can account for various time-dependent contact conditions which normally arise between the various structural components during the impact analysis.

The input and the output files created are stored on Holtec's server disk and tape archived as required by Holtec's QA procedures under the following address:

F:\PROJECTS\5014\HISTAR\IS\ESOIL28\....

....\END21\...	end-drop height 21 inches;
....\SIDE72\...	side-drop height 72 inches;
....\TIPOVER\...	tipover-drop from CG-over-corner position;

Each one of the three subdirectories contain specific data related to the analyzed drop scenarios and are organized in five files: LS-DYNA3D input file (XXX.DYN), corresponding to the analyzed drop event, and four time-history files (MATSUM- the impactor velocity time-history, RCFORC- the impact force time-history, NODOUT- displacement, velocity and acceleration and PLOT- the model deformation time-history) generated during the numerical analysis.

All LS-DYNA3D simulations were performed on a PC environment, using a Dell Corporation Pentium II - 266 MHz computer.

3.A.9 Conclusion

The DYNA3D analysis of HI-STAR 100 reported in this appendix leads to the following conclusion:

a. If a loaded HI-STAR undergoes a free fall for a height of 21 inches in a vertical orientation on to a reference pad defined by Table 3.A.1, the maximum rigid body deceleration is limited to 52.26 g's.

b. If a loaded HI-STAR 100 undergoes a free fall in a horizontal orientation (side drop) for a height 72" onto a reference pad defined by Table 3.A.1, the maximum rigid body deceleration is limited to 49.67 g's.

c. If a loaded HI-STAR 100 overpack pivots about its bottom edge and tips over on to a reference pad defined by Table 3.A.1, then the maximum rigid body deceleration of the cask centerline at the plane of the top of the fuel basket cellular region is 59.81 g's.

Table 3.A.3 provides the key results for all drop cases studied herein.

Recalling that the design basis g-load is 60 g's, the above impact scenarios are comfortably enveloped by the level D design limit and allow ample margin for the introduction of appropriate dynamic load factors into the component stress analyses.

3.A.10 References

[3.A.1] Witte, M., et al., "Evaluation of Low-Velocity Impacts Tests of Solid Steel Billet onto Concrete Pads.", Lawrence Livermore National Laboratory, UCRL-ID-126274, Livermore, California, March 1997.

[3.A.2] Witte, M., et al., "Evaluation of Low-Velocity Impacts Tests of Solid Steel Billet onto Concrete Pads, and Application to Generic ISFSI Storage Cask for Tipover and Side Drop.", Lawrence Livermore National Laboratory, UCRL-ID-126295, Livermore, California, March 1997.

[3.A.3] Tang, D.T., Raddatz, M.G., and Sturz, F.C., "NRC Staff Technical Approach for Spent Fuel Cask Drop and Tipover Accident Analysis", SFPO, USNRC (1997).

[3.A.4] Simulescu, I., "Benchmarking of the Holtec LS-DYNA3D Model for Cask Drop Events", Holtec Report HI-971779, September 1997.

[3.A.5] LS-DYNA3D, Version 936-03, Livermore Software Technology Corporation, September 1996.

[3.A.6] Whirley, R.G., "DYNA3D, A Nonlinear, Explicit, Three-Dimensional Finite element Code for Solid and Structural Mechanics - User Manual.", Lawrence Livermore National Laboratory, UCRL-MA-107254, Revision 1, 1993.

Table 3.A.1: Essential Variables to Characterize the Reference ISFSI Pad

Thickness of concrete	36 inches
Nominal compressive strength of concrete	4,200 psi at 28 days
Concrete mass density	2.097E-04 lb-sec^2/in^4
Concrete shear modulus	1.514E+06 psi
Concrete Poisson's ratio	0.22
Mass density of the engineered fill (soil)	1.498E-04
Effective modulus of elasticity of the subgrade soil	28,000 psi
Poisson's ratio of the soil	0.3

Notes: 1. The concrete Young's Modulus is derived from the American Concrete Institute recommended formula $57{,}000\sqrt{f}$ where f is the nominal compressive strength of the concrete (psi).

2. The effective modulus of elasticity of the subgrade soil is to be measured by an appropriate "plate test" before pouring of the concrete ISFSI pad.

3. The pad thickness of 36 inches, concrete compressive strength of 4,200 psi (nom.) At 28 days of curing, and the subgrade soil effective modulus of 28,000 psi are the upper bound values to ensure that the deceleration limits under postulated impact events set forth in Table 3.1.2 are satisfied.

Table 3.A.2: Key Input Data in Drop Analyses

Cask weight	128,275 lb
Holtite weight	12,926 lb
Holtite connectors weight	11,879 lb
Length of the cask	203.125 inches
Length of the Holtite	173.125 inches
Diameter of the bottom plate	83.25 inches
Inside diameter of the cask	68.75 inches
Outside diameter of the cask shells	85.75 inches
Outside diameter of the enclosure plate	96.00 inches
Outside diameter of the Holtite	95.00 inches
MPC weight (including fuel)	88,857 lb
MPC height	190.5 inches
MPC diameter	68.375 inches
MPC bottom plate thickness	2.5 inches
MPC top plate thickness	9.5 inches

Table 3.A.3: FILTERED RESULTS FOR DROP AND TIPOVER SCENARIOS

Drop Event	Rigid Cask Model†			
	Max. Displ (in)	**Impact Velocity (in/sec)**	**Max. Acc. (g's)**	**Acc. Pulse Duration (msec.)**
End-21"	**1.144**	**127.4**	**52.26**	**2.1**
Side-72	**2.674**	**235.9**	**49.67**	**4.4**
Tipover Top of Cask††	4.231	348.4	66.02	4.4
Tipover Top of Basket Elevation	**--**	**--**	**59.81**	**--**

† The passband frequency of the Butterworth filter is 350 Hz.

†† The distance of the top of the fuel basket is 176.25" from the pivot point. The distance of the top of the cask is 194.375" from the pivot point. Therefore, all displacements, velocities, and accelerations of the top of the basket are 90.6% of the cask top (176.25/194.4).

MISCELLANEOUS NUMERICAL CALCULATIONS SUPPORTING APPENDIX 3.A

This calculation generates the initial angle velocity of the cask when it contacts the ISFSI. Each input or calculation references an equation number or a reference for the data. The nomenclature follows the definitions in the main body of this Appendix 3A. References to Table numbers refer to the FSAR tables. References to Equation numbers refer to Appendix 3.A numbers.

The following data is taken from Holtec Drawings

$d := 83.25 \cdot in$ $a := 8.5 \cdot in$ $b := 6.375 \cdot in$ $D := 96 \cdot in$ $l := 203.125 \cdot in$

$h := 101 \cdot in - a$ $h = 92.5\,in$ From Table 3.2.2

$W := 241937 \cdot lbf$ This is a representative weight of HI-STAR

Next calculate the distance from the centroid to the points of rotation

$$r := \sqrt{\left(\frac{d}{2}\right)^2 + (h + a)^2} \qquad \text{Eq. 3.A.1} \qquad r = 109.241\,in$$

$$r_1 := \sqrt{\left(\frac{D}{2}\right)^2 + h^2} \qquad r_1 = 104.213\,in$$

The moment of inertia is computed using the input weight and considering the cask as a homogeneous cylindrical body. From Appendix 3.Y

$$I := \frac{W}{12 \cdot g} \cdot \left[3 \cdot \left(\frac{D}{2}\right)^2 + l^2\right] \qquad I = 2.516 \times 10^6\,lbf \cdot in \cdot sec^2$$

Next, calculate the inertia properties for rotations about axes through pints A and B

$$I_a := I + \frac{W}{g} \cdot r^2 \qquad I_a = 9.994 \times 10^6\,lbf \cdot sec^2 \cdot in$$

$$I_b := I + \frac{W}{g} \cdot r_1^2 \qquad I_b = 9.321 \times 10^6\,lbf \cdot sec^2 \cdot in \qquad \frac{I_a}{I_b} = 1.072$$

The next calculation determines the angle ψ_1

$$Ps_1 := \operatorname{atan}\left(\frac{a}{b}\right) \qquad Ps_2 := \operatorname{atan}\left(\frac{d}{2 \cdot h}\right)$$

$$Ps_1 = 53.13\,\text{deg} \qquad Ps_2 = 24.228\,\text{deg}$$

$$\psi_1 := Ps_1 - Ps_2 \qquad \psi_1 = 28.902\,\text{deg}$$

With the angle determined, the distance X is computed.

$$X := r \cdot \sin(\psi_1) - \left(a^2 + b^2\right)^{\frac{1}{2}}$$ Figure 3.A.17

Computing the appropriate angles needed to determine the factor β

$$\theta_{20} := \operatorname{asin}\left(\frac{X}{r_1}\right) \qquad \theta_{20} = 23.871\,\text{deg}$$ Eq 3.A.10

$$\theta_{2f} := \operatorname{acos}\left(\frac{D}{2 \cdot r_1}\right) \qquad \theta_{2f} = 62.574\,\text{deg}$$ Eq. 3.A.12

The parameter β is determined as

$$\beta := \frac{I_a}{I_b} \cdot \frac{r}{r_1} \cdot \left(1 - \cos(\psi_1)\right) + \cos(\theta_{20}) - \cos(\theta_{2f})$$ Eq. 3.A.14

$$\beta = 0.594$$

The initial pre-impact angular velocity is computed as

$$\theta dot_{2f} := \sqrt{2 \cdot \frac{W \cdot r_1}{I_b} \cdot \beta} \qquad \theta dot_{2f} = 1.792\,\text{sec}^{-1}$$

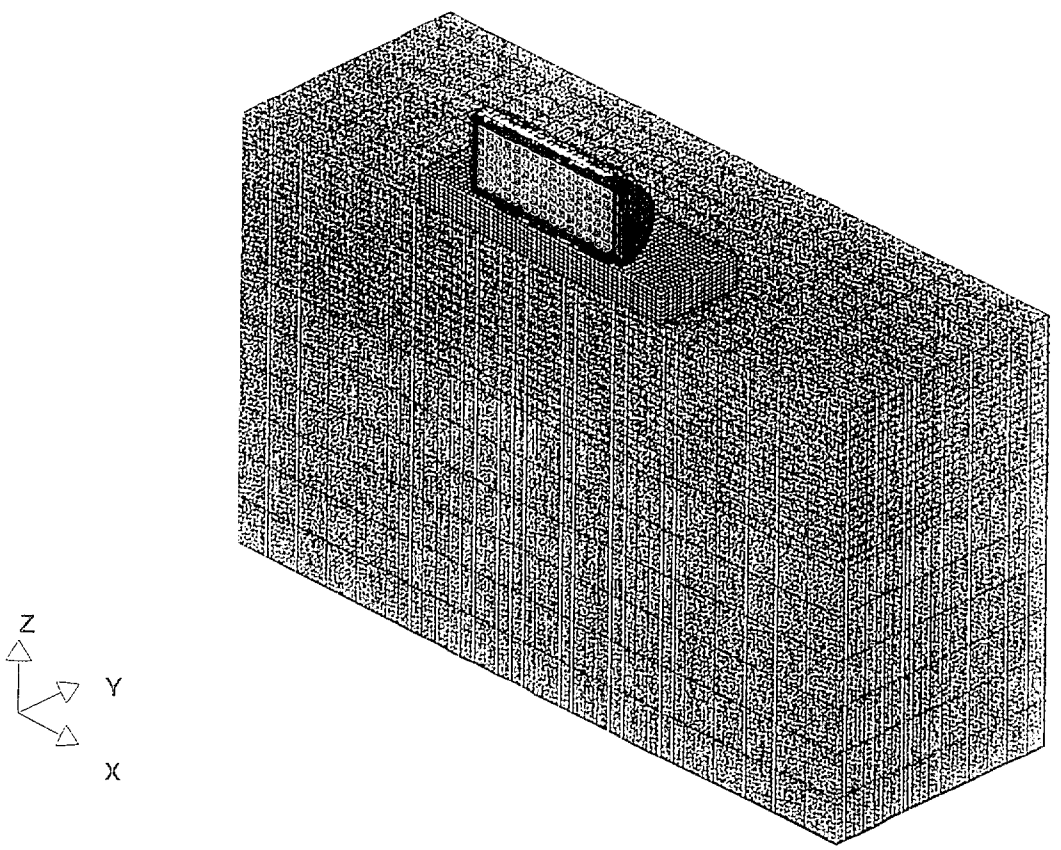

Fig. 3.A.1 Side-Drop and Tipover Finite-Element Model (3-D View)

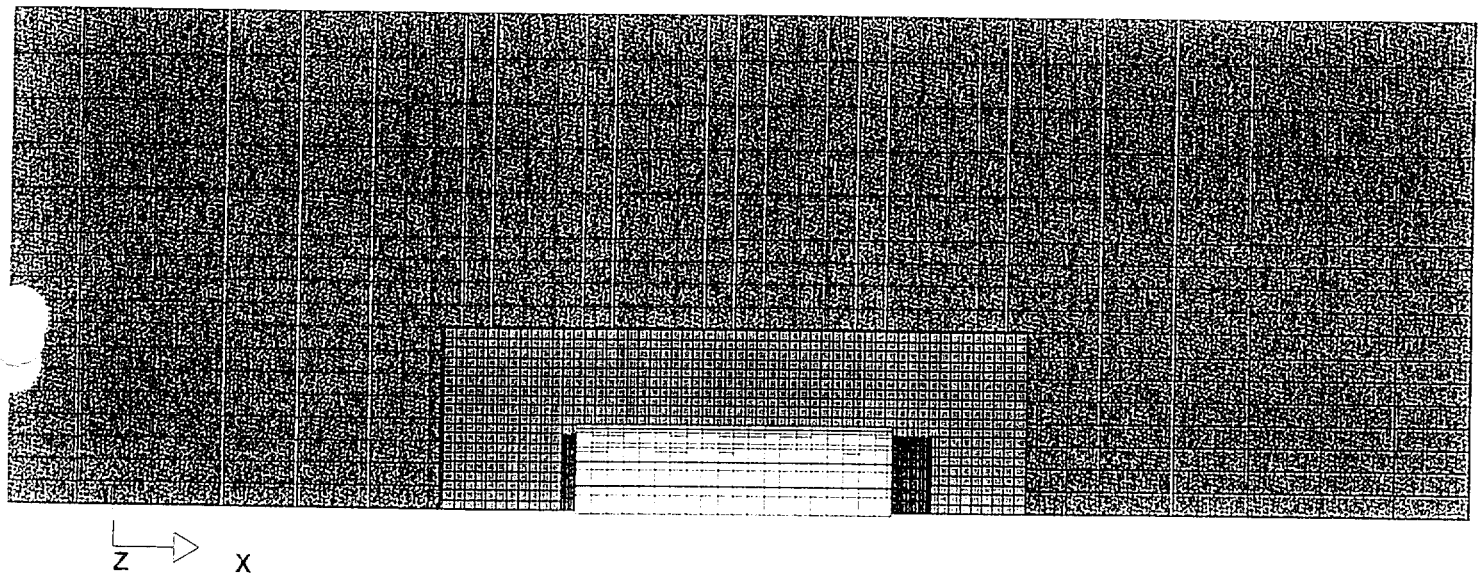

Fig. 3.A.2 Side-Drop and Tipover Finite-Element Model (Plan View)

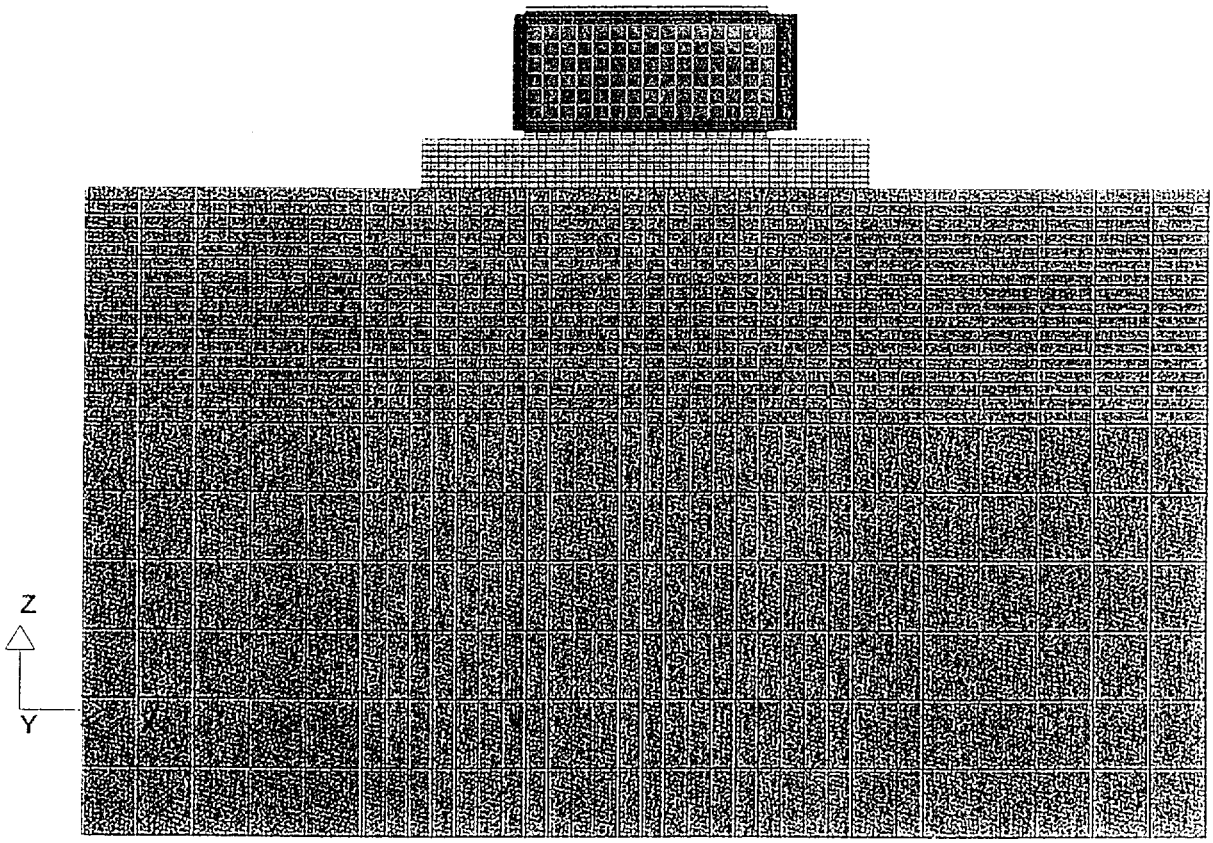

Fig. 3.A.3 Side-Drop and Tipover Finite-Element Model (XZ View)

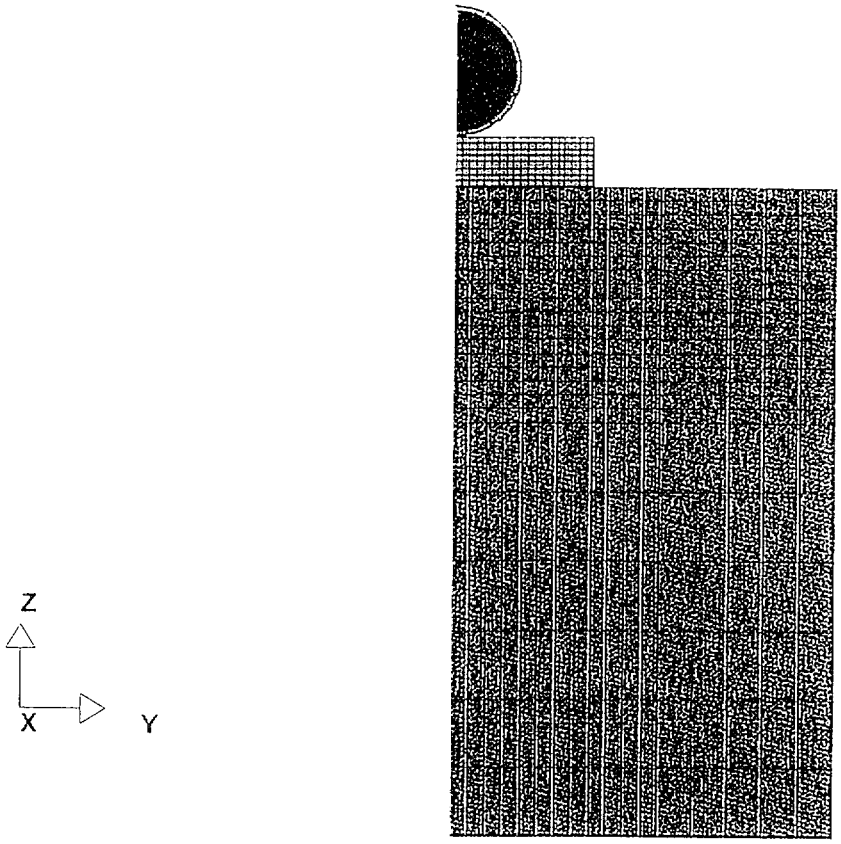

Fig. 3.A.4 Side-Drop and Tipover Finite-Element Model (YZ View)

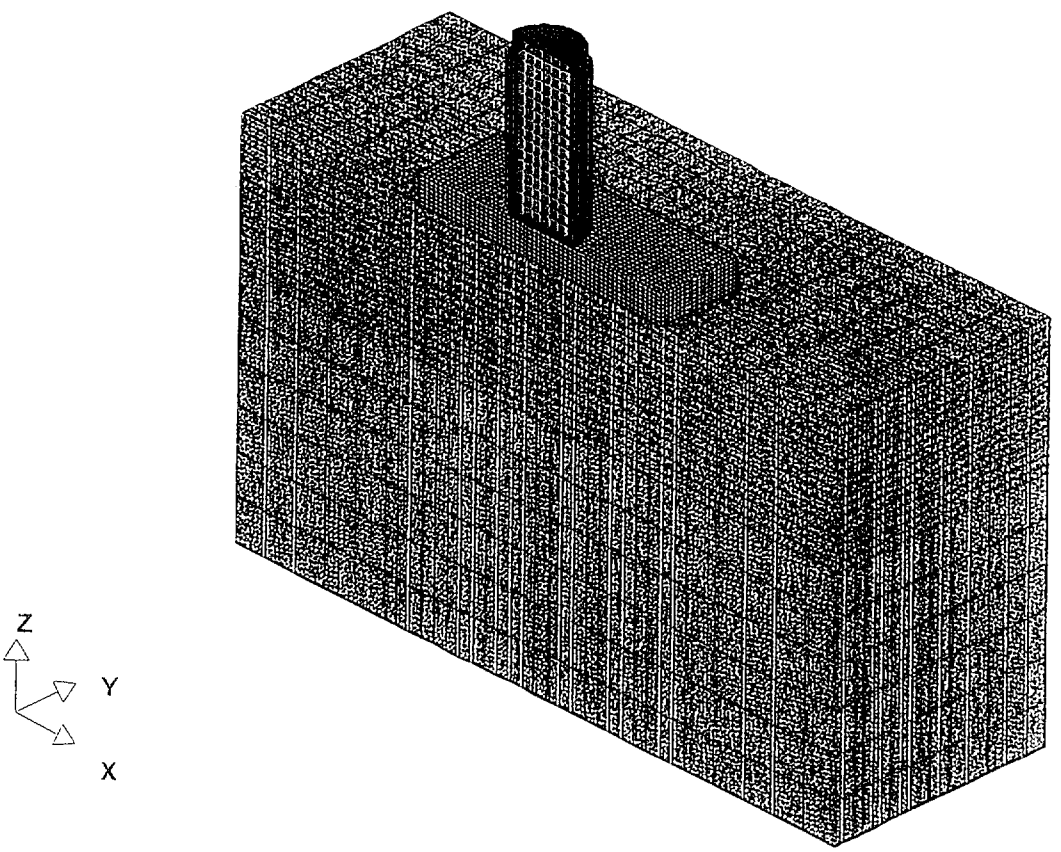

Fig. 3.A.5 End-Drop Finite-Element Model (3-D View)

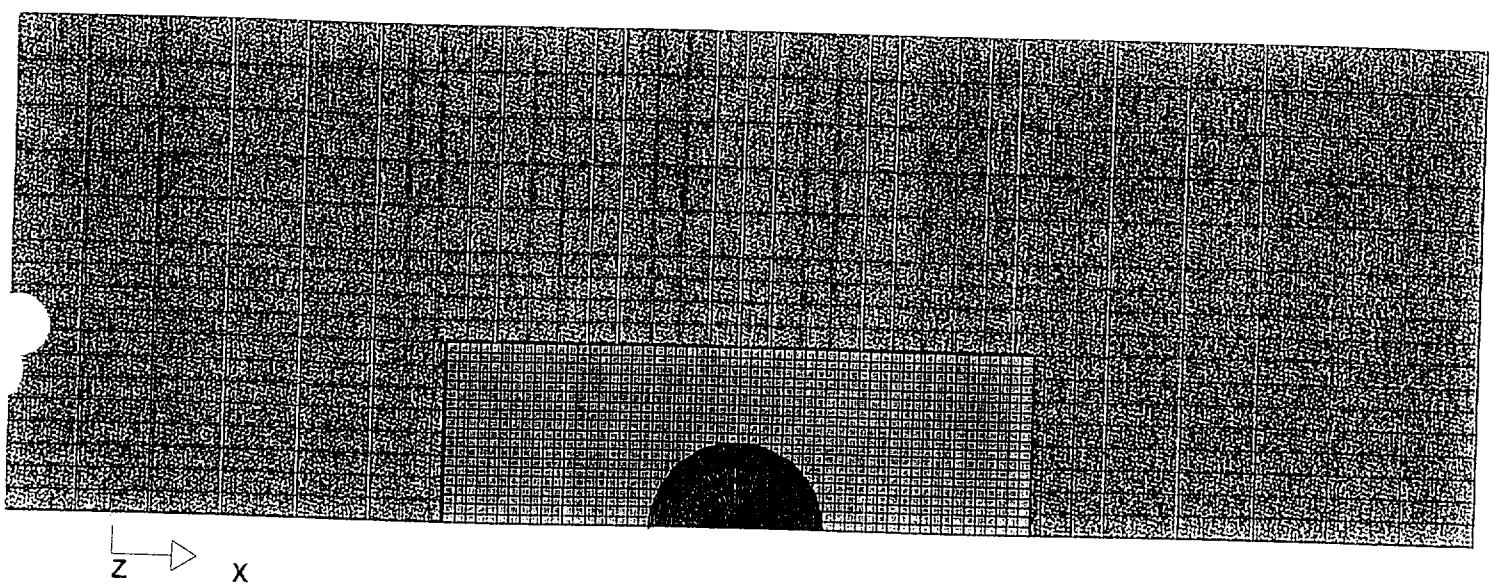

Fig. 3.A.6 End-Drop Finite-Element Model (Plan View)

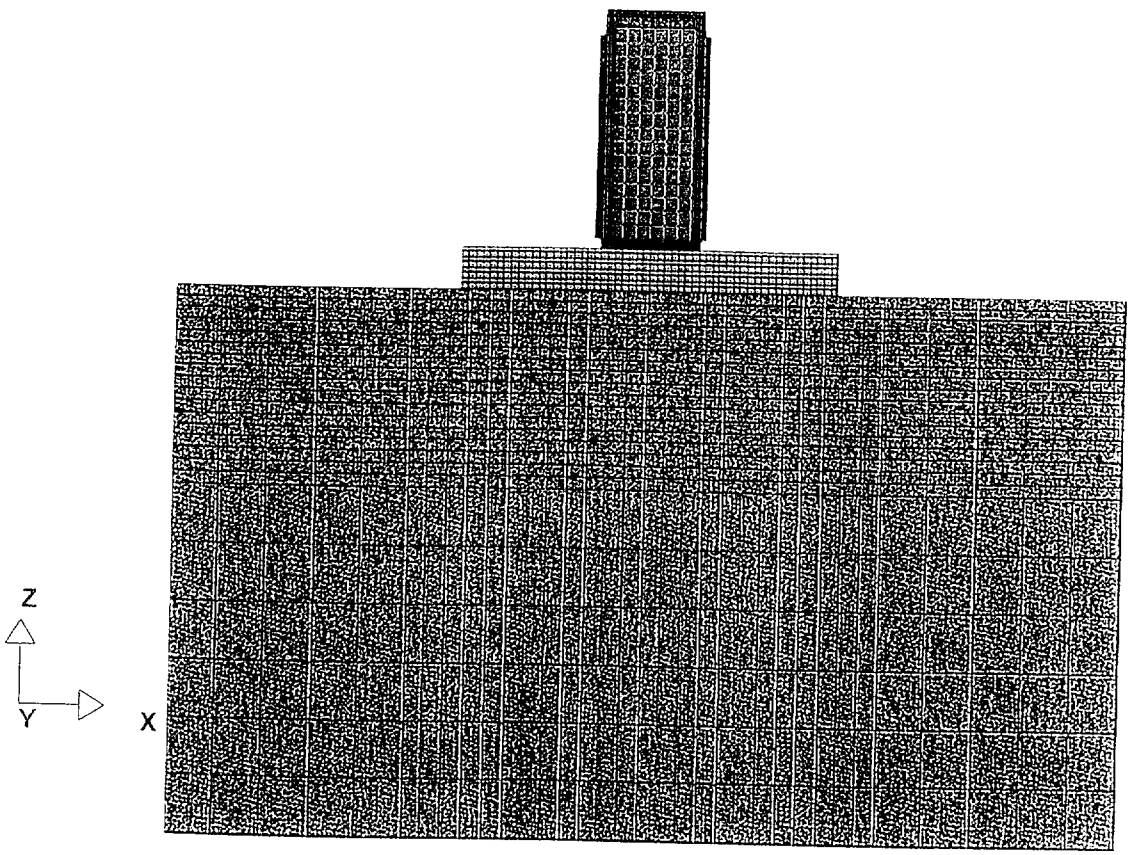

Fig. 3.A.7 End-Drop Finite-Element Model (XZ View)

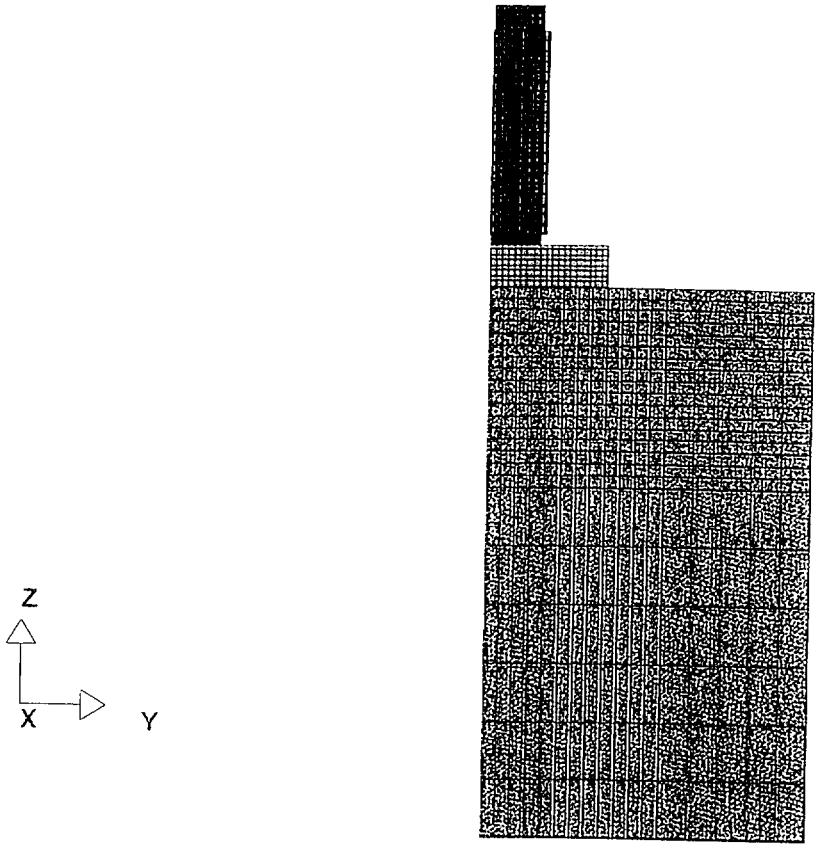

Fig. 3.A.8 End-Drop Finite-Element Model (YZ View)

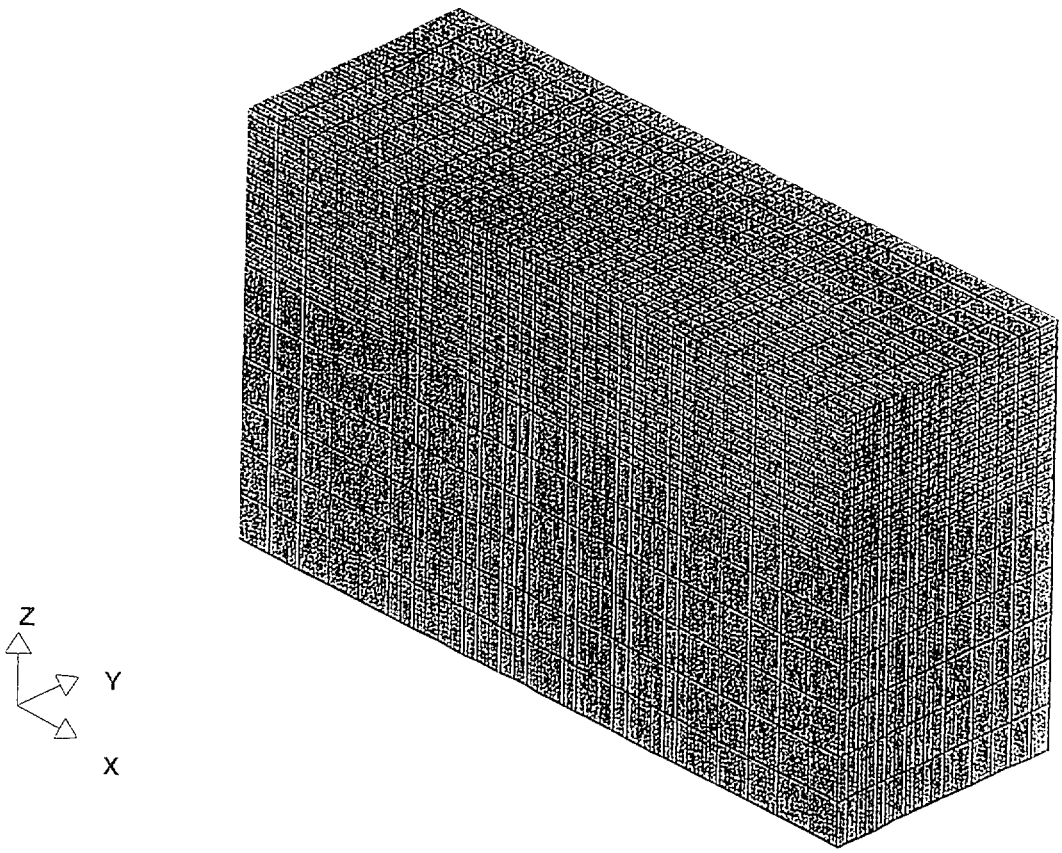

Fig. 3.A.9 Soil Finite-Element Model (3-D View)

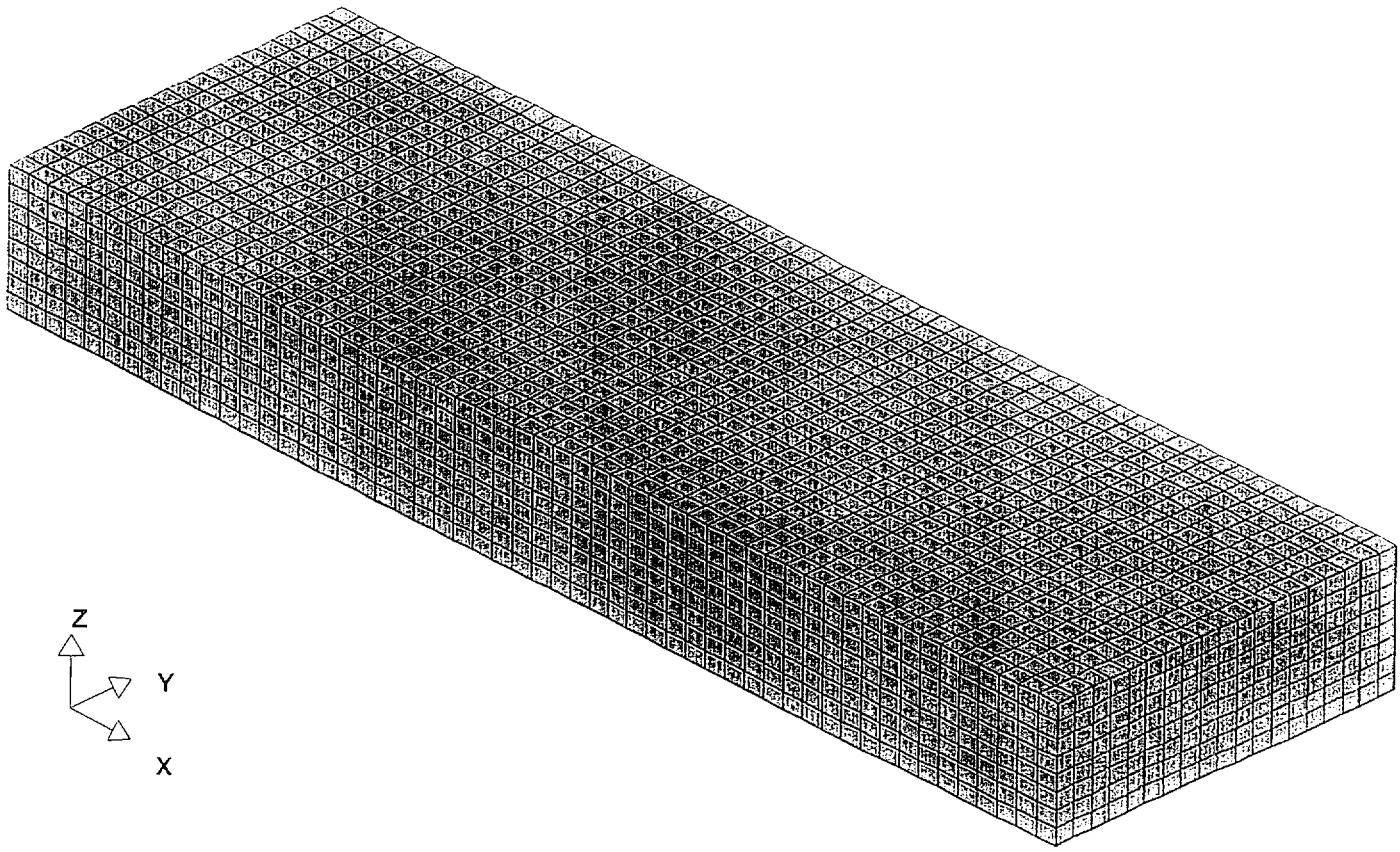

Fig. 3.A.10 Concrete Pad Finite-Element Model (3-D View)

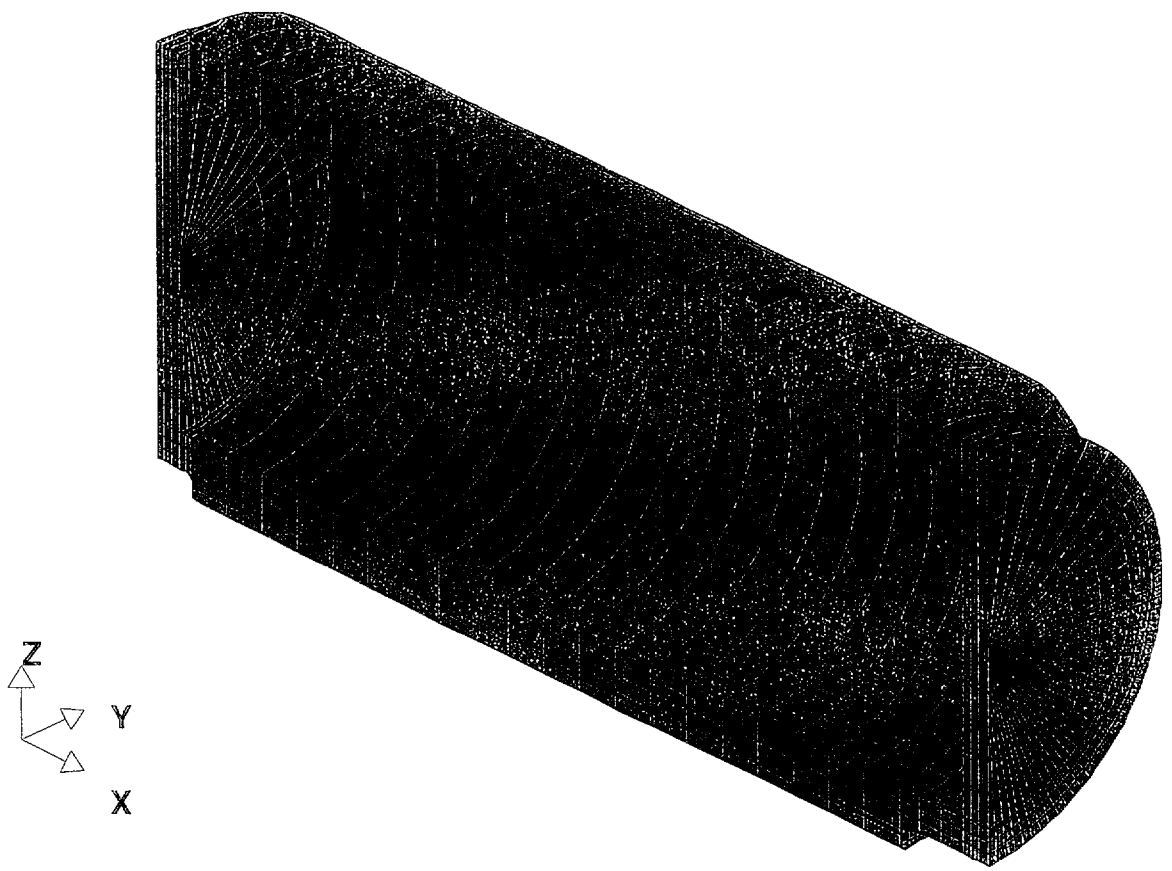

Figure 3.A.II Cask Finite-Element Model (3-D View)

FIGURE 3.A.12 DELETED

FIGURE 3.A.13 DELETED

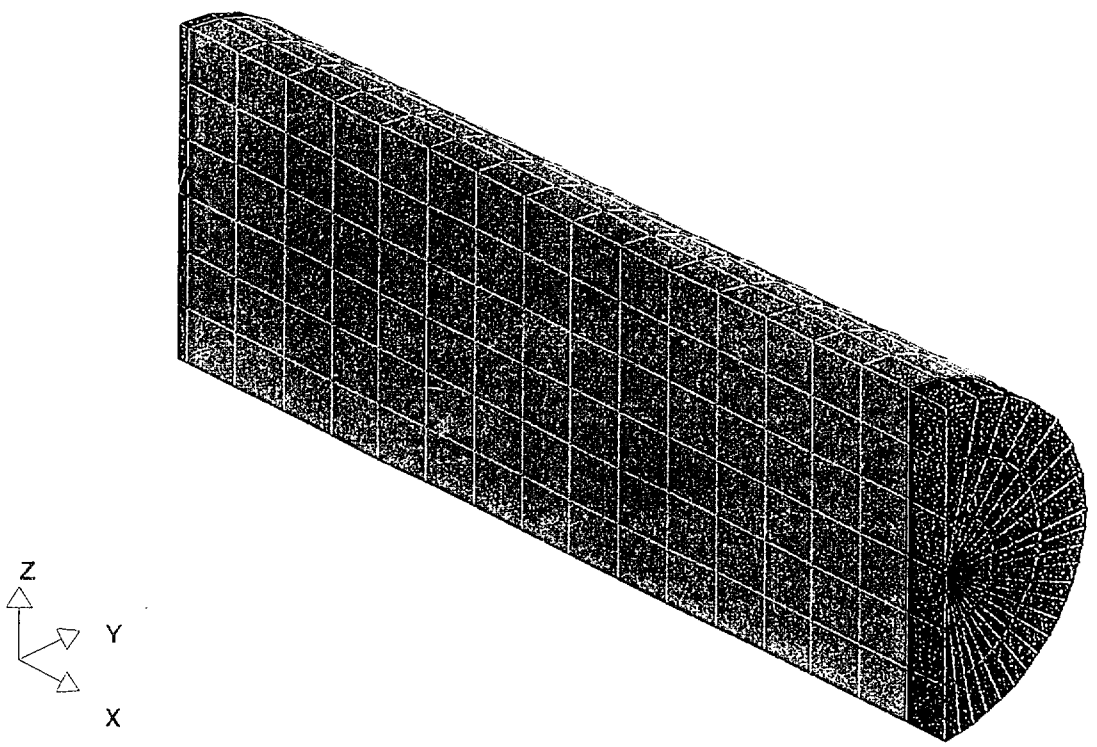

Fig. 3.A.14 MPC Finite-Element Model (3-D View)

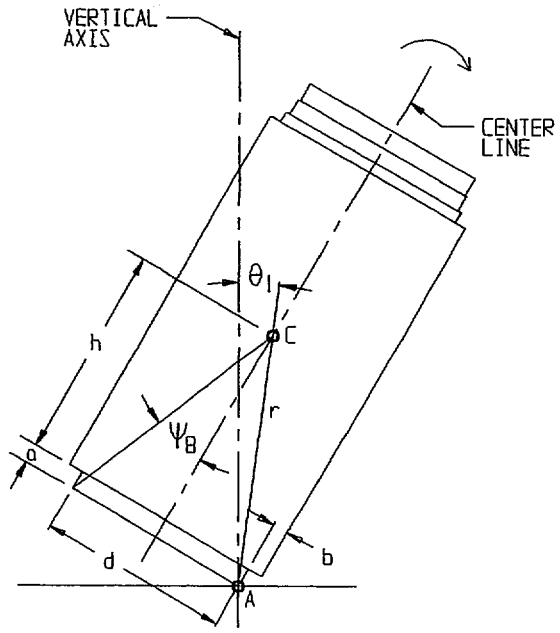

FIGURE 3.A.15; PIVOT POINT SHIFT DURING TIP-OVER
INITIAL CONDITION

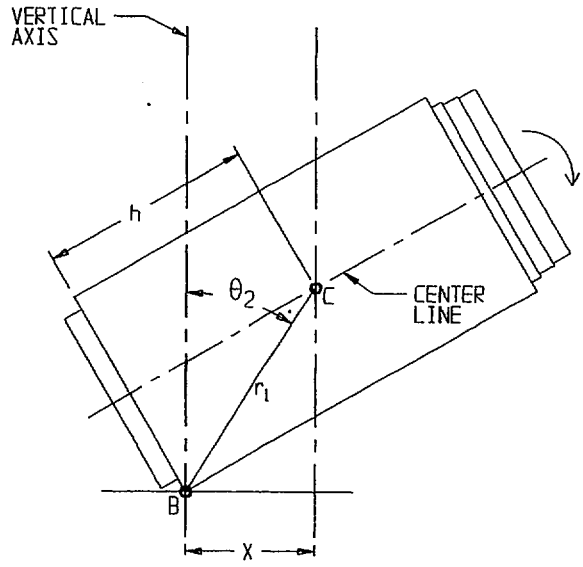

FIGURE 3.A.16; PIVOT POINT SHIFT DURING TIP-OVER
INTERMEDIATE CONDITION

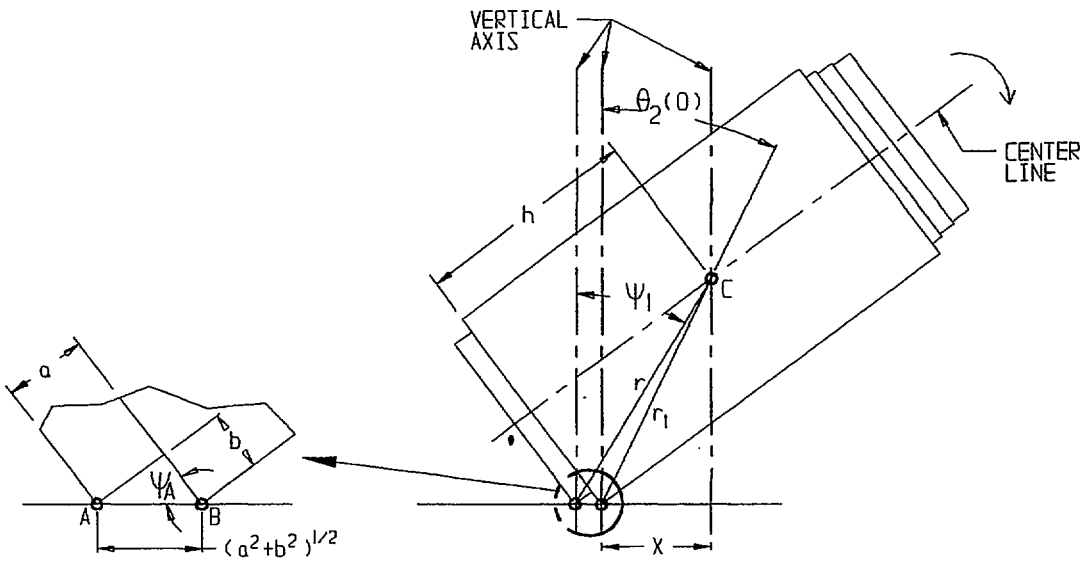

FIGURE 3.A.17; TIP-OVER EVENT AT THE INSTANT WHEN POINTS A AND B ARE BOTH IN CONTACT WITH THE GROUND

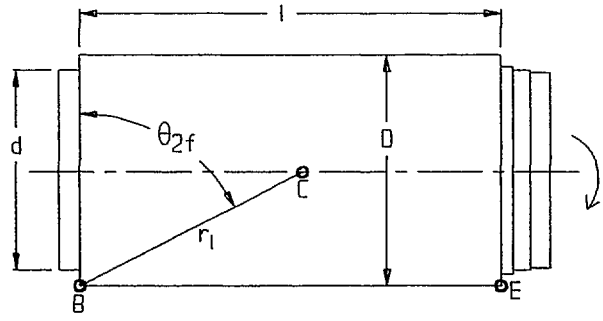

FIGURE 3.A.18; TIP-OVER EVENT OVERPACK SLAMS AGAINST THE FOUNDATION DEVELOPING A RESISTIVE FORCE

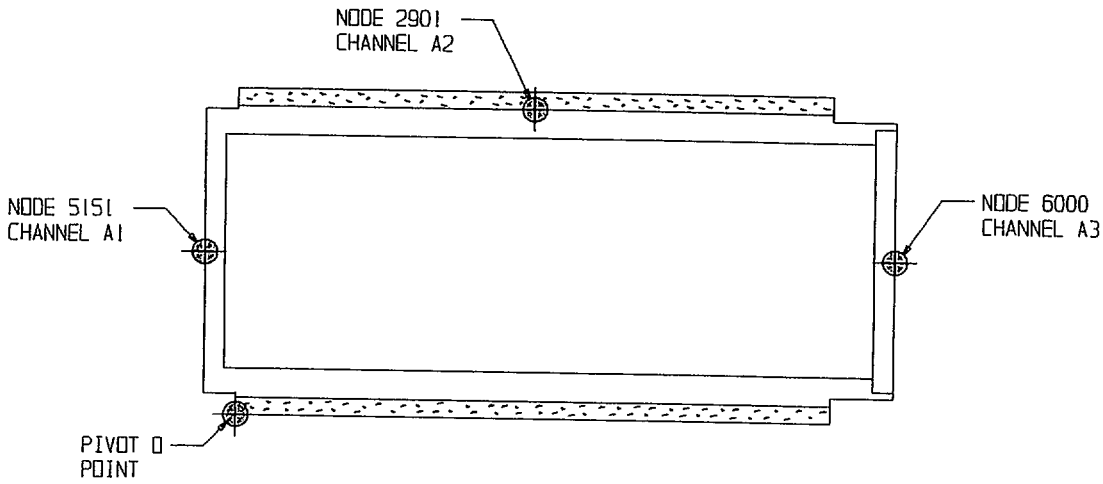

FIGURE 3.A.19; MEASUREMENT POINTS AND CORRESPONDING FINITE-ELEMENT MODEL NODES

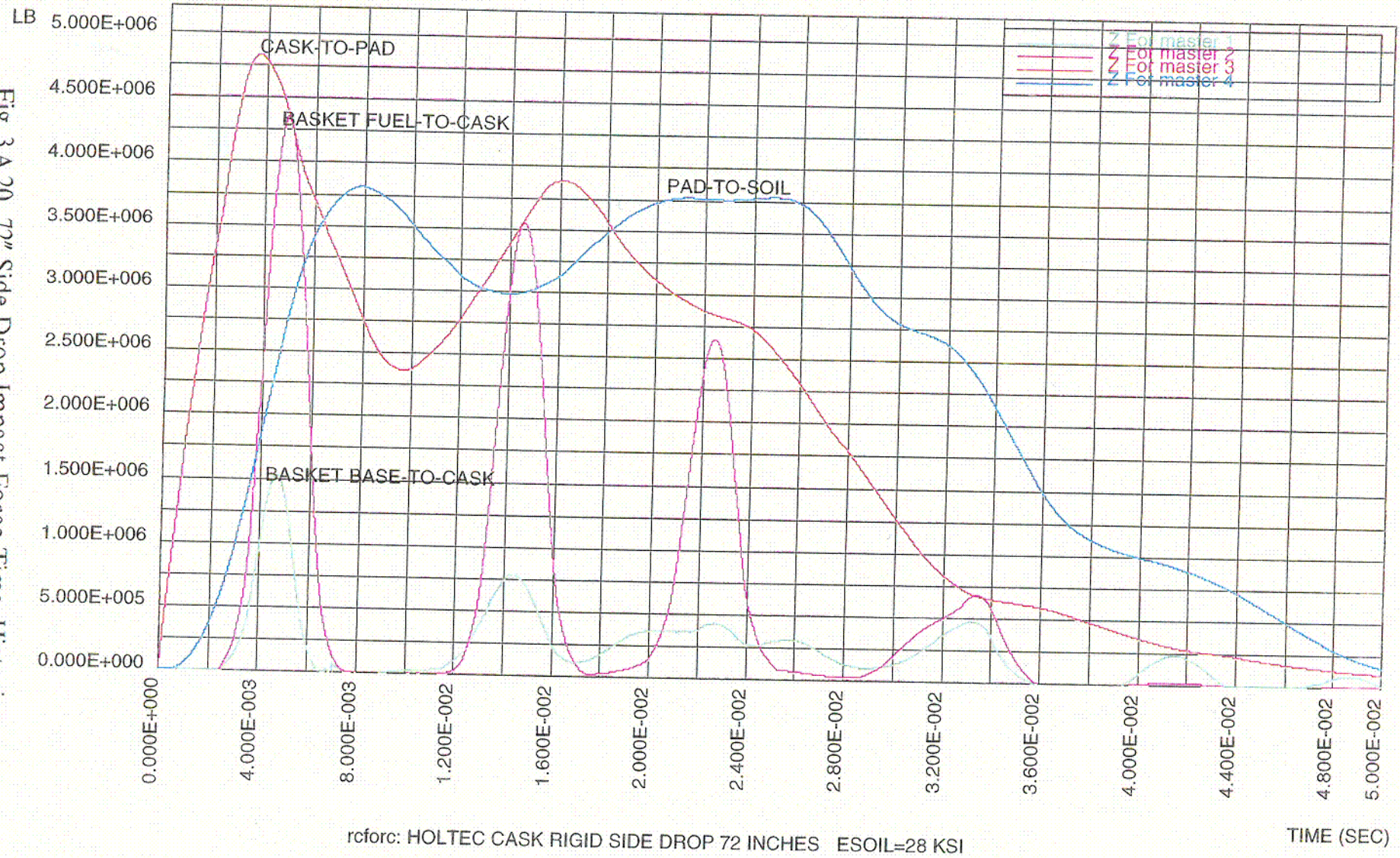

Fig. 3.A.20 72" Side Drop Impact Force Time-Histories

C03

Fig. 3.A.21 72" Side Drop Displacement Time-Histories

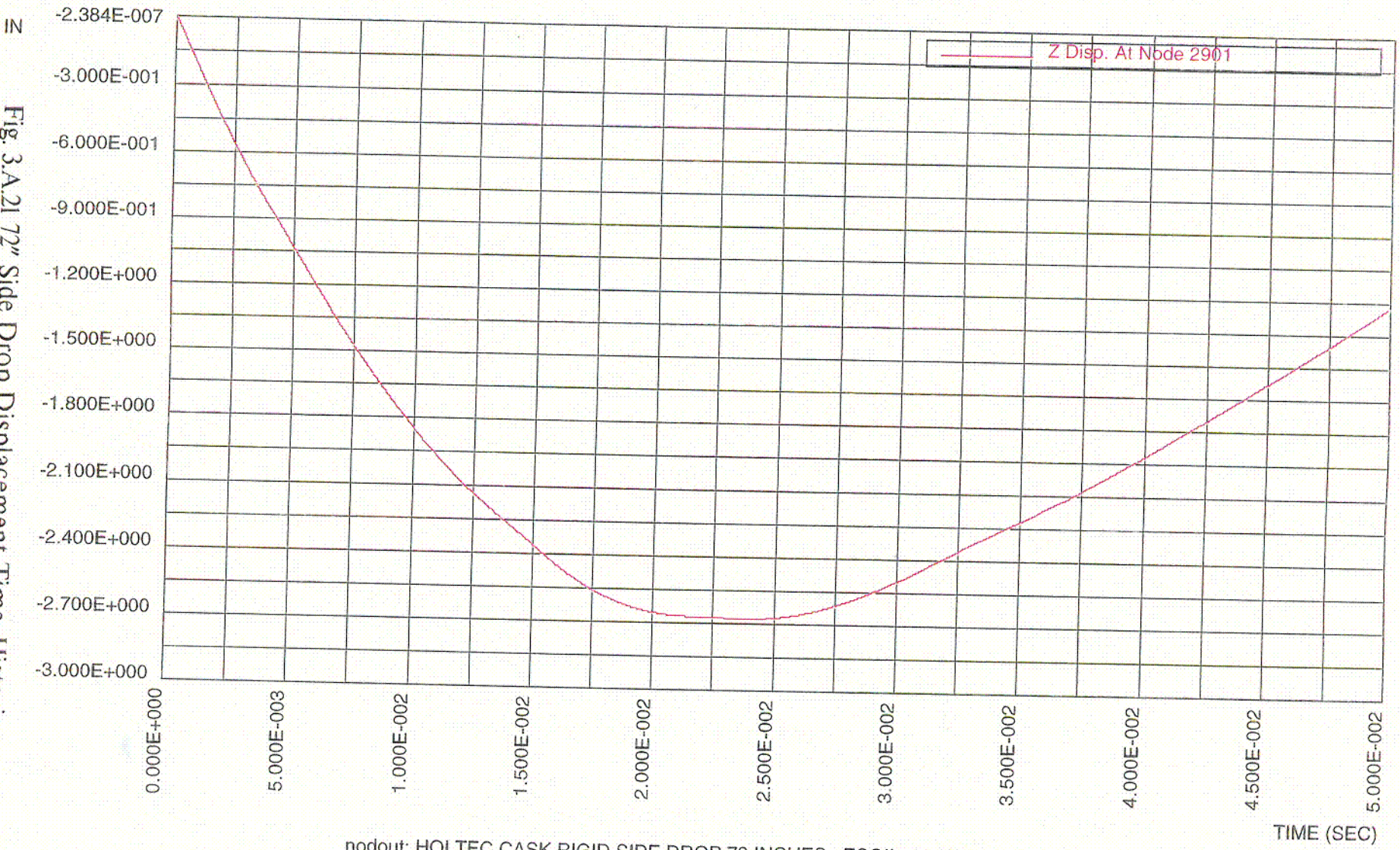

C04

Wed Nov 11 13:38:17 1920

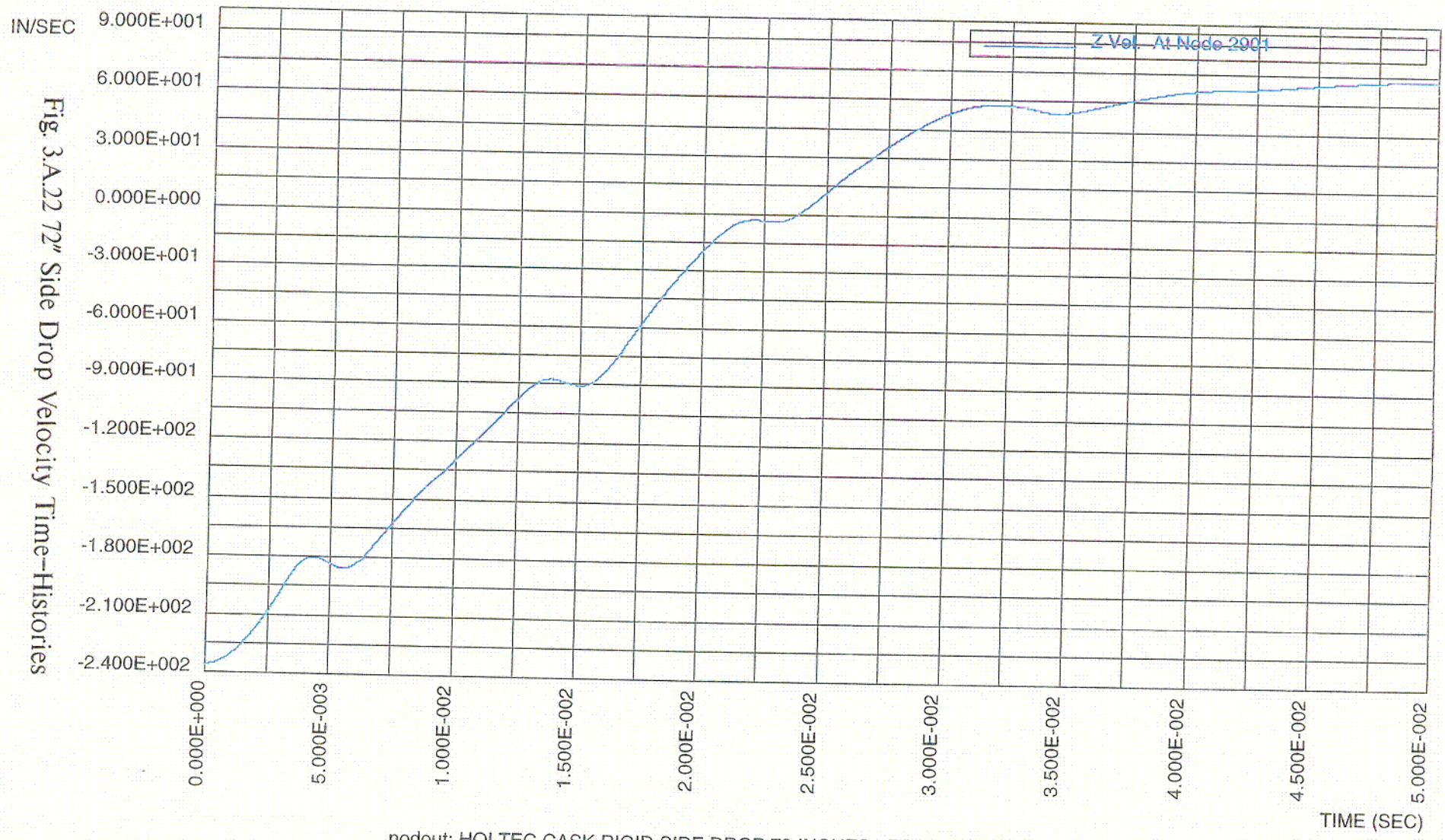

Fig. 3.A.22 72" Side Drop Velocity Time-Histories

C05

Wed Nov 11 13:38:40 1998

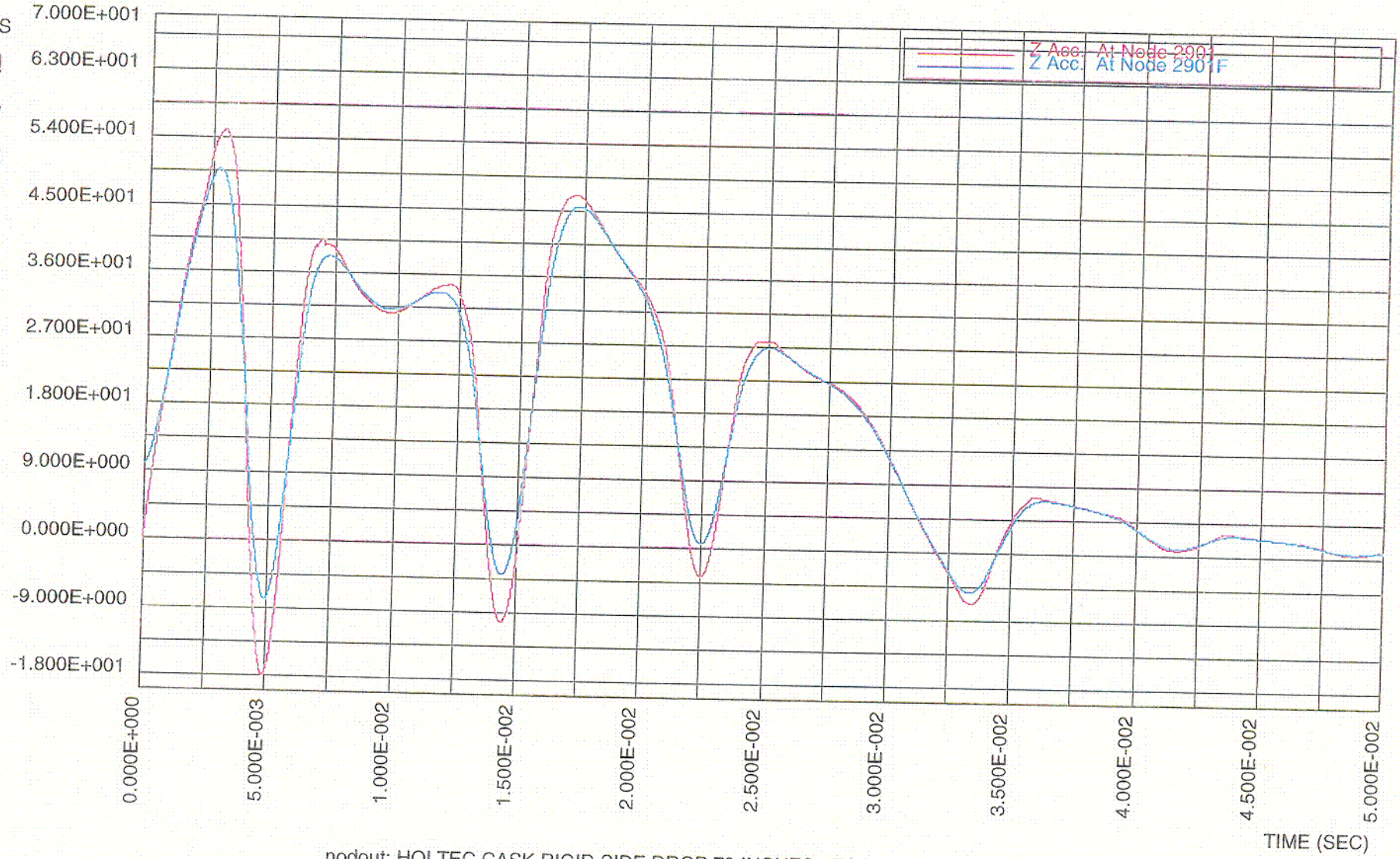

Fig. 3.A.23 72" Side Drop Acceleration Time-Histories

C04

Wed Nov 11 13:24:07 1999

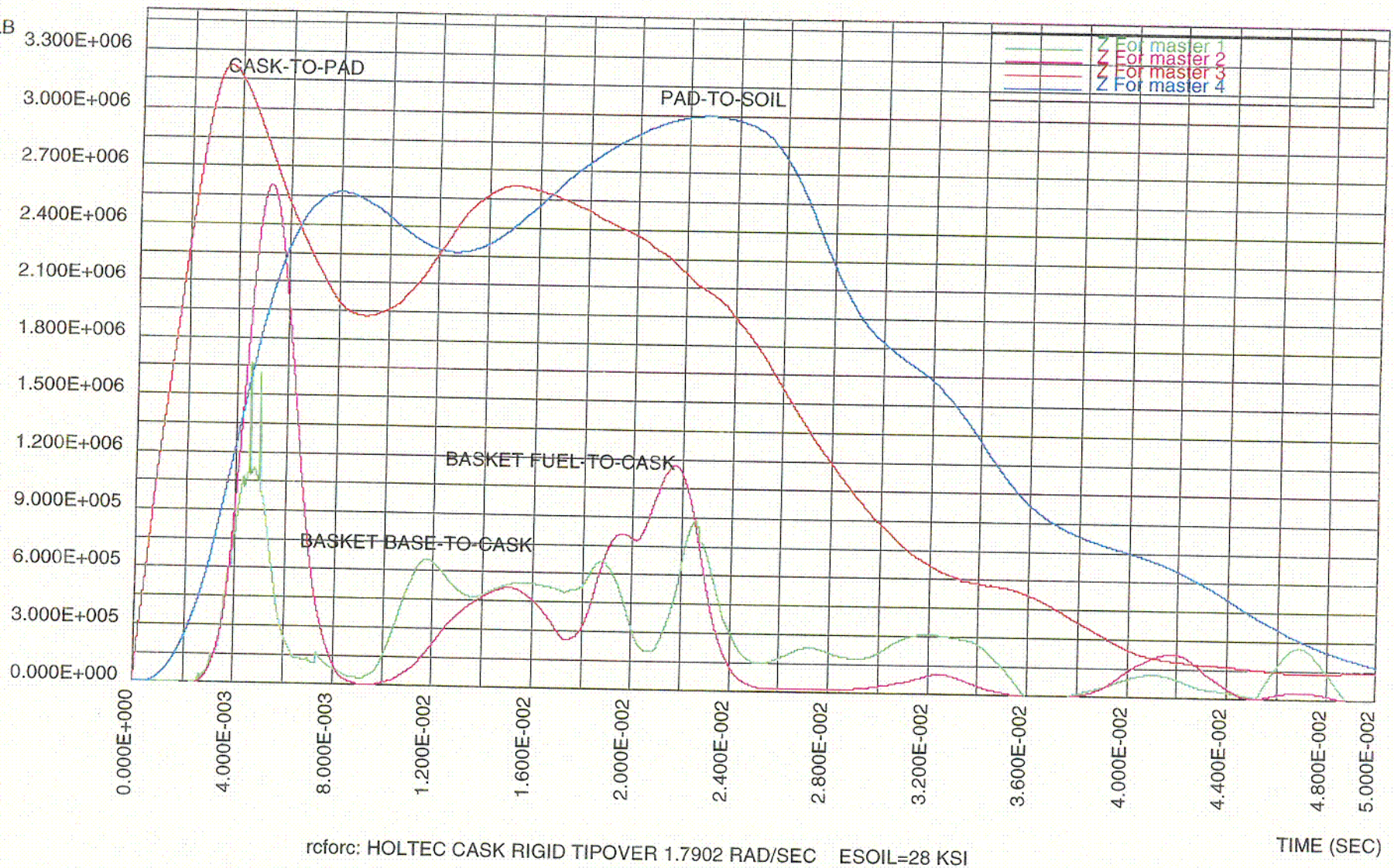

Fig. 3.A.24 Tipover Top Center of Overpack Closure Plate Impact Force Time-Histories

C07

Wed Nov 11 13:13:13 1998

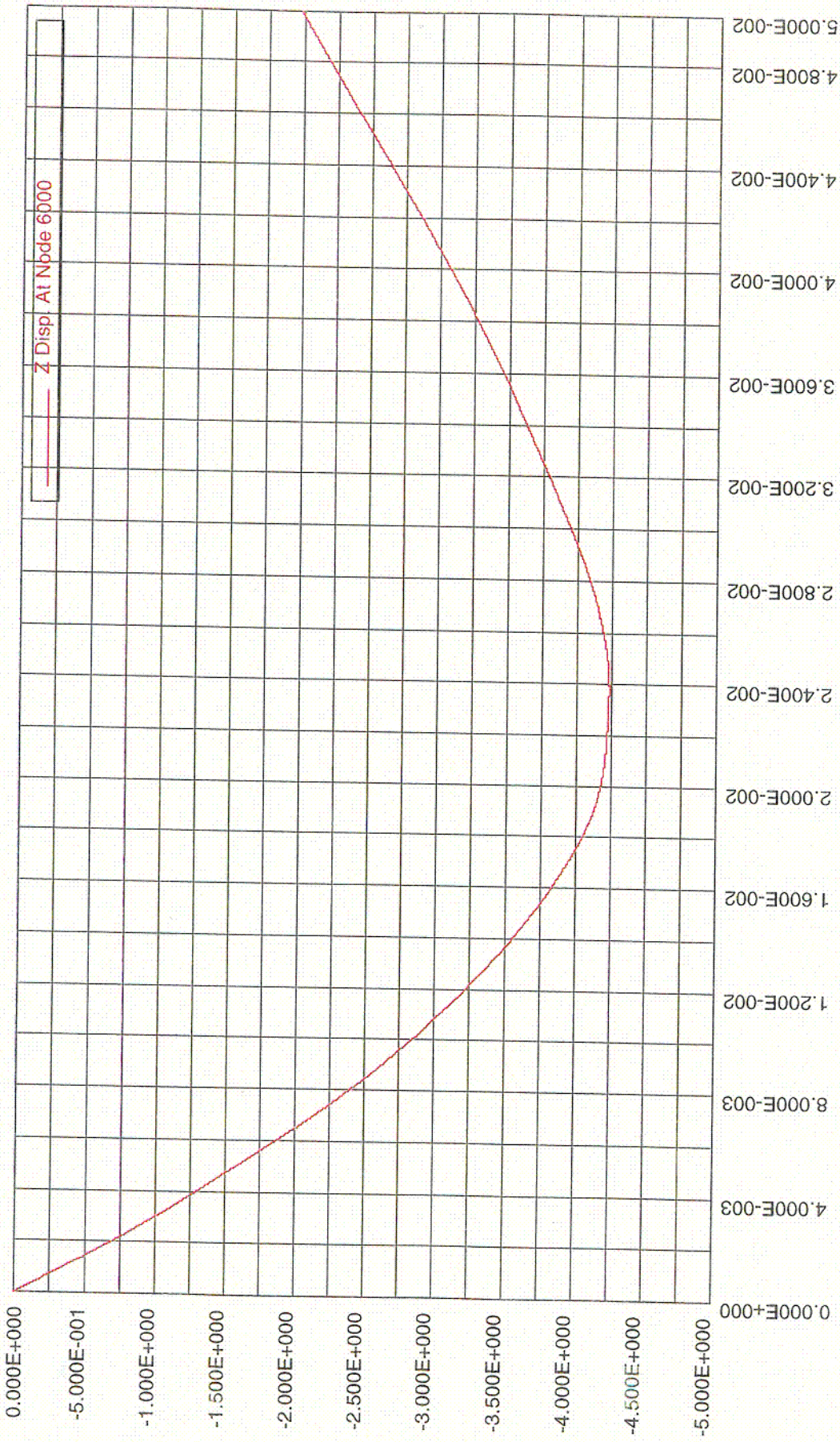

C08

Fig. 3.A.25 Tipover Top Center of Overpack Closure Plate Displacement Time-Histories

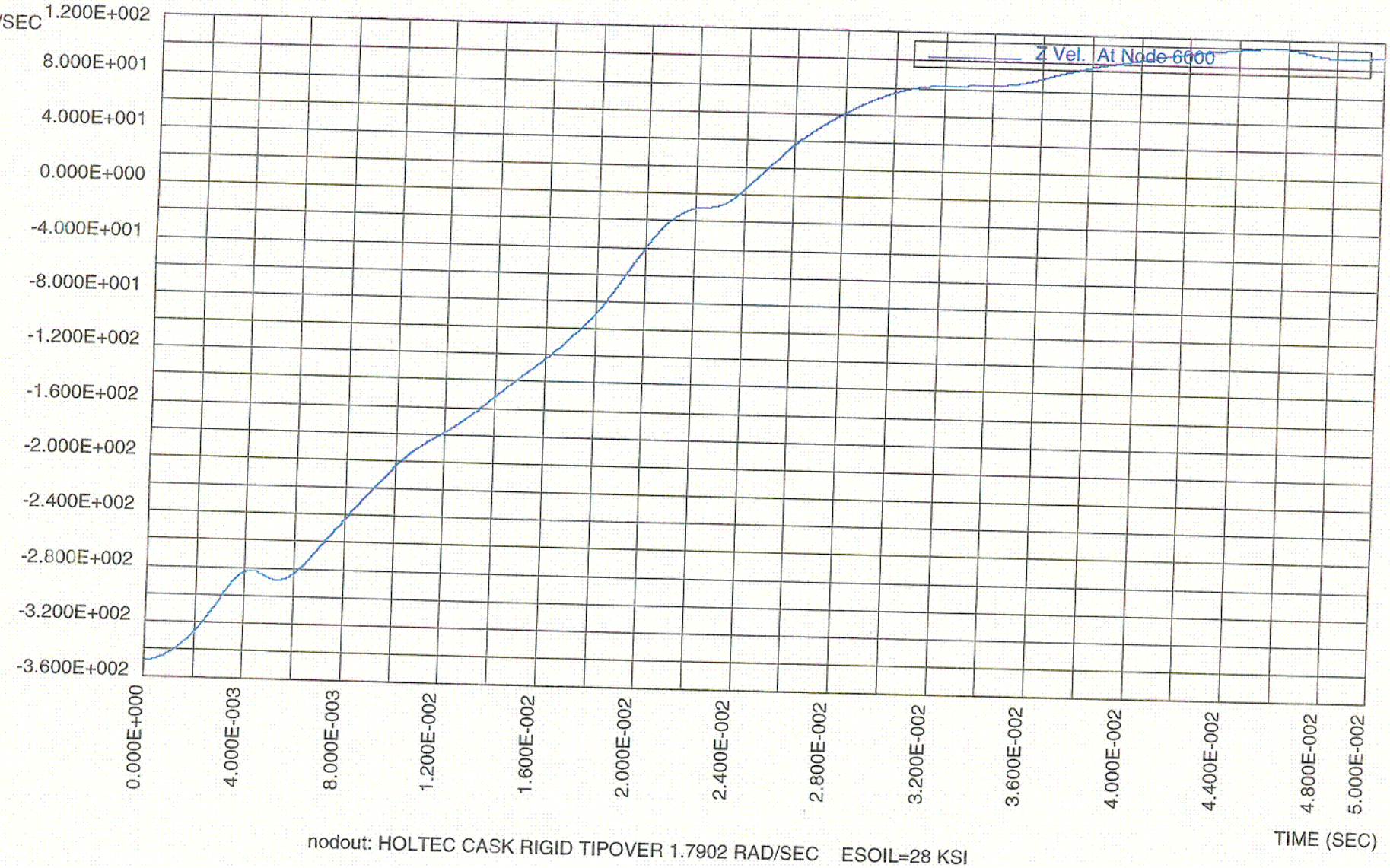

Fig. 3.A.26 Tipover Top Center of Overpack Closure Plate Velocity Time-Histories

C09

Wed Nov 11 13:17:58 1998

Fig. 3.A.27 Tipover Top Center of Overpack Closure Plate Accelertion Time-Histories

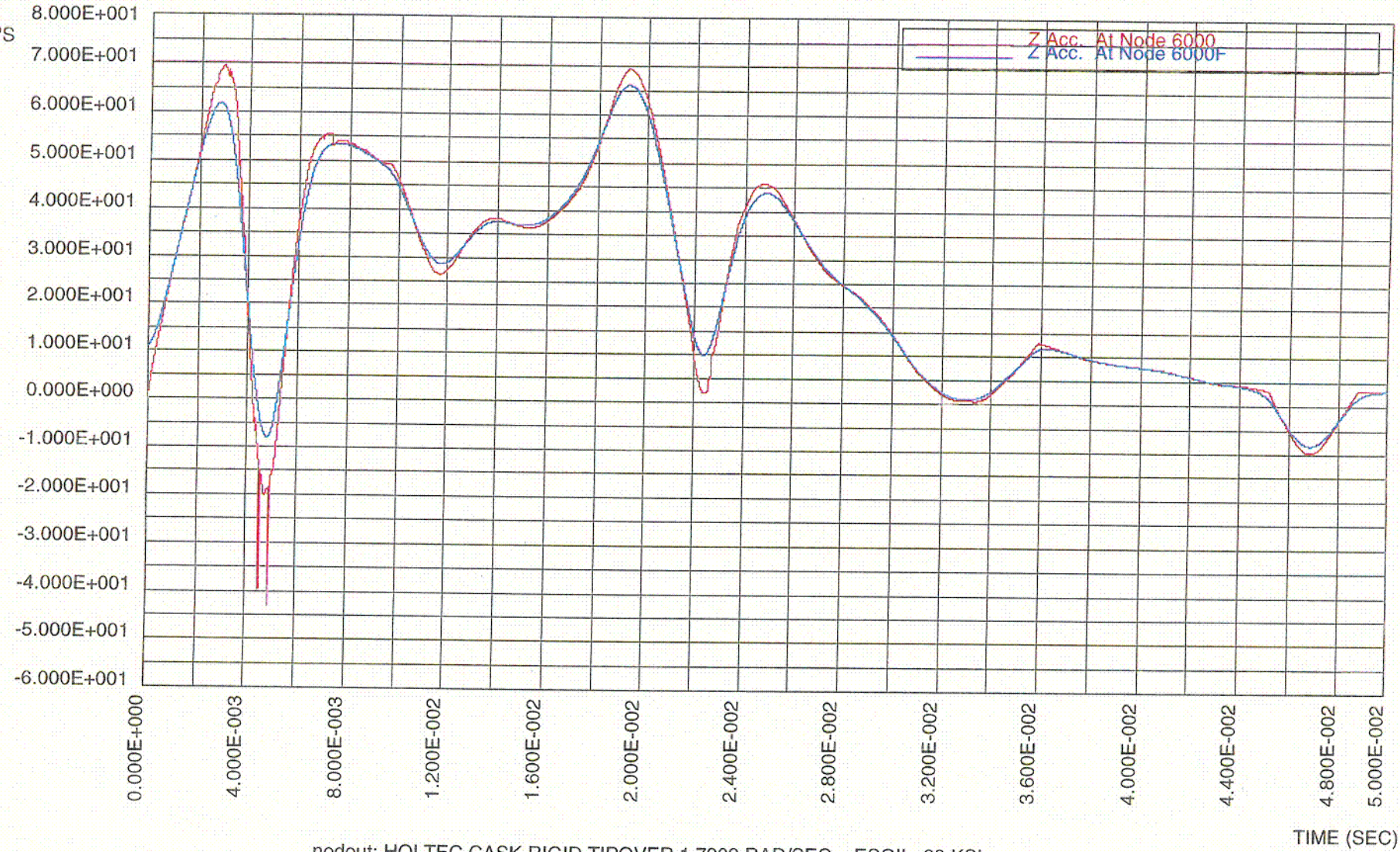

C10

Wed Nov 11 13:22:37 1998

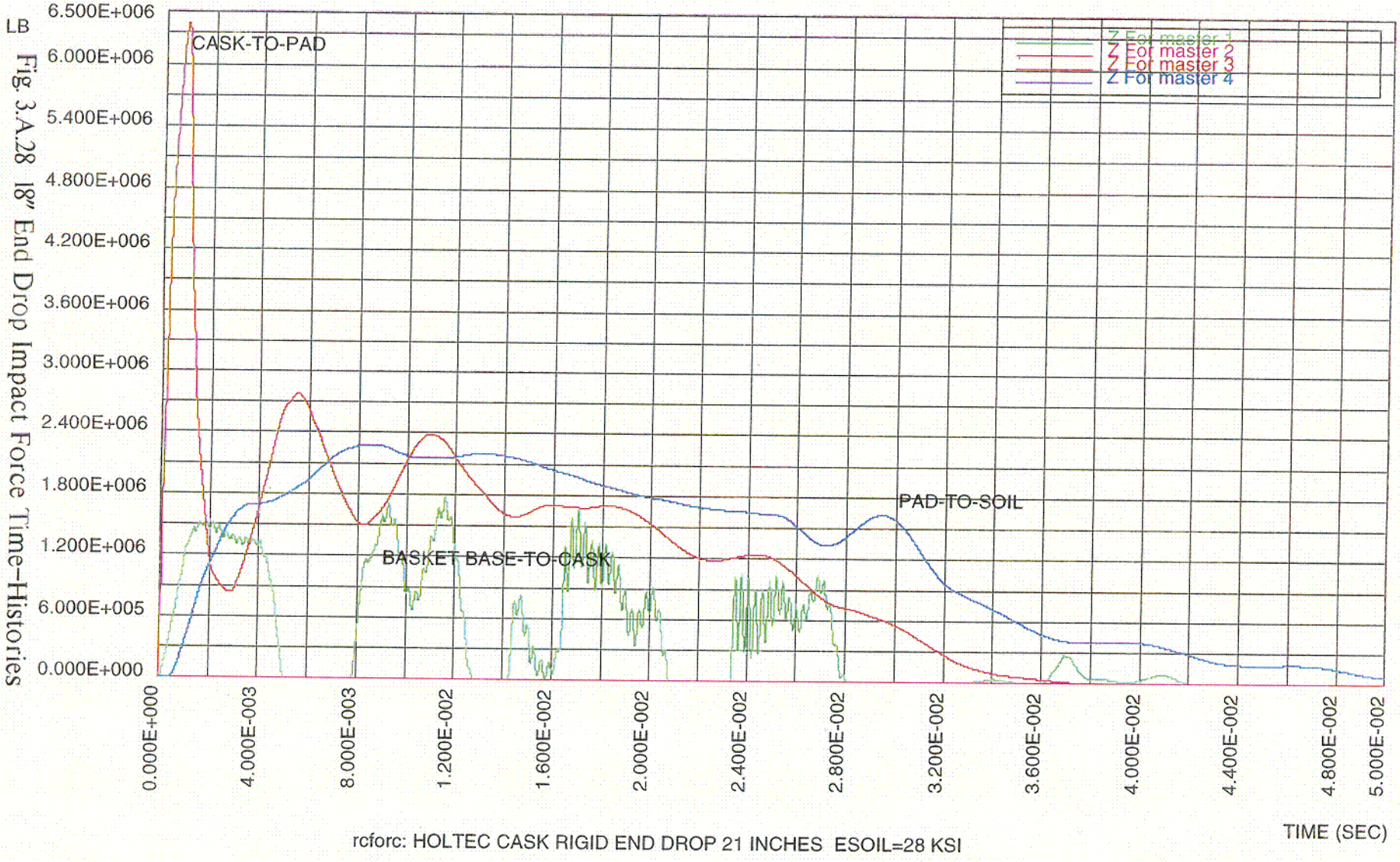

Fig. 3.A.28 18" End Drop Impact Force Time-Histories

C11

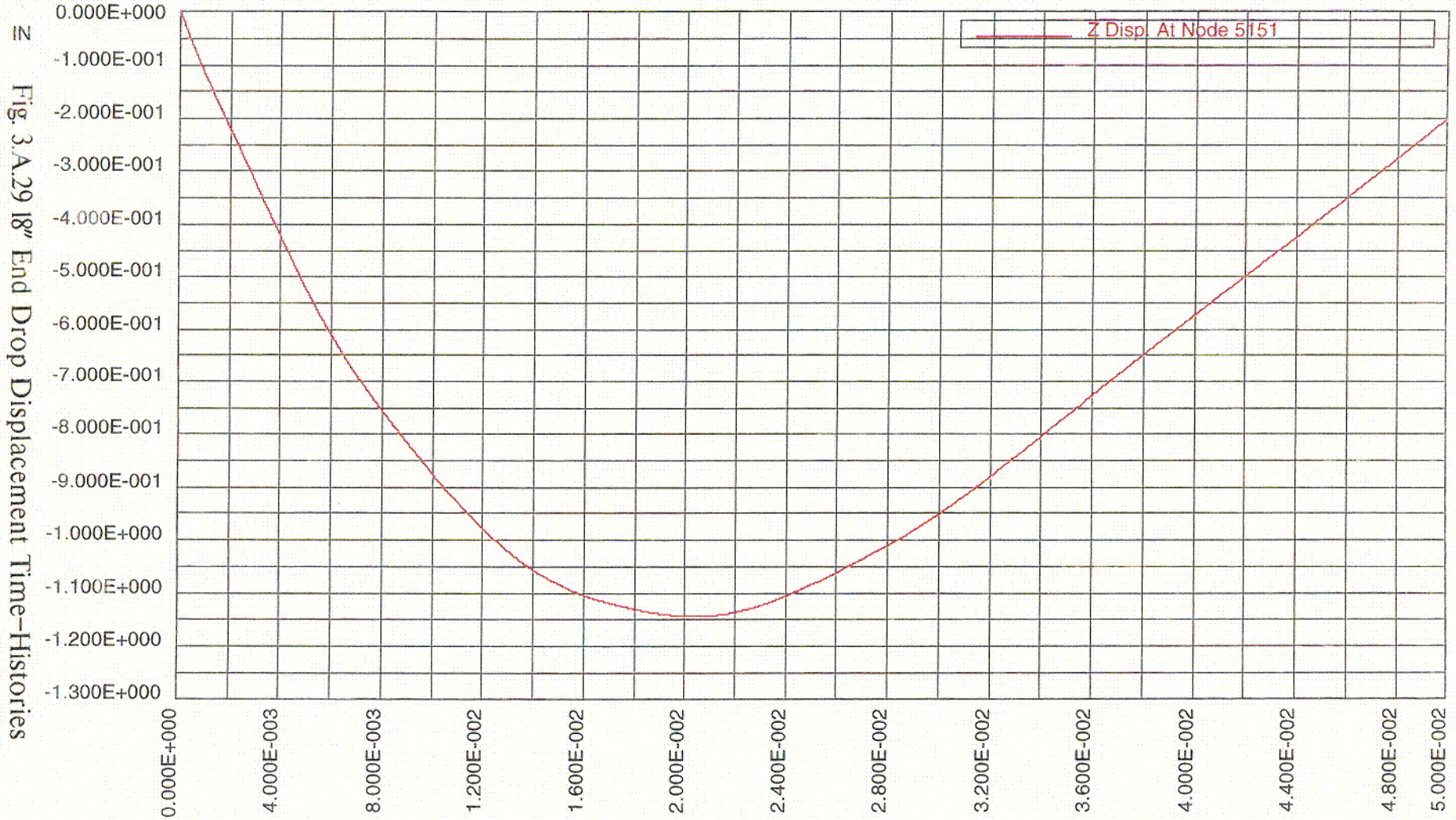

Fig. 3.A.29 18" End Drop Displacement Time-Histories

C12

Wed Nov 11 13:31:45 1998
KBS2 : LSDyna3d PrePost

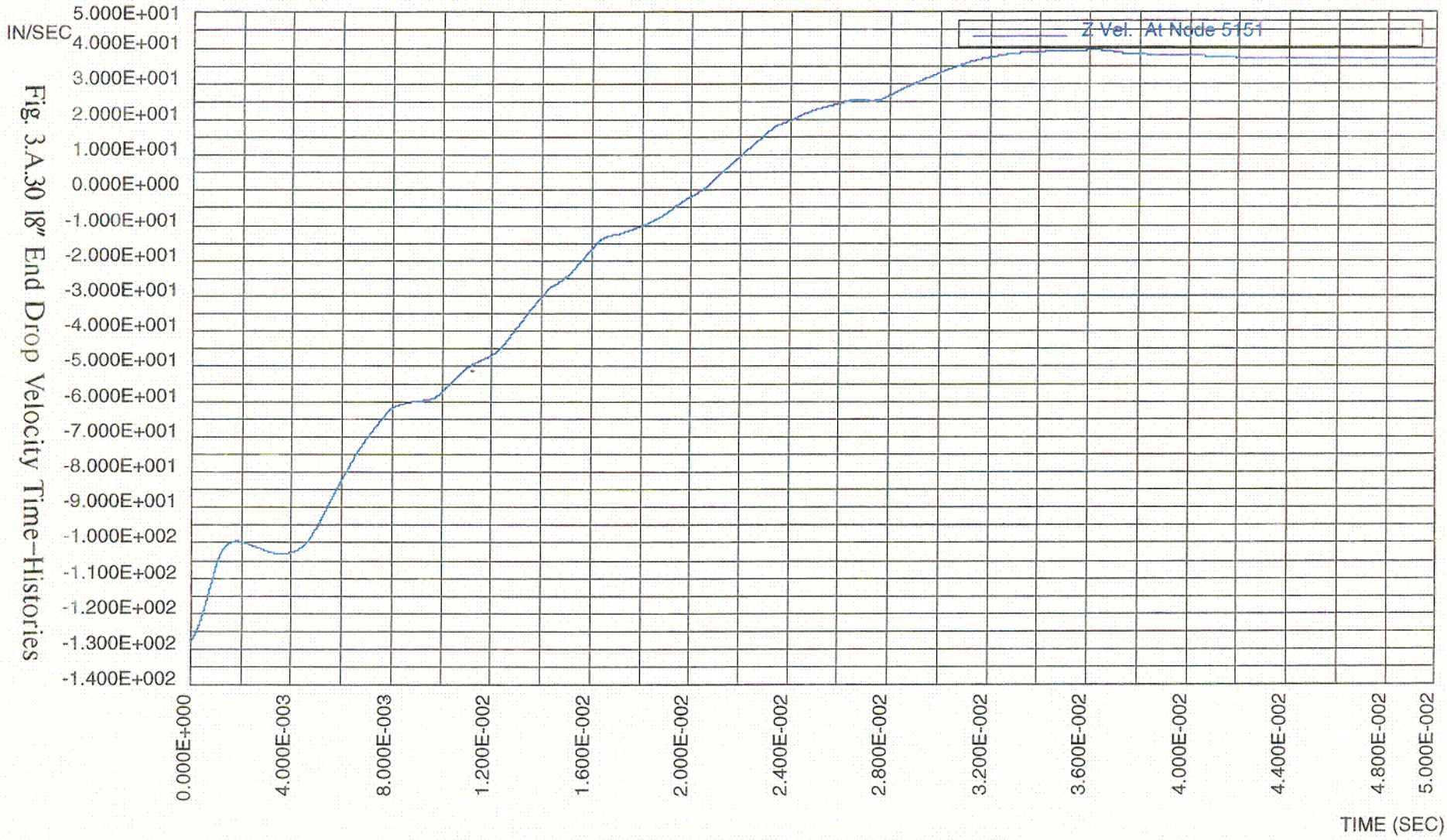

Fig. 3.A.30 18" End Drop Velocity Time-Histories

C13

Wed Nov 11 13:33:15 1998
KBS2 : LSDyna3d PrePost

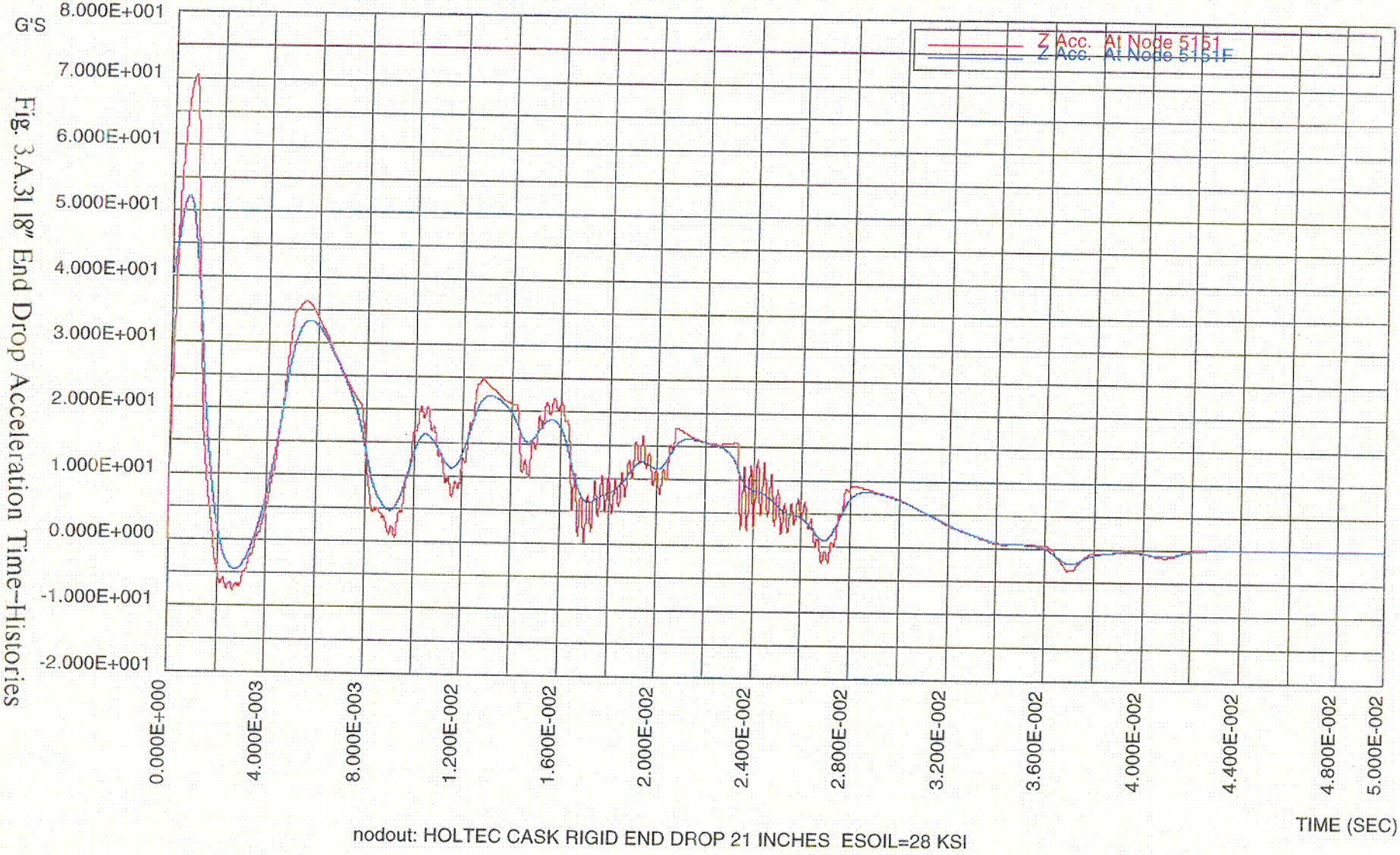

Fig. 3.A.31 18" End Drop Acceleration Time-Histories

C14

Wed Nov 11 13:35:49 1998